THE GARRETT CORPORATION
AiResearch Manufacturing Division
LOS ANGELES 45, CALIFORNIA

REPORT NO. AP-67-2161

HYPERSONIC RESEARCH ENGINE PROJECT - PHASE IIA
FIRST INTERIM TECHNICAL DATA REPORT
~~ITEM NO. 55-7.01~~
~~STRUCTURES AND COOLING DEVELOPMENT~~
3 FEBRUARY THROUGH 3 MAY 1967
NASA CONTRACT NO. NAS 1-6666

AP-67-2161 12 May 1967

NO. OF PAGES 139

DATE 12 May 1967

Dwgs Attached to Section 5

L980600	SK51306
L980604	SK51307
L980608	SK51308
SK51305	

PREPARED BY O. A. Buchmann

EDITED BY R. J. Downs

APPROVED BY Henry J. Lopez
Henry J. Lopez
Program Manager

REVISIONS				ADDITIONS			
PAGE	DATE	PAGE	DATE	PAGE	DATE	PAGE	DATE

FOREWORD

This Technical Data Report is submitted to the NASA Langley Research Center by the AiResearch Manufacturing Company, Los Angeles, California, a division of the Garrett Corporation. The document was prepared in compliance with Part VII, Paragraph A of NASA Contract No. NAS 1-6666, and Paragraph 6.3.3.2 of NASA Statement of Work L-4947-B.

Interim Technical Data Reports are generated on a quarterly basis for each major program task under the Hypersonic Research Engine Project. Upon completion of a given program task, a Final Technical Data Report will be submitted.

The document in hand presents a detailed technical discussion of Structures and Cooling Development for the period of 3 February through 3 May 1967.

CONTENTS

CONTENTS (Continued)

ILLUSTRATIONS

ILLUSTRATIONS (Continued)

ILLUSTRATIONS (Continued)

DRAWINGS ATTACHED TO SECTION 5

1.0 PROBLEM STATEMENT

The objective of the structures and cooling development program is to analyze, design, and fabricate the regeneratively cooled surfaces and their associated structures, and to verify the performance of these surfaces and structures at conditions which simulate the operating conditions expected in the flight test engine.

The Hypersonic Research Engine requires regenerative cooling on all surfaces that contact the engine airstream. The use of ablative coating on the engine aerodynamic surfaces is barred by the Statement of Work to minimize extraneous effects on engine performance. No such restriction is imposed on the engine cowl, therefore ablative protection is used for this component.

The characteristic design problem in regeneratively cooled structures for this type of application is associated with the large heat fluxes encountered over major portions of the engine surfaces. These heat fluxes range from values of approximately 10 Btu/sec-ft^2 to 1400 Btu/sec-ft^2 on the stagnation line of the support strut leading edge. The conservation of fuel requires that these heat fluxes be accommodated at temperature differences across the regeneratively cooled surfaces which range up to approximately 600°F in flat surfaces and 1000°F in leading edge areas. These temperature differences, in turn, result in strains which cause plastic deformation of the hot surfaces. Design is therefore controlled by low cycle fatigue. Uncertainties associated with the prediction of low cycle fatigue performance have led to heavy emphasis, in the experimental portion of the program, on the evaluation of the low cycle fatigue performance of the engine components.

The general objectives set for performance of the cooled structures are as follows:

> Design life - 10 hr of hot operation, of which 3 hr are to be taken at Mach 7 to 8 flight conditions
>
> Cycle life - 100 cycles, at conditions which produce the highest plastic strain

2.0 TOPICAL BACKGROUND

The cooled structures being investigated and fabricated as part of this task, together with their associated connecting structures, constitute the basic engine structure. The cooled surfaces also, and of necessity, form the aerodynamic engine surfaces.

2.1 GENERAL DESIGN GUIDELINES

Considerations which determine the design of the cooled structures are as described in the following paragraphs.

The regeneratively cooled surfaces must be compatible with engine performance requirements, i.e., they must be so designed as to minimize engine performance losses. In addition to providing the basic contours, the cooled surfaces must be fabricated and assembled in such a way as to avoid discontinuities; leading edges must use the minimum radius compatible with reliable structural design to minimize losses.

The research nature of the engine requires that temperatures and pressures be measured throughout the engine. Consequently, the engine structure must allow the use of static pressure taps and metal temperature thermocouples.

The total amount of fuel available to the engine and for cooling of the structure is severely limited by X-15 storage capabilities. Consequently, the cooling of the structure must minimize fuel usage in excess of combustion requirements. This gives incentive to operating at the maximum metal temperatures and temperature differences compatible with sound structural design.

The internal structures and plumbing of the engine must be volumetrically efficient to permit installation of fuel system components, engine controls, instrumentation transducers, and signal conditioning equipment. Also, for best reliability, the electronic equipment should be installed in areas of the engine which have the least severe environment.

To permit operation over the Mach number range from 3 to 8, it is necessary that the inlet spike be translated to various positions. To conserve coolant prior to and after engine operation, the inlet spike must be closed off against the outer body leading edge. Consequently, it is necessary to have an actuation system capable of the desired modulation and positioning accuracy, with control provided by the on-board computer.

Fuel pressurization in the engine is provided by a hydrogen turbopump. Pressure drops in the regeneratively cooled surfaces, manifolds, and associated plumbing must be compatible with the output of the turbopump.

In addition to control of temperatures and temperature differences, the integrity of the coolant structures requires that the flow routes within the engine be matched in such a way as to minimize temperature differences at axial stations for inner body and outer body surfaces. This will minimize distortion of the engine internal passages. Axial temperature discontinuities, as produced, for example, by the termination of two flow routes that differ greatly in temperature at the same station are objectionable because of the severe thermal strains that result.

Measurement of engine internal thrust during flight is required. Consequently, external loads (drag and lift) that are transmitted directly to the thrust measuring device must be minimized. Specifically, the engine cowl has drag loads which are of the same order of magnitude as the engine thrust. Mounting of the cowl in such a way as to minimize this external drag load, and thus the uncertainties in calculation of thrust, is therefore required.

A basic requirement in engine design is that malfunction of the engine not endanger safety of the aircraft or life of the pilot. Therefore, provision must be made to jettison the engine. Since hydrogen leakage to the engine cavities must be assumed possible, the inner body engine cavity must either be inerted or be capable of containing an explosion that results from the mixing of hot hydrogen and air. Venting of the engine cavity to near nozzle base pressure and provision for explosion containment is the approach selected for this program. During ground checkout, the engine cavity is inerted with nitrogen.

The cooled structures, inlet spike actuation system, internal supporting structures, and plumbing constitute the major portion of the total engine weight. Although optimization of the structures and structural components for minimum weight is not an objective, the specified weight limitation requires careful use of structural weight.

The instrumentation, controls, and fuel subsystems contained in the engine cavity require servicing prior to and after each test. Consequently, the mechanical assembly of the engine cooled structure components must provide access to and replacement of components of the subsystems in field and within reasonable time, as specified in the Statement of Work.

2.2 OPERATIONAL BOUNDARIES

The flight envelope and maximum operating conditions that the engine will experience have been derived from the conditions of the Statement of Work.

2.2.1 General Design Ground Rules

The maximum dynamic pressure specified for the current phase of the program is 2000 psf. This compares with a specified dynamic pressure of 2500 psf that was used during Phase I of the program. Consequently, the minimum altitude at

Mach 8 during which cooling must be provided is 85,000 ft, compared to a minimum altitude of 81,000 ft used during Phase I. The minimum design altitude for the current program is 88,000 ft. The increased altitude results in a reduction of heat flux throughout the engine, which is locally offset in part by an increase in contraction ratio of the engine from 10 to 14.6. The contraction ratio of 10 was used during Phase I. In summary, the operating envelope for the engine is as follows:

<u>Engine Structural Design</u> - With engine either lit or not lit, 2000q dynamic pressure.

<u>Engine Cooling Design</u>

Normal design, engine lit: 1750q, 88,000 ft minimum.

Emergency design, engine lit: 2000q, 85,000 ft minimum.

For the emergency design, engine lit conditions, all of the pump output pressure is available for coolant pressure drop (700 psia). Dump valve opens and fuel injection valves close as aircraft approaches these conditions from the normal operating line.

2.2.2 Engine Operating Cycles

A preliminary and qualitative definition of engine operating cycles is given below. Its purpose is to provide a basis for heat transfer transient analysis, structural evaluation of the effect of transient temperature differences, general control requirements, establishing typical environmental conditions, and for defining acceptable operating cycles. The types of missions or conditions which the engine must survive are summarized in the following cases:

<u>Case I</u> - Constant M, with aircraft power on, at constant, high q

<u>Case II</u> - Constant M, with aircraft power off, aircraft diving

<u>Case III</u> - Variable M, expected to involve a change in M of 0.5 during 20-sec engine operating cycle

<u>Case IV</u> - Subsonic-supersonic combustion transition at M = 6

<u>Case V</u> - Inlet unstart, with shock expelled

Figure 2.1-1 is a qualitative representation of critical cases. The most important variations among missions occur during the combustion phase and will be treated separately. The common features, typical for all missions, are numbered on the figure and are as follows:

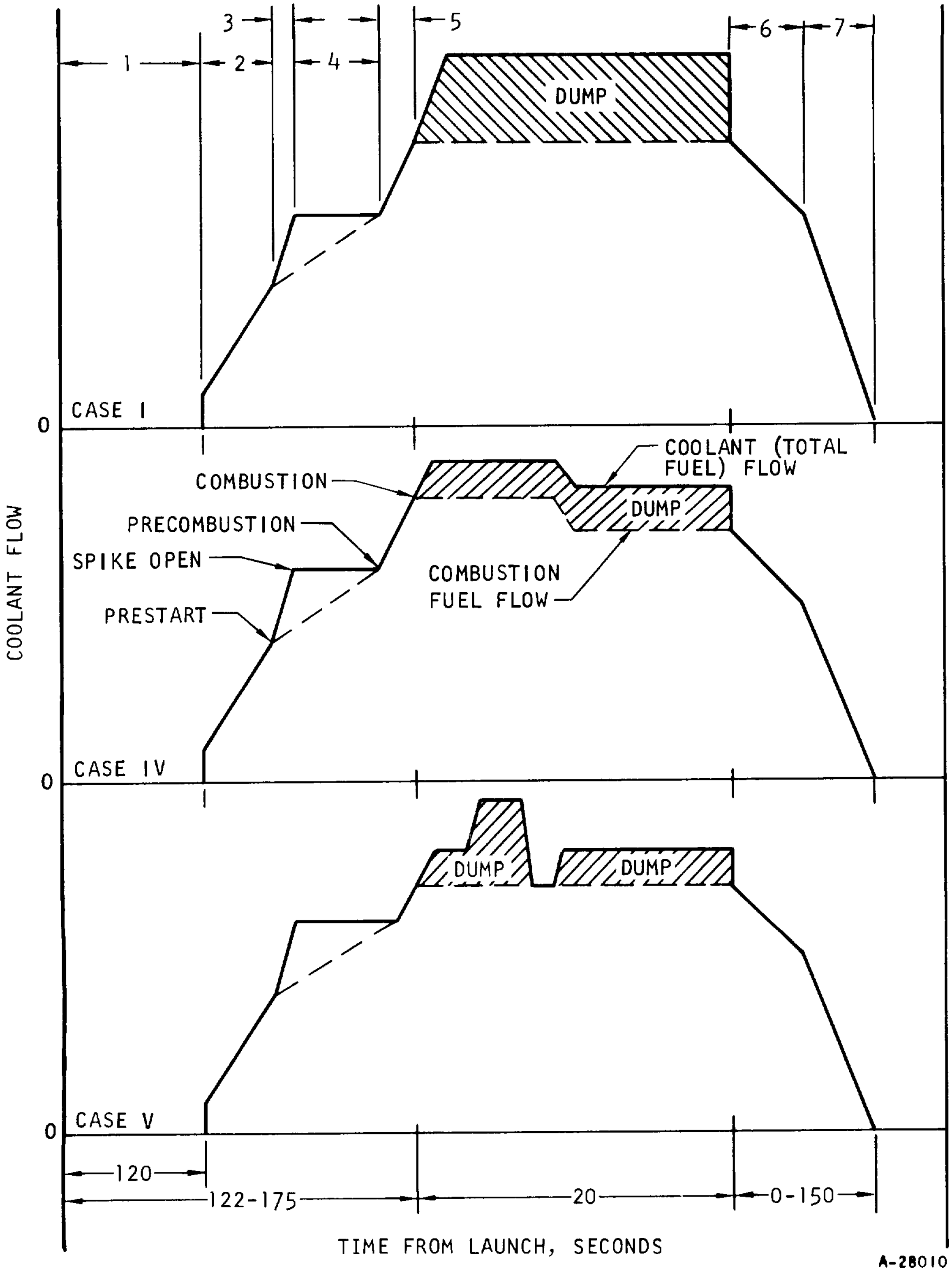

Figure 2.1-1. Typical Engine Operating Cycles

1. Launch to M=3+, during which the engine structure is assumed to go from soak at -65°F to soak at 1140°F. No cooling is required. At the end of this period, the helium purge is performed and coolant flow started through all portions of the cooled structure.

2. Approach to test M, inlet closed (leakage flow only), during which coolant flow is increased to maintain maximum structure temperature (cold surface) at 1140°F.

3. Time for retraction of inlet spike to desired position. The solid line assumes programmed cooling flow, the dashed line, controlled cooling flow based on temperature sensing. The approach selected will be a function of control system response and actuating system response. Controlled cooling is preferred.

4. Inlet spike in starting position, full airflow through the engine, no combustion.

5. Programmed increase in cooling flow to starting combustion equivalence ratio (ER). This ER will be less than the test ER. ER will ramp to test ER (not shown).

6. Combustion terminated and inlet spike being extended to closed position.

7. Inlet closed (leakage flow only), deceleration to M=4+, with coolant flow decreased to maintain maximum structure temperature at 1140°F. Helium purge.

As combustion starts, cooling ER must be controlled to accommodate increasing heat fluxes. The following considers each of the missions:

<u>Case I</u> - Shown in Figure 2.1-1. Cooling ER is in excess of combustion ER. Combustion ER will ramp at beginning and end of test. Ramps of 5-sec duration to and from ER=1 may be assumed at beginning and end of test.

<u>Case II</u> - Not shown. Represents a gradual change in conditions shown for Case I and will involve less severe transients. Not considered a design point.

<u>Case III</u> - Same comments as Case II.

<u>Case IV</u> - Shown in Figure 2.1-1. Involves a near-step change in gas-side engine conditions during test run.

<u>Case V</u> - Shown in Figure 2.1-1. The general rise in pressure would be expected to cause a step-change type increase in heat flux. Spike will extend and close, then retract to operating position for second attempt at starting. At this point, either normal operation or a second unstart is possible.

3.0 OVERALL APPROACH

The diverse requirements imposed on the cooled structures require iteration of the cooled structural design with the engine aerodynamic design; the instrumentation, control, and fuel subsystems designs; and with the airplane interface design. Internal constraints on cooled structural design are imposed by the close coordination required in thermal design, structural design, mechanical design, and manufacturing. It is generally not possible to treat any one of these areas independently of the others. During Phase I of the program, the basic design concepts for the engine were defined and are basically feasible in terms of the constraints imposed on the design. These concepts and the design data generated during Phase I are being used as the starting point for design of the Phase IIA cooled structures. Component layout drawings of acceptable mechanical design and with acceptable manufacturing features form the initial step in the iteration. These layout drawings have been evaluated to establish the required thermal and structural design features. Based on these inputs, layout drawings are revised to incorporate the required features, followed by substantiation of the thermal and structural performance of the revised design.

Although the Phase I design is being used as the starting point of Phase IIA cooled structure design, each of the components is being reviewed with the objective of simplification in terms of mechanical design and manufacturing features. The interfaces between two or more components, in particular, will be re-evaluated. The interfaces include engine-to-airplane mounting, outer shell-to-inner body mounting by means of the support struts, nozzle-to-inner shell assembly, inlet spike-to-inner body assembly, inlet spike actuator-to-inlet spike and inner body mounting, leading edge-to-outer shell mounting, and cowl-to-outer shell support.

The general approach to cooled structures development places heavy emphasis on fabrication and testing of the full-scale components. A limited number of types of cooled structural elements and models are being fabricated and tested to evaluate the problems which are basic to the overall engine design, or which are sufficiently localized in nature to permit use of subscale evaluation. All significant manufacturing development and evaluation is being accomplished using the full-scale components. The nature of the required manufacturing operations for the components is such that use of subscale components would be expected to lead to only limited information on the adequacy of manufacturing techniques and processes.

3.1 THERMAL DESIGN

The overall approach to thermal design is use of analysis based on previous experimental verification of analysis in similar but not identical geometries and heat transfer situations. These experimental-based analyses will, in turn, be verified by experiments where the geometry or fluid conditions, or both, will be like those existing for the flight engine. This approach is a direct continuation of that used in preliminary thermal design activities reported in References 7 through 14, and especially in References 7, 11, 12, and 15.

The discrepancy between calculated and experimental heat flux described in Reference 12 is large. Steps are being taken to improve the analytical techniques so that the correlation between calculation and experimental results can be improved. The initial results of this effort are described in Paragraph 4.1.3.

The basic goals of all thermal analysis and design are (1) the limitation of temperature and temperature differences to structurally acceptable values while keeping hydrogen flow, required for cooling, equal to or less than hydrogen flow required for fuel, and (2) at the same time maintaining hydrogen pressure drop compatible with cooling jacket pressure containment and pump outlet pressure capabilities. The limiting values for these parameters, previously used during Phase I, and still being used at present, are (1) a maximum gas side metal temperature of 1700°F (2160°R), (2) a maximum primary structure temperature of 1200°F (1660°R), (3) a hydrogen pump outlet pressure of 700 psia, and (4) a fuel control valve (fuel plenum) pressure of 400 psi. An arbitrary reduction in gas side metal temperature of 100°R to a maximum of 1600°F (2060°R) is used to accommodate coolant control response and aerothermodynamic fluctuations about the mean. The 300 psi cooled structures pressure drop implied above is divided, approximately 100 psi for cooling jacket finned passages and 200 psi for all manifolding and interconnecting ducting.

The design procedure involves separate calculation of aerodynamic heating and cooling jacket performance. The aerodynamic heating conditions are calculated (as during Phase I) primarily by use of the computer program H1940 (Reference 15). Special conditions, such as, shock wave-boundary layer interaction are computed by slide rule with the method outlined in Paragraph 4.1.3. Cooling jacket fin performance is calculated (as in Phase I) by use of computer program H1930 (Reference 16). Special conditions, such as, for inlets, outlets, and bolted flange/manifolds require slide rule calculation of pressure and flow distributions. Verification of aerodynamic and cooling jacket heat transfer and pressure drop calculations will be accomplished by separate techniques. Specifically, aerodynamic heat transfer calculations will be and have been verified by tests of engine component models such as the combustor and with the boiler plate engine, yet to be tested. Calculated performance of cooled structures will be verified by full-scale component and some subscale component testing at heat flux levels and distributions nearly equal to those calculated for the flight engine components. The primary areas requiring verification in the cooled structures performance are flow distribution and associated temperature distribution and its effects on structural performance in terms of life and contour.

3.2 STRUCTURAL DESIGN

The structural design approach utilizes a combination of analytical and experimental methods. Experimental verification of detailed parts is employed wherever necessary, such as, short term burst, creep rupture, and thermal fatigue tests on sandwich plate-fin elements. Generally, the structural tests will be performed on composite structural elements, such as, the inlet spike and the inner body assembly.

The bulk of the HRE is composed of ring-stiffened orthotropic shell structures of variable thicknesses and contours. The ring stiffeners are also used for coolant flow manifolding and fuel injection rings for the engine combustor section. The structural loadings will produce axisymmetric and asymmetric forces and moments due to static normal pressures, acceleration, vibrational inputs, and aerodynamic flutter and buffeting effects.

Fully operational computer solutions are available to analyze axisymmetric isotropic thin shells of variable thicknesses and contours for stresses due to axisymmetric loads and temperature profiles. In addition, the isotropic shell analysis had been extended to treat orthotropic cylindrical shells with axisymmetric loads. Two MIT finite difference nodal circle solutions (SABOR III and DASHER I), which have been adapted for use on the AiResearch computer system (IBM-360/50), are available for use.

The SABOR III program is applicable for axisymmetric isotropic shells (local departures from ideal isotropy can be treated) that may be subjected to nonsymmetrical static forces. The SABOR III program may also be used to obtain the stiffness and mass matrixes for direct input into the DASHER I program to obtain dynamic response.

It would have required an extensive programming effort to modify the SABOR III and DASHER I programs to accurately treat many of the problems that will be encountered in the HRE. Rather than attempt this approach, a further survey of existing shell programs was carried out, and it was determined that an extremely applicable program had been developed under the auspices of the Analysis Group of the Theoretical Mechanics Branch, Structures Division of the Wright Patterson Air Force Base, Dayton, Ohio. This program is based upon the very recent improvements in matrix shell solutions generated by A. Kalnins (Department of Mechanics, Lehigh University). It solves the general axisymmetric orthotropic thin shell problem for symmetric and nonsymmetric loads due to static as well as dynamic inputs. The program is presently being adapted for use on the AiResearch computer system. Although the program has been debugged, the final report describing the useability, limitations, and methods of data input has not been completed, and will not be released by the Wright Patterson Air Force Base for at least twelve months. Until a program of this magnitude has been completely checked out by trying numerous test cases, a note of caution must be exercised regarding its capabilities. Another important point is the fact that the problem inputs and the data reduction of the outputs require considerable effort on the part of the user. The existence of the program also does not eliminate or substantially reduce the work needed to generate a sound design; however, it is the objective of careful analysis to discover design inadequacies that would otherwise not be recognized.

The eventual objective of the test program is to verify the actual performance capabilities of the structures as fabricated. Although it will not be possible to analytically predict the influence of realistic fabrication restrictions and limitations on the end product, the initial analysis will identify the serious design problem areas. Results of the test program will be used to assess the extent of the changes required to achieve the structural integrity goals.

3.3 MECHANICAL DESIGN

The guidelines used in mechanical design of the cooled structures components and assembly of the components into the engine require the use of known materials and joining techniques. Standard fasteners and seals are used to the greatest extent possible. Design for brazing is aimed at minimizing the total number of braze cycles to which a given part must be subjected. In some cases, this is done by redesigning the parts to allow use of prebrazed subassemblies, substitution of machined or welded subassemblies, or substitution of bolted interfaces for brazed or welded interfaces. Also, as a general rule, all welding into or close to braze joints is being avoided, although in certain cases, such a procedure may be acceptable.

The mechanical design effort will be supported by experimental verification in selected areas. In particular, selected configurations that present analytical problems and raise questions as to manufacturing feasibility will be fabricated and tested on a subscale basis. The purpose of such tests will be to provide design data and guidance for possible design revision. Currently planned tests, which are in support of mechanical design, rather than thermal or structural design, include the following:

Test specimen to evaluate feasibility of bolting the nozzle flange manifold to the inner shell through the removable nozzle cap.

Fabrication of a section of the inlet spike near the spike tip to help resolve questions regarding the best manufacturing approach and hence the best design for this portion of the inlet spike.

Fabrication of the spike-to-inner body seal to evaluate the adequacy of the design solution.

Fabrication of a straight section of the bolted nozzle manifold to verify both the manufacturing aspects and structural integrity of the design solution.

Fabrication and evaluation of the various mechanical seals used in the components to verify the adequacy of the design solution.

Fabrication of flat panels using the various instrumentation and fuel injector fittings that penetrate the regeneratively cooled surfaces to verify manufacturing feasibility and structural integrity of the design. Tests results will be used to select the final configuration used in the engine.

3.4 MANUFACTURING

The manufacturing approach being used on this program has two aspects: (1) that dealing with the approach to development of manufacturing techniques and processes, and (2) that dealing with the specific manufacturing processes planned for use.

3.4.1 Development Approach

The development of the manufacturing techniques and processes will rely primarily on full-scale components. Except where isolated problems or basic data must be obtained, the use of subscale components represents a duplication of development effort. The compound forming of the shell-face sheets in half-scale, for example, results in working with radii of curvature which are half those encountered in the full-scale part. Use of lighter gauge material to facilitate forming, on the other hand, is impractical. In addition, the size of the full-scale tooling, the machines required to use this tooling, and the unique problems associated with the forming of large thin wall shells cannot be duplicated in half-scale. As a result, a half-scale compound-curved model of the isentropic surface of the inlet spike is the only subscale component on which fabrication development work is being done. This part is being used to establish forming characteristics, evaluate electro-hydraulic forming parameters, and investigate brazing problems.

3.4.2 Fabrication Approach

The most critical area of cooled structures fabrication is in the cooled surface shell face sheets. The starting point for these shells can either be rolled and welded cone sections or flat sheets. The rolled and welded cones are bulge formed, then final sized, using electrohydraulic forming. Using flat sheets as a starting point, the shells must be deep drawn in about three stages. Final sizing of the shells occurs as for the welded cones. Of the two approaches, the one using the seam welded cone has been selected. The weld seam is not considered structurally objectionable and the approach involves fewer steps than are required for deep drawing.

To ensure adequate braze fitup, forming accuracy for the shells must be high. Specifically, it is expected that the clearance between shells must be maintained within a tolerance of approximately ±0.001 in. Given this accuracy, the brazing of the fins between the face shape still requires special attention. To ensure sound braze joints, pressure must be exerted on the shells in such a way as to provide a crushing load on the fins. The methods available for providing this braze fixturing load include the following, as a function of the component being brazed:

Graphite fixtures, with an external piece containing the assembly and an internal piece using expanding segments to exert pressure.

Steel bags placed inside the shell and pressurized to a level sufficient to deform the shell with which the bag is in contact. Containment on the external face sheet may or may not be required with this approach.

Evacuation and backfilling of the space between the two shell face sheets, using atmospheric pressure to provide the load.

Integrity of the shell joining will be experimentally evaluated and adjustments in shell forming tools and brazing procedures and fixtures made to correct problems that appear.

3.4.3 Nondestructive Testing

The critical area in fabrication of the full-scale components involves the shells themselves, as discussed in the two previous paragraphs. For structural integrity of the shells, only very limited areas of unbrazed joint areas are tolerable. These joints are detectable by proof pressure testing at sufficiently high pressure levels. Only in exceptional cases, however, will a defect that is revealed by proof pressure test be repairable. In general, a nondestructive test capable of revealing braze voids is preferable and offers better opportunity for subsequent repair. The two techniques available are radiographic inspection of the entire shell surface and the use of temperature-sensitive paint on one of the face sheets with a heating transient imposed on the other face sheet. These methods will show a braze void; that is, an unbonded joint. Weak joints are not discernable as such. In general, however, the existence of a brazed joint is reasonable assurance that adequate joint strength can be achieved. Verification of the result of radiographic or thermal inspection of the shells will be done by proof pressure testing.

The repair techniques available for unbonded joints in the shells would generally be the following:

Recycling of the complete shell to a slightly higher temperature than used during the first braze cycle. In this way, remelt and flow of the braze alloy is obtained with the objective of filling the void. Orientation of the shell in the brazing furnace can be used to assist the process.

Removal of a portion of the face sheet in the unbrazed area, addition of filler alloy and closeout using a patch, with the entire shell recycled in the brazing furnace. The applicability of this repair procedure will be a function of the location of the affected shell area in the engine gas stream.

4.0 ANALYTICAL DESIGN

4.1 OVERALL DESIGN REVIEW

4.1.1 Shell Design

The Phase I overall design was reviewed to define material thickness of the Hastelloy X material used in the shell designs. The effort was limited to the review of Phase I pressure-load design calculations. The following summary describes the findings (Station numbers are referenced to Drawing 950007):

Spike Fore Body (Station 1.2 to Station 36)--Design calculations for both the structural and thermal skins were based on 0.015-in. material thickness. Combined bending and axial stresses were found to be well within allowable limits and the critical elastic buckling pressure is much higher than the actual pressure.

Spike Aft Body (Station 36 to Station 56)--The thickness of the outer skin is 0.015-in., while the inner face is 0.060 in. thick. It was assumed that only the inner skin will resist external pressure loads and the outer skin will resist thermal loads. Since a safety factor of 1.72 (elastic buckling, ultimate) was calculated in this area, there may be difficulties if pressures will go higher than used in the analysis. In that event, the addition of another stiffener ring near Station 46 can be considered as an alternative to an increase of skin thickness.

Inner Body (Station 56 to Station 86.2)--The inner shell between the struts (Station 56 to 65) carries lower pressure and temperature loads than the area forward of the struts. Thus, the 0.015-in. outer and 0.060-in. inner surface configuration already investigated for these higher loads will be satisfactory here too. Between Station 65.5 and Station 71.5, both inside and outside surfaces will be 0.015-in. thick. If the assumption of neglecting the outer (thermal) skin to resist pressure loads is maintained, the critical buckling pressure exceeds the actual pressure. Using both surfaces to resist pressure loads will, however, give a safety factor of 7.1 against buckling without considering thermal stresses. Based on the fact that the average metal temperature of the outer surface is approximately 500°F and the inside (structural) wall is at 100°F, the assumption of using both surfaces to resist pressure loads is justifiable. The fin height aft of Station 71.5 is doubled; thus, the effective stiffness and strength of the two walls are increased in an area where both pressure and temperature values decrease. This fact, coupled with the decrease of shell radius, results in increasing buckling strength in this area.

Outer Body Leading Edge (Station 36 to Station 43)--The 0.015-in. outside (thermal) wall and the 0.060-in. inside (structural) wall of the inside face were investigated on the assumption that only the structural wall resists pressure loads and the combination is satisfactory from the view of pressure loads alone. Pressure on the outside face of the cowl is 15 psi maximum and is not critical. Since the scheme of cooling in this area is still a subject of modifications and since the stresses due to temperature distribution are high, further detailed investigation of this critical area will be performed.

Outer Shell (Station 43 to Station 76)--Hoop stresses in the 0.060-in. thick inner wall are one-fourth of the ultimate tensile strength. The 0.015-in. internal (thermal) wall will carry some tensile stresses resulting from pressure, and these stresses will be subtracted from the thermal stresses. This fact, which should be beneficial, was neglected during the Phase I cowl thermal stress analysis, when 1630 cycles to failure were calculated.

Ablatively-Cooled Cowl--Pressure loads on the outside surface of the ablatively-coated cowl will be small, and it should not govern the determination of the metal thickness. This outside surface will require ring stiffening to prevent supersonic panel flutter.

These results are summarized in Table 4.1-1.

4.1.2 Fin Design

A preliminary survey of fin designs for the HRE cooling system was performed. The purpose of the analysis was to (1) determine adequate fin geometries for design operating conditions, and (2) estimate short-time burst and 10-hr rupture pressures of uniform-temperature test specimens. Table 4.1-2 presents a summary of the results of this calculation, which use fin data reported in AiResearch Phase I Report AP-66-0168-2. The table includes a tabulation of the margins of safety for the various fin geometries at design temperature with a 700-psi internal pressure. A safety factor of 1.5 on the short-time yield strength or the 10-hr rupture life of Hastelloy X, whichever is less, is used. A comments column is provided which indicates a satisfactory minimum weight fin with the associated margin of safety.

The fin calculated stress is based on the combined loads due to an internal pressure of 700 psi and differential radial thermal expansion of the shells. The following equations apply:

a. Internal pressure--

$$\sigma_{fin} = P_{int} (b_{fin} - t_{fin})/(f\ t_{fin})$$

where P_{int} = internal pressure

b_{fin} = fin spacing (reciprocal of fins/in.)

TABLE 4.1-1

SHELL DESIGN SUMMARY

Location	Wall Thickness, in.		F.O.S.$_{ultimate}$		Remarks
	Outer	Inner	Buckling	$\sigma_{H\ or\ B}$*	
Spike Fore Body Sta. 1.2-36	0.015	0.015	51.5	16.2	
Spike Aft Body Sta. 36-56	0.015	0.060	1.72	4.37	
Inner Body Sta. 56-86.2	0.015	0.060	2.64	--	To Sta. 65.5±
	0.015	0.015	7.1	--	Between Sta. 65.5 and 71.5
Outer Body Leading Edge Sta. 36-43	0.015	0.060	--	4.58	Inside face
	0.015	0.015	--	--	Outside face
Outer Shell Sta. 43-76	0.015	0.060	--	3.78	Inside
	--	0.060	--	--	Outside, ablative coated

*σ_H = hoop stress

σ_B = bending stress

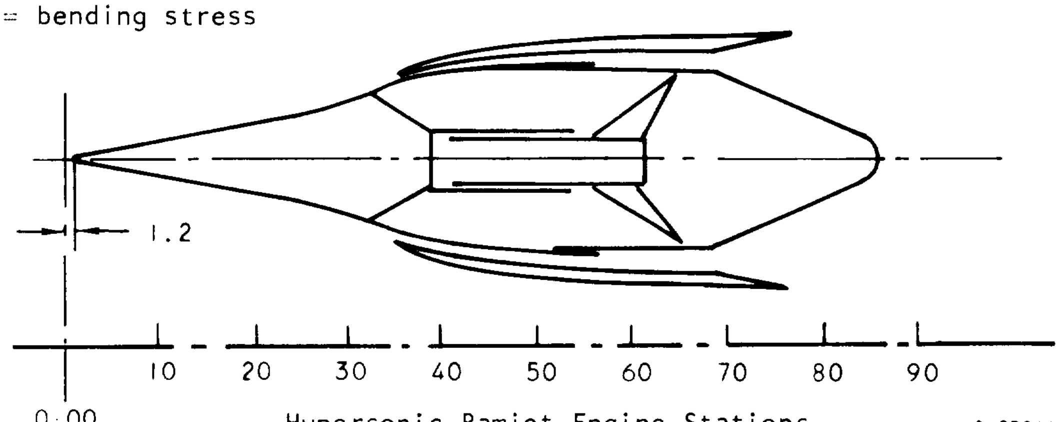

TABLE 4.1-2

FIN DESIGN SUMMARY

Location	Reference Page of AP66-0168-2	Fin Geometry	Max Fin Temp, °F	Estimated Pressure, psi		Lowest Margin of Safety	Comments
				Short-Time Burst	10-hr Rupture		
Spike Fore Body	198	16R-.153-.006	210	3900	NA	0.41	M.S. = 0.17 for 16R-.153-.005
Spike Aft Body	200	20R-.050-.006	1420	3100	1300	0.12	
Nozzle	201	16R-.153-.006	180	4150	NA	0.40	M.S. = 0.17 for 16R-.153-.005
Nozzle	204	20R-.050-.006	1500	2850	950	-0.23	M.S. = 0.02 for 20R-.050-.008
Strut side	207	16R-.025-.006	930	3400	NA	0.42	M.S. = 0.19 for 16R-.025-.005
Strut Lead-ing Edge	210	16R-.012-.006	1180	3000	2250	0.37	M.S. = 0.14 for 16R-.012-.005
Inside cowl	211	40R-.025-.003	1370	3200	1550	0.87	M.S. = 0.25 for 30R-.025-.003
Outer Body Leading Edge	214	20R-.050-.006	1470	2950	1050	-0.12	M.S. = 0.02 for 20R-.050-.007
Outer Shell	212	40R-.025-.003	1340	3300	1700	0.35	
Outer Shell	215	40R-.035-.003	1400	3150	1350	0.08	
Outer Shell	216	20R-.050-.006	1420	3100	1300	0.04	

Notes:
1. Estimated pressure for failure is based on fin pressure stress only.
2. Lowest safety margin (M.S.) is based on a 1.5 safety factor on combined fin thermal and pressure stresses.
3. NA = not applicable.
4. Fin geometry units: For numbers such as 16R-.153-.006, the units are fins/in.; height, in.; and thickness, in.

t_{fin} = fin thickness

f = fin strength efficiency factor

b. Differential thermal expansion--

$$\sigma_{fin} = P_{\alpha} b_{fin}/(f\ t_{fin})$$

where P_{α} = equivalent fin pressure required to restrain the hotter shell

The fin efficiency factor is defined as the ratio of actual burst pressures to burst pressures as calculated from ultimate stress properties. The apparent reduction in strength is attributable to nonuniform load distribution across the fins due to differences in height, misaligned fins, and stress concentrations at the braze joint. This strength reduction factor is based upon performance of successfully brazed heat exchangers, i.e., the failure mode at burst is tensile rupture of the fins. Fin strength efficiency factors have been found to range from 0.25 to 0.50 for Type 347 stainless steel fins brazed with Nicrobraz. The median value of 0.33 was used in this calculation in lieu of applicable test data for Hastelloy X fins at the time of this analysis.

Material allowable stresses are based on the lesser of the 10-hr stress rupture life or the short-time yield stress divided by a safety factor of 1.5. The margin of safety of the fins is determined from

$$M.S. = \sigma_{all}/\sigma_{calc} - 1$$

where σ_{all} = allowable stress at temperature

σ_{calc} = calculated stress level at 700 psi

The estimated pressures for short-time burst and 10-hr rupture are obtained by equating the fin tensile stress due to internal pressure and the published material strength. Actual pressure tests of fins will then provide an experimental check on the fin strength efficiency factor used in the calculations.

4.1.3 Aerodynamic Heating Analysis

Continued use of Computer Program H1940 (Reference 15) for aerodynamic hot-gas conditions has led to generation of Table 4.1-3 for the Mach-8, 81,000-ft altitude conditions. The differences between these data and data previously calculated (Reference 1) are (1) enthalpy was used rather than an approximation to enthalpy based on specific heat, and (2) a hot-gas total temperature of 5840°R was used downstream from Station 51 instead of the 5450°R temperature previously used in Phase I. The headings for the various columns are somewhat modified from those previously used and are now more self-explanatory. The

TABLE 4.1-3 AERODYNAMIC HEATING CONDITIONS

MACH NUMBER= 8.0000 ALTITUDE= 81000.0FT.

X = 1.187 SPIKE BLUNT TIP L.E.

X = 39.2 COWL L.E.

X (IN.)	SIN (IN.)	SOUT (IN.)	PSTAT (PSIA)	VEL (FPS)	TTOT (DEG R)	TSTAT (DEG R)	TWALL (DEG R)	TRECOV (DEG R)	TOTAL H INNER (BTU/ SEC.R FT SQ)	TOTAL H OUTER (BTU/ SEC.R FT SQ)	TOTAL FLUX INNER (BTU/ SEC FT SQ)	TOTAL FLUX OUTER (BTU/ SEC FT SQ)	RADIANT FLUX (BTU/ SEC FT SQ)	TOTAL HEAT INNER (BTU/ SEC)	TOTAL HEAT OUTER (BTU/ SEC)	TOTAL HEAT (BTU/ SEC)
1.00	1.02	0.0	26.1	6000.	4650.	4650.	260.	4650.	0.042	0.0	186.	0.	0.0	1.46	0.	1.
2.00	2.03	0.0	2.5	6032.	4650.	2459.	270.	4324.	0.012	0.0	49.	0.	0.0	2.22	0.	2.
3.00	3.05	0.0	2.5	6086.	4650.	2392.	279.	4312.	0.010	0.0	40.	0.	0.0	3.15	0.	3.
4.00	4.06	0.0	2.4	6140.	4650.	2325.	289.	4410.	0.022	0.0	90.	0.	0.0	5.97	0.	6.
5.00	5.08	0.0	2.4	6194.	4650.	2258.	299.	4401.	0.021	0.0	87.	0.	0.0	9.36	0.	9.
6.00	6.09	0.0	2.4	6247.	4650.	2191.	309.	4392.	0.021	0.0	84.	0.	0.0	13.29	0.	13.
7.00	7.11	0.0	2.4	6301.	4650.	2124.	318.	4382.	0.020	0.0	82.	0.	0.0	17.74	0.	18.
8.00	8.12	0.0	2.4	6355.	4650.	2057.	328.	4373.	0.020	0.0	80.	0.	0.0	22.72	0.	23.
9.00	9.14	0.0	2.3	6408.	4650.	1989.	338.	4364.	0.019	0.0	78.	0.	0.0	28.20	0.	28.
10.00	10.15	0.0	2.3	6462.	4650.	1922.	348.	4354.	0.019	0.0	77.	0.	0.0	34.18	0.	34.
11.00	11.17	0.0	2.3	6516.	4650.	1855.	357.	4344.	0.019	0.0	75.	0.	0.0	40.66	0.	41.
12.00	12.19	0.0	2.3	6570.	4650.	1788.	367.	4334.	0.019	0.0	74.	0.	0.0	47.62	0.	48.
13.00	13.20	0.0	2.2	6623.	4650.	1721.	377.	4325.	0.019	0.0	73.	0.	0.0	55.05	0.	55.
14.00	14.22	0.0	2.2	6677.	4650.	1654.	387.	4314.	0.018	0.0	72.	0.	0.0	62.97	0.	63.
15.00	15.23	0.0	2.2	6731.	4650.	1586.	396.	4304.	0.018	0.0	72.	0.	0.0	71.35	0.	71.
16.00	16.25	0.0	2.2	6785.	4650.	1519.	406.	4294.	0.018	0.0	71.	0.	0.0	80.20	0.	80.
17.00	17.26	0.0	2.2	6838.	4650.	1452.	416.	4284.	0.018	0.0	70.	0.	0.0	89.50	0.	90.
18.00	18.28	0.0	2.1	6892.	4650.	1385.	426.	4273.	0.018	0.0	69.	0.	0.0	99.27	0.	99.
19.00	19.29	0.0	2.1	6946.	4650.	1318.	435.	4262.	0.018	0.0	69.	0.	0.0	109.49	0.	109.
20.00	20.31	0.0	2.1	6999.	4650.	1251.	445.	4252.	0.018	0.0	68.	0.	0.0	120.16	0.	120.
21.00	21.32	0.0	2.1	7053.	4650.	1184.	455.	4241.	0.018	0.0	68.	0.	0.0	131.27	0.	131.
22.00	22.34	0.0	2.0	7107.	4650.	1116.	465.	4230.	0.018	0.0	67.	0.	0.0	142.83	0.	143.
23.00	23.35	0.0	2.0	7161.	4650.	1049.	474.	4218.	0.018	0.0	67.	0.	0.0	154.83	0.	155.
24.00	24.37	0.0	2.0	7205.	4650.	1000.	484.	4210.	0.018	0.0	67.	0.	0.0	167.49	0.	167.
25.00	25.39	0.0	2.2	7222.	4650.	1000.	494.	4210.	0.019	0.0	71.	0.	0.0	181.43	0.	181.
26.00	26.40	0.0	2.4	7239.	4650.	1000.	504.	4210.	0.020	0.0	75.	0.	0.0	196.68	0.	197.
27.00	27.42	0.0	2.5	7255.	4650.	998.	513.	4210.	0.021	0.0	77.	0.	0.0	212.99	0.	213.
28.00	28.44	0.0	2.5	7270.	4650.	992.	523.	4209.	0.021	0.0	76.	0.	0.0	229.89	0.	230.
29.00	29.46	0.0	2.5	7285.	4650.	986.	533.	4208.	0.021	0.0	75.	0.	0.0	247.37	0.	247.
30.00	30.48	0.0	2.5	7300.	4650.	980.	543.	4208.	0.020	0.0	75.	0.	0.0	265.43	0.	265.
31.00	31.50	0.0	2.6	7307.	4650.	974.	552.	4207.	0.021	0.0	76.	0.	0.0	284.75	0.	285.
32.00	32.54	0.0	2.7	7314.	4650.	969.	562.	4206.	0.021	0.0	77.	0.	0.0	305.37	0.	305.
33.00	33.57	0.0	2.8	7321.	4650.	963.	572.	4206.	0.022	0.0	78.	0.	0.0	327.32	0.	327.
34.00	34.62	0.0	2.8	7325.	4650.	960.	582.	4205.	0.022	0.0	79.	0.	0.0	350.64	0.	351.
35.00	35.67	0.0	2.9	7325.	4650.	960.	591.	4205.	0.022	0.0	79.	0.	0.0	375.37	0.	375.
36.00	36.74	0.0	2.9	7325.	4650.	960.	601.	4205.	0.022	0.0	79.	0.	0.0	401.55	0.	402.
37.00	37.81	0.0	2.9	7343.	4650.	960.	611.	4205.	0.022	0.0	79.	0.	0.0	429.20	0.	429.
38.00	38.89	0.0	3.0	7369.	4650.	960.	621.	4205.	0.022	0.0	79.	0.	0.0	458.33	0.	458.
39.00	39.96	0.0	3.0	7395.	4650.	960.	630.	4205.	0.022	0.0	79.	0.	0.0	488.94	0.	489.
40.00	41.04	0.81	3.7	7417.	4650.	957.	640.	4205.	0.023	0.050	81.	178.	0.0	521.72	73.	595.
41.00	42.06	1.82	4.9	7425.	4650.	904.	650.	4199.	0.029	0.054	102.	191.	0.0	562.36	151.	714.
42.00	43.07	2.83	5.2	7322.	4650.	826.	744.	4193.	0.029	0.051	102.	175.	0.0	603.23	224.	827.
43.00	44.08	3.83	5.9	7194.	4650.	828.	838.	4195.	0.031	0.051	104.	170.	0.0	645.43	295.	940.
44.00	45.08	4.84	9.7	7013.	4650.	1118.	932.	4241.	0.057	0.089	189.	296.	0.0	722.75	420.	1142.
45.00	46.09	5.84	13.6	6832.	4650.	1408.	1026.	4285.	0.068	0.103	223.	337.	0.00	814.65	563.	1378.

TABLE 4.1-3 (Continued)

	X (IN.)	SIN (IN.)	SOUT (IN.)	PSTAT (PSIA)	VEL (FPS)	TTOT (DEG R)	TSTAT (DEG R)	TWALL (DEG R)	TRECOV (DEG R)	TOTAL H INNER (BTU/ SEC.R FT SQ)	TOTAL H OUTER (BTU/ SEC.R FT SQ)	TOTAL FLUX INNER (BTU/ SEC FT SQ)	TOTAL FLUX OUTER (BTU/ SEC FT SQ)	RADIANT FLUX (BTU/ SEC FT SQ)	TOTAL HEAT INNER (BTU/ SEC)	TOTAL HEAT OUTER (BTU/ SEC)	TOTAL HEAT (BTU/ SEC)
	46.00	47.09	6.84	17.4	6651.	4650.	1698.	1120.	4327.	0.077	0.113	246.	362.	0.00	916.95	718.	1635.
	47.00	48.10	7.85	21.2	6470.	4650.	1988.	1214.	4367.	0.083	0.119	261.	375.	0.00	1026.51	881.	1907.
	48.00	49.10	8.85	25.1	6288.	4650.	2278.	1308.	4405.	0.087	0.123	270.	380.	0.06	1140.86	1047.	2188.
	49.00	50.10	9.86	31.7	6072.	4811.	2622.	1402.	4595.	0.093	0.129	298.	412.	0.29	1267.98	1228.	2496.
	50.00	51.10	10.86	47.1	5742.	5494.	3138.	1496.	5283.	0.109	0.149	413.	563.	1.31	1444.53	1479.	2924.
	51.00	52.10	11.86	56.4	5666.	5840.	3582.	1590.	5668.	0.117	0.157	478.	642.	2.82	1649.30	1768.	3417.
	52.00	53.10	12.87	59.3	5852.	5840.	3951.	1684.	5728.	0.116	0.153	468.	619.	5.50	1849.61	2048.	3898.
X = 53.6 START INNERBODY →	53.00	54.10	13.87	62.1	6038.	5840.	4321.	1778.	5775.	0.114	0.150	458.	598.	9.52	2045.49	2320.	4366.
	54.00	55.10	14.87	65.0	6223.	5840.	4690.	1872.	5809.	0.114	0.147	448.	578.	15.23	2237.30	2585.	4823.
	55.00	56.10	15.88	67.8	6409.	5840.	5059.	1966.	5831.	0.114	0.145	441.	560.	23.31	2425.95	2844.	5270.
X = 55.76 END SPIKE →	56.00	57.10	16.88	47.0	6571.	5840.	5256.	2060.	5839.	0.085	0.106	321.	402.	25.65	2560.15	3032.	5592.
	57.00	58.10	17.88	34.5	6658.	5840.	4907.	1987.	5835.	0.067	0.084	259.	324.	14.08	2668.34	3183.	5851.
	58.00	59.10	18.88	24.9	6747.	5840.	4627.	1914.	5828.	0.053	0.066	206.	257.	7.47	2754.45	3304.	6058.
X = 59.6 START STRUT →	59.00	60.10	19.89	24.3	6843.	5840.	4573.	1841.	5826.	0.053	0.065	209.	260.	7.19	2842.10	3426.	6268.
	60.00	61.10	20.89	23.8	6909.	5840.	4533.	1768.	5825.	0.052	0.064	212.	261.	6.93	2930.84	3549.	6480.
	61.00	62.10	21.89	23.2	6933.	5840.	4516.	1695.	5823.	0.052	0.063	213.	261.	6.71	3020.04	3673.	6693.
	62.00	63.10	22.89	22.6	6956.	5840.	4498.	1622.	5822.	0.051	0.062	214.	261.	6.49	3109.62	3797.	6906.
	63.00	64.10	23.89	22.0	6979.	5840.	4481.	1549.	5820.	0.050	0.061	215.	260.	6.25	3199.51	3920.	7120.
	64.00	65.10	24.89	21.4	7002.	5840.	4463.	1476.	5818.	0.050	0.060	215.	260.	6.02	3289.65	4044.	7334.
	65.00	66.10	25.89	20.9	7026.	5840.	4446.	1403.	5817.	0.049	0.059	216.	259.	5.77	3379.96	4168.	7548.
	66.00	67.10	26.89	20.3	7049.	5840.	4428.	1330.	5815.	0.048	0.058	216.	258.	5.52	3470.37	4291.	7761.
	67.00	68.10	27.89	19.7	7072.	5840.	4411.	1257.	5813.	0.047	0.057	216.	258.	5.27	3560.86	4414.	7975.
X = 68.2 END STRUT →	68.00	69.10	28.89	19.1	7095.	5840.	4393.	1184.	5812.	0.047	0.055	216.	256.	5.03	3651.30	4537.	8188.
	69.00	70.13	29.89	18.1	7346.	5840.	4372.	1111.	5808.	0.046	0.055	218.	257.	4.60	3743.95	4660.	8404.
	70.00	71.18	30.90	15.3	7624.	5840.	4325.	1038.	5797.	0.042	0.050	202.	238.	3.93	3831.10	4776.	8607.
	71.00	72.25	31.93	11.4	7808.	5840.	4248.	965.	5779.	0.035	0.041	169.	199.	2.93	3903.32	4876.	8779.
	72.00	73.33	32.95	9.2	7938.	5840.	4059.	892.	5750.	0.031	0.037	151.	177.	2.13	3965.36	4967.	8932.
	73.00	74.41	33.97	7.2	8063.	5840.	3859.	819.	5715.	0.027	0.032	132.	155.	1.33	4017.03	5047.	9064.
	74.00	75.49	34.98	5.2	8188.	5840.	3659.	746.	5675.	0.022	0.026	108.	126.	0.74	4057.28	5113.	9170.
	75.00	76.57	35.99	4.2	8215.	5840.	3610.	673.	5666.	0.019	0.022	95.	110.	0.58	4090.78	5172.	9262.
	76.00	77.64	37.00	3.4	8232.	5840.	3577.	600.	5660.	0.016	0.019	82.	95.	0.44	4118.07	5222.	9340.
	77.00	78.72	38.01	2.6	8248.	5840.	3543.	569.	5654.	0.013	0.015	66.	76.	0.32	4138.93	5264.	9403.
	78.00	79.80	39.01	2.3	8340.	5840.	3522.	538.	5651.	0.012	0.014	61.	70.	0.28	4156.98	5301.	9458.
X = 79.6 END AFT OUTER SHELL →	79.00	80.88	40.01	2.0	8440.	5840.	3502.	508.	5649.	0.011	0.013	56.	65.	0.24	4172.65	5337.	9509.
	80.00	81.96	41.01	1.9	8514.	5840.	3445.	477.	5640.	0.011	0.012	54.	62.	0.20	4186.79	5369.	9556.
	81.00	83.04	42.01	1.9	8550.	5840.	3432.	446.	5638.	0.010	0.012	54.	62.	0.16	4199.88	5398.	9597.
	82.00	84.12	43.01	1.8	8586.	5840.	3418.	415.	5636.	0.010	0.012	54.	62.	0.11	4211.93	5422.	9634.
	83.00	85.19	44.01	1.8	8622.	5840.	3405.	385.	5635.	0.010	0.012	54.	62.	0.08	4222.93	5442.	9665.
	84.00	86.27	45.01	1.8	8658.	5840.	3392.	354.	5633.	0.010	0.012	55.	62.	0.04	4232.87	5458.	9691.
	85.00	87.35	46.01	1.8	8694.	5840.	3379.	323.	5631.	0.010	0.012	54.	62.	-0.01	4241.77	5470.	9712.
	86.00	88.43	47.01	1.7	8730.	5840.	3366.	292.	5629.	0.010	0.012	55.	62.	-0.04	4249.61	5478.	9728.
	87.00	89.51	48.01	1.7	8766.	5840.	3352.	262.	5627.	0.010	0.012	55.	62.	-0.00	4256.41	5482.	9738.
	88.00	90.58	49.01	1.7	8800.	5840.	3339.	231.	5625.	0.010	0.011	54.	62.	0.03	4261.97	5482.	9744.
X = 89.47 END NOZZLE →	89.00	91.59	50.01	1.6	8800.	5840.	3312.	200.	5622.	0.010	0.011	52.	58.	-0.02	4263.55	5482.	9746.
	90.00	92.60	51.01	1.4	8800.	5840.	3286.	169.	5618.	0.009	0.010	49.	55.	-0.02	4261.87	5482.	9744.

calculation procedure was not modified except as mentioned in (1) above and in the calculation of the station at which transition from laminar to turbulent Reynolds number occurs. The transition position is moved to X = 4 at a Reynolds number of 1,000,000. The aerodynamic conditions of pressure, temperature, and velocity are those previously used for the Mach 8, 81,000-ft altitude condition presented in Reference 1. Although the 81,000-ft altitude is below the minimum line in the NASA work statement, it was used during Phase I because of a requirement for operation with a 2500 psf dynamic pressure. The new NASA work statement (Reference 2) indicates a maximum dynamic pressure of 2000 psf for engine lit and not-lit conditions. However, this is not considered an ordinary operating condition; therefore, the normal pressure drop required for fuel injectors need not be maintained, and thus, the cooling jacket hydrogen pressure drop design condition is on the B-B line at an altitude of 88,000 ft with a dynamic pressure of 1750 psf. New design condition aerodynamic data are being prepared and will be used for subsequent aerodynamic heating analysis. A 29-percent reduction in heat flux is expected by changing the design point altitude with a significant easing of the fin design problems in terms of reduced fin ΔT as well as reduced flow required for cooling, not only because of the overall reduced heat fluxes, but because the hydrogen outlet temperature can be higher and can approach the 1660^0R maximum permissible temperature more closely. A factor that will tend to increase the heat fluxes, but which is limited to the 9 or 10 in. section immediately upstream of the strut leading edge, is the use of an inlet contraction ratio of 14.6 instead of an inlet contraction ratio of 10 on which the pressure, temperature, and velocity data were based and which was used in Computer Program H1940 to obtain the results shown in Table 4.1-3.

For the design condition, approximately 300 psia ΔP is available from the pump outlet to the fuel plenum. For the 2000 psf line in Figure A4 of Reference 2, the entire 700 psi will be available for the Mach 8, 85,000-ft altitude off-design condition, since it is assumed that the fuel injectors will not be operating normally and, therefore, the fuel control valves will not require normal pressure of up to 400 psia.

4.1.4 Cooling Jacket Design

The coolant flow routing has been revised to the configuration shown in Figure 4.1-1 to reduce thermal stresses on the outer body leading edge and forward outer shell by eliminating the large sawtooth axial temperature profile which previously resulted from having flow routes 3, 4, and 5 flowing away from the bolted flange which attaches the leading edge to the outer shell (page 217, Reference 1). Flow routes 3, 4, and 5 have been combined into a single flow route, which flows forward toward the leading edge along the outer surface, aft from the leading edge along the inner surface, passes through the bolted flange, and into the cooling jacket in the forward part of the outer shell.

To provide acceptable strut leading-edge temperatures with a heat flux of 1400 Btu/sec-ft^2 on an 80-mil-radius leading edge rather than the previously calculated 1000 Btu/sec-ft^2 on a 30-mil radius leading edge, the flow to the nozzle is routed through the strut leading edge rather than through a tube passing through the interior of the strut. This change is discussed in detail

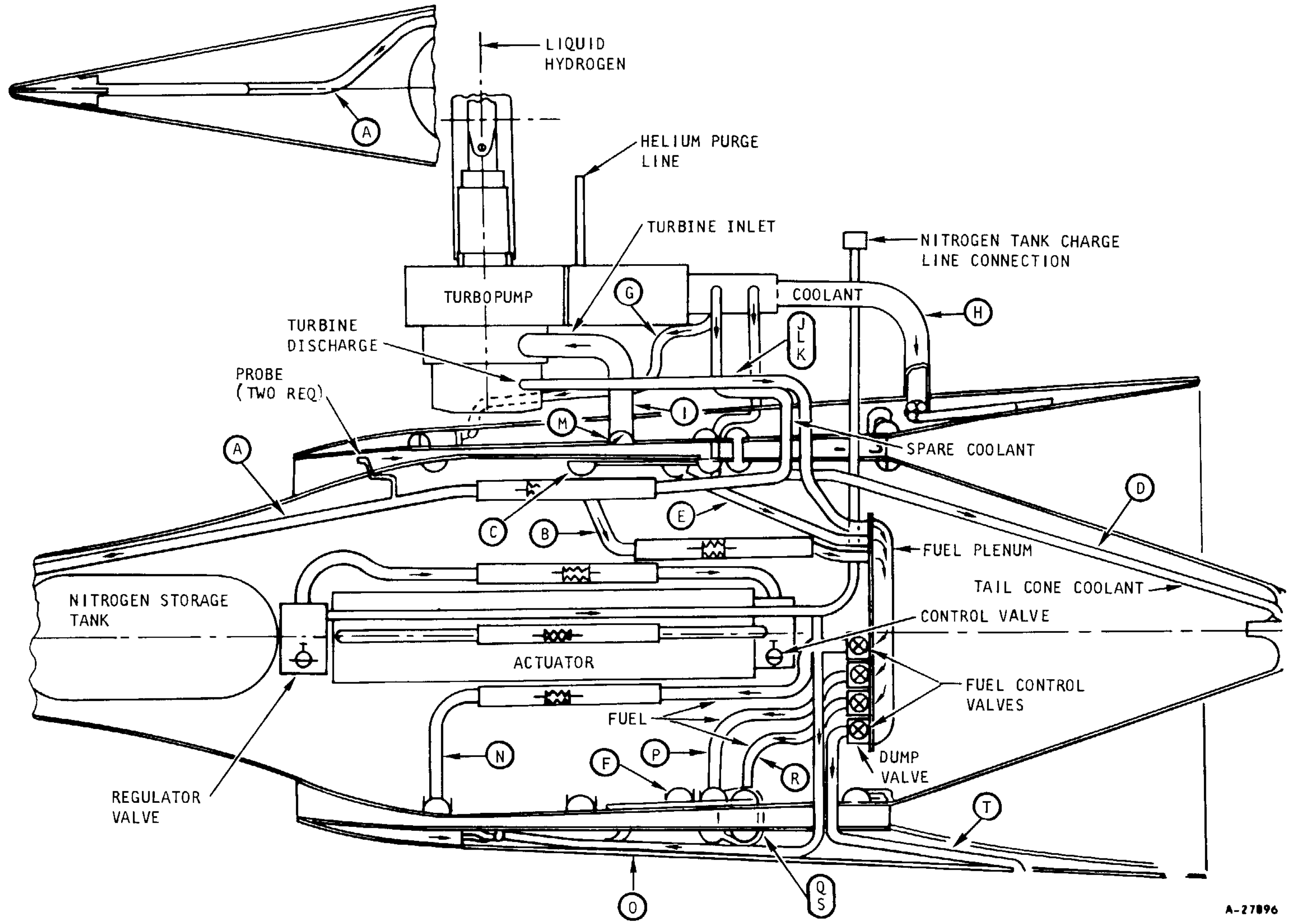

Figure 4.1-1. Plumbing Schematic

in Paragraph 4.3. An additional flow routing change associated with strut cooling is the use of coolant from flow route 6 on the aft outer shell to cool the strut sides rather than coolant from the bolted flange/manifold on the inner body. Also, the strut side coolant does not return to the cooling jackets as in the Phase I design, but is routed directly to the fuel plenum. A negligible increase in hydrogen flow results. The coolant from the strut sides is approximately 1400°R rather than 1600°R, but the strut hydrogen flow is very small.

The above changes in flow routing are reflected in the cooling jacket fin performance estimates included in Tables 4.1-4 and 4.1-5 for the inner body and outer shell respectively. Tables 4.1-6 through 4.1-8 include outputs from Computer Program H1930 for the most probable fin candidates, based on the Mach 8, 81,000-ft altitude conditions.

Table A-36, page 229 of Reference 1, is a summary of the fins selected during Phase I. The number of fin sizes required has been reduced from that indicated by Table A-36 to a total of three. The forward part of the inlet spike will still have the 16R-.153-.143-.006 fin geometry. All other cooling jackets, except the strut and a 0.5 in. section of the outer body leading edge, will have a fin of approximately 20R-.050-.083-.006. Further detailed design and analysis will determine the precise number, thickness, and height of these fins with the number of fins potentially ranging from 20 to 40 fins per in., fin heights ranging ±0.010 in. about the 0.050 in. fin height, and fin thickness ranging downward from 0.006 in. to 0.003 in. The 0.5 in. length adjacent to the outer body leading edge and the entire surface of the strut will be covered by a fin approximately 20R-.020-plain-.006. Passages of 0.006 in. height, as indicated in Table A-36 of Reference 1, for cowl and strut leading edges have been eliminated because the small passages are both difficult to fabricate and difficult to maintain open for flow. The cowl leading edge passage will be 20 mils or larger by combining flow routes 3, 4, and 5, and/or by having flow in a separate tubular passage parallel to the outer body leading edge. This is discussed in greater detail in Paragraph 4.4. The strut leading edge will be cooled by hydrogen flow in a tube that is parallel to the strut leading edge and has an inside diameter of 0.13 in. Details of the strut flow routing and passage geometry are discussed in Paragraph 4.3.

4.1.4.1 Inner Body

Fin candidates for the inner body, including the inner shell and nozzle, are listed in Table 4.1-4, along with some of the more important performance characteristics for these fins. The hydrogen flow rate to provide an outlet temperature below 1660°R is increased from 0.28 lb/sec used in Phase I to 0.34 lb/sec. All of the candidates listed have an acceptable fin ΔT less than 500°R and acceptable pressure drop of less than 100 psi except the 20R-.040-.060-.006, which has a pressure drop of about 125 psi. Detailed performance for this fin is included in Table 4.1-6 because it may be needed to provide acceptable fin ΔT in the forward part of the outer shell. When the pressure drops associated with the nozzle cap, the bolted flange/manifold at the aft edge of the strut, and the outlet manifold are added to this 125 psi fin pressure drop, the total may be incompatible with a 700 psi pump outlet pressure and a pressure drop of about 100 psi in the strut leading edge passages, thus, making this fin an unacceptable candidate.

TABLE 4.1-4

FIN CANDIDATES FOR INNER BODY

Fin Geometry	Wall Temp T_W, ^oR	Outlet Hydrogen Temp T_{OUT}, ^oR	Overall Fin ΔP, psi	Fin ΔT ΔT_{FIN}, ^oR
20R-.04-.060-.006	1948	1628	125	304
20R-.05-.091-.004	2019	1608	45	398
20R-.05-.088-.006	1991	1615	58	363
20R-.05-.086-.008	1968	1622	78	335
20R-.06-.095-.006	2028	1604	34	415
30R-.05-.073-.003	1980	1619	55	348
40R-.05-.060-.003	1937	1630	73	299

Notes:

1. Inlet conditions: $\dot{W}$ = 0.34 lb/sec
   P = 600 psia
   T = 120^{o}R
2. Overall and outlet conditions are for entire inner body length.
3. Mach 8 at 81,000 ft, T_T max = 5840^{o}R

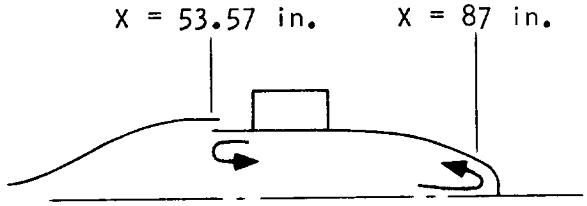

TABLE 4.1-5

FIN CANDIDATES FOR OUTER SHELL

Fin Geometry	$\dot{W}$ lb/sec	ΔP psi	$T_{WTOUT-MAX}$ °R	$\Delta T_{FIN-MAX}$ °R	T_{HOUT} °R	Remarks
FORWARD OUTER SHELL						
16R-.153-.1/7-.006	NA	NA	NA	NA	NA	Fin not acceptable due to excessive ΔT_{FIN} and T_{WTOUT}
20R-.04-.080-.006	0.60	100	2085	560	1375	$\Delta T_{FIN} > 500$ for 3 in. (Station 49.6 to 52.6)
20R-.05-.093-.003	0.68	42	2087	733	1208	$\Delta T_{FIN} > 500$ for 10 in. (Station 45.6 to 55.3)
20R-.05-.091-.004	0.68	47	2067	703	1214	$\Delta T_{FIN} > 500$ for 7 in. (Station 48.6 to 55.3)
20R-.05-.088-.006	0.66	57	2059	609	1254	$\Delta T_{FIN} > 500$ for 6 in. (Station 49.6 to 55.3)
20R-.05-.086-.008	0.62	66	2084	616	1328	$\Delta T_{FIN} > 500$ for 6 in. (Station 49.6 to 53.6)
20R-.06-.095-.006	0.68	35	2085	738	1206	$\Delta T_{FIN} > 500$ for 10 in. (Station 45.6 to 55.3
20R-.076-.110-.004	NA	NA	NA	NA	NA	Excessive ΔT_{FIN} and T_{WTOUT}
20R-.1-.120-.006	NA	NA	NA	NA	NA	Excessive ΔT_{FIN} and T_{WTOUT}
30R-.05-.073-.003	0.64	53	2069	637	1290	$\Delta T_{FIN} > 500$ for 6 in. (Station 49.6 to 54.6)
30R-.05-.071-.004	0.62	59	2074	604	1331	$\Delta T_{FIN} > 500$ for 5 in. (Station 49.6 to 53.6)

TABLE 4.1-5 (continued)

Fin Geometry	$\dot{W}$ lb/sec	ΔP psi	$T_{WTOUT-MAX}$ °R	$\Delta T_{FIN-MAX}$ °R	T_{HOUT} °R	Remarks
FORWARD OUTER SHELL (continued)						
40R-.05-.060-.003	0.62	68	2045	552	1341	$\Delta T_{FIN} > 500$ for 4 in. (Station 49.6 to 52.6)
20R-.03-.068-.006	0.58	275	2050	441	1440	
40R-.03-.050-.003	0.56	264	2058	397	1492	
40R-.04-.060-.003	0.58	115	2068	480	1431	
AFT OUTER SHELL						
16R-.153-1/7-.006	NA	NA	NA	NA	NA	Excessive ΔT_{FIN} and T_{WTOUT}
20R-.04-.080-.006	0.50	88	2026	432	1566	
20R-.05-.093-.003	0.52	33	2088	597	1492	$\Delta T_{FIN} > 500$ for 1 in. (Station 55.6 to 55.3)
20R-.05-.091-.004	0.52	41	2069	567	1497	$\Delta T_{FIN} > 500$ for 1 in. (Station 55.6 to 55.3)
20R-.05-.088-.006	0.52	47	2038	516	1505	$\Delta T_{FIN} > 500$ for 1 in. (Station 55.6 to 55.3)
20R-.05-.086-.008	0.50	56	2052	469	1459	
20R-.06-.095-.006	0.52	31	2083	587	1493	$\Delta T_{FIN} > 500$ for 1 in. (Station 55.6 to 55.3)

TABLE 4.1-5 (continued)

Fin Geometry	$\dot{W}$ lb/sec	ΔP psi	$T_{WTOUT-MAX}$ °R	$\Delta T_{FIN-MAX}$ °R	T_{HOUT} °R	Remarks
AFT OUTER SHELL (continued)						
20R-.076-.110-.004	NA	NA	NA	NA	NA	Excessive ΔT_{FIN} and T_{WTOUT}
20R-.100-.120-.006	NA	NA	NA	NA	NA	Excessive ΔT_{FIN} and T_{WTOUT}
30R-.05-.073-.003	0.50	49	2063	494	1555	
30R-.05-.071-.004	0.48	54	2087	454	1611	
40R-.05-.06-.003	0.48	62	2060	414	1619	
20R-.03-.068-.006	0.48	262	2011	333	1633	
40R-.03-.050-.003	0.48	272	1986	297	1640	
40R-.04-.060-.003	0.46	112	2026	360	1628	

MACH 8 AT 81,000 FT
T_T = 5840°R
X = 39.2 TO 55.3 IN.

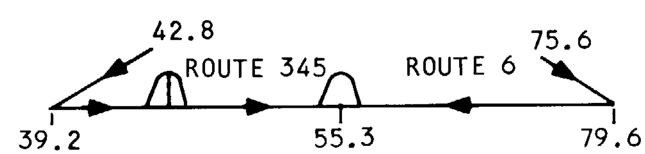

A-28042

TABLE 4.1-6

INNER BODY FIN CANDIDATES FOR M = 8 AT 81,000 FT

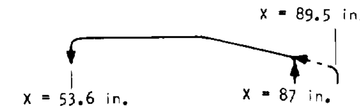

Fin Geometry: 20R-.04-.080-.006
Hydrogen Flow Rate: W_H = 0.34 lb/sec
ΔT_{FIN} does not exceed 400°F

XX	TIN	HH	HHH	HG	PHIN	DELTFN	TWTOUT	DELTWL	HEATFLUX	EFFFIN	EFFTOT
86.988	120.000	1.61569	0.19354	0.01000	600.00	37.52	228.	67.	53.99921	0.08429	0.34257
85.988	126.138	1.41122	0.19581	0.01000	591.00	42.34	239.	67.	53.90961	0.09047	0.34700
84.988	133.336	1.25127	0.19782	0.01000	584.29	47.08	251.	66.	53.81090	0.09642	0.35128
83.988	141.584	1.12352	0.19978	0.01000	579.05	51.72	264.	66.	53.70488	0.10225	0.35546
82.988	150.303	0.99341	0.19751	0.01000	574.82	57.43	277.	64.	53.58585	0.11024	0.36120
81.988	160.760	0.89870	0.19754	0.01000	571.36	62.49	291.	62.	53.45898	0.11687	0.36596
80.988	171.439	0.82028	0.19783	0.01051	568.42	70.80	313.	64.	55.99017	0.12329	0.37057
79.988	183.310	0.76763	0.20059	0.01100	565.86	78.16	334.	66.	58.41225	0.12825	0.37413
78.988	196.259	0.72608	0.20495	0.01151	563.59	85.43	357.	68.	60.93175	0.13281	0.37740
77.988	210.304	0.68021	0.20687	0.01251	561.50	97.44	388.	72.	65.86891	0.13874	0.38166
76.988	226.178	0.65317	0.21288	0.01454	559.58	115.92	433.	81.	75.93462	0.14338	0.38499
75.988	245.359	0.62823	0.21838	0.01754	557.72	142.46	494.	94.	90.64293	0.14842	0.38861
74.988	269.106	0.62304	0.22923	0.02054	555.91	165.54	555.	106.	105.05240	0.15133	0.39070
73.988	297.602	0.63383	0.24622	0.02456	554.09	192.21	629.	121.	124.43826	0.15275	0.39172
72.988	332.728	0.63254	0.25989	0.02905	552.25	223.97	714.	135.	145.78702	0.15658	0.39446
71.988	376.032	0.63080	0.27337	0.03305	550.36	250.83	798.	145.	164.13007	0.16066	0.39739
70.988	427.736	0.63039	0.28226	0.03858	548.39	285.69	903.	157.	188.47232	0.16515	0.40062
69.988	490.409	0.65827	0.29517	0.04405	546.33	306.19	1000.	166.	211.54709	0.16663	0.40168
68.988	561.841	0.68821	0.30208	0.04651	544.18	304.32	1067.	162.	220.59206	0.16842	0.40297
67.988	636.667	0.70743	0.31153	0.04700	541.86	294.31	1123.	153.	220.38489	0.17093	0.40477
66.988	712.252	0.72054	0.31901	0.04751	539.27	286.75	1183.	145.	220.01785	0.17397	0.40695
65.988	787.469	0.73397	0.32682	0.04851	536.38	281.77	1247.	138.	221.64587	0.17721	0.40928
64.988	863.242	0.74365	0.33333	0.04951	533.16	277.76	1313.	131.	223.03979	0.18099	0.41199
63.988	939.491	0.76728	0.34544	0.05000	529.61	267.11	1370.	123.	222.42905	0.18353	0.41382
62.988	1015.551	0.78807	0.35632	0.05051	525.74	258.02	1431.	117.	221.77203	0.18601	0.41560
61.988	1091.229	0.80445	0.36545	0.05151	521.53	252.63	1496.	112.	222.86775	0.18874	0.41756
60.988	1167.187	0.81480	0.37226	0.05200	516.99	246.50	1560.	106.	221.72565	0.19206	0.41994
59.988	1242.771	0.82120	0.37767	0.05251	512.10	241.42	1625.	100.	220.57286	0.19593	0.42272
58.988	1317.818	0.83143	0.38460	0.05300	506.85	235.46	1689.	95.	219.32304	0.19936	0.42518
57.988	1392.182	0.84373	0.39248	0.06017	501.25	255.34	1793.	101.	242.99846	0.20268	0.42756
56.988	1474.143	0.86143	0.40284	0.07621	495.24	303.09	1948.	116.	296.39551	0.20585	0.42984
55.988	1573.264	0.87615	0.41139	0.04154	488.72	166.32	1833.	63.	166.25282	0.20828	0.43158
54.988	1628.259	0.88574	0.41623	0.00010	481.84	0.41	1629.	0.	0.41908	0.20876	0.43193
								904-LAGIN2	XTRPLTD	XA= 0.5348810E 02	
								905-LAGIN2	XTRPLTD	XA= 0.5348810E 02	
53.988	1628.397	0.88580	0.41626	0.00010	474.82	0.41	1629.	0.	0.41626	0.20877	0.43193

Fin Geometry: 20R-.05-.088-.006
Hydrogen Flow Rate: W_H = 0.34 lb/sec
ΔT_{FIN} does not exceed 400°F

XX	TIN	HH	HHH	HG	PHIN	DELTFN	TWTOUT	DELTWL	HEATFLUX	EFFFIN	EFFTOT
86.988	120.000	1.26098	0.15457	0.01000	600.00	46.90	237.	67.	53.90663	0.08096	0.31072
85.988	126.127	1.09971	0.15638	0.01000	595.57	52.91	249.	67.	53.80531	0.08695	0.31522
84.988	133.311	0.97389	0.15802	0.01000	592.28	58.82	262.	66.	53.69531	0.09273	0.31955
83.988	141.541	0.87364	0.15965	0.01000	589.73	64.57	276.	65.	53.57840	0.09838	0.32378
82.988	150.739	0.77952	0.15918	0.01000	587.67	71.07	291.	64.	53.44539	0.10508	0.32881
81.988	160.728	0.69767	0.15810	0.01000	585.97	77.87	306.	62.	53.30742	0.11254	0.33440
80.988	171.377	0.63644	0.15845	0.01051	584.54	88.13	330.	64.	55.81097	0.11875	0.33907
79.988	183.212	0.59531	0.16075	0.01100	583.30	97.21	353.	66.	58.20656	0.12356	0.34267
78.988	196.120	0.57087	0.16633	0.01151	582.19	104.92	376.	68.	60.71208	0.12707	0.34530
77.988	210.117	0.55066	0.17233	0.01251	581.17	116.62	407.	72.	65.63507	0.13081	0.34811
76.988	225.938	0.52477	0.17631	0.01454	580.19	139.44	456.	81.	75.60211	0.13570	0.35178
75.988	245.041	0.50776	0.18192	0.01754	579.25	170.25	521.	94.	90.17110	0.14004	0.35503
74.988	268.670	0.50361	0.19106	0.02054	578.34	197.59	586.	105.	104.41850	0.14277	0.35708
73.988	297.002	0.51339	0.20561	0.02456	577.42	228.80	664.	120.	123.57790	0.14395	0.35796
72.988	331.890	0.51145	0.21681	0.02905	576.49	266.59	755.	134.	144.60979	0.14766	0.36074
71.988	374.833	0.50982	0.22809	0.03305	575.54	298.28	843.	144.	162.65196	0.15152	0.36364
70.988	426.044	0.50648	0.23447	0.03858	574.55	340.76	955.	156.	186.48692	0.15617	0.36714
69.988	488.013	0.53216	0.24650	0.04405	573.53	363.20	1052.	165.	209.23425	0.15705	0.36779
68.988	558.607	0.55403	0.25140	0.04651	572.46	362.17	1120.	161.	218.14381	0.15900	0.36925
67.988	632.498	0.57275	0.26062	0.04700	571.30	348.78	1172.	152.	218.10632	0.16095	0.37072
66.988	707.316	0.58389	0.26714	0.04751	570.01	339.67	1230.	144.	217.81377	0.16366	0.37274
65.988	781.779	0.59286	0.27302	0.04851	568.57	334.62	1293.	137.	219.42926	0.16692	0.37519
64.988	856.794	0.59797	0.27753	0.04951	566.98	330.98	1358.	131.	220.79242	0.17084	0.37813
63.988	932.275	0.61646	0.28748	0.05000	565.24	318.62	1414.	123.	220.27338	0.17324	0.37993
62.988	1007.601	0.63335	0.29671	0.05051	563.35	307.76	1471.	116.	219.71504	0.17556	0.38167
61.988	1082.646	0.64661	0.30444	0.05151	561.31	301.34	1535.	111.	220.85500	0.17812	0.38359
60.988	1157.922	0.65417	0.30993	0.05200	559.12	294.32	1598.	106.	219.77080	0.18132	0.38599
59.988	1232.851	0.66264	0.31587	0.05251	556.77	287.20	1660.	100.	218.73723	0.18449	0.38836
58.988	1307.300	0.67211	0.32226	0.05300	554.26	279.78	1722.	95.	217.57510	0.18751	0.39063
57.988	1381.115	0.68367	0.32962	0.06017	551.57	302.59	1828.	100.	240.38437	0.19040	0.39280
56.988	1462.433	0.69616	0.33774	0.07621	548.71	359.04	1991.	116.	293.14697	0.19367	0.39525
55.988	1560.609	0.70548	0.34397	0.04154	545.64	198.79	1852.	63.	165.44147	0.19630	0.39722
54.988	1615.447	0.71201	0.34752	0.00010	542.42	0.50	1616.	0.	0.42036	0.19686	0.39765
								904-LAGIN2	XTRPLTD	XA= 0.5348810E 02	
								905-LAGIN2	XTRPLTD	XA= 0.5348810E 02	
53.988	1615.585	0.71205	0.34754	0.00010	539.18	0.50	1616.	0.	0.41753	0.19686	0.39765

Further detailed analysis is required to establish this point because the flow rate may be reduced below 0.34 lb/sec when the aerodynamic heating conditions are calculated for the Mach 8, 88,000 ft altitude case.

4.1.4.2 Outer Shell

The fin candidates for the outer body, including the outer shell and leading edge, are listed in Table 4.1-5. The total length of the outer body leading edge and the forward outer shell are included together. The outer surface of the leading edge and the outer surface of the aft outer shell are given ficticious station numbers to allow convenient inclusion in the computer tabulations (Tables 4.1-7 and 4.1-8) for the fins which have the best characteristics for these flow routes. For the aerodynamic heating conditions imposed, the only fin geometry with fin ΔT's less than $500^{\circ}R$ everywhere and a pressure drop of near 100 psi is the 40R-.04-offset-.003. The flow rate for this fin is 0.58 lb/sec compared to a flow rate of 0.66 lb/sec for the 20R-.05-offset-.006 fin and the total flow rate of 0.53 lb/sec for flow routes 3, 4, and 5 during Phase I.

4.1.4.3 Hydrogen Ducting

The detailed results of the preliminary hydrogen ducting analysis are included in Table 4.1-9 and Figure 4.1-2. In general, the following results were obtained:

> The preliminary fuel line sizes were determined for all fuel lines. In cases where two or more parallel lines may be desirable, the line sizes for various combinations are shown.
>
> It was found that the outlet torus for Route 1 and the outlet torus for Route 2 have cross sections large enough to provide good flow distribution with one outlet each. The outlet torus for Route 345 and 6 will require cross-section enlargement or more than one outlet tube to have good flow distribution.

The review of the HRE fuel system pressure drops was conducted in order to provide preliminary fuel line sizes, pinpoint areas of high pressure drops, and check for possible flow maldistributions in manifolds. Calculations were made prior to the decision to route the inner body coolant (flow Route 2) through the strut leading edge and, hence, do not reflect the effects of this change. However, the tubing connecting the aft cover to the fuel plenum is indicated as having 170 psi pressure drop. This can be reduced to a 20 psi pressure drop and also at the same time ensure better flow distribution in the inner body by increasing the number of 0.491-in. dia tubes from 1 to 6. These comments are relative to location E in Figure 4.1-2.

The following assumptions were used to determine the fuel line sizes:

(a) The pressure drop in each individual leg was assumed to correspond to the Phase I pressures. The pressures in Figure 4.1-2 are from Reference 1, Pages 75 and 76.

TABLE 4.1-7

AFT OUTER SHELL (INNER AND OUTER SURFACES)
FIN CANDIDATES FOR M = 8 AT 81,000 FT

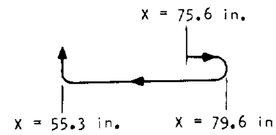

Fin Geometry: 20R-.04-.080-.006
Hydrogen Flow Rate: $W_H = 0.50$ lb/sec
ΔT_{FIN} does not exceed 500°F

[illegible]	[illegible]	[illegible]	[illegible]	[illegible]	PHIN	DELTFN	TWTOUT	DELTWL	HEATFLUX	EFFFIN	EFFTOT
[illegible]	[illegible]	[illegible]	0.31212	0.01300	680.00	90.26	282.	63.	50.93423	0.14341	0.38502
82.	[illegible]	[illegible]	[illegible]	0.01300	679.53	89.47	297.	62.	50.74515	0.14484	0.38604
81.[illegible]	[illegible]	[illegible]	0.31186	0.01300	678.99	89.62	311.	59.	50.55186	0.14798	0.38829
[illegible]	[illegible]	[illegible]	[illegible]	0.01300	678.39	89.02	326.	58.	50.36815	[illegible]	[illegible]
[illegible]	[illegible]	[illegible]	[illegible]	0.01300	677.74	114.33	386.	75.	66.55576	[illegible]	[illegible]
[illegible]	[illegible]	[illegible]	[illegible]	0.01300	677.00	123.94	421.	80.	72.70216	[illegible]	[illegible]
77.	[illegible]	0.57747	0.31312	0.01490	676.16	131.39	453.	83.	77.50255	0.15277	0.39173
76.	[illegible]	[illegible]	0.31913	0.01860	675.22	160.06	522.	98.	95.58859	0.15466	0.39309
75.	275.774	0.60451	[illegible]	0.02170	674.17	178.25	580.	110.	110.38210	0.15425	0.39280
74.	[illegible]	[illegible]	[illegible]	0.02560	672.97	197.03	644.	124.	128.79530	[illegible]	0.39170
73.	[illegible]	[illegible]	[illegible]	0.03141	671.59	231.04	735.	144.	156.27146	[illegible]	[illegible]
72.	[illegible]	[illegible]	[illegible]	0.03651	669.99	255.48	820.	158.	179.86455	0.15441	0.39291
71.[illegible]	427.677	0.71547	[illegible]	0.04060	668.12	273.47	895.	166.	198.21529	0.15576	0.39388
70.599	480.352	[illegible]	[illegible]	0.04911	665.93	304.24	1003.	187.	235.33266	0.15459	0.39304
69.599	541.472	0.79508	[illegible]	0.05451	663.39	315.55	1085.	193.	257.36353	C.15496	0.39330
[illegible]	[illegible]	[illegible]	[illegible]	[illegible]	660.46	303.60	1130.	182.	[illegible]	0.15682	0.39464
[illegible]	[illegible]	[illegible]	[illegible]	[illegible]	657.14	[illegible]	1194.	178.	262.34131	[illegible]	0.39642
[illegible]	[illegible]	[illegible]	[illegible]	[illegible]	653.44	[illegible]	1252.	170.	[illegible]	[illegible]	0.39840
65.599	817.195	0.86007	0.42593	0.05890	649.35	294.78	1310.	162.	265.42749	0.16535	0.40076
64.599	887.451	0.87614	0.43648	0.05990	644.86	289.02	1368.	154.	266.57788	0.16817	0.40279
63.599	957.903	0.90372	[illegible]	[illegible]	639.96	280.42	1422.	147.	267.82007	0.17012	0.40419
[illegible]	[illegible]	0.92881	[illegible]	[illegible]	634.63	[illegible]	1479.	140.	[illegible]	0.17195	0.40550
61.[illegible]	[illegible]	[illegible]	[illegible]	[illegible]	628.86	266.41	1537.	135.	269.57349	0.17397	0.40695
60.[illegible]	[illegible]	[illegible]	[illegible]	[illegible]	622.60	261.73	1599.	129.	[illegible]	0.17658	0.40883
59.599	1240.690	0.97510	[illegible]	[illegible]	615.82	257.58	1659.	123.	270.43994	0.17957	0.41097
58.599	1311.246	0.99002	0.49984	[illegible]	608.52	252.66	1719.	118.	270.75366	0.18221	0.41287
57.599	[illegible]	[illegible]	0.50961	0.08222	600.64	297.53	1860.	136.	[illegible]	0.18475	0.41469
[illegible]	[illegible]	[illegible]	[illegible]	[illegible]	592.08	350.63	2026.	156.	395.86816	[illegible]	[illegible]
								904-LAGIN2	XTRPLTD	XA=	[illegible]
								905-LAGIN2	XTRPLTD	XA=	0.5509879E 02
								904-LAGIN2	XTRPLTD	XA=	0.5509879E 02
								905-LAGIN2	XTRPLTD	XA=	0.5509879E 02
55.599	1565.590	[illegible]	[illegible]	0.14115	582.67	432.47	2253.	188.	505.12036	0.19082	0.41905

Fin Geometry: 20R-.05-.088-.006
Hydrogen Flow Rate: $W_H = 0.52$ lb/sec
$\Delta T_{FIN} > 500$°F from X = 55.6 in.

XX	TIN	HH	HHH	HG	PHIN	DELTFN	TWTOUT	DELTWL	HEATFLUX	EFFFIN	EFFTOT
[illegible]	[illegible]	[illegible]	[illegible]	0.01300	680.00	105.64	297.	53.	[illegible]	[illegible]	[illegible]
[illegible]	136.051	[illegible]	[illegible]	0.01300	679.73	104.96	311.	51.	[illegible]	[illegible]	[illegible]
[illegible]	[illegible]	[illegible]	[illegible]	0.01300	679.43	105.35	325.	59.	50.37184	[illegible]	[illegible]
80.599	168.327	0.45970	0.26353	0.01300	679.09	104.78	339.	58.	50.19516	0.13961	0.35471
79.599	183.688	[illegible]	0.26500	0.01300	678.73	135.22	404.	75.	66.32602	0.13912	0.35434
78.599	202.892	0.47421	0.26920	0.01390	678.32	145.32	439.	80.	72.45502	0.13987	[illegible]
[illegible]	[illegible]	[illegible]	[illegible]	[illegible]	677.85	154.36	471.	[illegible]	[illegible]	[illegible]	[illegible]
[illegible]	[illegible]	[illegible]	[illegible]	[illegible]	677.33	138.03	544.	[illegible]	[illegible]	[illegible]	[illegible]
[illegible]	[illegible]	[illegible]	[illegible]	[illegible]	676.75	209.79	605.	110.	109.83797	[illegible]	[illegible]
74.599	298.243	0.52749	0.28969	0.02560	676.08	231.81	671.	124.	128.10025	[illegible]	[illegible]
73.599	330.793	[illegible]	0.29775	0.03141	675.32	271.24	766.	144.	155.29451	[illegible]	[illegible]
[illegible]	[illegible]	0.56271	0.30265	0.03651	674.44	301.91	854.	159.	178.61536	0.14365	[illegible]
71.	[illegible]	[illegible]	[illegible]	0.04060	673.42	321.69	[illegible]	167.	[illegible]	[illegible]	[illegible]
[illegible]	[illegible]	[illegible]	[illegible]	0.04911	672.22	362.42	1046.	188.	[illegible]	[illegible]	[illegible]
[illegible]	[illegible]	[illegible]	[illegible]	0.05451	670.84	373.27	1124.	195.	[illegible]	[illegible]	[illegible]
[illegible]	[illegible]	[illegible]	0.34021	0.05500	669.25	358.92	1164.	184.	255.64261	[illegible]	[illegible]
[illegible]	[illegible]	0.68760	0.34771	0.05530	667.46	357.50	1223.	180.	260.69529	[illegible]	[illegible]
[illegible]	718.614	0.70047	0.35530	0.05790	665.48	351.94	1278.	173.	262.71411	[illegible]	[illegible]
[illegible]	[illegible]	[illegible]	[illegible]	[illegible]	663.29	346.71	1332.	165.	[illegible]	[illegible]	[illegible]
[illegible]	[illegible]	0.71680	[illegible]	0.05930	660.90	343.01	1389.	158.	[illegible]	[illegible]	[illegible]
[illegible]	[illegible]	0.73715	[illegible]	0.06090	658.30	333.95	1440.	151.	266.73779	[illegible]	[illegible]
[illegible]	[illegible]	0.75987	0.39032	0.06190	655.48	324.45	1492.	144.	268.04102	[illegible]	[illegible]
61.[illegible]	1055.811	[illegible]	0.40137	0.06290	652.43	316.16	1545.	138.	269.06152	[illegible]	[illegible]
60.[illegible]	1123.687	[illegible]	0.40914	0.06390	649.12	310.45	1602.	133.	269.83203	[illegible]	[illegible]
[illegible]	[illegible]	[illegible]	[illegible]	0.06490	645.58	305.44	1660.	127.	[illegible]	[illegible]	[illegible]
[illegible]	[illegible]	[illegible]	[illegible]	[illegible]	641.79	301.05	1718.	122.	[illegible]	[illegible]	[illegible]
[illegible]	[illegible]	[illegible]	[illegible]	[illegible]	637.73	354.68	1865.	141.	[illegible]	[illegible]	[illegible]
[illegible]	[illegible]	0.84235	0.43598	0.10383	633.35	417.67	2038.	161.	394.61549	0.17332	[illegible]
								904-LAGIN2	XTRPLTD	XA=	[illegible]
								905-LAGIN2	XTRPLTD	XA=	[illegible]
								904-LAGIN2	[illegible]	XA=	[illegible]
								905-LAGIN2	XTRPLTD	XA=	[illegible]
[illegible]	[illegible]	[illegible]	[illegible]	0.14115	628.58	516.27	2278.	193.	[illegible]	[illegible]	[illegible]

TABLE 4.1-8

LEADING EDGE (INNER AND OUTER SURFACES) AND FORWARD OUTER SHELL FIN CANDIDATES FOR M = 8 AT 81,000 FT

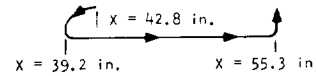

Fin Geometry: 20R-.04-.080-.006
Hydrogen Flow Rate: W_H = 0.60 lb/sec
$\Delta T_{FIN} > 500^oF$ from X = 49.6 in. to X = 52.6 in.

XX	TIN	HH	HHH	HG	PHIN	DELTEN	TWTOUT	DELTWL	HEATFLUX	EFFFIN	EFFTOT
35.601	120.000	0.60791	0.35348	0.02980	680.00	145.85	418.	139.	112.84715	0.11994	0.36816
36.601	145.833	0.78897	0.34462	0.02980	678.77	147.35	439.	133.	112.23999	0.12404	0.37110
37.601	171.008	0.79613	0.36452	0.03185	677.29	154.10	474.	136.	118.81935	0.12563	0.37225
38.601	197.955	0.84728	0.33240	0.05000	675.35	219.55	630.	197.	178.75621	0.12397	0.37136
39.601	230.811	0.80077	0.32037	0.05041	673.00	227.98	663.	198.	178.52002	0.13052	0.37575
40.601	262.6[illegible]	0.78645	0.31846	0.05370	670.30	241.70	710.	199.	187.29558	0.13436	0.37452
41.601	295.412	0.82368	0.33578	0.05100	667.47	219.56	704.	174.	177.93539	0.13364	0.37800
42.601	326.391	0.83936	0.34592	0.05485	664.40	228.56	749.	178.	189.26064	0.13501	0.37898
43.601	359.575	0.85061	0.35528	0.09042	661.07	348.41	998.	263.	293.66138	0.13725	0.38059
44.601	412.991	0.86296	0.36568	0.10401	657.31	384.77	1109.	280.	330.83887	0.14007	0.38261
45.601	473.4[illegible]	0.90727	0.38840	0.11361	653.05	394.50	1188.	285.	357.10837	0.14076	0.38311
46.601	541.51[illegible]	0.9[illegible]143	0.41176	0.11941	648.22	391.74	1250.	279.	372.65598	0.14134	0.38389
47.601	614.749	0.98184	0.43050	0.12361	642.78	389.79	1315.	270.	384.36157	0.14413	0.38553
48.601	692.828	0.99505	0.44307	0.13103	636.67	420.41	1438.	281.	422.73508	0.14728	0.38779
49.601	773.259	1.01144	0.45809	0.14981	629.83	526.67	1699.	335.	542.78149	0.15151	0.39083
50.601	881.470	1.03752	0.47841	0.15659	622.05	560.43	1854.	338.	598.15381	0.15640	0.39434
51.601	1016.006	1.07807	0.50416	0.15270	613.25	523.01	1905.	303.	584.48047	0.16030	0.39714
52.601	1134.328	1.10338	0.52373	0.14970	603.38	494.37	1968.	273.	570.33252	0.16469	0.40029
53.601	1258.420	1.11578	0.53841	0.14680	592.40	470.04	2036.	246.	554.17285	0.17004	0.40413
54.601	1375.506	1.13542	0.55615	0.14002	580.32	433.58	2085.	218.	524.90405	0.17461	0.40741

Fin Geometry: 20R-.05-.088-.006
Hydrogen Flow Rate: W_H = 0.66 lb/sec
$\Delta T_{FIN} > 500^oF$ from X = 49.6 in. to X = 54.6 in.
$\Delta T_{FIN} > 600^oF$ from X = 49.6 in. to X = 52.6 in.

XX	TIN	HH	HHH	HG	PHIN	DELTEN	TWTOUT	DELTWL	HEATFLUX	EFFFIN	EFFTOT
35.601	120.000	0.68849	0.30706	0.02980	680.00	167.09	438.	139.	112.26944	0.11017	0.33263
36.601	143.302	0.67590	0.30065	0.02980	679.24	168.17	456.	133.	111.72041	0.11330	0.33498
37.601	166.194	0.67743	0.31624	0.03185	678.32	176.87	491.	136.	118.27756	0.11521	0.33641
38.601	190.551	0.72714	0.29553	0.05000	677.14	248.77	653.	198.	177.61299	0.11284	0.33463
39.601	220.879	0.68906	0.28045	0.05041	675.72	258.98	694.	190.	177.43825	0.11843	0.33892
40.601	249.926	0.66562	0.27491	0.05370	674.08	278.24	734.	191.	186.00676	0.12293	0.34219
41.601	279.783	0.68536	0.28549	0.05100	672.39	256.73	726.	176.	176.80215	0.12314	0.34236
42.601	307.936	0.71046	0.29833	0.05485	670.57	263.77	768.	181.	188.24933	0.12301	0.34225
43.601	337.926	0.72044	0.30662	0.09042	668.60	400.12	1029.	267.	290.84888	0.12498	0.34374
44.601	384.908	0.73316	0.31432	0.10401	666.40	440.88	1139.	286.	327.65137	0.12707	0.34530
45.601	439.121	0.74875	0.32746	0.11361	663.92	462.83	1224.	292.	352.94629	0.12921	0.34691
46.601	499.786	0.78999	0.34871	0.11941	661.14	458.58	1280.	298.	369.12036	0.12940	0.34705
47.601	564.743	0.82242	0.36729	0.12361	658.03	454.35	1335.	281.	381.86133	0.13074	0.34806
48.601	634.421	0.84160	0.38126	0.13103	654.57	486.88	1453.	292.	420.78442	0.13294	0.34970
49.601	712.888	0.85506	0.39442	0.14981	650.72	609.38	1725.	351.	538.90332	0.13618	0.35213
50.601	814.178	0.86481	0.40272	0.15659	646.36	656.58	1885.	357.	593.28882	0.14042	0.35562
51.601	925.479	0.89402	0.42550	0.15270	641.46	617.78	1923.	322.	591.74902	0.14450	0.35837
52.601	1037.394	0.92629	0.44685	0.14970	636.01	581.02	1967.	293.	570.55518	0.14745	0.36059
53.601	1146.622	0.94290	0.46163	0.14680	630.02	552.11	2020.	257.	555.48730	0.15125	0.36344
54.601	1253.883	0.95034	0.47282	0.14002	623.47	515.24	2059.	237.	528.55884	0.15573	0.36680

Fin Geometry: 40R-.04-.060-.003
Hydrogen Flow Rate: W_H = 0.58 lb/sec
ΔT_{FIN} does not exceed 500^oF

XX	TIN	HH	HHH	HG	PHIN	DELTEN	TWTOUT	DELTWL	HEATFLUX	EFFFIN	EFFTOT
35.601	120.000	0.75620	0.36662	0.02980	680.00	140.84	414.	139.	112.98073	0.10229	0.26966
36.601	146.779	0.76020	0.36732	0.02980	678.81	138.59	431.	133.	112.46454	0.10438	0.27136
37.601	172.823	0.77891	0.39390	0.03185	677.31	143.02	465.	136.	119.10222	0.10499	0.27178
38.601	200.259	0.82503	0.36533	0.05000	675.30	203.93	618.	197.	179.34488	0.10388	0.27096
39.601	234.621	0.81717	0.35989	0.05041	672.88	204.23	643.	188.	179.51071	0.10491	0.27342
40.601	267.599	0.82659	0.36746	0.05370	669.93	211.18	685.	199.	198.63305	0.10846	0.27469
41.601	301.651	0.86624	0.38764	0.05100	666.77	191.55	683.	173.	179.04512	0.10797	0.27428
42.601	333.859	0.88152	0.39923	0.05485	663.33	199.49	728.	177.	190.45334	0.10921	0.27526
43.601	368.455	0.89553	0.41136	0.09042	659.58	304.42	964.	263.	296.74780	0.11091	0.27667
44.601	423.486	0.91690	0.42738	0.10401	655.35	333.65	1070.	280.	334.95762	0.11273	0.27830
45.601	488.093	0.96941	0.45640	0.11361	650.50	340.35	1149.	284.	361.53345	0.11316	0.27950
46.601	559.678	1.00796	0.48100	0.11941	644.98	339.55	1215.	277.	376.78906	0.11476	0.27990
47.601	637.194	1.03654	0.50171	0.12361	638.76	338.18	1285.	269.	388.03149	0.11662	0.28132
48.601	718.729	1.04761	0.51639	0.13103	631.77	364.89	1407.	278.	426.86230	0.11963	0.28377
49.601	809.013	1.06216	0.53520	0.14981	623.93	457.85	1657.	331.	549.03101	0.12343	0.28685
50.601	926.440	1.10802	0.56740	0.15659	614.95	479.92	1805.	333.	605.89844	0.12666	0.28948
51.601	1055.961	1.14817	0.59763	0.15270	604.69	447.09	1866.	297.	590.49929	0.12938	0.29219
52.601	1184.662	1.16692	0.61883	0.14970	593.07	423.20	1938.	267.	574.88965	0.13420	0.29562
53.601	1309.765	1.18307	0.63931	0.14680	580.08	400.13	2011.	240.	557.84033	0.13855	0.29916
54.601	1431.341	1.20365	0.66159	0.14002	565.69	367.83	2068.	211.	527.22021	0.14233	0.30221

TABLE 4.1-9

PRELIMINARY SIZING OF HRE FUEL LINES AND ASSOCIATED FLOW PARAMETERS

Assumed Parameters →	K	$\dot{W}$	ΔP	T	P_{avg}	A_F	D_1	D_2	D_4	D_6	D_8	D_{10}	D_{12}	M		LOCATION Fig. 4.1-2
Route 1																
Manifold to Spike	8.0	0.37	30	100	685	0.252	0.566							0.085		A
Manifold to Fuel Plenum	5.0	0.37	147	1600	481	0.429	0.739									B
Torus	1.0	0.185	1.51	1600	555	0.884										C
Route 2																
Manifold to Aft Cover	5.5	0.28	7	100	681.5	0.328	0.647									D
Aft Cover to Fuel Plenum	2.0	0.28	170	1600	493	0.189	0.491							0.157		E
Torus	1.0	0.14	2.86	1600	578	0.475										F
Route 345																
Manifold to Forward Cowl	7.0	0.54	2.0	100	684	1.3088			0.646							G
Route 6																
Manifold to Aft Cowl	5.5	0.408	5.0	100	682.5	0.5652			0.425							H
Routes 345 and 6																
Cowl Manifold to Turbine Inlet	2.5	0.938	10	1600	578.0	2.68	1.85									I
Turbine to Fuel Plenum	4.0	0.342	16.4	1600	425.5	1.130		0.849								J
Turbine to Fuel Plenum	4.0	0.138	16.4	1600	425.5	0.456		0.540								K
Turbine to Fuel Plenum	4.0	0.48	16.4	1600	425.5	0.502		0.566								L
Torus	1.0	0.469	9.2	1600	583	0.884										M
Injector Routes																
1st Injector Set (Inboard)	4.0	0.879	40	1600	338	2.085	1.630	1.154	0.815	0.665	0.577	0.515	0.470			N
1st Injector Set (Outboard)	3.5	0.4395	20	1600	310	1.442	1.356	0.960	0.678	0.554	0.480	0.429	0.392			O
2nd Injector Set (Inboard)	4.0	1.125	40	1600	338	2.66	1.840	1.304	0.922	0.750	0.652	0.582	0.532			P
2nd Injector Set (Outboard)	3.5	0.5625	20	1600	310	1.854	1.536	1.081	0.769	0.628	0.544	0.486	0.444			Q
3rd Injector Set (Inboard)	4.0	0.304	40	1600	338	0.720	0.958	0.678	0.479	0.391	0.339	0.303	0.2765			R
3rd Injector Set (Outboard)	3.5	0.152	20	1600	310	0.499	0.797	0.564	0.399	0.326	0.282	0.252	0.230			S
Dump to Ambient	4.0	0.721	358	1600	179	0.788	1.0									T

K = Loss coefficient

$\dot{W}$ = Total flow rate thru leg (lb/sec)

ΔP = Assumed pressure drop (psi)

T = Temperature (^{o}R)

P_{avg} = Assumed average pressure (psia)

D_1* = Line ID (in.)

$\rho = 0.118 \frac{P_{avg}}{T}$ = density (lb/ft^3)

M = Mach No.

*Subscript indicates number of lines.

$$\Delta P = \frac{KW^2}{2g\rho A_F^2}$$

$$A_F = \frac{\pi D^2}{4} = \sqrt{\frac{KW^2}{2g\rho\Delta P}}$$

$$D = \sqrt{\frac{4A}{\pi}}$$

Note: All cooling jackets are assumed to have ΔP = 100 psi.

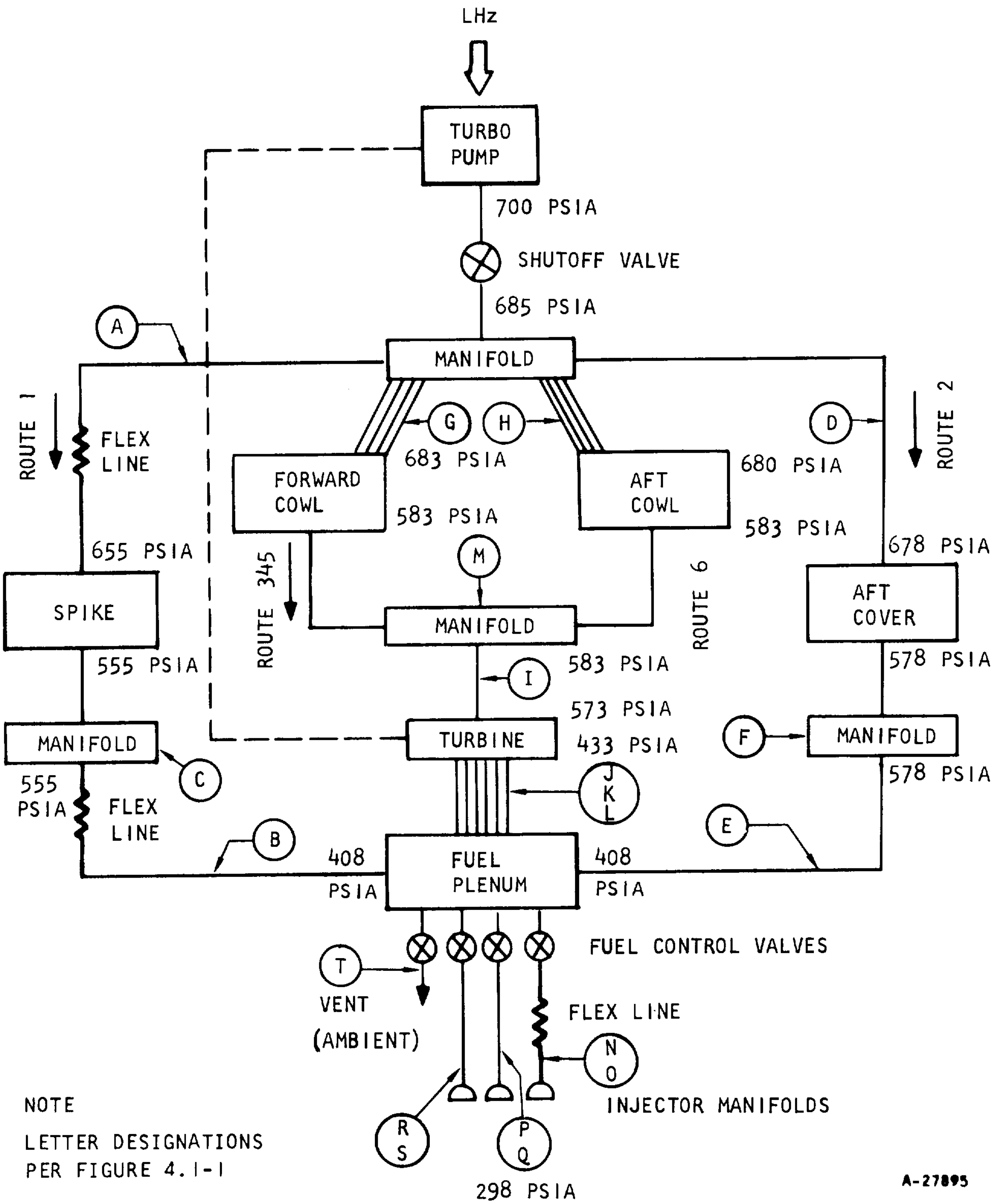

Figure 4.1-2. Fuel Route Schematic

(b) The flow rates upstream of the fuel plenum are from Reference 1. The flow rates downstream of the fuel plenum are new values.

(c) The pressure drops for specific component (i.e., shutoff valve, spike, etc.) are from Reference 1, Pages 74 to 76.

(d) The loss coefficients for the fuel lines were calculated by assigning the following head loss coefficient values:

$K = 1.0$ (expansion)

$K = 0.5$ (contraction)

$K = 1.0$ (90-deg turn)

$K = 0.5$ (friction loss)

The total head loss coefficient for each fuel line was the summation of the individual component losses.

(e) The fuel temperatures were assumed to be (1) $100^\circ R$ upstream of finned surfaces, and (2) $1600^\circ R$ downstream of finned surfaces.

(f) The flow areas, A_F, were calculated using assumptions a through e.

4.2 NOZZLE

4.2.1 Applied Structural Loads

The nozzle structure is flange bolted to the inner shell as described in Paragraph 4.2.3. The nozzle cap is connected to the nozzle by a screwed flange connection which is safety locked after assembly.

The external normal static pressure forces applied to the nozzle are relatively small, even at the bolted flange ring, and the pressure diminishes very rapidly in the expansion portion of the nozzle. The nozzle skin is sized to contain 30 psi internal pressure.

The bolted flangeconnection from the nozzle to the inner shell also provides for coolant manifolding and crossover ports from the nozzle to the inner shell. These flange rings have been analyzed for critical stresses due to coolant containment. In particular, the joint connections to the skins are being carefully designed, since such local areas are usually the most difficult structural and detailed design problems. This work is discussed in detail in Paragraph 4.2.3.

The screwed flange connection between the nozzle cap and the nozzle has also been thoroughly investigated. The principle stresses in this portion of the engine are due to joint connections required for satisfactory pressure containment strength and for a seal-tight joint. This is discussed in detail in Paragraph 4.2.2.

The dual mainfold rings at the connection between the nozzle and the inner shell behave as a single structural member. An instrumentation and control package will be located inside the nozzle, and will be mounted directly to the dual rings. The cg of this package was taken to be 10 in. aft of the bolted connection, and its weight was estimated to be 50 lb for this analysis. A second package of equipment will be mounted at the aft end of the nozzle. The weight of this package was not known at the time of this analysis, but it is certain that the weight will not exceed 10 lb and that a 5 lb upper limit is entirely reasonable. The loads due to this equipment will be reacted by shear flow into the nozzle skin, and by very small membrane stresses in the nozzle longitudinal direction at the bolted flange.

The dual ring structure also reacts part of the loads from the internal equipment, such as, the actuator nitrogen storage tank and the actuator itself. Loads applied to the spike will also be transmitted into the combined inner shell-strut-outer shell structure. The structure is extremely redundant, and the preliminary analysis showed that approximately 50 percent of the loads went into the inner shell rings, while the remaining 50 percent was picked up by the outer shell rings. Due to uncertainty in these load fractions and further uncertainty in the load magnitudes, both sets of rings (inner shell set and outer shell set) were each sized to carry 75 percent of the applied loads from the internal structure. The weight of these internal parts plus the spike was estimated to be 150 lb for this analysis. Loads due to non-symmetric pressure loads arising from a 10 deg angle of attack at the spike were considered in this particular analysis.

4.2.2 Nozzle Cap

4.2.2.1 Structural Design

The nozzle cap was analyzed for the following conditions:

Normal operating condition

Pressure = 700 psia

Temperature = outside surface metal ranging from 400^0R to 900^0R, as indicated by thermal analysis

Proof pressure condition

Pressure = 1050 psi

Temperature = ambient

The proof pressure condition proved critical and formed the basis for the detail design.

The skin and tube structure is fabricated from Hastelloy X, with the following room temperature mechanical properties:

Ultimate stress = 114,000 psi

Yield stress = 65,000 psi

The allowable stress was taken as the lesser, or 85 percent of the yield stress, or 2/3 of the ultimate stress.

$$S_{allowable} = 0.85\ (65,000) = 55,100 \text{ psi}$$

A brief description of two nozzle cap designs that were considered is given below.

a. The initial design proposed was such that the force required to react the pressure thrust on the cap and to seat the main seal, be applied through the center of the cap. This would be done by structurally connecting the cap center to the inner shell through a bolt-tie bar arrangement.

b. The second design utilized a threaded flange connection between the end of the nozzle cap and the inner shell. The pressure thrust and the gasket seating load would be reacted through the total periphery of the inner shell (ref Drawing L-980604).

Transmission of the reacting loads through the center of the cap (design a above) resulted in a high axial concentrated load in the cap and in the connecting bolt and tie bar, causing excessive stresses in the skin. In addition, the accumulated axial deflection in the skin and tie bar would have exceeded, by a considerable amount, the compression on the main "K" seal (0.012 in.). The amount of skin reinforcing and additional tie bar metal cross-section required to reduce the stresses and deflections to acceptable levels would have resulted in higher temperatures and temperature gradients in the skin, as well as considerably increased component weight.

The second design (b), which carries the thrust load in the total periphery of the skin, proved to be far better. The center bolt and tie bar become essentially nonstructrual, and the size is governed purely by design considerations (i.e., flow passage required, locking device required, etc.). This, in turn, reduced the size of the hole required in the end of the cap (a 1/4-in. bolt can be used rather than the 5/8-in. bolt, which would have been required in design a), which results in less reinforcing at the center of the cap. There is no tendency for the pressure thrust to open up the seal because the load path is short and stiff.

The sealing load required for the main "K" seal is approximately 2300 lb. The inner shell ring mating with the seal was stiffened in order to resist this load. The maximum pressure (circumferential) stress in the 0.070-in. wall of the skin is 41,200 psi, which is well within the allowable. The threaded end of the cap was reinforced slightly, in order to accommodate the additional local bending stesses. The maximum axial stress (membrane plus bending) in the threaded end is 38,600 psi. The shear stress in the threads is less than 15,000 psi; again, well within the allowable.

4.2.2.2 Thermal Design

The design objectives were to evolve a cooling method that would (1) maintain nozzle cap exterior surfaces below 1000°R, (2) keep temperature difference between metal surfaces below 400°R, though localized values higher than 400°R can be tolerated, and (3) maintain a low coolant pressure drop, preferably under 10 psi. Aerodynamic heating parameters used in the analysis corresponded to the design flight condition of Mach 8, 81,000 ft altitude, and were obtained from Table 4.1-3, sheet 2. The hot gas convective heat transfer coefficient in the nozzle cap vicinity is 0.01 Btu/sec-ft^2-°R and the adiabatic wall temperature is 5300°R. A hydrogen flow of 0.34 lb/sec at 120°R and 600 psia is available to cool the nozzle cap surfaces. With these conditions, the pressure drop for the cap passages is 10 psi. This coolant subsequently cools the inner body surfaces.

A cross-section of the nozzle cap is shown in Figure 4.2-1. A coolant flow rate of 0.34 lb/sec is fed to the cap through a 5/8-in. ID tube. Eight oval holes (total area = 0.070 sq in.) near the end of the tube allow most of the coolant to flow directly into a channel formed by the cap hemispherical surface and a 0.025-in. thick baffle placed nominally 0.10 in. from the cap surface. The remainder of the coolant in the tube is fed through six 0.050-in.

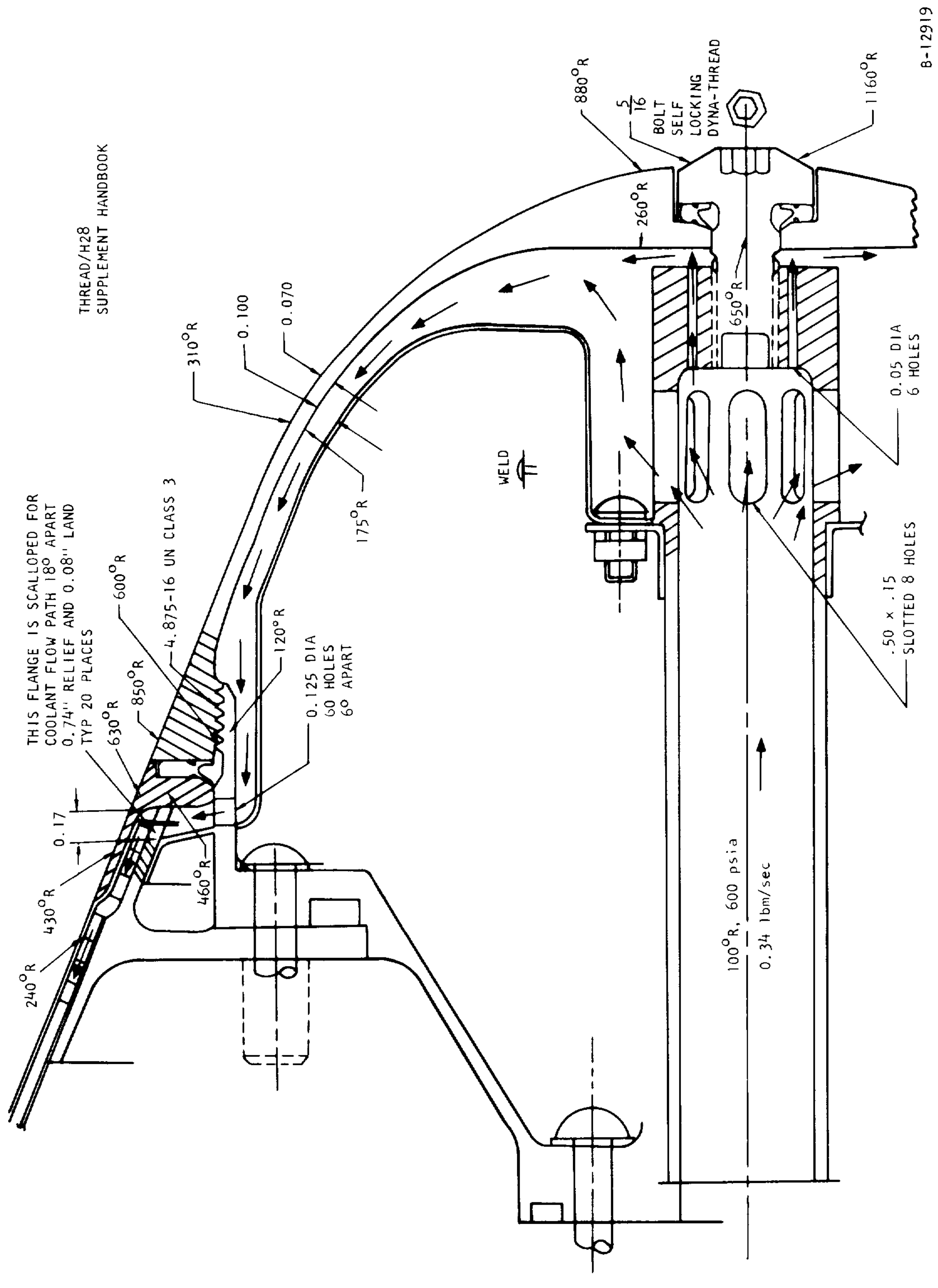

Figure 4.2-1. Cross-Section of Nozzle Cap

dia holes drilled through the solid end section of the tube. This coolant impinges on the inner surface of the nozzle cap tip, adjacent to the bolt, and provides forced convection coolant in the gap between tube and inner cap surface that would otherwise be filled with near stagnant coolant. Coolant leaves the nozzle cap through sixty holes of 1/8 in. dia adjacent to the threaded flange section and enters the rectangular offset fins in the aft inner body flow route.

Metal temperatures and coolant temperature and pressure are indicated in Figure 4.2-1. The maximum metal temperature (1160°R) occurs on the surface of the bolt exposed to the hot gas and the maximum metal temperature difference (700°R) occurs at the thick section of the threaded flange. A similarly high metal temperature difference of 620°R occurs at the thick wall section adjacent to the bolt. Although these temperature differences exceed the objective of 400°R, they are localized values. Generally, nozzle cap temperature differences are much less than 400°R, as indicated for the 0.070-in. thick metal section midway between the bolt and thread flange. The bolt temperature of 1160°R is not critical. The 1000°R temperature was arbitrarily established to provide ample assurance against overheating and maintain moderate metal temperature differences between nozzle cap and adjacent finned cooling jackets.

4.2.3 Bolted Flange/Manifold

4.2.3.1 Structural Design

Preliminary analysis of the nozzle-to-inner shell bolted joint was initiated during this reporting period. A cross-section of this joint (at about Station 65) is shown in Figure 4.2-2. One of the high stress regions for this joint area is the coolant ring-to-sandwich shell intersection, shown schematically in Figure 4.2-2a. Loads at this joint arise due to:

Differential thermal expansion

Internal coolant pressure

External (and possibly enternal) gas pressure

Inertia effects

The analysis conducted to date (but not completed) indicates that the ring design discussed below will sustain the applied loads but that the mating shell is highly stressed. The loads arising due to the requirement that ring and shell move together (continuity) affect the shell more than the ring by introducing discontinuity bending stresses in the shell.

Additional analysis is being conducted to determine stresses in the ring itself due to the internal pressure of the coolant (1050 psi proof pressure). Figure 4.2-3 shows the nozzle ring cross-section which appears to be adequate for internal pressure loads. Preliminary analysis of the quarter torus geometry, treated as a two-dimensional problem, gives a maximum bending moment of 126 lb-in. at the sandwich-to-quarter sphere joint. The bending stress at the corner

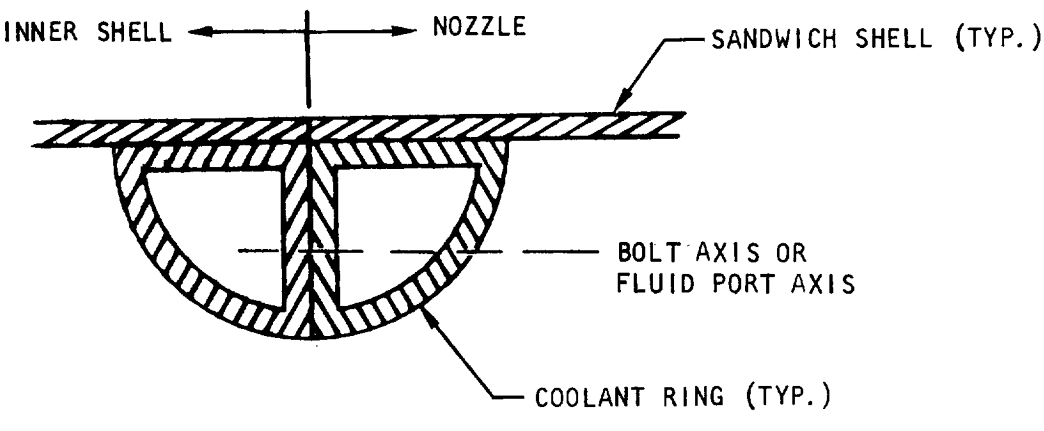

a. JOINT CROSS-SECTION

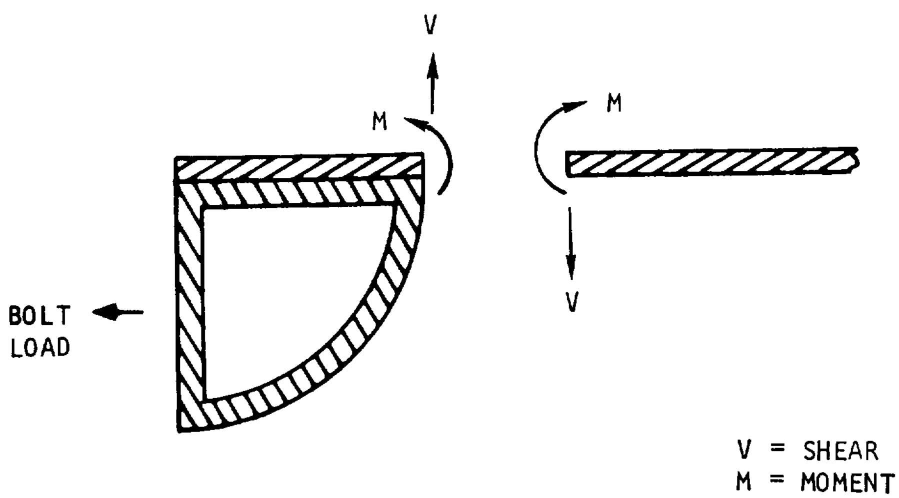

b. TYPICAL JOINT BREAKDOWN FOR ANALYSIS

A-27907

Figure 4.2-2. Nozzle-to-Inner Shell Detachable Joint

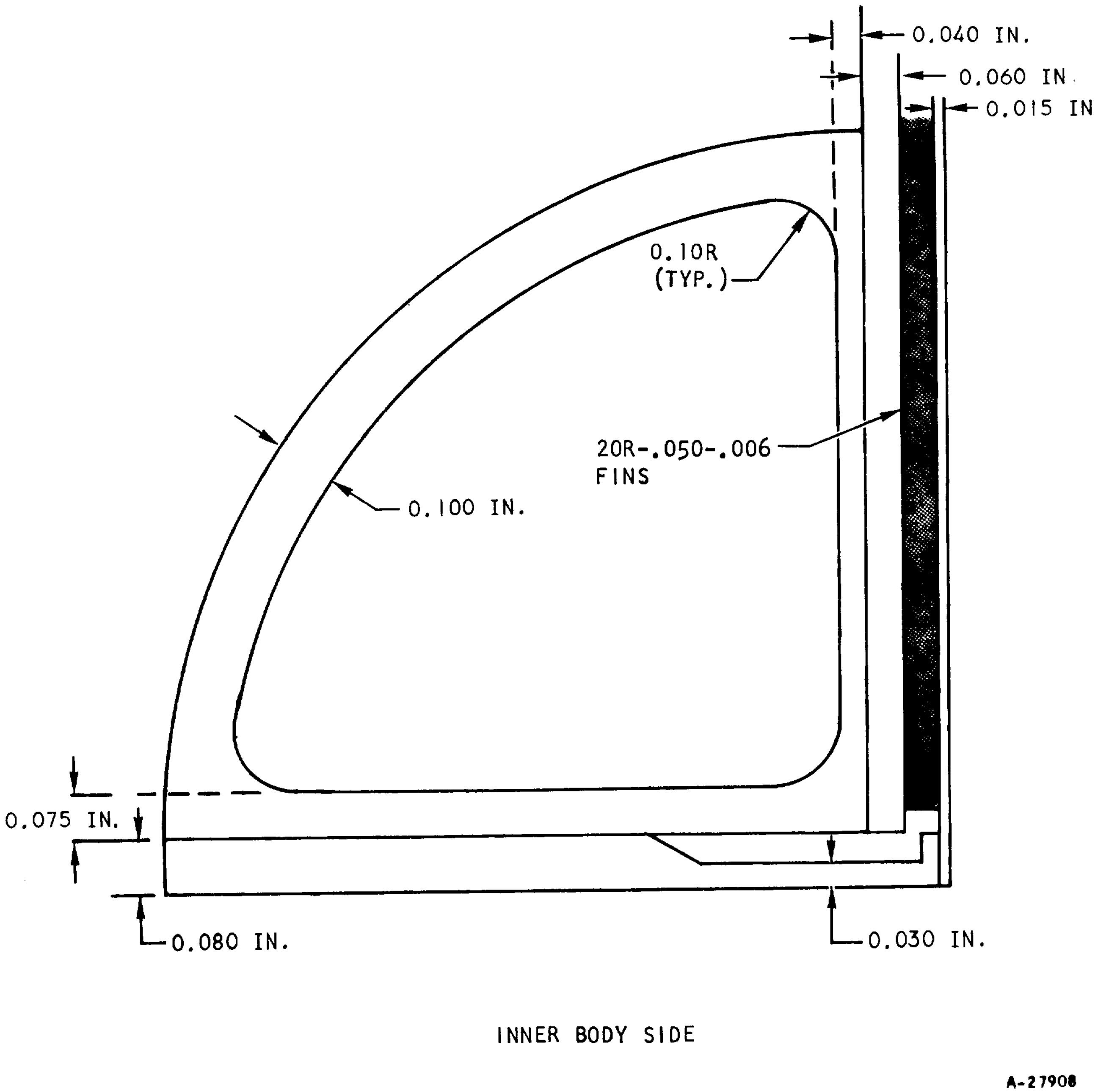

Figure 4.2-3. Nozzle Ring Cross-Section

for a ring of 0.100-in. thickness, will be 78,000 psi. A design value of 50 percent of this value was used, since a generous fillet will be used at the corner. (The bending moment decreases rapidly away from the corner.) A pressure test of this joint will be conducted to determine the adequacy of the design based on the dimensions shown in Figure 4.2-3.

The following is an outline of the calculations performed to estimate the ring material sizes required to contain internal fluid pressures up to a 1050 psi proof pressure.

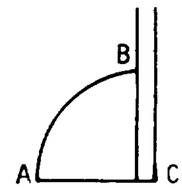

A-28043

a. <u>Results of Calculation</u> -

Maximum Bending Moments:

$$M_B = M_A = 0.12\ q$$

Assume the following for sizing $\overline{AB}$, $\overline{BC}$, $\overline{AC}$:

(1) Fillets at A, B, and C allow use of 50 percent of the maximum bending moment

(2) Stiffness of $\overline{AC}$ is 2 times either $\overline{AB}$ or $\overline{BC}$ to ensure validity of calculated results

(3) Design for q = 1050 psi proof pressure, $\sigma All \approx$ 40,000 psi

(4) Two-dimensional results are valid

(5) Fins and hot sheet of heat exchanger to be ineffective (for strength, but not for bending stiffness)

b. <u>Thickness Calculations</u> -

Are from A to B:

$$\sigma = \frac{M}{z} = \frac{6M}{t^2}$$

$$M = 0.06\ q = 0.06(1050) = 63\ \text{lb-in./in.}$$

$$t_{REQ} = \left(\frac{6M}{\sigma ALL}\right)^{1/2} = \left[\frac{6(63)}{40,000}\right]^{1/2}$$

$$t_{REQ} = 0.097\ \text{in.}$$

Segment $\overline{BC}$:

Use

$$\left.\begin{array}{l} t = 0.080 \text{ for ring} \\ t = 0.015 \text{ for back sheet} \end{array}\right\} \text{nozzle side}$$

$$\left.\begin{array}{l} t = 0.040 \text{ for ring} \\ t = 0.060 \text{ for back sheet} \end{array}\right\} \text{on inner shell side}$$

Segment $\overline{CA}$:

$$I = 2 \ \frac{0.10^3}{12} = 0.167 \times 10^{-3}$$

$$t_{REQ} = \left[12 \ (0.167 \times 10^{-3})\right]^{1/3} = 0.142 \text{ in.}$$

Consider

0.080 back piece

Use

0.075 ring segment

c. Shear and Bending Moment Results -

The shear and bending moment results are shown in Figure 4.2-4.

Figure 4.2-5 shows the structure assumed for this analysis. The requirement that the slope and deflection of the structure be zero (fixed end conditions) at C leads to a matrix in V_x, V_y, and M shown below.

Matrix to determine loads at C:

$$\left(\frac{1}{3I_2} + \frac{\pi}{4I_1}\right) V_x - \left(\frac{1}{2I_1}\right) V_y + \left(\frac{1}{2I_2} + \frac{1}{I_1}\right) M + \left(\frac{1}{8I_2} + \frac{1}{2I_1}\right) q = 0$$

$$- \left(\frac{1}{2I_1}\right) V_x + \left(\frac{\pi}{4I_1}\right) V_y - \left(\frac{1}{I_1}\right) M - \left(\frac{1}{2I_1}\right) q = 0$$

$$\left(\frac{1}{2I_2} + \frac{1}{I_1}\right) V_x - \left(\frac{1}{I_1}\right) V_y + \left(\frac{1}{I_2} + \frac{\pi}{2I_1}\right) M + \left(\frac{1}{6I_2} + \frac{\pi}{4I_1}\right) q = 0$$

q = internal pressure, psi

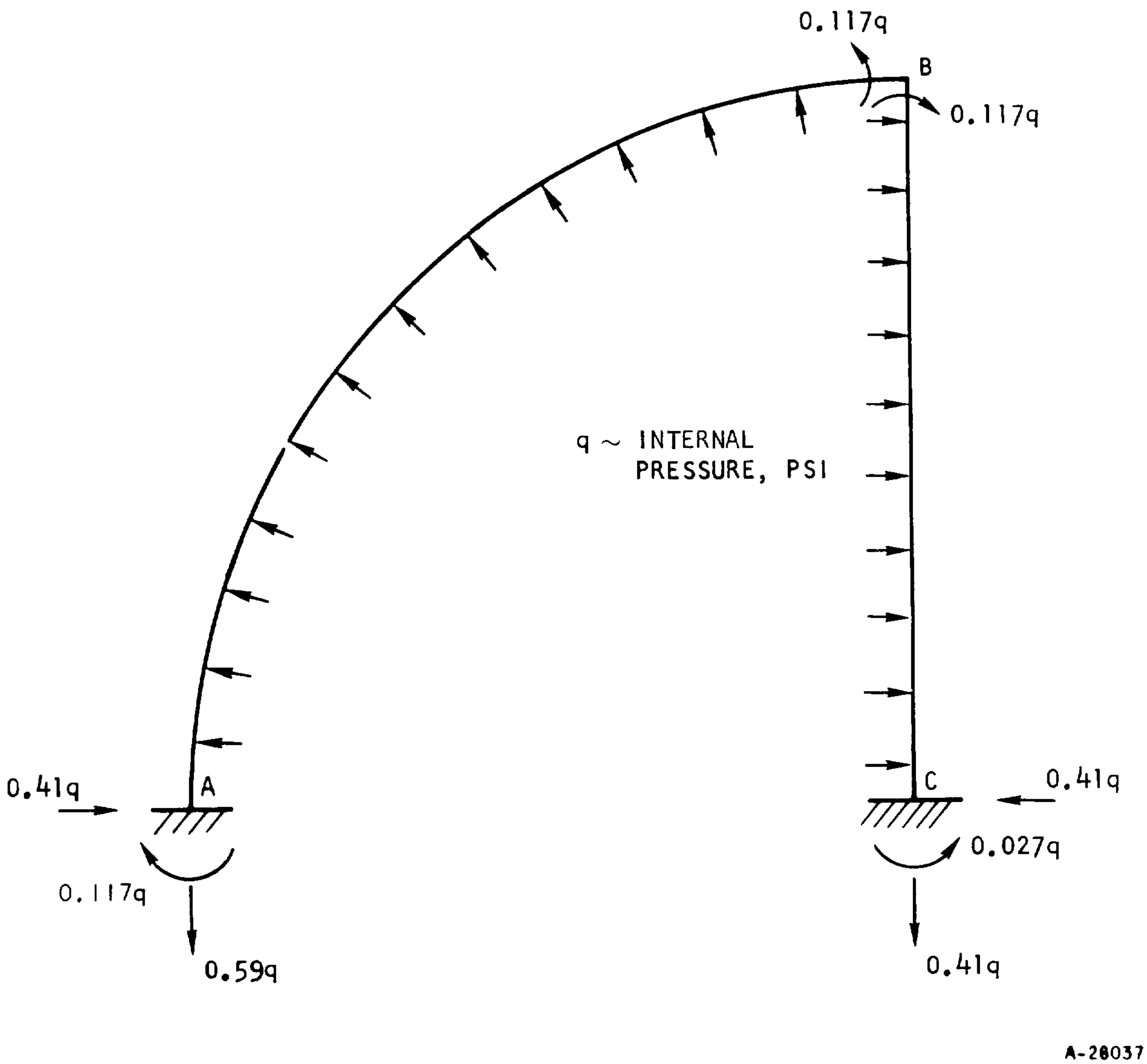

Figure 4.2-4. Shear and Bending Moment Results

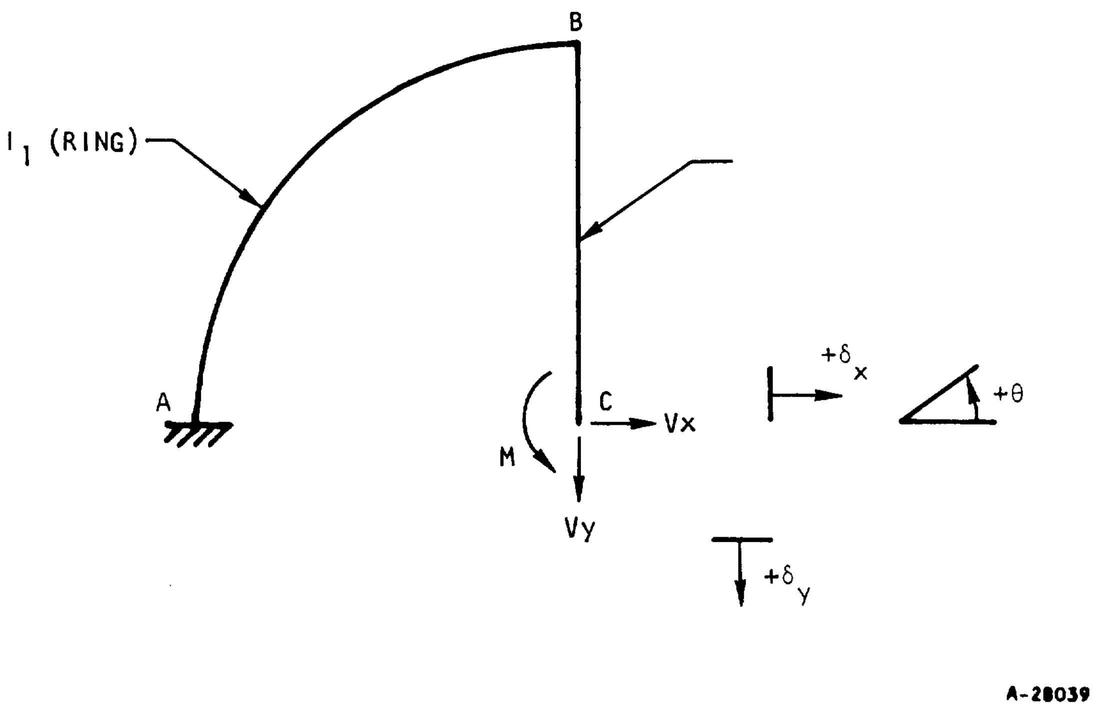

Figure 4.2-5. Structure Assumed for Analysis

For

$$I_1 = 8.33 \times 10^{-5} \text{ in.}^4/\text{in.} \quad (t = 0.10 \text{ in.})$$

$$I_2 = 14.5 \times 10^{-5} \text{ in.}^4/\text{in.}$$

$$V_x = -0.41\ q$$

$$V_y = 0.41\ q$$

$$M = 0.027\ q$$

4.2.3.2 Thermal Design

Results of a heat transfer and pressure drop analysis are presented for the bolted flange/manifold at axial Station 68.91 (Mach 8 geometry) on the HRE inner body. The objectives were (1) to size the coolant holes between halves of the flange/manifold so that a 10 psi pressure drop would occur, and (2) to determine whether metal surface temperatures are acceptable at the flange/manifold interface where no cooling fins are present. A sketch of the bolted flange/manifold is shown in Figure 4.2-6 with the results. Coolant in the nozzle flow route (0.34 lb/sec) is at 630°R and 535 psia in the 20R-.050 offset-.006 fins just prior to the flange/manifold. The aerodynamic hot gas heat transfer coefficient and adiabatic wall temperature are 0.046 Btu/sec-ft^2-°R and 5808°R, respectively, at Station 68.91, and correspond to the design flight condition of Mach 8 at 81,000 ft altitude.

Results of hole sizing and pressure drop are presented in Figure 4.2-6. Three hole size combinations were used in the analysis and were selected because they are compatible with fabrication. The second combination of hole sizes were selected for design because (1) these holes gave a pressure drop (8.85 psi) within the maximum allowable (10 psi) and (2) the two sets of 115 holes at 1/8 in. dia each gave a larger pressure drop than the common holes between manifolds (9 holes at 3/8 in. dia each), which is needed for good flow distribution in the fins.

Results of a heat transfer analysis indicate a flange/manifold interface surface temperature of 1260°R. Metal surface temperatures of adjacent fin cooled panels are 1170°R. Therefore, interface overheating or large temperature differentials with adjacent sections should not occur.

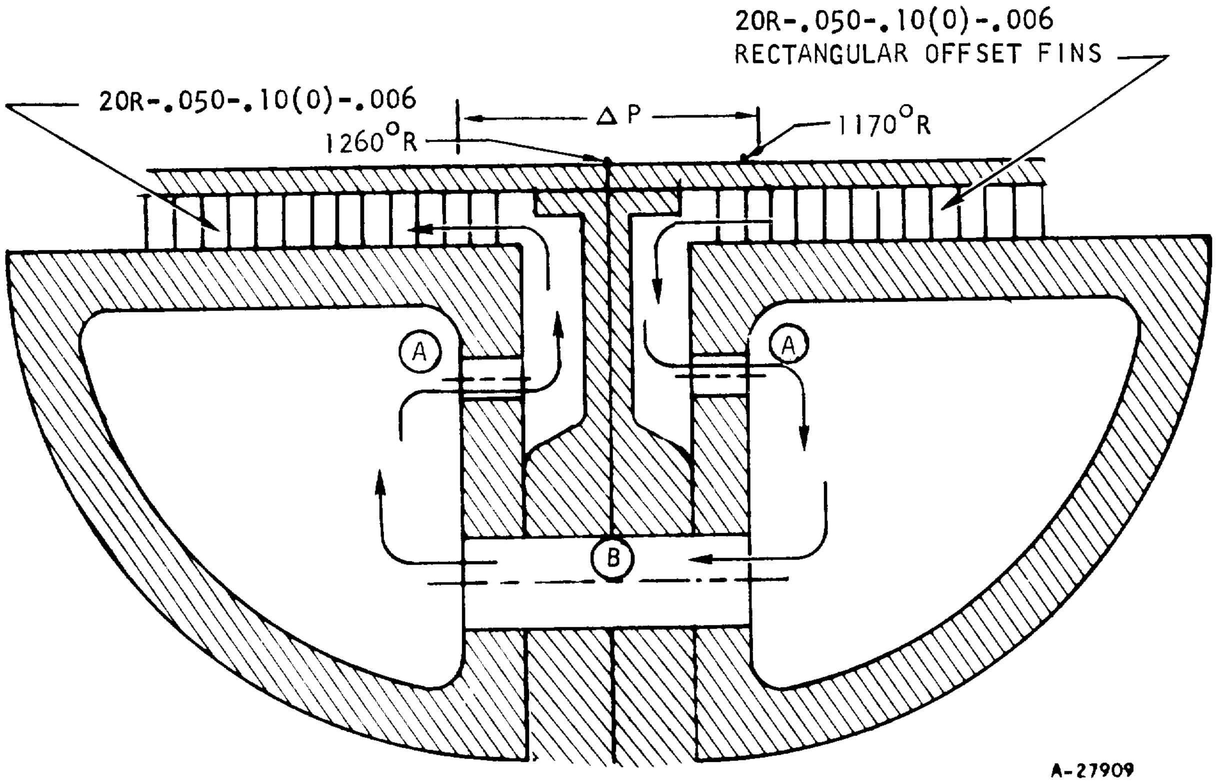

HOLES COMBINATION		HOLES GEOMETRY	TOTAL PRESSURE DROP
I	A	230 HOLES AT 1/8 DIA	3.8 PSI
	B	12 HOLES AT 3/8 DIA	
II*	A	115 HOLES AT 1/8 DIA	8.85 PSI
	B	9 HOLES AT 3/8 DIA	
III	A	230 HOLES AT 1/8 DIA	11.25 PSI
	B	12 HOLES AT 1/4 DIA	

*SELECTED FOR DESIGN

Figure 4.2-6. Bolted Flange/Manifold Hole Sizing and Thermal Analysis

4.3 INNER BODY - OUTER SHELL SUPPORT STRUT

4.3.1 Aerodynamic Heating

The aerodynamic heating conditions used for strut design correspond to the Mach 8, 81,000-ft altitude design point flight condition. The aerodynamic heating parameters for this flight condition were determined from Phase I aerodynamic hot gas conditions (Reference 1), except the hot gas total temperature was increased from 5400°R to 5840°R in the vicinity of the strut.

Aerodynamic heating data for the strut sides, from Computer Program H1940, is presented in Table 4.3-1. The average heat transfer coefficient over the strut sides from Table 4.3-1 is 0.093 Btu/sec-ft^2-°R. However, an average coefficient of 0.085 Btu/sec-ft^2-°R was used in the Phase II, Concept I design analysis prior to availability of the results presented in Table 4.3-1. This difference in average hot-gas coefficient and localized high values of hot-gas coefficient near leading edges accounts for the difference in strut sides flow rate between the Phase II, Concept I (0.094 lb/sec) and Concept II (0.165 lb/sec) design discussed in Paragraph 4.3.3.

Re-examination of the strut leading edge heating at the critical conditions of Mach 8, 81,000-ft altitude, has resulted in the calculation of leading edge stagnation heat flux approximately twice that of the Phase I calculations (2000 Btu/sec-ft^2 instead of 1000 Btu/sec-ft^2). The Mach 6, 68,000-ft altitude subsonic and supersonic combustion conditions will have heat flux of 1400 Btu/sec-ft^2 or less. The strut leading edge radius was later increased from 30 mils to 80 mils to reduce the heat flux at Mach 8, 81,000-ft altitude conditions to about 1400 Btu/sec-ft^2.

Significant factors accounting for the deviating results are (1) the somewhat different free-stream properties (the total temperature and pressure are slightly higher for the recent data), (2) the techniques to evaluate the gas properties behind the normal (bow) shock (the previous calculation considers the gas as air, while the gas properties for the recent analysis consider the water vapor in the mixture), (3) the difference in the analytical equations used, and (4) evaluated wall at total pressure downstream of shock. The previous calculation used Reshotko-Cohen, Reference 3, while the recent calculation used Fay-Riddell, Reference 4. The axi-symmetric stagnation solution was completed first, then the result was modified for two-dimensional effects. The resulting heat fluxes due to these methods could vary as much as 25 to 30 percent. Since Reference 4 solves the differential equations exactly at the stagnation point and is widely accepted, this method is preferred where critical heating exists. The final results and the input data for these two computations are presented in Table 4.3-2. These data are for equilibrium flow with a Lewis number of 1.0. When the Lewis number is 1.4, and considering only the $1/2\ H_2 + O_2 \rightarrow H_2O$ reaction, the total flux increases by 3 percent.

In addition to these two methods, other equations often used for the stagnation are from Lees, Reference 5, and Krieth, Reference 6. In order to compare the various available stagnation heating equations, heat flux and film

TABLE 4.3-1

STRUT SIDES AERODYNAMIC HEATING DATA (COMPUTER PROGRAM H1940 OUTPUT)

X (IN.)	SIN (IN.)	SOUT (IN.)	PSTAT (PSIA)	VEL (FPS)	TTOT (DEG R)	TSTAT (DEG R)	TWALL (DEG R)	TRECOV (DEG R)	TOTAL H (BTU/SEC.R FT SQ)	[redacted]	TOTAL FLUX (BTU/SEC FT SQ)	[redacted]	RADIANT FLUX (BTU/SEC FT SQ)	[redacted]
20.40	0.01	0.01	41.9	5004.	5840.	4998.	1799.	5780.	0.394	[redacted]	1569.	[redacted]	1.73	[redacted]
20.60	0.21	0.21	39.5	5104.	5840.	4938.	1780.	5775.	0.199	[redacted]	796.	[redacted]	1.42	[redacted]
20.80	0.41	0.41	37.1	5204.	5840.	4878.	1761.	5771.	0.169	[redacted]	678.	[redacted]	[illegible]	[redacted]
21.00	0.61	0.61	34.7	5304.	5840.	4818.	1742.	5767.	0.151	[redacted]	607.	[redacted]	[illegible]	[redacted]
21.20	0.81	0.81	32.3	5404.	5840.	4758.	1723.	5762.	0.137	[redacted]	555.	[redacted]	[illegible]	[redacted]
21.40	1.01	1.01	30.0	5500.	5840.	4700.	1704.	5758.	0.126	[redacted]	511.	[redacted]	[illegible]	[redacted]
21.60	1.21	1.21	30.2	5491.	5840.	4704.	1685.	5759.	0.122	[redacted]	498.	[redacted]	0.48	[redacted]
21.80	1.41	1.41	30.4	5483.	5840.	4709.	1666.	5759.	0.119	[redacted]	487.	[redacted]	0.51	[redacted]
22.00	1.61	1.61	30.5	5474.	5840.	4713.	1647.	5759.	0.116	[redacted]	479.	[redacted]	0.53	[redacted]
22.20	1.81	1.81	30.7	5466.	5840.	4717.	1628.	5760.	0.114	[redacted]	[illegible]	[redacted]	0.55	[redacted]
22.40	2.01	2.01	30.9	5457.	5840.	4721.	1610.	5760.	0.112	[redacted]	467.	[redacted]	0.57	[redacted]
22.60	2.21	2.21	31.0	5449.	5840.	4726.	1592.	5760.	0.111	[redacted]	[illegible]	[redacted]	[illegible]	[redacted]
22.80	2.41	2.41	31.2	5440.	5840.	4730.	1576.	5760.	0.109	[redacted]	458.	[redacted]	0.61	[redacted]
23.00	2.61	2.61	31.4	5432.	5840.	4734.	1560.	5761.	0.108	[redacted]	455.	[redacted]	0.64	[redacted]
23.20	2.81	2.81	31.6	5424.	5840.	4738.	1544.	5761.	0.107	[redacted]	452.	[redacted]	0.66	[redacted]
23.40	3.01	3.01	31.7	5415.	5840.	4742.	1528.	5761.	0.106	[redacted]	450.	[redacted]	0.68	[redacted]
23.60	3.21	3.21	31.9	5407.	5840.	4747.	1512.	5762.	0.106	[redacted]	448.	[redacted]	0.70	[redacted]
23.80	3.41	3.41	32.1	5398.	5840.	4751.	1496.	5762.	0.105	[redacted]	447.	[redacted]	0.73	[redacted]
24.00	3.61	3.61	32.3	5390.	5840.	4755.	1480.	5762.	0.104	[redacted]	446.	[redacted]	0.75	[redacted]
24.20	3.81	3.81	32.4	5381.	5840.	4759.	1464.	5763.	0.104	[redacted]	445.	[redacted]	0.77	[redacted]
24.40	4.01	4.01	32.6	5373.	5840.	4764.	1448.	5763.	0.103	[redacted]	444.	[redacted]	0.80	[redacted]
24.60	4.21	4.21	32.8	5364.	5840.	4768.	1432.	5763.	0.102	[redacted]	444.	[redacted]	0.82	[redacted]
24.80	4.41	4.41	33.0	5356.	5840.	4772.	1416.	5764.	0.102	[redacted]	444.	[redacted]	0.84	[redacted]
25.00	4.61	4.61	33.1	5348.	5840.	4776.	1400.	5764.	0.102	[redacted]	443.	[redacted]	0.87	[redacted]
25.20	4.81	4.81	33.3	5339.	5840.	4780.	1384.	5764.	0.101	[redacted]	443.	[redacted]	0.89	[redacted]
25.40	5.01	5.01	33.5	5331.	5840.	4785.	1368.	5764.	0.101	[redacted]	443.	[redacted]	0.91	[redacted]
25.60	5.21	5.21	33.6	5322.	5840.	4789.	1352.	5765.	0.100	[redacted]	443.	[redacted]	0.94	[redacted]
25.80	5.41	5.41	33.8	5314.	5840.	4793.	1336.	5765.	0.100	[redacted]	444.	[redacted]	0.96	[redacted]
26.00	5.61	5.61	34.0	5305.	5840.	4797.	1320.	5765.	0.100	[redacted]	444.	[redacted]	0.99	[redacted]
26.20	5.81	5.81	13.5	6519.	5840.	4147.	1304.	5719.	0.058	[redacted]	257.	[redacted]	-0.19	[redacted]
26.40	6.01	6.01	13.2	6576.	5840.	4136.	1288.	5718.	0.057	[redacted]	254.	[redacted]	-0.19	[redacted]
26.60	6.21	6.21	12.9	6633.	5840.	4126.	1272.	5717.	0.056	[redacted]	251.	[redacted]	-0.19	[redacted]
26.80	6.41	6.41	12.6	6689.	5840.	4116.	1256.	5716.	0.056	[redacted]	248.	[redacted]	-0.19	[redacted]
27.00	6.61	6.61	12.3	6746.	5840.	4105.	1240.	5716.	0.055	[redacted]	245.	[redacted]	-0.19	[redacted]
27.20	6.81	6.81	12.0	6803.	5840.	4095.	1224.	5715.	0.054	[redacted]	242.	[redacted]	-0.19	[redacted]
27.40	7.01	7.01	11.7	6860.	5840.	4085.	1208.	5714.	0.053	[redacted]	239.	[redacted]	-0.18	[redacted]
27.60	7.21	7.21	11.4	6917.	5840.	4074.	1192.	5714.	0.052	[redacted]	235.	[redacted]	-0.18	[redacted]
27.80	7.41	7.41	11.1	6974.	5840.	4064.	1176.	5713.	0.051	[redacted]	232.	[redacted]	-0.18	[redacted]
28.00	7.61	7.61	10.8	7031.	5840.	4053.	1160.	5712.	0.050	[redacted]	229.	[redacted]	-0.18	[redacted]
28.20	7.81	7.81	10.5	7088.	5840.	4043.	1144.	5711.	0.049	[redacted]	225.	[redacted]	-0.17	[redacted]
28.40	8.01	8.01	10.2	7145.	5840.	4033.	1128.	5711.	0.048	[redacted]	221.	[redacted]	-0.17	[redacted]
28.60	8.21	8.21	9.9	7202.	5840.	4022.	1112.	5710.	0.047	[redacted]	218.	[redacted]	-0.17	[redacted]
28.80	8.41	8.41	9.6	7258.	5840.	4012.	1096.	5709.	0.046	[redacted]	214.	[redacted]	-0.17	[redacted]
29.00	8.61	8.61	9.3	7315.	5840.	4002.	1080.	5708.	0.045	[redacted]	210.	[redacted]	-0.16	[redacted]

Notes:

1. X is axial distance from outer body leading edge (Mach 8 engine geometry).
2. SIN or SOUT are distance from strut leading edge along strut surface.
3. Leading edge tip heat flux not included in this table.

TABLE 4.3-2

STRUT LEADING EDGE HEAT TRANSFER FOR SUPERSONIC BURNING, M_∞ = 8.0, 81,000 FT ALTITUDE

Properties	Units	Data for Phase I Analysis	Data for Phase II Analysis	Consistent Data for Theories Comparison	Ref. (6) Kreith	Ref. (3) Reshotko and Cohen	Ref. (5) Lees	Ref. (4) Fay and Riddell
h	Btu/sec-ft²-°F	0.322	0.56	before	0.50	0.488	0.522	0.632
				aero				
q/A	Btu/sec-ft²-°F	1080	2060	data of	1720	1700	1800	2180
				3-9-67			140	190
Free Stream				ρ_o = 0.012 lb/ft³				
T_∞	°R	4000	4500	4100				
$T_{T\infty}$	°R	5400	5840	5450				
P_∞	psia	20	21.5	21.5				
U_∞	ft/sec	7000	6900	6900				
M.W.	lb/mole		24.5	24.5				
Aft of Shock			(equilibrium)					
T_2	°R		5670	5200				
T_{T2}	°R	5400	5740	5450				
P_2	psia	112	108	132				
P_{T2}	psia		132	165 (used in ρ_w)				
ρ_{T2}	lb/ft³		0.051	0.069				
Air μ_{T2}	lb/ft-sec		5.32×10^{-5}	5.05×10^{-5}				
u_2	ft/sec	1665	2000	2250				
M.W.	lb/mole		23.25	24.5				
γ_2	lb	1.13	1.14	1.25				
H_2	Btu/lb		2080	1980				
ρ_2				0.058				
Wall								
T_w	°R	2060	2060	2000				
ρ_w	lb/ft³	0.124	0.14	0.18				
Air μ_w	lb/ft²-sec	3×10^{-5}	3×10^{-5}	3×10^{-5}				
P_{r_w}		0.7 air	0.8 mix	0.8 mix				
H_w	Btu/lb		630	630				

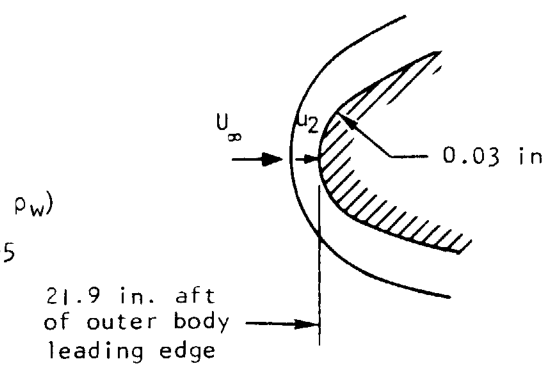

coefficients were computed with a set of consistent data. The results, together with the input data and the various equations, are also shown in Table 4.3-2. All calculations were made by assuming equilibrium flow, with a Lewis number of 1.0.

The chemical constituents behind the shock are as follows:

$H_2O \simeq 0.25$ mole fraction

$N_2 \simeq 0.61$ mole fraction

$NO \simeq 0.012$ mole fraction

$O \simeq 0.006$ mole fraction

$O_2 \simeq 0.013$ mole fraction

$OH \simeq 0.03$ mole fraction

$H_2 \simeq 0.05$ mole fraction

$H \simeq 0.02$ mole fraction

Although the quantities of all these species are known, in order to simplify the solution without introducing significant error, the viscosity of air was used while the specific heat values were weight averages of the nitrogen gas and water vapor.

The following symbols and subscripts apply to Table 4.3-2 and the equations given below.

Symbols

D = leading edge diameter, ft

H = enthalpy, Btu/lb

h = fil coefficient, Btu/sec-ft^2-^{o}F

k = conductivity, Btu/sec-ft-^{o}F

L = Lewis number, D ρ Cp/k

M.W. = molecular weight

Nu = Nusselt No. = $\frac{h\ D}{k}$

P = pressure, psia

Pr = Prandtl No. = $\frac{Cp\ \mu}{k}$

Re = Reynolds No. = $\frac{\rho\ u\ D}{\mu}$

r = leading edge radius, ft

T = temperature, ^{0}R

U = velocity, ft/sec

γ = specific heat ratio

μ = viscosity, lb/ft-sec

ρ = density, lb/ft^3

Subscripts

∞ = free-stream condition before shock (see sketch in Table 4.3-2)

f = properties evaluated at the arithmetic average temperature between the hot gas and the wall

T = total (otherwise static)

w = wall

2 = aft of the bow shock (see sketch in Table 4.3-2)

Equations

$$\frac{q}{A} = 1.14\, k_f \left(\frac{u_2}{D} \frac{\rho_f}{\mu_f} \right)^{\frac{1}{2}} Pr_f^{\,0.4} (T_{T2} - T_w) \qquad \text{(Reference 6)}$$

$$\frac{q}{A} = k_w \sqrt{\frac{\rho_w}{\mu_w}} \; \frac{Nu}{\sqrt{Re_w}} \; \sqrt{\frac{1.414\, u_2}{r}} \; (T_{T2} - T_w) \qquad \text{(Reference 3)}$$

$$\frac{q}{A} = \frac{0.664}{\sqrt{2}\, Pr_w^{\,2/3}} \sqrt{\beta\, \mu_{2T}\, \rho_{2T}} \; (H_T - H_w) \qquad \text{(Reference 5)}$$

$$\frac{q}{A} = \frac{0.76}{\sqrt{2}\, Pr_w^{0.6}} (\mu \rho)_w^{0.1} (\rho \mu)_{2T}^{0.4} \sqrt{\beta} \left| H_T - H_w \right| \left[H \left(L^{0.52} - 1 \right) \left(\frac{H_D}{H_{2T}} \right) \right]$$

(Reference 4)

$$\beta = \frac{du_e}{dx} = \frac{1}{r} \sqrt{\frac{288 \left(P_{2T} - P_\infty \right) g}{\rho_{2T}}}$$

4.3.2 Loads Analysis

The loads considered in the structural analysis of the strut body and strut mounting are as follows:

Internal pressure

Operating condition: 700 psia at operating temperature

Proof pressure condition: 1050 psia at ambient temperature

External pressure forces occurring at a flight mode of Mach 8 with a dynamic pressure of q_∞ = 2500 psf and an aircraft 30 degree angle of attack, spike fully extended (see Figure 4.3-1).

A 20-g inertia load acting in any direction with the mass centers as indicated below for the inner body.

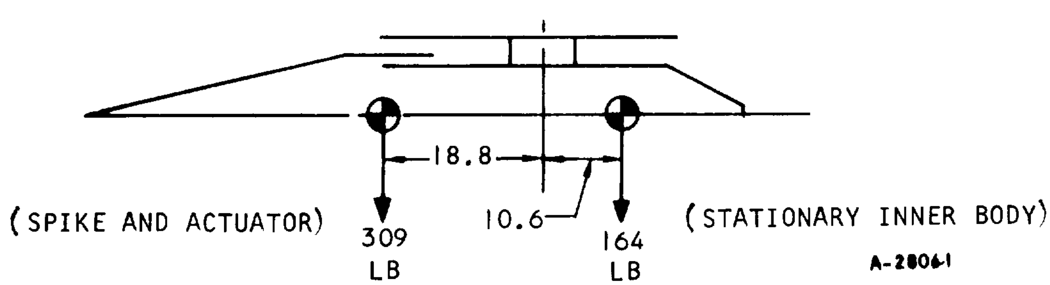

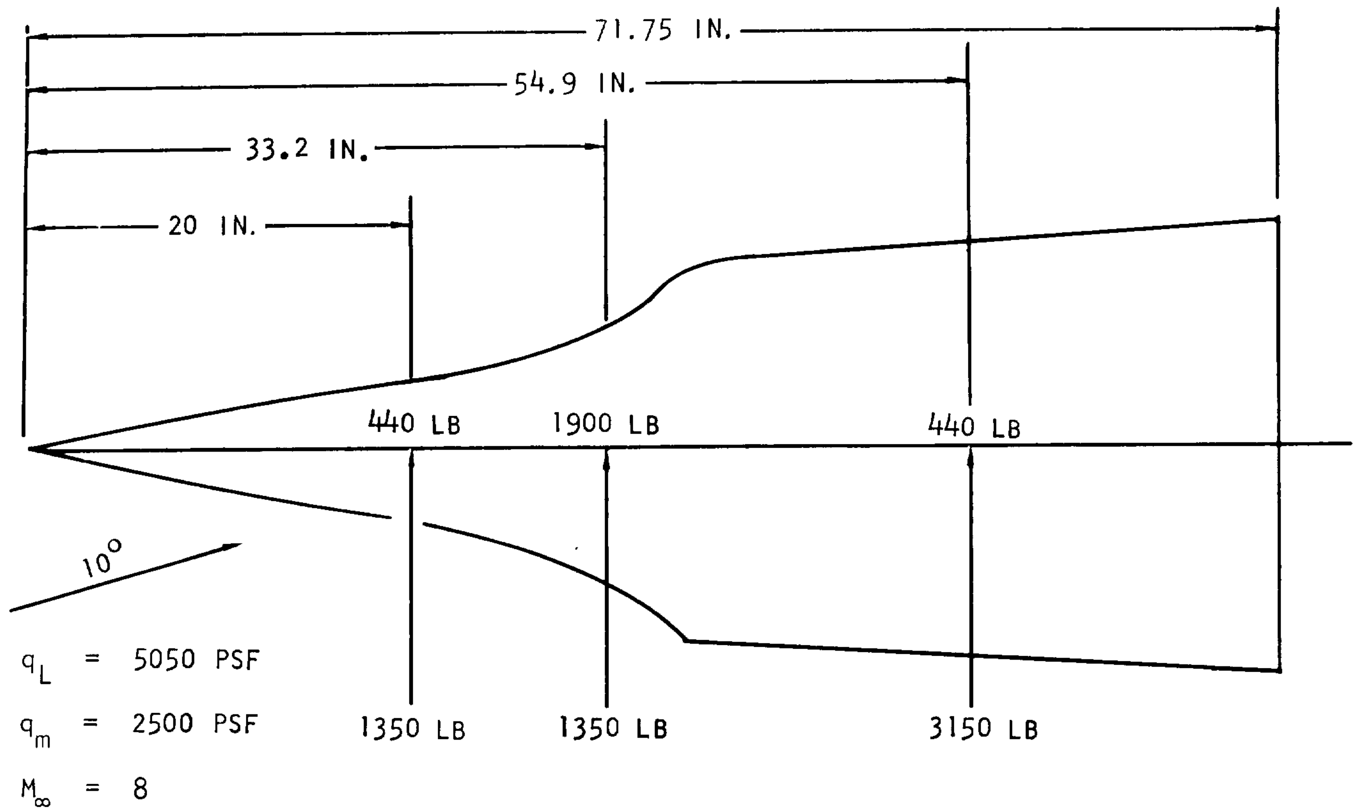

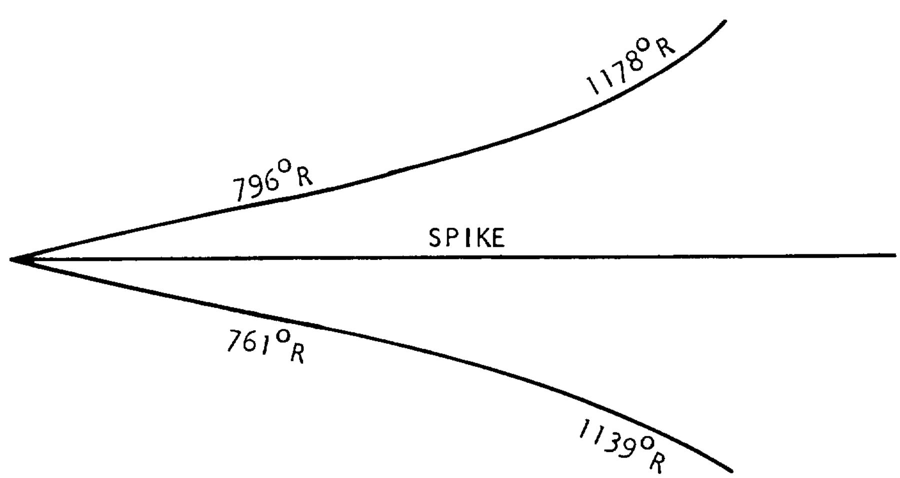

A-27897

Figure 4.3-1. External Force Distributions and Flow Temperatures

The strut body and mounting were checked for the following loading combinations:

a. The inertia and the external pressure load acting simultaneously in the vertical direction.

b. The inertia load acting in the horizontal direction with the external pressure load acting simultaneously in the vertical direction.

Condition b proved to be the critical condition and formed the basis for the detail design.

Spike-actuator loads were assumed to be reached at the four struts which support the actuator, while the stationary inner body loads were reacted by all six struts. Moment loads were reacted by axial shears in the struts at approximately the inner body radius, with lateral forces being reacted by radial loads in the struts.

4.3.3 Strut Cooling Design

The purpose of cooling design and analyses for the strut was to determine the simplest hydrogen coolant flow routing and passage geometry required to (1) maintain all aerodynamically heated surfaces temperature below 2060°R, (2) maintain structural temperature differences between strut and adjacent inner body and outer shell below 300°R, (3) provide a coolant pressure drop less than 100 psi, and (4) keep fin temperature differences generally below 400°R (higher localized fin temperature differences are acceptable).

The latest strut design (Phase II, Concept II) is shown in Dwg L-980608 and schematically in Figure 4.3-2. This design was developed from two previous designs: (1) the Phase I strut design, and (2) a design considered at the start of Phase II (Concept I). Coolant for strut sides is taken from the aft outer shell (flow Route 6) at the structural support torus, which is located at axial Station 69 in the Mach 8 geometry, and delivered to the aft of each of the six struts. The flow to the strut sides is distributed to 20R-.020-plain-.003 rectangular fins that are oriented parallel to the engine axis. Coolant flow paths on the sides are not identical with respect to the strut inner body because of space limitations (see Dwg L-980608). The trailing edge is cooled with coolant flowing through 0.020-in. deep grooves milled into the 3/8-in. radius semi-cylindrical trailing edge. The trailing edge coolant subsequently provides coolant for one strut side. Coolant leaves the strut sides at about one inch aft of the leading edge and is routed directly to the inner body fuel plenum. The strut leading edges are cooled separately from the sides with 100°R coolant flowing through a 0.13 in. dia circular passage adjacent to the 0.015 in. thick leading edge wall. Coolant from the six strut leading edges is collected and delivered to the aft inner body at the nozzle cap (flow Route 2). The leading edge radius has been increased to 0.08 in. from 0.03 in. shown in the two previous designs. An increased leading edge radius reduces the hot gas stagnation point heat flux, provides more coolant passage free flow area and reduced coolant pressure drop. Neither coolant

Design Schematic (Strut Sides / Leading Edge)	Advantages	Disadvantages	Aero Heating Parameters Used in Analysis	Coolant and Pressure Drop Requirements
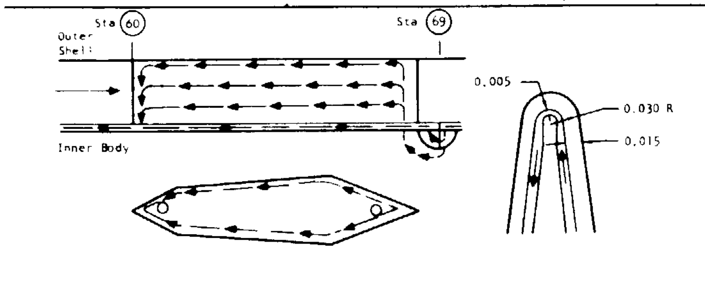 Phase I (Dwg No. 950007)	1) Acceptable structural ΔT's with inner body and outer shell (<300°R) 2) Surface temperature and fin ΔT's OK except at L.E. with 2180 Btu/sec ft² L.E. heat flux	1) 0.005" gap at L.E. unacceptable to manufacturing 2) Coolant concept cannot cool L.E. under new heat flux conditions (2180 Btu/sec ft²) 3) Recombination of strut flow and inner body flow at station 60 unacceptable to manufacturing	1) At L.E. tip, $q = 1080$ Btu/sec ft² 2) $H_{avg} = 0.065$ Btu/sec ft² °R $T_{aw} = 5400°R$ on sides. See ref 1 for details	1) 0.07 lb/sec total for six struts including leading edges. Pressure drop = 50 psi. 2) 0.21 lb/sec in adjacent inner body passages or 0.28 lb/sec total in aft inner body route.
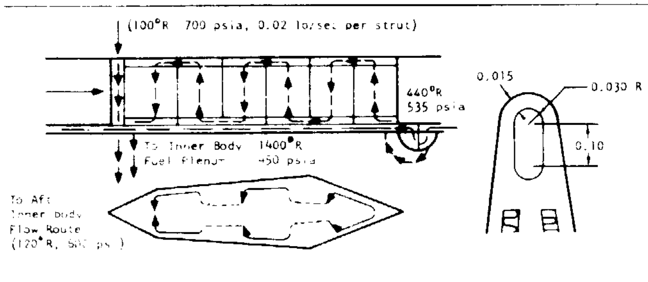 Phase II, Concept I (Dwg No. L-380605)	1) Acceptable structural ΔT's with inner body and outer body (315°R maximum excluding the effect of 100°R hydrogen in L.E. passage). 2) Surface temperatures and fin ΔT's OK	1) Leading edge tip temperature marginal (1980°R) 2) Strut manifolds reduce structural strength 3) Leading edge pressure drop marginal (OK if smooth transitions are made) 4) L.E. flow in parallel with remainder of aft inner body flow 5) L.E. metal ΔT's are approximately [illegible]00°R	1) At L.E. tip, $q = 2180$ Btu/sec ft² 2) $H_{avg} = 0.085$ Btu/sec ft² °R $T_{aw} = 5800°R$ on sides No details available	1) Side coolant = 0.094 lb/in. for six struts or 27% of aft inner body flow rate (0.34 lb/sec). Pressure drop = 85 psi 2) L.E. coolant = 0.13 lb/sec for six struts. Pressure drop = 100 psi if smooth transitions are used
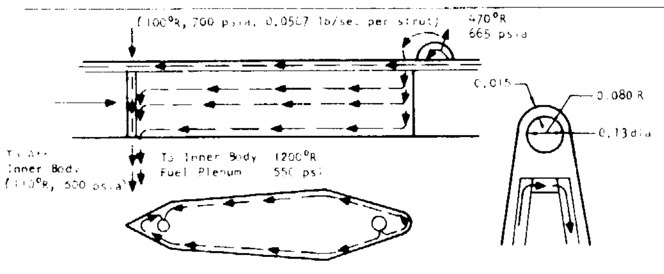 Phase II, Concept II (Dwg No. L-980608)	1) Acceptable structural ΔT's (<200°R), excluding 100°R hydrogen in L.E. passage 2) L.E. temperatures and pressure drop OK (no smooth transitions needed) 3) L.E. carries entire aft inner body flow. 4) Surface temperature and fin ΔT's OK 5) L.E. metal ΔT's are reduced to approximately 600°R.	1) Design problem to equalize flow on strut sides	1) At L.E. tip, $q = 1350$ Btu/sec ft² 2) $H_{avg} = 0.093$ Btu/sec ft² $T_{aw} = 5800°R$ on side See Table [illegible] for details	1) Side coolant = 0.165 lb/sec for six struts or about 25% of aft outer shell flow rate (0.[illegible] lb/sec). Pressure drop = 115 psi 2) L.E. coolant = 0.34 lb/sec for six struts or 100% of aft inner body flow rate. Pressure drop = 100 psi without smooth transitions

B-12922

Figure 4.3-2. Summary of HRE Strut Cooling Design from the strut sides nor adjacent inner body or outer shell flow routes can be used to cool the strut leading edge because the coupled effects of high temperature and low pressure of these coolant sources is insufficient to guarantee an acceptable leading edge maximum temperature and coolant pressure drop.

All surfaces of the strut design described above can be maintained below 2060°R. A maximum of 1930°R on the strut sides and 1370°R at the leading edge stagnation line have been calculated. Structural temperature differences are less than 300°R except at the leading edge where localized differences of up to 1000°R will occur because the 100°R leading edge passage coolant is in close proximity with 1200°R coolant in adjacent strut sides, inner body and outer shell (Figure 4.3-3). Fin temperature differences on the strut sides can be kept at about 400°R or less except in the fins adjacent to the leading edge passage where a difference of 560°R will occur. The wall temperature difference of the leading edge tip is estimated at 600°R.

The coolant required for the sides of the six struts is 0.165 lb/sec with 470°R, 665 psia inlet conditions and 1200°R, 550 psia outlet conditions and a coolant pressure drop of 115 psi. A coolant rate of 0.0567 lb/sec is supplied to each of the six strut leading edges with 100°R, 700 psia inlet and 120°R, 600 psia outlet conditions. A total coolant rate of 0.34 lb/sec for all six struts is more than the minimum rate required to keep the leading edge tip temperature at 2060°R. An excess of coolant is used because 0.34 lb/sec is required to adequately cool the inner body (flow Route 2) and at the same time provide ample assurance against leading edge overheating due to uncertainties in hot gas heat flux.

The Mach 8, 81,000-ft altitude design point flight condition (which the Phase II, Concept II design presented herein is based on) has been superseded by a new design point at Mach 8, 88,000 ft altitude. Although the aerodynamic heating parameters for this new design point have not been determined, it is estimated that the hot gas heat fluxes on the strut sides will be about 20 percent lower than at the Mach 8, 81,000-ft altitude condition. Strut coolant consumption, maximum metal temperatures, and fin temperature differences should decrease accordingly and will be determined when the new aerodynamic heating data is made available.

4.3.3.1 Phase I Design

The strut design presented in Figure 4.3-2 (Phase II, Concept II) is an outgrowth of two previous strut designs, also presented in Figure 4.3-2 (Phase I) and Phase II, Concept I). The Phase I strut design was cooled with hydrogen from the aft inner body flow route at the bolted flange/manifold adjacent to the strut trailing edge (Station 69, Mach 8 geometry). The coolant was distributed to 20R-.020-.006 plain rectangular fins oriented parallel to the engine axis. Hydrogen cooling strut side surfaces also cooled leading and trailing edge surfaces. Coolant leaving the strut through a tube aft of the leading edge was redistributed to the inner body flow route at Station 60.

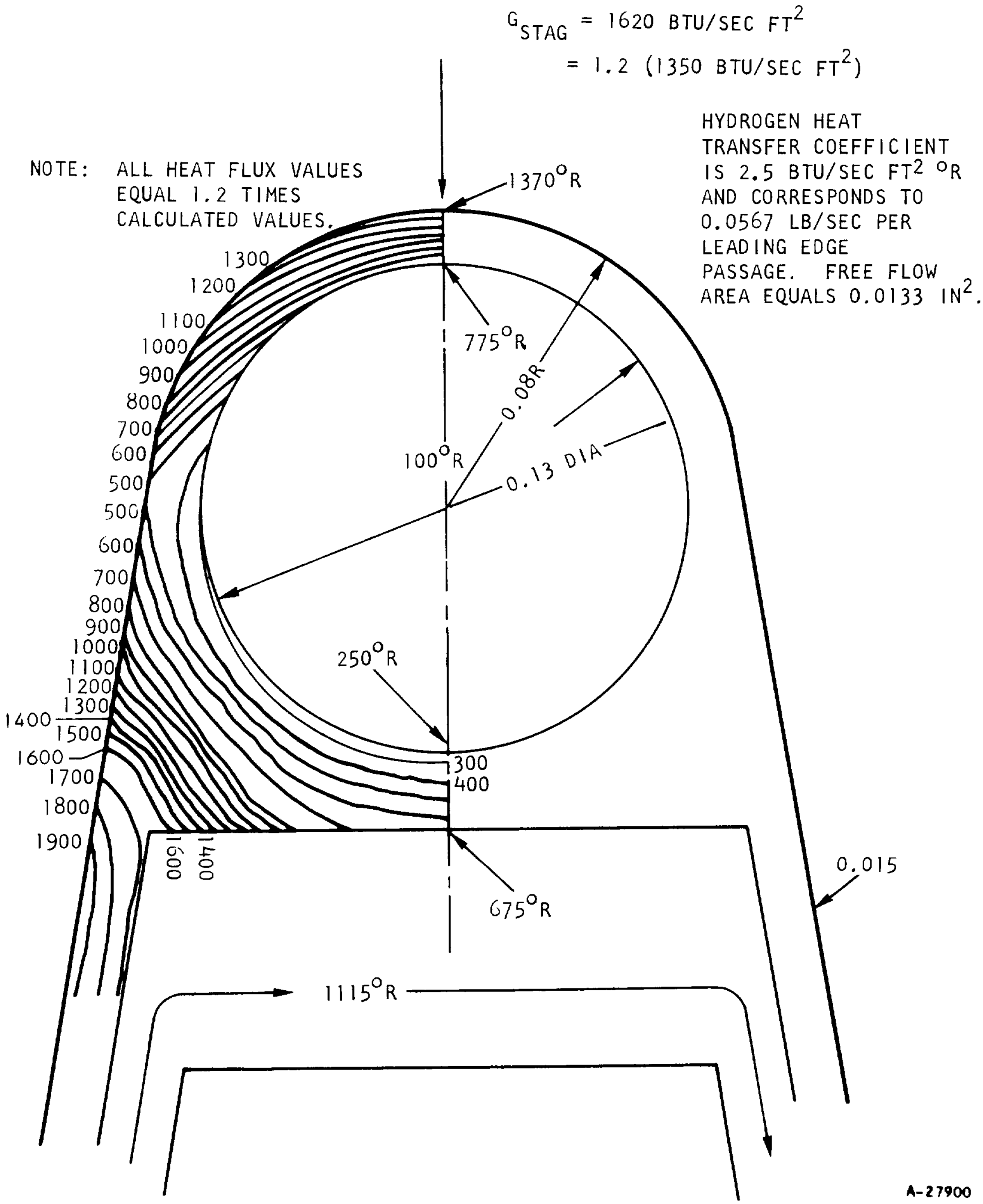

Figure 4.3-3. Leading Edge Temperature Isotherms, Phase II, Concept II Design

The disadvantages of the Phase I design are threefold. First, the 0.005 in. coolant passage clearance at the leading edge cannot be fabricated easily. The difficulty lies in maintaining this small clearance free from blockage. Second, the incident heat flux at the leading edge tip has been recently recalculated at 2180 Btu/sec-ft^2 (Reference 7) for the 0.03 in. radius or about twice the 1080 Btu/sec-ft^2 reported during Phase I. At a leading edge tip heat flux of 1080 Btu/sec-ft^2 coolant flow through the 0.005 in. clearance was sufficient to maintain leading edge tip temperature at 2060°R. However, for a tip flux of 2180 Btu/sec-ft^2, the coolant flow rate (0.036 lb/sec for each of six leading edges) is not high enough, and coolant temperature of about 1150°R not low enough to maintain the tip temperature at 2060°R or less.

The third disadvantage of the Phase I strut design is redistribution of strut flow into cooled surface panels in the inner body flow route at about Station 60. Coolant was to leave the strut through a tube oriented perpendicular to the engine axis just aft of each strut leading edge. Holes in these tubes allow strut coolant to flow into 20R-.050-.10(0)-.006 fins in the inner body flow route.

The manufacturing difficulties of this redistribution technique are considerable and most applicable for a brazed-in-place strut. Adoption of mechanically attached strut designs in Phase II, in addition to basic manufacturing difficulties, has caused this strut flow discharge technique to be discarded.

The major advantage of the Phase I strut design (retained in the chosen Phase II, Concept II design) was that it provided a low structural temperature difference between the strut and adjacent inner body and outer shell. Strut coolant flowed parallel to the engine axis and in the same direction as the adjacent inner body and outer shell flow routes, i.e., from aft to forward. Thus, the structural temperature difference between strut and inner body was approximately 100°R and slightly over 200°R between strut and outer shell (Reference 1).

4.3.3.2 Phase II, Concept I Design

The Phase II, Concept I design (Figure 4.3-4) is considerably different from Phase I in the following ways: (1) 20R-.020-.006 plain rectangular fins were oriented radially with respect to engine axis, and heater bars placed along the strut sides formed a multipass flow circuit (two, four, and six passes per strut side were investigated), (2) the leading edges were cooled separately from the sides with 100°R hydrogen, and (3) hydrogen coolant leaving the strut sides just aft of the leading edges were routed directly to the inner body fuel plenum. Coolant for strut sides enters the aft end of the strut from a mechanical joint torus at Station 69 on the inner body. Grooves (1/8 by 1/4 in.) milled into the strut structure, parallel to engine axis, and beneath the heated surfaces on the inner body and outer shell formed manifolds between coolant passes.

A two-pass flow circuit was considered because this gave the largest coolant flow width and allowed the entire inner body coolant flow to cool the struts, even though this coolant rate is more than required to cool the strut

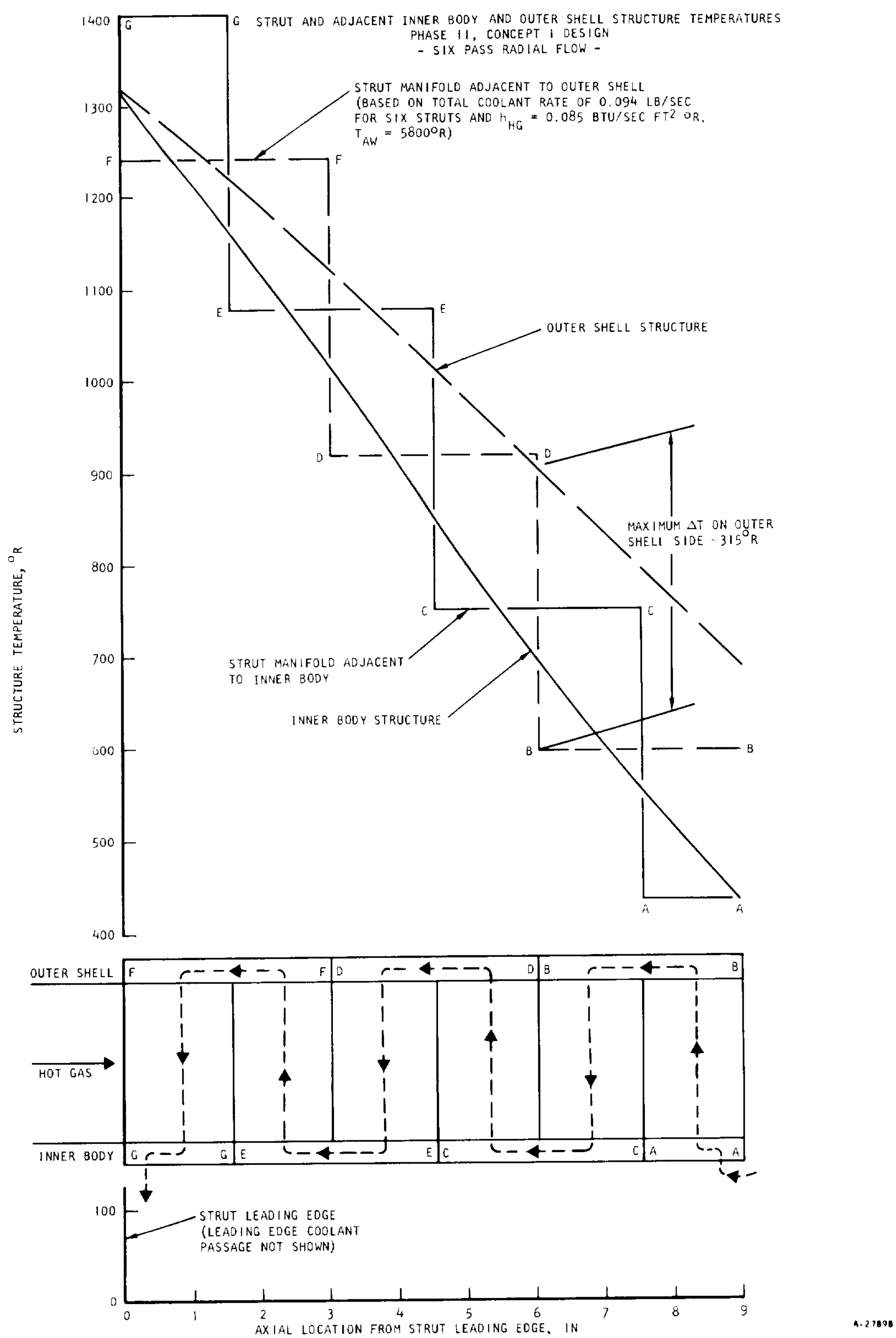

Figure 4.3-4. Strut and Adjacent Inner Body and Outer Shell Structure Temperatures, Phase II, Concept I Design

sides. Coolant leaving the forward end of the struts on the inner body side is routed back to Station 69 to cool the remainder of the inner body from Station 69 to 56. This cooling concept eliminates the difficulty in achieving a correct flow split between the strut and inner body by eliminating the parallel flow circuit used in the Phase I design. However, this concept has a disadvantage which overshadows its simplicity. Structural temperature differences between strut and adjacent inner body and outer shell exceed 300°R over most of the strut length and is locally 725°R just aft of the leading edge (excluding the effect of 100°R hydrogen in the leading edge passage). The manifold between passes and adjacent to the outer shell has a length almost equal to the length of the strut. The coolant in this manifold is approximately 600°R (nearly equal to structure temperature) while the outer shell structure temperature increases from 700°R at strut trailing edge to 1325°R at the leading edge. Increasing the number of passes to four increases the coolant pressure drop by over tenfold (half the flow width, double the flow length, plus four additional 90° turns) for the same flow rate, and does not substantially decrease temperature differences.

In order to decrease structural temperature differences, the strut coolant rate was decreased to one-third of the aft inner body coolant and the number of passes was increased to six. The coolant was split at the bolted flange/manifold on the inner body at Station 69, as in the Phase I design. In this concept, the simplicity of a series flow circuit between strut and inner body was eliminated in favor of a parallel circuit so that the six-pass radial flow would give structural temperature differences similar to one-pass axial flow. Structure temperatures of strut and adjacent inner body and outer shell for this concept are shown in Figure 4.3-4. Results indicate that the maximum temperature difference is 315°R and occurs between strut and outer body approximately 6 in. aft of the leading edge.

Coolant leaving the strut in this design (Phase II, Concept I) was routed directly into the inner body fuel plenum rather than back into the inner body flow route at Station 60. Using one-third of the inner body flow, the strut coolant pressure drop for six-pass radial flow is approximately 85 psi, while the coolant pressure drop in the inner body route is parallel with the strut (Stations 69 to 60) is 9 psi (at 0.23 lb/sec). To recombine these flows, the inner body flow route must have orifices with 76 psi (85-9 psi) pressure drop. However, to eliminate the need for orificing and to eliminate fabrication difficulties resulting from a flow recombination circuit, the strut flow is routed to the fuel plenum. If this flow routing were selected, the total inner body flow rate must be increased slightly above 0.34 lb/sec to provide adequate cooling from Stations 60 to 56 on the inner body in place of recombined strut flow.

Strut leading edges in both Phase II designs are cooled separately from the strut sides with 100°R hydrogen. Several leading edge cooling configurations proposed and considered are presented in Figure 4.3-5. Two of these

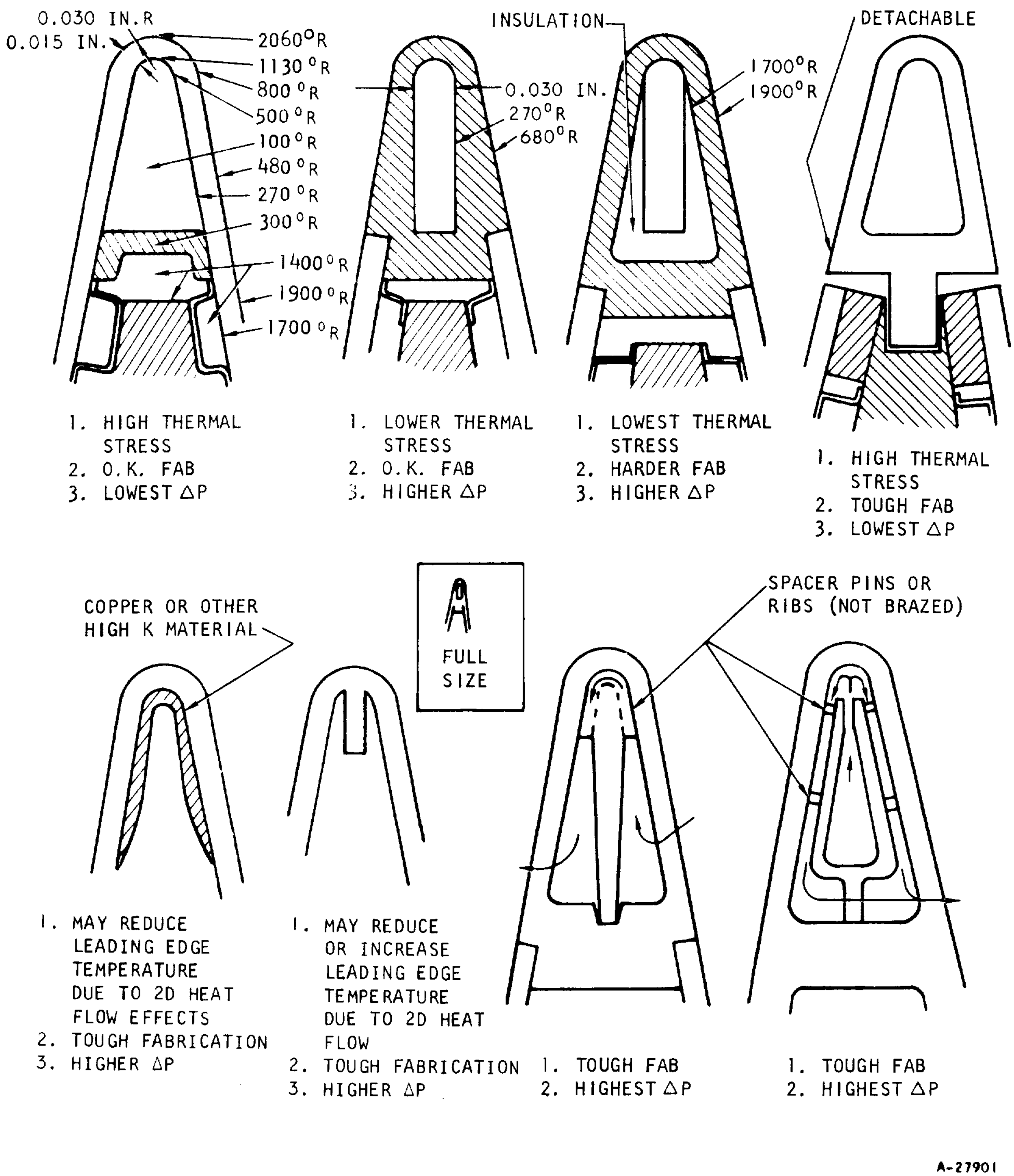

Figure 4.3-5. Strut Leading Edge Configurarions

configurations were analyzed in detail. The first analyzed configuration, shown in Figure 4.3-6, has the largest coolant free-flow area (0.0055 sq in.) with a constant metal thickness of 0.015 in. A two-dimensional steady-state heat transfer analysis was performed on this configurating using Computer Program H2530. The coolant heat transfer coefficient of 3.70 Btu/sec-ft^2-^{o}R corresponds to a coolant rate of 0.03 lb/sec per strut leading edge at 100^{o}R. Temperatures indicated in Figure 4.3-6 are results of this computer analysis. The tip temperature is acceptable (2010^{o}R), but the metal cross-sectional temperature difference is 1025^{o}R.

The second configuration, which was similarly analyzed using Computer Program H2530, is shown in Figure 4.3-7. The free-flow area of the configuration (0.0037 sq in.) was reduced to thicken metal cross-sections on the sides of the passage. Increased metal cross-section thickness provides more strength for pressure containment and thermal stresses, and gives higher side metal temperatures for lower temperature differences between leading edge tip and adjacent finned passages. The coolant heat transfer coefficient of 3.7 Btu/sec-ft^2-^{o}R corresponds to a coolant rate of 0.02 lb/sec per strut leading edge at 100^{o}R. Figure 4.3-7 indicates maximum metal temperature and maximum metal cross-sectional temperature difference at the tip are almost identical to the first configuration (Figure 4.3-6). Metal temperatures on the sides of the passage are about 300^{o}R higher than the first configuration.

Hydrogen at 100^{o}R was selected to cool the strut leading edges because it provides greatest assurance of an acceptable leading edge temperature and it is available from the turbopump at 100^{o}R and 700 psia. The pressure drop required to pump 100^{o}R coolant at 0.02 lb/sec through one leading edge (Figure 4.3-7) is estimated at 75 psi, exclusive of manifolding. The inlet and outlet velocity heads are 55 and 85 psi, respectively, so the pressure drop could be as high as 215 psi (one velocity head loss at inlet and outlet) if no provisions for smooth transition to and from the leading edge passage are made. If smooth transitions are fabricated, the inlet and outlet pressure losses can be minimized. However, smooth transitions cannot guarantee a pressure drop less than 100 psia. The leading edge flow (0.12 lb/sec total for six struts) is subsequently used to cool surfaces of the inner body and is connected in a parallel circuit with the remainder of the inner body coolant (0.23 lb/sec). The remainder of the inner body coolant is orificed by 100 psi to match leading edge pressure drop and routed through the interior of the strut before connection with strut leading edge outlet flow.

Hydrogen from the strut sides, the adjacent inner body, or the adjacent outer shell cooling jackets, which are at a higher temperature and lower pressure (approximately 300 psia, 500^{o}R) than supplied from the turbopump, cannot be used to cool strut leading edges because the decreased coolant density would cause the flow to choke (Mach no. equals unity) at the leading edge passage outlet. Choking at passage outlet limits the flow to a coolant rate that is less than required to adequately cool the leading edges.

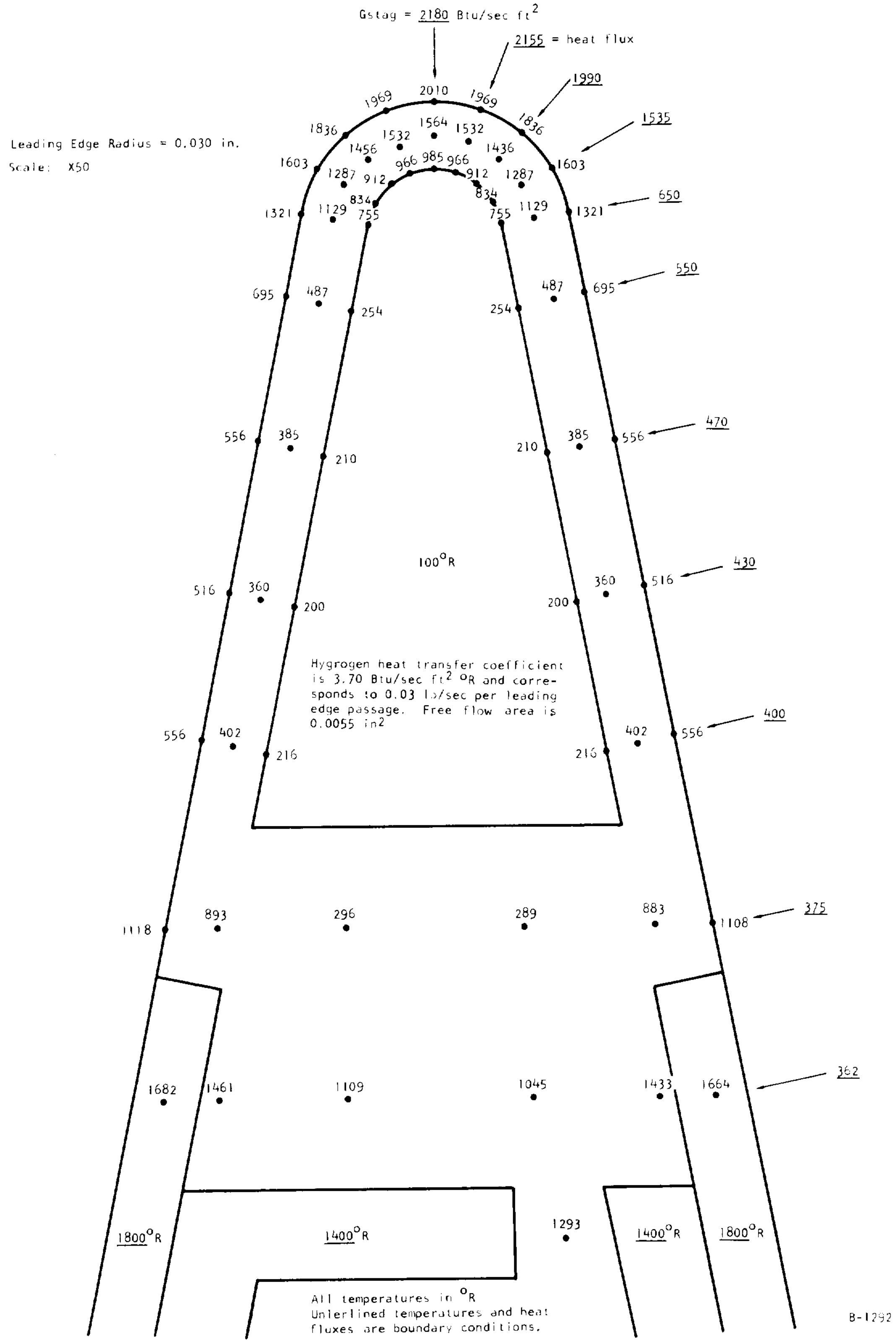

Figure 4.3-6. Strut Leading Edge Thermal Analysis

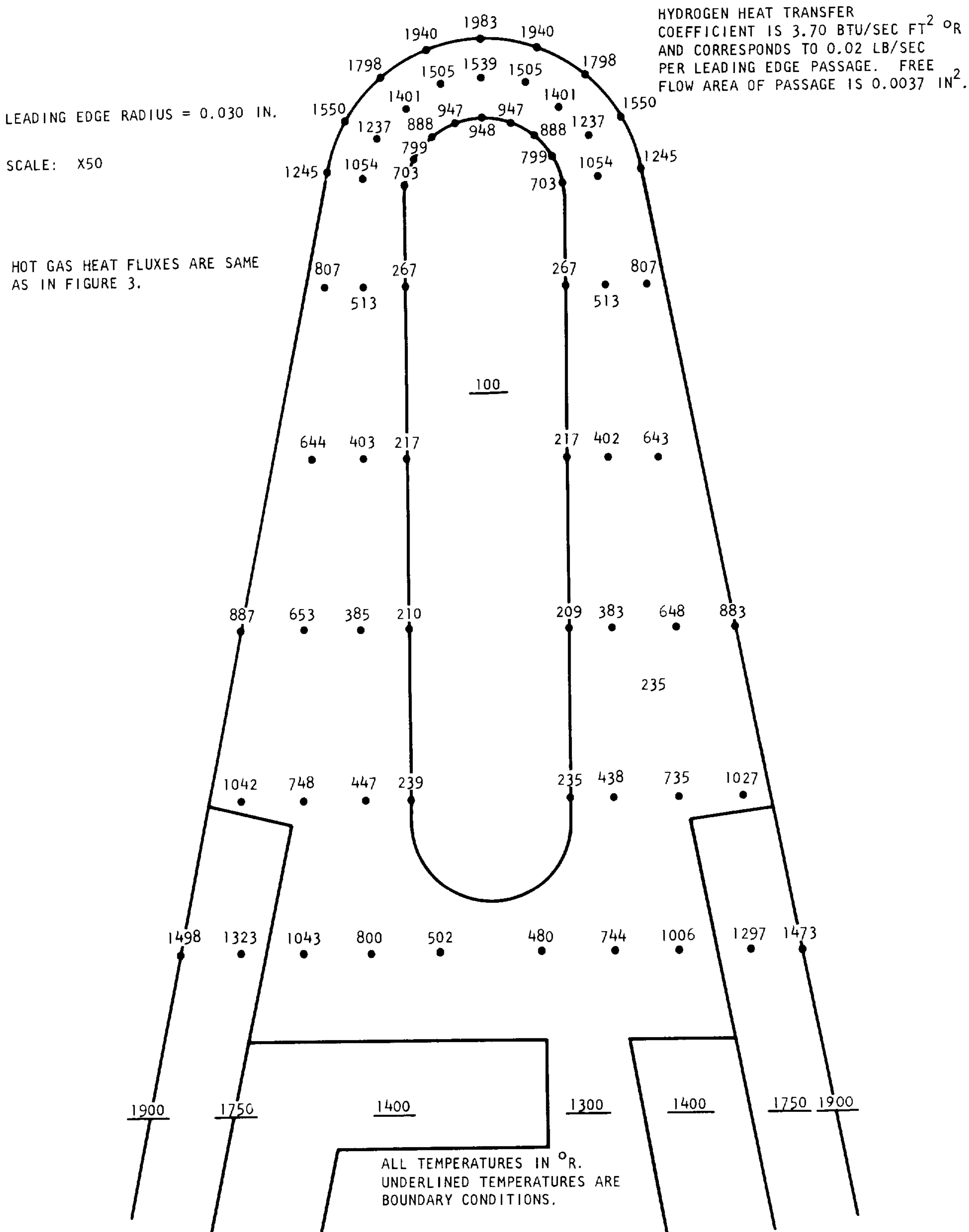

Figure 4.3-7. HRE Strut Leading Edge Thermal Analysis, Phase II, Concept I Design

In spite of several improvements made in the Phase II, Concept I design over the Phase I design, the Phase II, Concept I design is not completely satisfactory. To obtain a leading-edge coolant pressure drop of 100 psi, smooth converging and diverging transition pieces must be fabricated at each end of leading edge passages, respectively. Transition pieces are expensive and difficult to fabricate because an EDM process with close tolerances must be used. The outlet coolant Mach number in leading edge passages is about 0.5 with smooth transitions. If the free-flow area is reduced by as much as 30 percent,due to unexpected blockage or flow contraction, the flow will choke at outlet. If choking occurs, leading edge flow rate will decrease below the required 0.02 lb/sec per strut because leading edge flow is in a parallel circuit with the remainder of the inner body flow (fixed pressure drop). A decrease in leading edge coolant rate below 0.02 lb/sec cannot be tolerated because results of thermal analysis with 0.02 lb/sec in Figure 4.3-7 indicate a leading-edge tip temperature of 1983°R, or within 80°R of the maximum allowable temperature. Another disadvantage of the Phase II, Concept I design are the 1/4 by 1/8 in. manifolds on the sides of the struts. These manifolds reduce the structural strength of the struts. Thus, the thermal coolant distribution and structural characteristics of the Phase II, Concept I design are marginal.

4.3.3.3 Phase II, Concept II Design

The Phase II, Concept II design (Figure 4.3-2 and Dwg L-980608) has the following features that are different and/or similar to the two previous designs:

a. The leading edge radius is increased from 0.03 to 0.08 in. in two previous designs; the coolant passage is separate from side coolant passages as in Phase II, Concept I design but is circular with a 0.13-in. dia.

b. 20R-.020-.006 plain rectangular fins on strut sides are oriented parallel to engine axis, as in Phase I design (see discussion in Paragraph 4.3.3.1 for advantages of this concept).

c. Strut sides coolant is tapped off the aft outer shell flow route rather than the aft inner body flow route used in the two previous designs.

d. Coolant leaving the strut sides is routed directly to the inner body fuel plenum,as in the Phase II, Concept I design.

Figure 4.3-8 indicates the advantages of an increased leading edge radius. As radius increases, leading edge temperature and coolant pressure drop decrease substantially for similar coolant inlet conditions. Hot-gas heat flux at the leading edge decreases as the inverse square root of the radius increases. Also, as radius increases, the hot gas-to-coolant surface area ratio decreases for constant wall thickness. For example, for a 0.03-in. outside radius and a 0.015-in. thick wall, the hot gas-to-coolant area ratio is 0.030/0.015 or 2, while for a 0.08-in. outside radius and a 0.015-in. thick wall, the ratio is

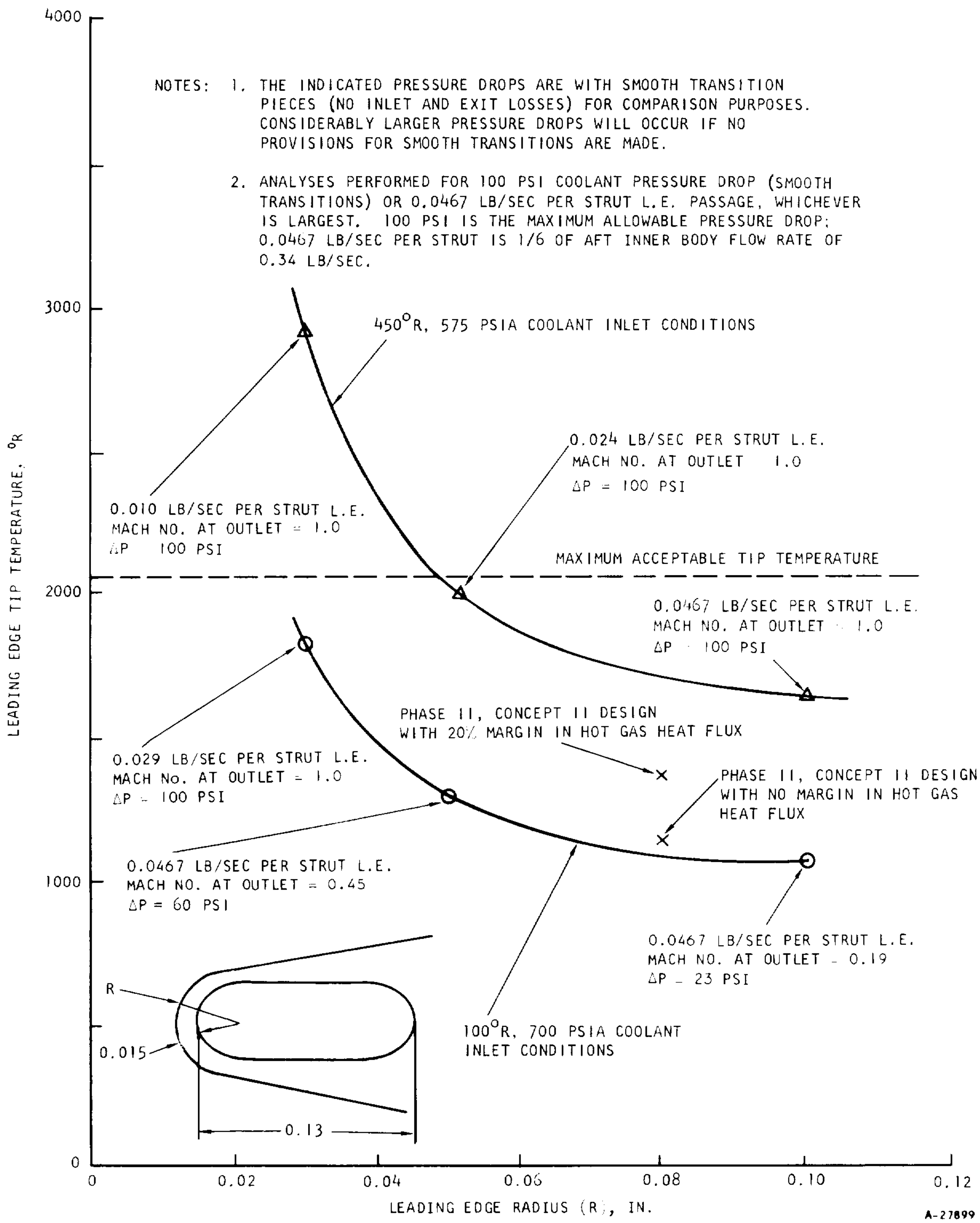

Figure 4.3-8. Strut Leading Edge Radius Variation

0.080/0.065 or 1.23. Coolant pressure drop decreases because the required mass flux is smaller and hydraulic radius is larger. Although the curves in Figure 4.3-8 correspond to an oval passage similar to Phase II, Concept I design, a circular passage of 0.13-in. dia was selected because it is much simpler to fabricate. Metal temperature isotherms in the circular leading edge section are shown in Figure 4.3-3. The leading edge tip temperature is about 600°R, or about 400°R less than in the Phase II, Concept I design.

In the Phase II, Concept II design, a structural support torus was placed on the outer shell adjacent to the trailing edge of the struts. Coolant for strut sides was taken from this torus because (1) coolant in this torus relieves transient thermal differentials between the torus and adjacent finned passages, (2) strut inlet manifolding is more accessible on the outer shell than on the inner body, (3) the geometry of the spike actuator mounting pad can be simplified, and (4) the outer shell flow route has a relatively small pressure drop, therefore, more coolant pressure drop can be allotted to the strut sides.

4.3.4 Structural Analysis

4.3.4.1 Leading Edge

The strut leading edge design was analyzed for pressure containment of 700 psi at operating metal temperatures, and for thermal stresses due to the large temperature variations that will occur. The initial design (Phase II, Concept I), which was to have used a 0.030-in. leading edge outside radius, showed critical stresses for both containment and thermal fatigue. The containment problem could have been improved by reducing the unsupported flat portion in the leading edge to a more reasonable value. However, plastic thermal strains due to the extreme temperature variations were estimated, and a cycle life expectancy of 100 full operating engine uses could not be achieved.

A second design (Phase II, Concept II) was adopted that will use a leading edge radius of 0.080 in. The containment stresses for this design are about 3500 psi, which is clearly acceptable, even for an operating maximum metal temperature of 1600°F. Preliminary estimates of temperatures indicate that the temperature profiles are greatly improved. Based upon a very cursory computation of cycle life, there appears to be no serious problem. A more comprehensive analysis will be conducted to properly assess the design margins, although the new strut leading edge should not be a source of difficulties.

4.3.4.2 Strut Body

The critical strut loading is as indicated below:

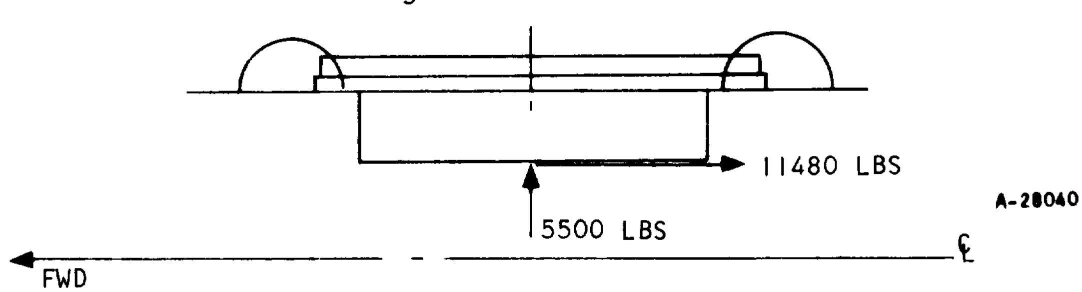

The critical bolt flange loads occur at the aft end of the strut where the design temperature was taken as 300°F. The allowable stress for the Hastelloy X strut was taken as 85 percent of the yield stress.

$$S_{allowable} = 0.85\ (58{,}000) = 49{,}500 \text{ psi}$$

The critically loaded bolt has a tensile load of 1470 lb and a shear load of 820 lb, which is well within the allowable for a 1/4 in. dia Inco 718 bolt. The maximum flange stress is equal to 42,100 psi.

The maximum tensile stress in the main body of the strut is 13,700 psi, while the maximum shear stress equals 4500 psi. Again, these are well within the allowable stresses at the operating temperatures.

4.3.4.3 Strut Mounting

The struts are integrally bolted to sockets which are brazed to the inner and outer shells. The bolts form adequate "shear ties" and it was considered that the sockets and strut resist bending as an integral member. Maximum stress in this section was previously noted in Paragraph 4.3.4.2. The sockets will have local ribbing where they junction with the rings in order to maintain structural continuity.

The high internal pressure in the structural rings (half circles, approximately two inches in diameter) necessitated a 0.060-in. reinforcing sheet adjacent to the shell in conjunction with a radial tie, which reduces the unsupported length along the shell to somewhat less than one inch. The maximum local stress in the reinforced ring (due to the proof pressure) was equal to 44,200 psi. The ring material is Hastelloy X with an allowable stress of 55,100 psi at room temperature.

The maximum radial load in the structural ring is equal to 4230 lbs, which results in a maximum moment (at the socket ring junction) of 7080 in.-lbs. This analysis takes into account the relief provided by the distortion in the shell. Shell shear and bending stresses proved to be negligible. The allowable stress in the ring is equal to 49,000 psi ($T \cong 225°F$). Since the ring is cut away at the socket-ring junction, a 0.125-in. reinforcing plate is required on the curved part of the ring. This results in a section modulus of 0.154 cu in. and a maximum bending stress of 46,000 psi.

4.4 OUTER BODY LEADING EDGE

4.4.1 Cooling Analysis

The purpose of the outer body leading edge thermal analysis was to find a leading edge configuration that is acceptable for temperatures, stress, and fabrication at the Mach 8, 81,000-ft design point. Some of the candidate designs and flow routings are shown in Figures 4.4-1, 4.4-2, and 4.4-3. These three design concepts (shown in Figure 4.4-1) have the entire forward flow of hydrogen (0.53 lb/sec) perpendicular to the leading edge, as shown in Figure 4.4-2, Concept 2. Concept 1 in Figure 4.4-1, has an additional flow of 0.008 lb/sec in each of two or four segments parallel to the leading edge. All of the leading edge configurations are about 7 in. long forward of the mechanical joint and have hydrogen coolant passages both on the interior and exterior surfaces. The mechanical joint allows for manifolding of various flow rates and temperatures, as shown in the four concepts in Figures 4.4-2 and 4.4-3. The flow routing concept and the temperature implications of each will be discussed prior to a discussion of the details of the small area adjacent to the leading edge stagnation line shown in Figure 4.4-1.

Of the four flow routes shown in Figures 4.4-2 and 4.4-3, the most satisfactory in all respects appears, at present, to be Concept 2. With Concept 2, the flow enters along the outside surface of the mechanically-attached section at 100°R, reaches a temperature of about 200°R at the leading edge, and about 550°R at the mechanical joint as it flows aft toward the outlet manifold. The flow length is about 7 in. from inlet to leading edge, about 7 in. from leading edge to mechanical joint, and about 11 in. from mechanical joint to outlet for a total length of 25 in. The flow length from inlet to leading edge was later reduced from 7 in. to 4 in. Concept 2 is beneficial because it has relatively simple flow routing and manifolding, as well as a moderate 500°R temperature difference between the inner and outer structural shell at the mechanical joint. Calculations reported in Tables 8-29 and 8-30 of Reference 1 indicate that Concept 2 was rejected at the time Reference 1 was prepared, because of fin ΔT greater than 500°R or ΔP greater than 100 psi. However, thermal stress now appears less with a fin ΔT up to about 580°R than with the axial sawtooth temperature profile (Figure A-80 of Reference 1) associated with Concept 1.

The flow routing for Concept 1 has 100°R hydrogen inlet at the mechanical joint and 1300°R outlet at the leading edge, combined with 1600°R outlet about 11 in. aft of the mechanical joint. The possibility of reducing the fin ΔT for Concept 2 below the 580°R indicated in Table A-30 of Reference 1 is small because the boilerplate combustor heat transfer test data show that heat flux greater than the values used in preparing Reference 1 may occur. Concept 1 is also undesirable because of the relatively awkward manifolding.

Concept 3 is undesirable because there is a difference of 1200°R between the hydrogen inlet manifold on the inner surface and the hydrogen outlet manifold for the leading edge lip at the mechanical joint. Another disadvantage of Concepts 1 and 3 is the need for an extra hydrogen outlet manifold in the crowded region at the mechanical joint, although the ducting for this manifold is not shown in Drawing 950009.

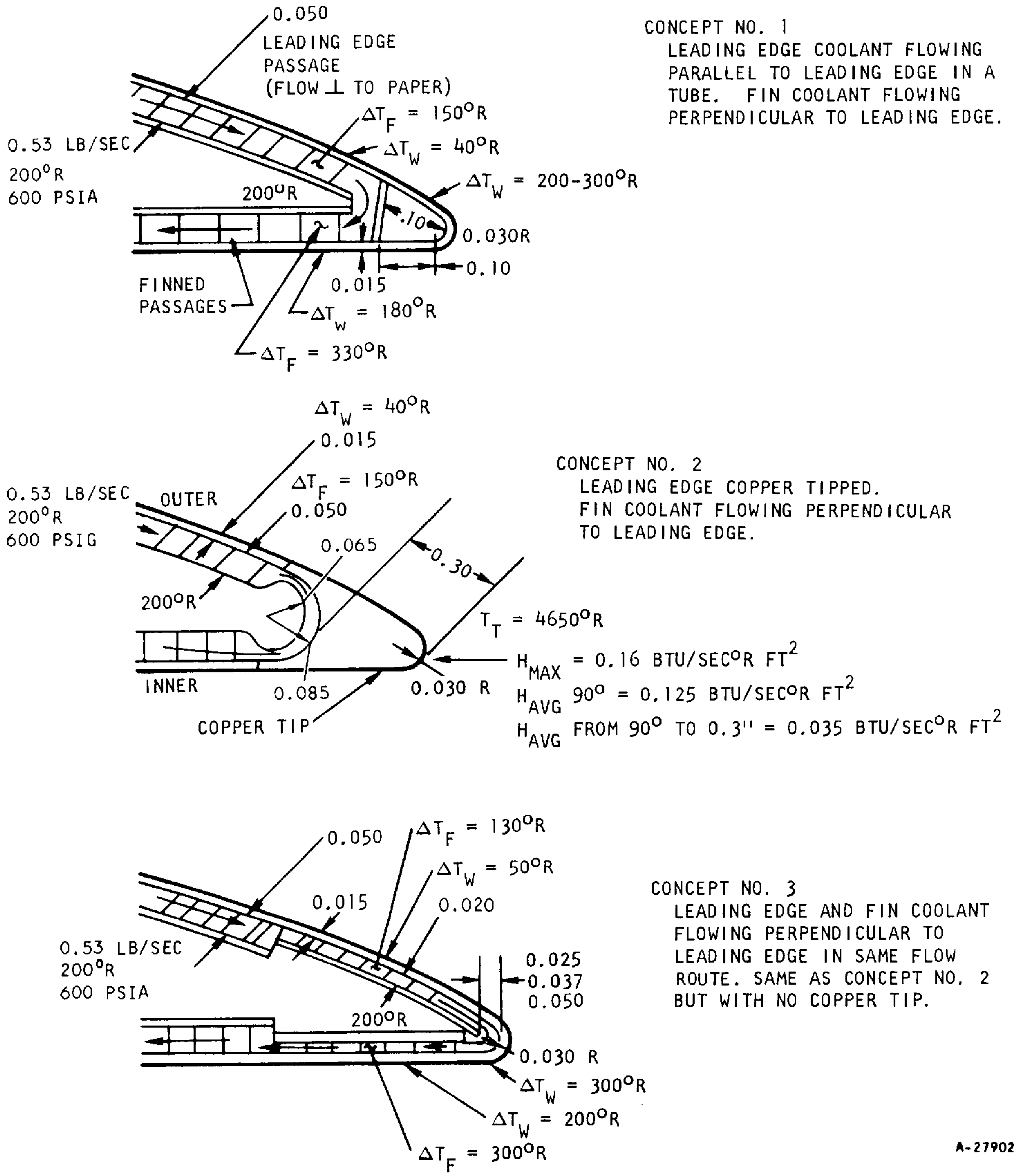

Figure 4.4-1. Outer Body Leading Edge Cooling Concepts

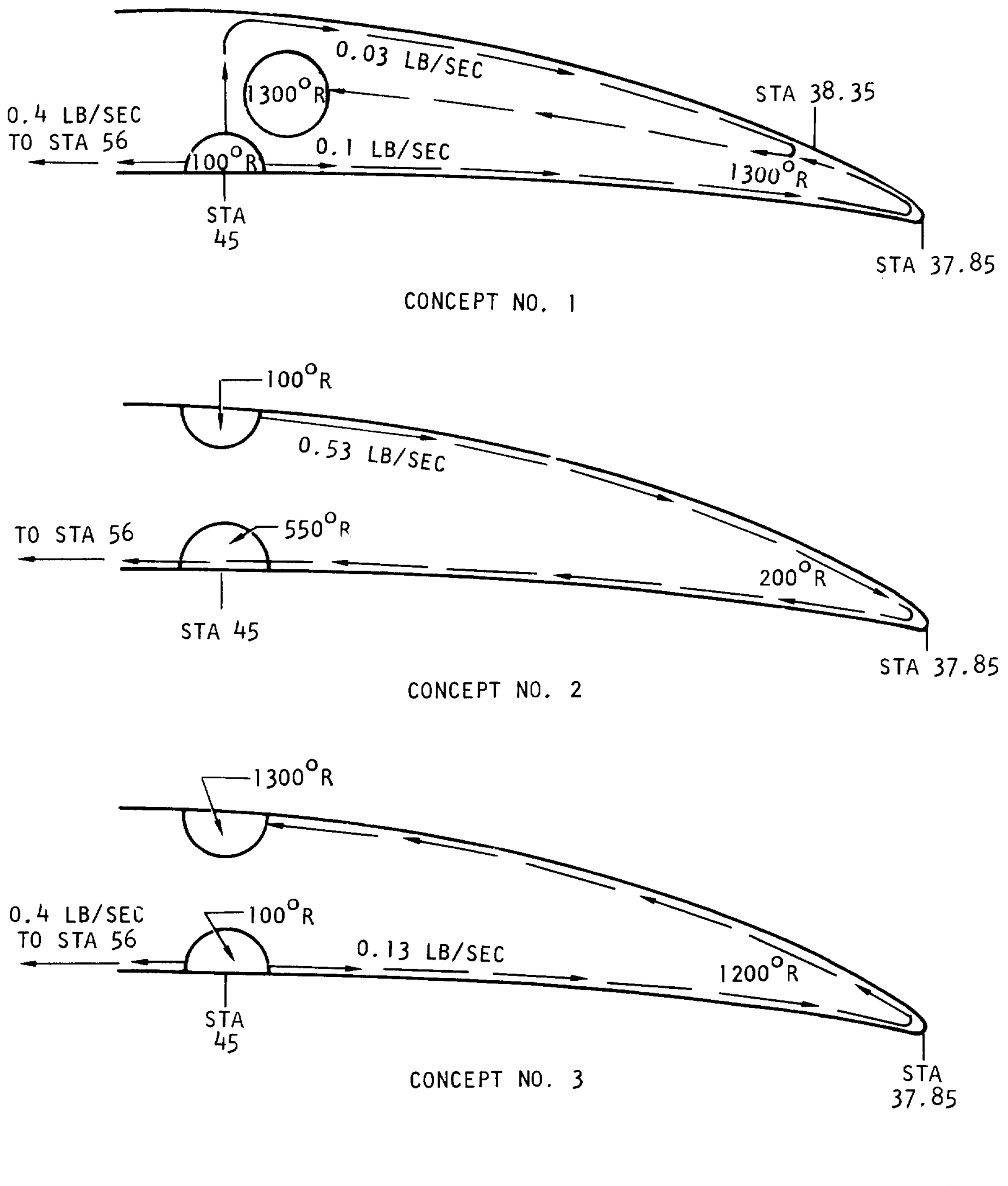

Figure 4.4-2. Outer Body Leading Edge Flow Route Concepts

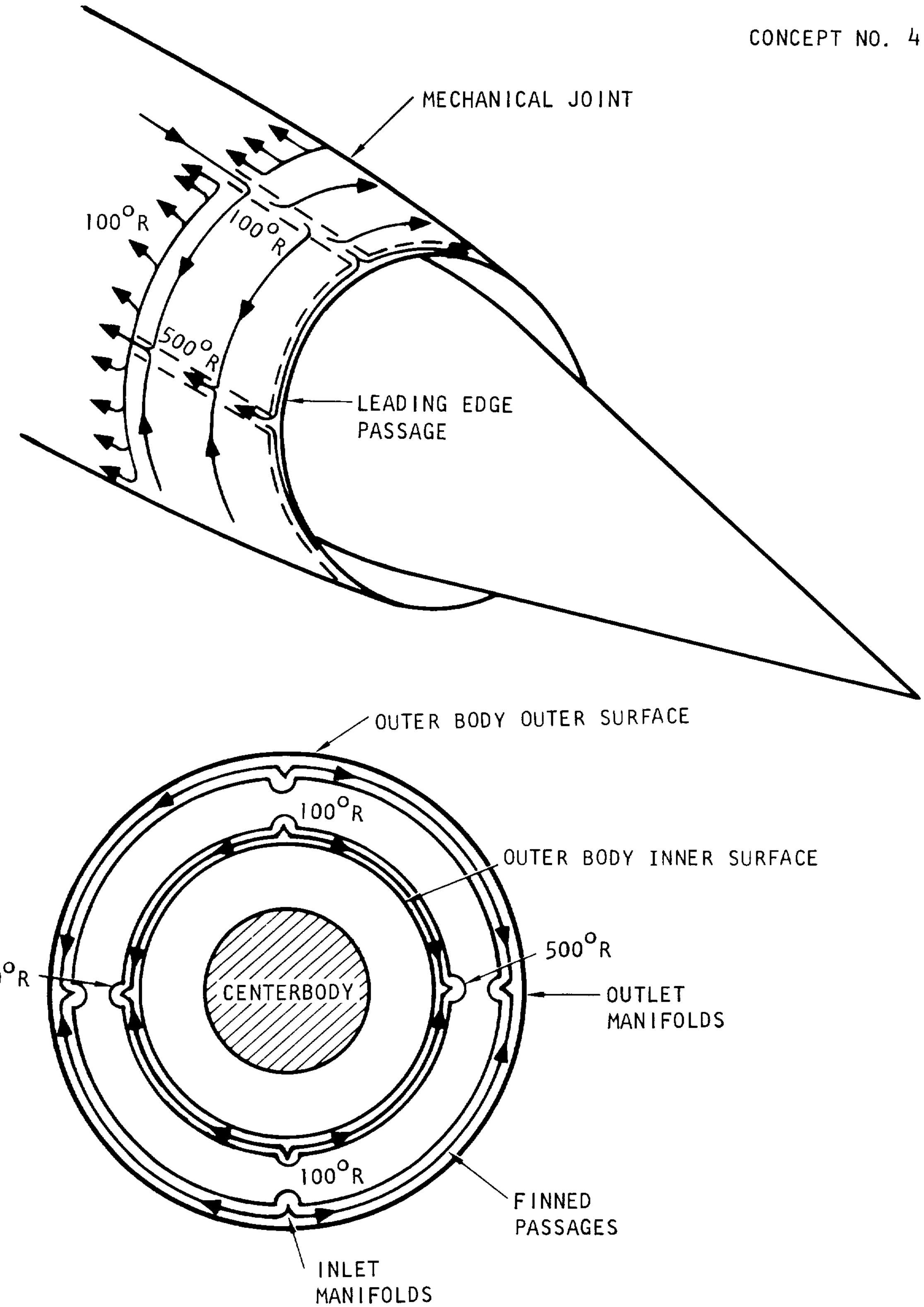

Figure 4.4-3. Outer Body Leading Edge Flow Route Concept No. 4

Concept 4 in Figure 4.4-3 is like Concept 2 on Drawing L-980600 and has been rejected because it has a large sawtooth temperature gradient around the mechanical joint. With the forward cowl flow of 0.53 lb/sec divided among four circumferential segments, structure temperatures will range from $100^{\circ}R$ to $500^{\circ}R$ forward of the joint, compared to the $100^{\circ}R$ uniform temperature around the circumference aft of the joint. The sawtooth temperature profile from $100^{\circ}R$ to $500^{\circ}R$ will exist regardless of the number of segments. The four segments indicated with two inlets and two outlets is the minimum number acceptable for a pressure drop limit of 100 psi at an inlet pressure of 600 psia.

The following discussion describes the fin heights suitable for the cowl forward and aft of the mechanical joint. Table A-36 in Reference 1 summarizes fin geometry for Flow Concept 1. It will be difficult to fabricate and maintain open for flow the short fin heights indicated for Flow Routes 3 and 4, especially within 0.5 in. of the leading edge on both the inner and outer surfaces. The short fins for Flow Routes 3 and 4 in Table A-36 were required because of the low flow rates quoted in Table A-43 of Reference 1. Concepts 1, 3, 4, 7, 8, and 10 in Drawing L-980600 were predicated on the fin heights in Table A-36 of Reference 7. Such short fin heights are not required for Flow Concept 2. Since Flow Concept 2 of Figure 4.4-2 appears most attractive at present, the fins for the cowl can have a geometry with about 20 rectangular offset fins per inch of 0.050-in. height, 0.006-in. thickness, and 0.087-in. offset length. Lower fin ΔT will result for the same pressure drop if more than 20 fins per inch with less than 0.006-in. thickness are used. The detailed choice of fins for the cowl and all other regions of the engine will depend on additional heat transfer, stress, and fabrication analyses.

A fin of 0.020-in. height is shown in the region up to about 0.5 in. aft of the leading edge in Concept 3 of Figure 4.4-1 (Concept 6 in Drawing L-980600), because this configuration will permit the closest approach of the coolant jet to the back of the leading edge bend with an acceptable clearance for fabrication. The use of a step in fin height for Concept 3 in Figure 4.4-1 is to stay within the 100-psi pressure drop limitation.

Each of the concepts in Figure 4.4-1 has beneficial features not available in the others. The Concept 1 configuration has no need for a small clearance at the 180-deg bend where the flow is first toward the leading edge and then away from the leading edge in the finned passages, because the leading edge heat flux is handled by the flow parallel to the leading edge in the separate passage. The flow rate in each segment of the leading edge passage for Concept 1 is 0.008 lb/sec, and a minimum of two 180-deg segments are required with a single common inlet and outlet. If a single inlet and outlet are to be used, then the total flow rate will be 0.016 lb/sec, and maximum wall temperature at the $100^{\circ}R$ hydrogen inlet location will be $1070^{\circ}R$ with a $300^{\circ}R$ wall ΔT, and at the $600^{\circ}R$ hydrogen outlet temperature location, the maximum stagnation line wall temperature will be $1400^{\circ}R$ with a wall ΔT of $200^{\circ}R$. Adjacent to the joint between the leading edge passage and the rest of the cowl flow rate, the wall temperature will be between the local hydrogen temperature in the leading edge passage and the approximately $200^{\circ}R$ temperature of the hydrogen flowing around the 180-deg turn in the finned passages. The leading edge passage pressure drop will be 100 psi if only two 180-deg segments are used. If more segments are used, the pressure drop will be lower but the flow rate in each segment cannot be less than 0.008 lb/sec unless higher stagnation line temperatures than quoted above are acceptable. It may be practical to have the inlet to the leading edge passage directly connected to the finned passages on the outside surface of the cowl; the pressure at the 180-deg turn will be nearly equal to the nominal 600-psia fin passage inlet pressure. A separate outlet tube from the leading edge passage will be required.

If a copper leading edge is used, a length of 0.3 in. from the inner surface of the hydrogen flow channel to the stagnation point will have a circumferentially uniform maximum temperature of about 990°F at the stagnation line and about 630°F at the hydrogen passage surface. Concept 2 in Figure 4.4-1 has some similarities to Concept 9 in Drawing L-980600, except there are no hydrogen passages in the copper tip, and flow is perpendicular rather than parallel to the leading edge. A hydrogen heat transfer coefficient of 1.26 Btu/sec-ft^2-°R can be obtained in a 20-mil clearance at a temperature of 200°R for a pressure drop of less than 2 psi. The pressure drop and the heat transfer coefficient quoted were increased for the effect of the passage radius of curvature. Twenty-mil diameter wires or ribs, spaced at intervals as required by fabrication processes, will probably be beneficial to assure maintenance of the 20-mil clearance. Although not shown in Figure 4.4-1, the presence of a Hastelloy X covering on the copper leading edge, with a thickness of 0.010 in. and a design point ΔT of about 100°F, is assumed. No ΔT was estimated or assumed for the metallurgical bond between the Hastelloy X covering and the copper. Clearly, this metallurgical bond must be maintained or the Hastelloy X covering will have an equilibrium temperature well above the presently calculated maximum temperature of 1090°F (copper maximum of 990°F + skin ΔT of 100°F). If a 0.2-in. copper length is used, the maximum temperature will be reduced from 1090°F to 1030°F, and the hydrogen passage surface will be at 635°F.

4.4.2 Manifolds

Outer body leading edge manifold preliminary design work was done to obtain a configuration with acceptable flow distribution. It was determined that an acceptable flow distribution could be realized without the use of inserts. Acceptable flow distribution was obtained by sizing of the inlet and outlet tubes and manifolds, as shown in Figure 4.4-4.

Two tube and manifold configurations (Case 1 and Case 2) were designed. The inlet and outlet manifold geometries were the same for both cases, but the inlet and outlet tube ID's were different. The two configurations are shown in Figure 4.4-4. The decision as to which case to use will depend on flight hardware dimensional limitations. The case with the larger tubes is preferred for flow distribution. A performance comparison for the two designs and a uniform flow case is presented in Table 4.4-1.

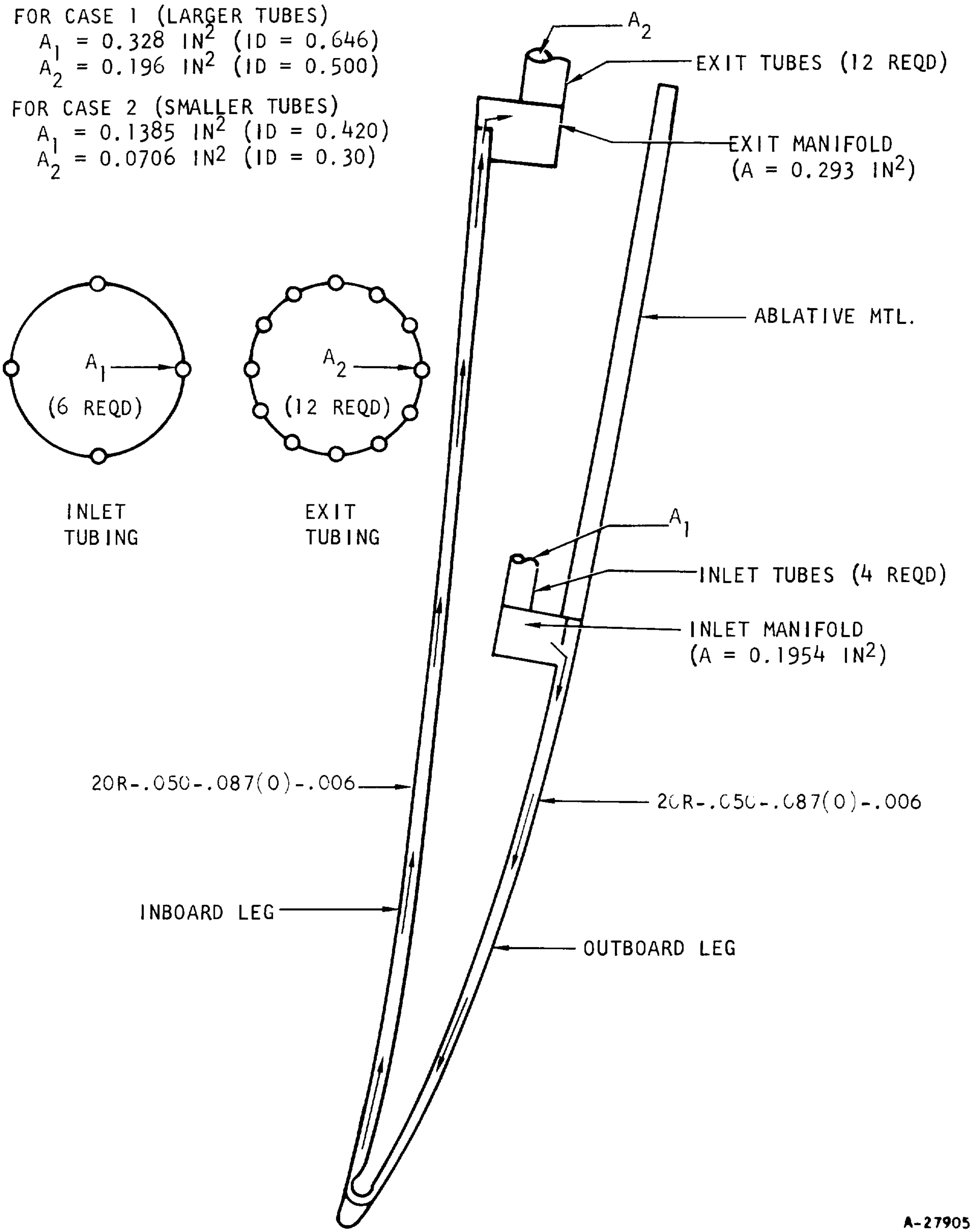

Figure 4.4-4. Outer Body Leading Edge Manifolds

TABLE 4.4-1

MANIFOLD DESIGN CASES PERFORMANCE

Case	Hydrogen Flow Rate (lb/sec)	$\left[\frac{W_{max}}{W_{min}}\right]_{local}$	Hydrogen and Structural Wall Temperature at Mechanical Joint, ^{0}R		$\Delta P_{overall}$ (psia)
			Maximum	Minimum	
Uniform Flow	0.53	1.00	457	457	Greater than Case 1 or Case 2
Case 1 (Larger Tubes)	0.53	1.02	464	450	16.88
Case 2 (Smaller Tubes)	0.53	1.06	478	448	18.87

The hydrogen flow rate is not increased due to nonuniform flow (as is usually required), because the wall temperature is far below the structural limit of $1600^{0}R$ and the circumferential temperature variation is not more than $30^{0}R$. The ratio of the local maximum to minimum flow rates is a function of the geometry of the shortest and longest paths that the hydrogen follows. The ratio is determined by defining the individual path resistance and resulting flow rates for a given overall pressure drop. The circumferential temperature variation is noted in Table 4.4-1 as the difference between the maximum and minimum hydrogen and structural wall temperatures. The wall temperatures are based on a constant circumferential heat flux and, therefore, are a direct function of flow rate. The overall ΔP is the average of the ΔP's from the exit or the inlet tube to the entrance of the exit tube for the local maximum and minimum flow rates for each case.

4.4.3 Structural Analysis

The outer body leading edge was analyzed for containment of hydrogen operating pressure of 700 psia at operating temperature. The proof pressure condition of 1050 psia at ambient temperature is not a severe problem. The combined effects of temperature distributions (as determined from the heat transfer analysis) and pressure loading were computed. The leading edge was found to have an adequate margin of safety on pressure containment capability. The estimated plastic strains during each operating cycle were also computed and a predicted life in excess of 225 cycles was obtained.

4.4.4 Test Section Design

4.4.4.1 Cooling Analysis and Test Simulation

The outer body leading edge test section was designed to provide a geometry like that in the flight engine for the area immediately adjacent to the stagnation region. While stagnation line heat flux is to be achieved, surface heat flux will be somewhat less than design point heat flux since the surfaces are not the area of primary concern.

A cooling hydrogen flow of 0.075 lb/sec at 200°F was assumed for inlet test conditions. At a heat flux of 74 Btu/sec-ft^2, the hydrogen temperature increases 114°R to an outlet temperature of 314°R. By use of a 20R-.075-.100-.004 fin (slightly taller than the flight engine fin of about 20R-.050-offset-.004), the fin ΔT is about 67°R for wall temperatures of 267°R at the hydrogen inlet and 381°R at the hydrogen outlet.

The manifolds and tubes were sized for the test section based on the results obtained from the analysis on the flight engine. The test section plumbing was sized to simulate the flight hardware. The results for the two test unit cases are shown in Figure 4.4-5.

4.4.4.1.1 Heat Flux Calculations

The objective of work on the outer body leading edge test section was to define the test apparatus and flow conditions so that the test specimen will experience the same level of heating as the flight engine would at the most critical conditions (M = 8; Alt = 81,000 ft). At this flight condition, the heat flux will be 670 Btu/sec-ft^2 at the stagnation line of the cowl lip. The average heating on the forward 4 in. of the cowl is 60 Btu/sec-ft^2 on the outer surface, and 180 Btu/sec-ft^2 on the inside surface. In the phase I calculation, the outer body leading edge heat flux was 450 Btu/sec-ft^2 for the same flight conditions. The reason for this difference is attributed, in part, to the heat transfer equations used and, in part, to use of total instead of static pressure aft of the bow shock. The present calculation was by the method of Fay and Riddell (Reference 4), while that for the previous calculation was by the method of Reshotko and Cohen (Reference 3), and resulted in values equal to Krieth (Reference 6). The leading edge heating calculation by the methods of References 4 and 6 are compared below.

Flight conditions and equations for cowl lip stagnation line heat transfer:

$M_\infty = 8$	$\gamma_2 = 1.29$
$P_{T_2} = 30.2$ psia	Alt = 81,000 ft
$T_{T_2} = 4650°R$	$P_2 = 27.8$ psia
$V_2 = 1140$ ft/sec	$P_\infty = 0.38$ psia

FOR CASE 1 (LARGER TUBES)
$A_1 = 0.328\ IN^2$ (ID = 0.646)
$A_2 = 0.196\ IN^2$ (ID = 0.500)
FOR CASE 2 (SMALLER TUBES)
$A_1 = 0.1385\ IN^2$ (ID = 0.420)
$A_2 = 0.0706\ IN^2$ (ID = 0.30)

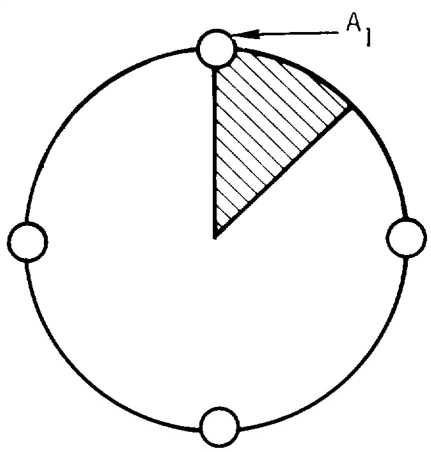

INLET TUBE ARRANGEMENT
FOR ENGINE CONFIGURATION

SCHEMATIC OF LEADING
EDGE COWL TEST SECTION

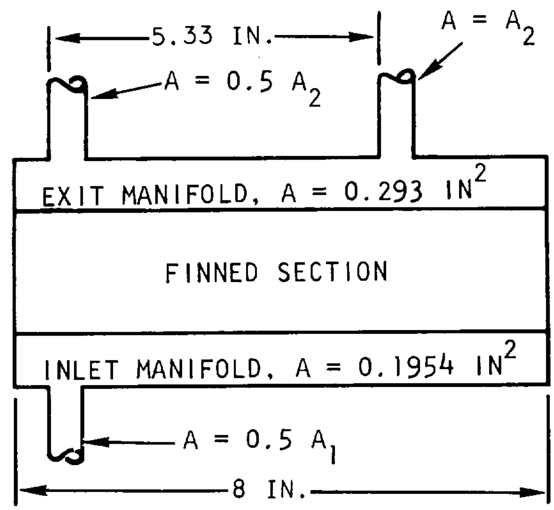

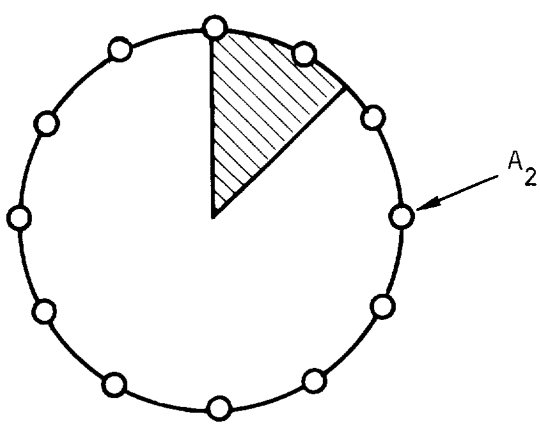

OUTLET TUBE ARRANGEMENT
FOR ENGINE CONFIGURATION

NOTE

THE CROSS-HATCHED AREAS REPRESENT THE AREA WHICH THE TEST SECTION WILL SIMULATE.

A-27906

Figure 4.4-5. Test Section Plumbing

Method (1), Fay and Riddell (modified for 2D):

$$q = \frac{0.56}{Pr_W^{0.6}} (\rho\mu)_{W_T}^{0.1} (\rho\mu)_{T_2}^{0.4} (H_T - H_W) \sqrt{\frac{du}{dx}}$$

where $\frac{du}{dx} = \frac{2}{D}\sqrt{\frac{288\ g\ (P_{T_2} - P_\infty)}{\rho_{T_2}}}$

$q = 670$ Btu/sec-ft^2

Method (2), Kreith:

$$q = 1.14 \frac{k_f}{D} \sqrt{\left(\frac{\rho u D}{\mu}\right)_f}\ Pr_f^{0.4} \quad (T_T - T_W)$$

where k_f, ρ_f, and μ_T are evaluated based on

$$T_f = \frac{T_{gas} + T_W}{2}$$

$q = 450$ Btu/sec-ft^2 by Kreith

<u>Symbols</u>

D = leading edge diameter, ft

H = enthalpy, Btu/lb

h = film coefficient, Btu/sec-ft^2-^{0}F

k = conductivity, Btu/sec-ft-^{0}F

P = pressure, psia

Pr = Prandtl No. $= \frac{Cp\ \mu}{k}$

q = heat flux, Btu/sec-ft^2

Re = Reynolds No. $= \frac{\rho u D}{\mu}$

T = temperature, ^{0}R

U = velocity, ft/sec

γ = specific heat ratio

μ = viscosity, lb/sec-ft

ρ = density, lb/cu ft

Subscriptions

∞ = free-stream condition (upstream of bow shock)

f = properties evaluated at the arithmetic average temperature between the hot gas and the wall

T = total (otherwise static)

w = wall

2 = aft of the bow shock

4.4.4.1.2 Test Tunnel

The test tunnel is a two-dimensional channel with a 6-in. straight section of 2 by 8 in., followed by an 18-1/2 deg half-angle divergent channel (Figure 4.4-6). The 6-in. straight section serves two purposes: (1) to allow the inviscid portion of the flow to settle any upstream disturbance, and (2) to permit the boundary layer in the tunnel wall to develop a turbulent flow at the test section. This latter condition will permit side wall radiation to contribute approximately 24 Btu/sec-ft^2 of net heat flux to the flat surfaces of the test unit.

4.4.4.1.3 Calculated Heat Loads

Maximum test heating conditions are listed below:

W = the mass flow rate = 6.4 lb/sec

P = the reservoir pressure = 100 psia

T = the reservoir gas temperature = 4000^{0}R

Calculated heat fluxes are listed below:

	q/A in Test Btu/sec-ft^2	q/A in Flight Btu/sec-ft^2
Leading edge stagnation line	670*	670
Outer Surface	64	60
Inner Surface	64	180

The required flow rate is 6.4 lb/sec and the corresponding velocity is 890 ft/sec at the leading edge in the test section. The stagnation line heat flux is 670 Btu/sec-ft^2 based on a wall temperature of 2000^{0}R. The test unit boundary layer will be laminar and the predicted average

*For wall temperature of 2000^{0}R.

NOTES:
1. ALL DIMENSIONS ARE IN INCHES
2. INTERIOR WALLS (EXCEPT THE MODEL) ARE TO BE LINED WITH ZrO_2 OR EQUIVALENT
3. WIDTH OF CHANNEL = 8 INCHES
4. ZrO_2 WALL NOT TO SCALE

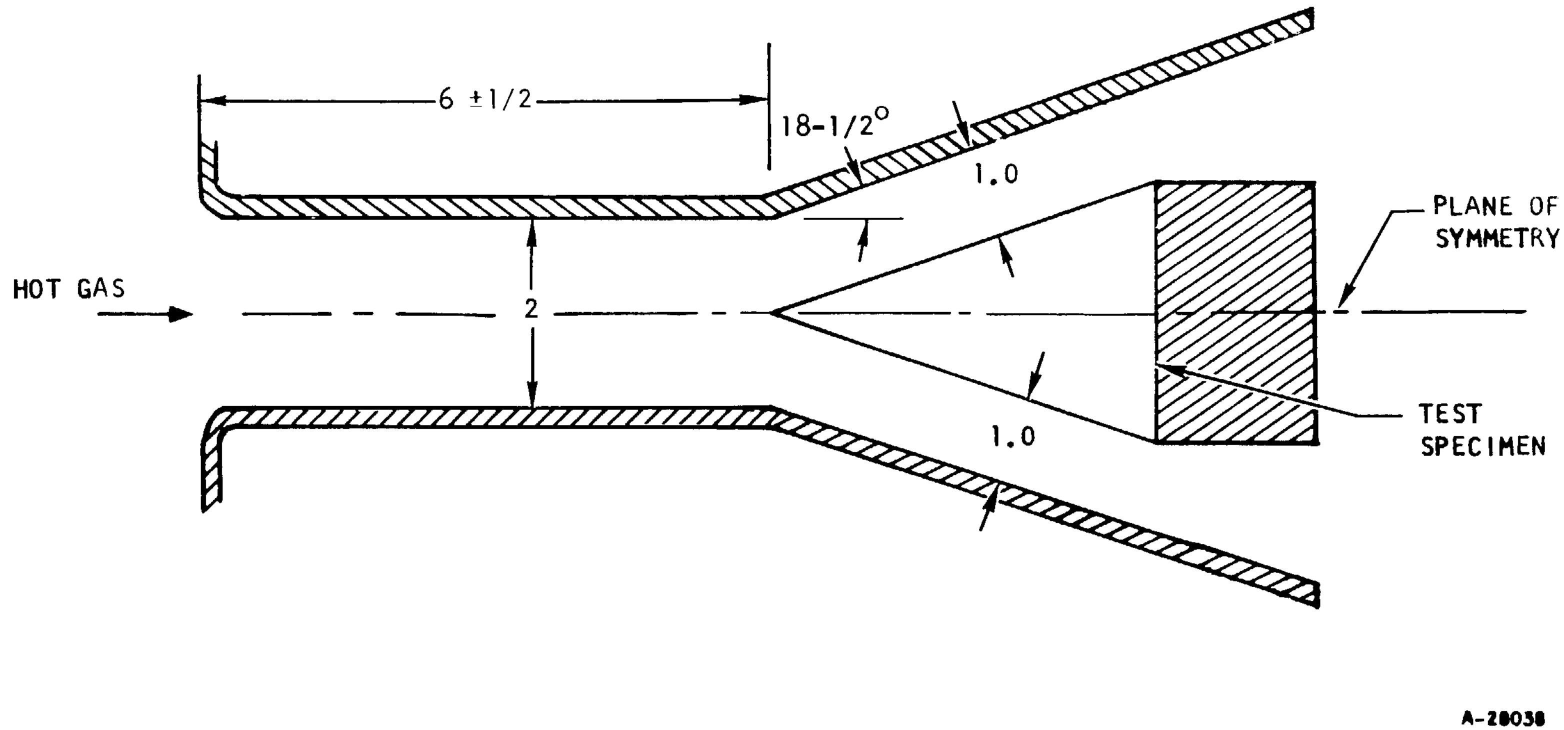

Figure 4.4-6. Schematic of Test Apparatus

convective heat flux is approximately 40 Btu/sec-ft^2. Since the tunnel wall is made of zirconium oxide, ZrO_2, there is little conduction loss. Hence, the convective heat load incident on the tunnel wall will be rejected primarily through radiation to the test unit. At a steady state, the net radiative heat flux of 24 Btu/sec-ft^2 equals the convective heat flux to the tunnel wall. The test conditions which meet the requirements of the stagnation line do not produce the flight condition heating to the flat surfaces. By having a 6-in. straight section upstream of the test sections so that $Re \simeq 5 \times 10^5$, turbulent conditions will increase convective heating. The tunnel wall equilibrium temperature will be 3320^{0}R and a net radiative heat flux of 24 Btu/sec-ft^2 is expected. The total net heat flux to the side wall of the test unit will be 64 Btu/sec-ft^2, which is very close to what the outer surface of the flight engine cowl will receive. No attempt will be made to simulate the higher heat flux encountered on the interior cowl surface.

4.4.4.2 Structural Analysis

The outer body leading edge test section was analyzed in order to evaluate possible configurations. Figure 4.4-7 shows the results of the investigation. Cases 1 and 5 can support the 100 psi external pressure, while the other combinations are not satisfactory.

Combined axial and bending stresses due to 700 psi internal pressure at the leading edge in the vicinity of the stagnation point will be around 8140 psi. Temperatures during testing will create plastic strains, but the magnitude of these strains will be such that the expected number of allowable cycles will exceed 4000 if the maximum ΔT does exceed 300^{0}F, and the maximum metal temperature will be below 1550^{0}F.

Fins at the leading edge will be 20R-.020-.003. The margin of safety is 0.112 based on the combined loads due to 700 psi internal pressure and the differential radial expansion of the face metal and using a fin efficiency factor of 0.33.

The analysis revealed that the maximum allowable span of 0.015-in. thick Hastelloy X sheet would be less than 0.1 in.

OUTER BODY LEADING EDGE TEST SECTION

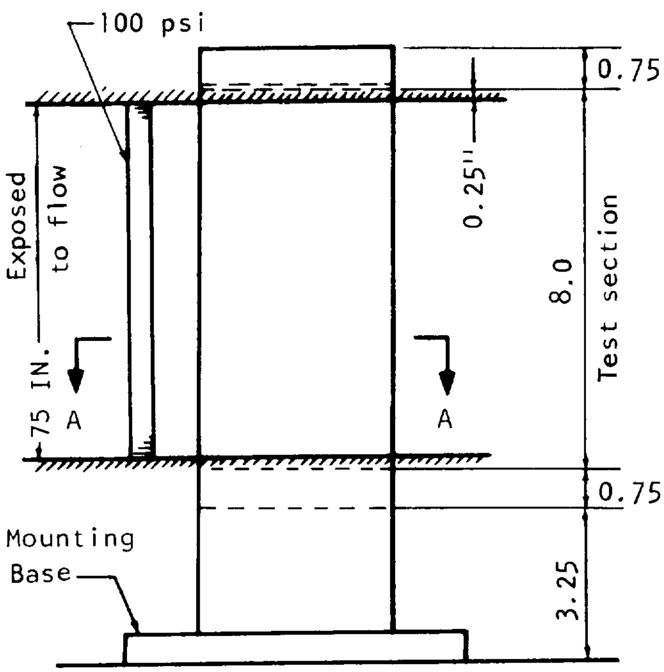

SIDE VIEW

CASE		CONFIGURATION	MARGIN OF SAFETY
0.015 / 0.015	1		0.03
	2		-0.762
	3		-0.362
0.015 / 0.060	4		-0.512 (0.065) -0.646 (0.015)
	5		0.96 (0.060) 0.43 (0.015)

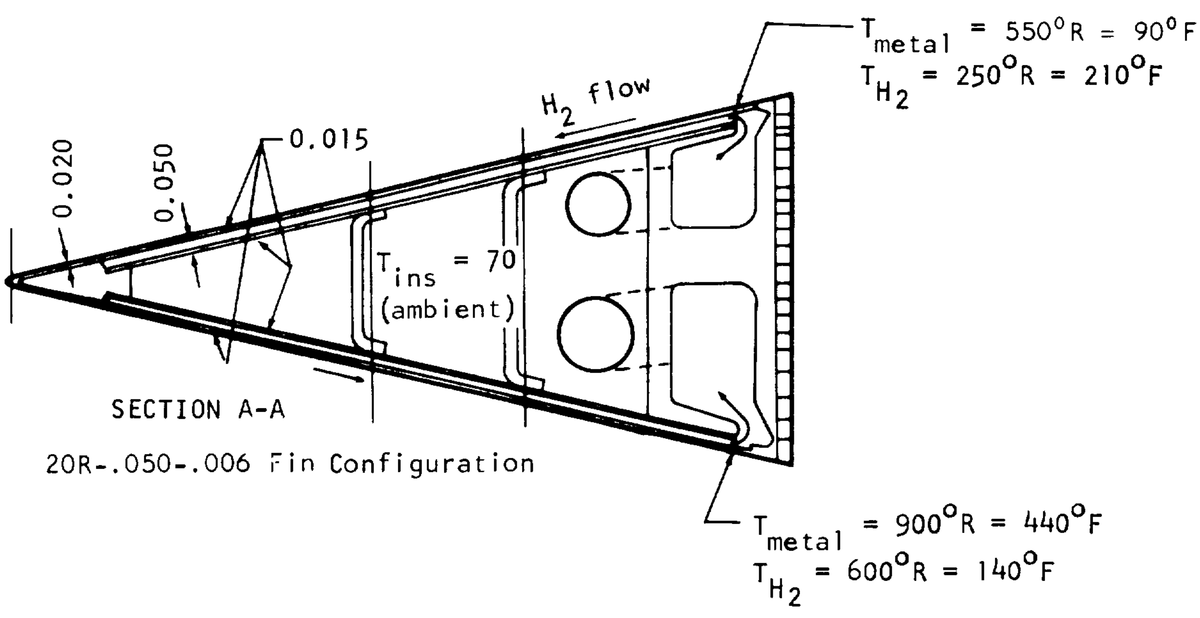

SECTION A-A

20R-.050-.006 Fin Configuration

Figure 4.4-7. Outer Body Leading Edge Test Section

4.5 INLET SPIKE ACTUATOR

The inlet spike actuator has two functions: (1) it is used to modulate the inlet spike to the position required by aerodynamic considerations, and (2) it serves as the support for the inlet spike, and consequently must be structurally designed to limit deflection of the inlet spike to levels acceptable for translation of the spike over the inner body.

4.5.1 Operating Requirements

Preliminary operating requirements established for the inlet spike actuator are as follows:

Aerodynamic loads	Maximum axial: 1733 lb Maximum normal: 6446 lb
Load due to bellows	0 to 1500 lb (spring rate load of parallel bellows for 0 to 5.3 in. actuator extension; load is in same direction as axial aerodynamic load, tending to retract actuator)
Internal pressure load	
Steady state	0 to 15,000 lb acting to extend actuator
Transient	0 to 20,000 lb acting to extend actuator during inlet unstart
Inertia load	100 lb
Operating gas	Nitrogen, 5 lb total, stored at 5000 psig, at $-35^{\circ}F$ to $160^{\circ}F$
Actuator	Stroke: 5.3 in. Piston diameter: 3.5 to 7.0 in.
Actuation rate	Minimum acceptable: 0.5 cps Desired: 1 cps
Positioning accuracy	$M = 3, 4$: ± 0.08 in. $M = 6$: ± 0.075 in. $M = 8$: ± 0.144 in.
Permissible overshoot	For sudden application of reverse load, actuator may extend against stops (inlet closed)
Load profiles	As shown in Figures 4.5-1 and 4.5-2 for inlet opening at $M = 3$ and $M = 8$ (extreme cases). Individual loads are shown, not totals. Load profile for closing is assumed identical to that for opening of inlet

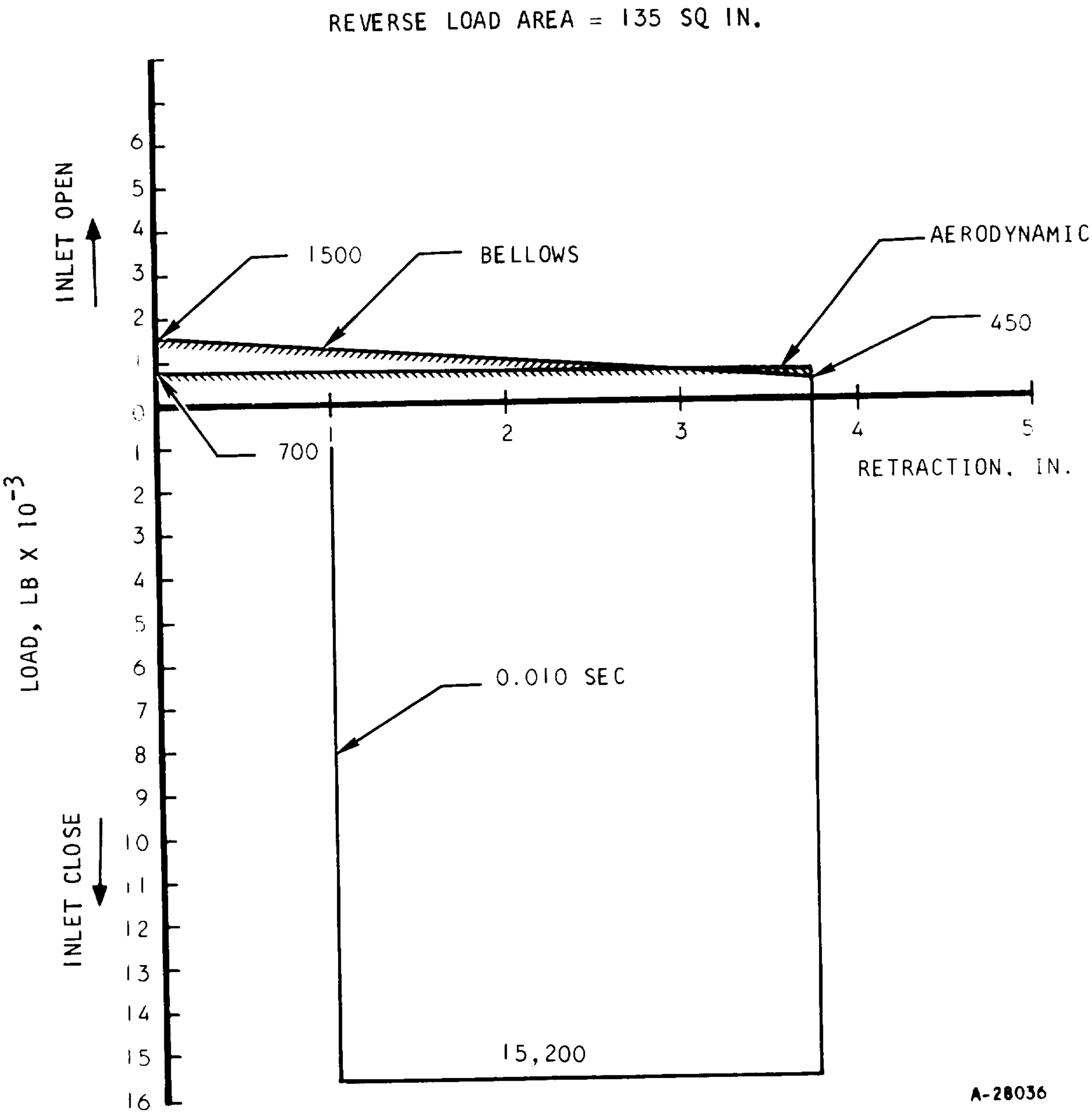

Figure 4.5-1. Actuator Load Profile for Mach 3

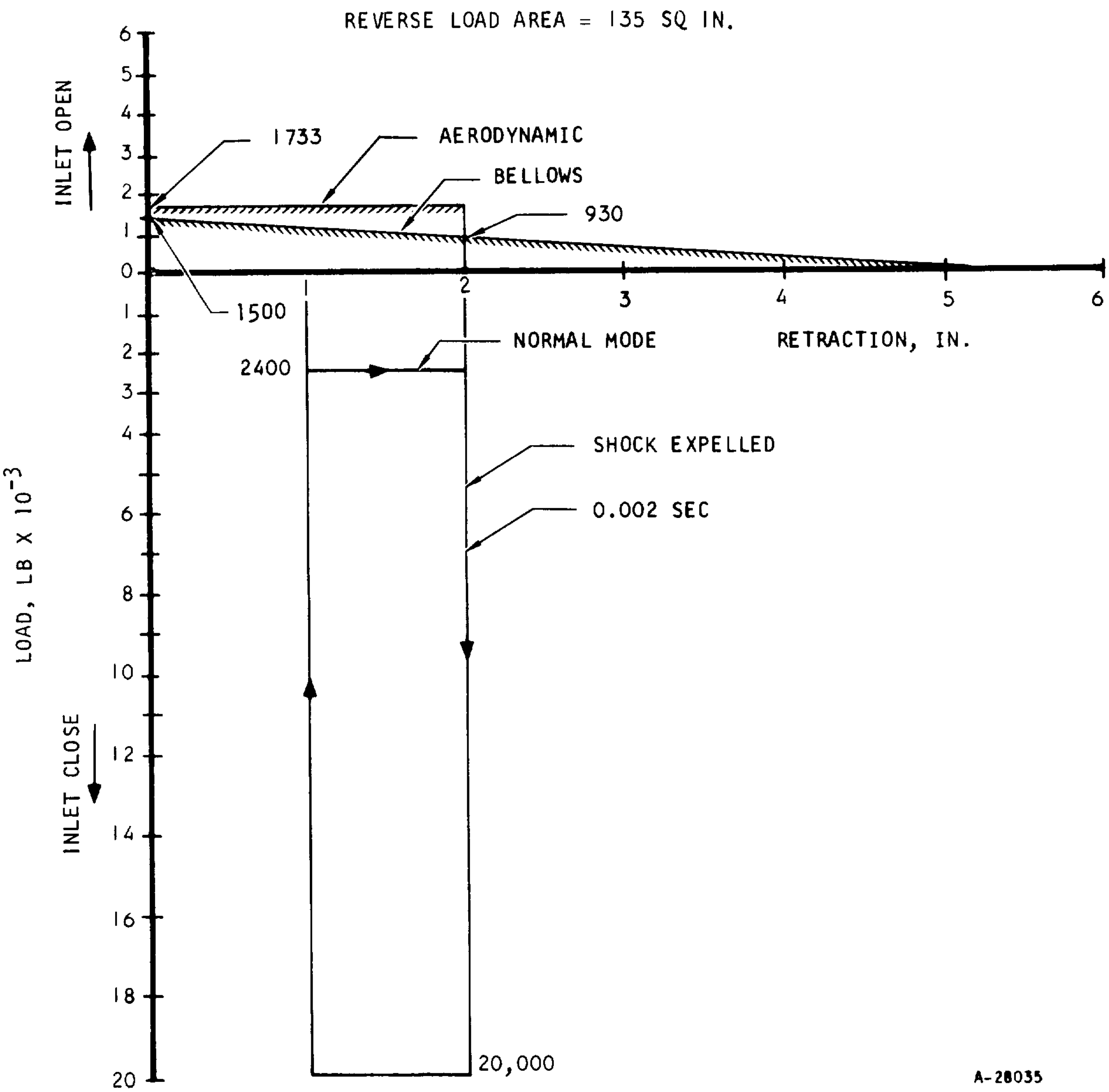

Figure 4.5-2. Actuator Load Profile for Mach 8

Vibration requirement	No natural frequencies or vibratory outputs from 15 to 17 cps Input to engine a. 0.06-in. double amplitude, 10 cps to 31 cps b. 3 g, 31 cps to 2000 cps c. Random, 6 g rms for 2 min, Gaussian band-limited from 20 cps to 2000 cps at 0.018 g^2/cps
Environment	Pressure: 14.7 psia to 0.3 psia Temperature: -65°F to 450°F (soak temperature of actuator mass can be reduced by insulation
Fall safe position	Actuator extended (inlet closed)
Design life	100 missions for the operating sequence outlined below

Typical Operating Sequence:

a. Actuator fully extended (inlet closed): 150 sec after launch from B-52 airplane

b. Actuator retracted (inlet open) to operating position: 0.5 sec

c. Engine operating, with either of the following conditions:

   (1) Normal engine operation, actuator modulating around selected operating position: 40 sec maximum

   (2) Inlet unstart:

      (a) Actuator fully extended (inlet closed): 0.5 sec

      (b) Actuator retracted (inlet open): 0.5 sec

      (c) Actuator modulating: 40 sec maximum

d. Actuator fully extended (inlet closed): 0.5 sec

e. Actuator fully extended: 150 sec for return to launch altitude

f. Soak: In flight on B-52 for 75 min at 45,000 ft. Actuator will be fully extended during these periods and latched.

4.5.2 Design Concept

Based on the operating requirements presented above, preliminary analyses show that a pneumatic actuator, using a hydraulic damper, is feasible. The large reverse loads developed during certain operating conditions, however, result in a relatively large piston diameter. Preliminary calculations indicate that piston diameter of approximately 7 in. may be required, in combination with a hydraulic damper.

5.0 DESIGN EFFORT

During the reporting period, design layout work has been accomplished on the nozzle, the inner body-outer shell support strut, and the outer body leading edge. Layout design of the nozzle and layout of the inner body-outer shell support strut assembly has been completed. Outer body leading edge configurations have been evaluated to the extent necessary to permit definition of candidate leading edge designs for further consideration. With definition of the inner body-outer shell support strut assembly, layout work on the shell was initiated.

5.1 NOZZLE

5.1.1 Design Ground Rules

The nozzle involves two critical design problems; (1) provisions for assembly of the nozzle to the inner shell must be made, and (2) access to permit such assembly must be provided. Conceptual design of these areas proceded on the assumption that all of the nozzle and structure brazed directly to the nozzle would soak to temperatures of approximately 1600°R prior to start of coolant flow in flight. This assumption is the most pessimistic that can be made but is justified by the uncertainity of predicting the exact temperatures achieved in the shell. The importance of this assumption is that the use of all organic seals is barred; metal seals only are acceptable. Many of the design features adopted stem directly from this basic assumption.

5.1.2 Features

Drawing L-980604 is the completed layout of the nozzle. This redesigned nozzle is expected to meet the thermal and structural requirements encountered during engine flight testing.

5.1.2.1 Nozzle Cap

The nozzle cap is used to make the final engine closeout. It is threaded into the brazed mounting provided on the shell and is locked into position using the center bolt. Although the locking bolt picks up load by its mere presence, its primary function is to lock the nozzle cap against rotation. The seal at the bolt end is a standard part suitable for use with threaded fittings. The large seal at the interface with the shell is a specially fabricated seal of the same type as the one used under the bolt. "K" seals are used to seal the nozzle cap cavity from the remainder of the nozzle. Removal, in turn, of the bolt, the cap, the male thread supporting the cap, and the central tube gives access to the nozzle cavity. Connections for instrumentation of the nozzle can be made and access to the bolts with which the nozzle is mounted to the inner shell is provided.

5.1.2.2 Bolted Flange/Manifold

The flange/manifold consists of the manifold itself, fabricated as a weldment from two machined pieces, and a brazed face. The coolant crossover connection to the burner is provided by ports sealed with conventional "K" seals. Fastening occurs on either side of the seal using blind inserts in the flange/manifold assembly. The tubes shown extending from the manifold serve to guide a flexible shaft used to torque the bolts. It is welded into the manifold to eliminate possibility of leakage.

5.1.2.3 Shell

The thermal design of the shell has been re-evaluated with the objective of using a single fin height along the entire length of the nozzle shell. During Phase I, different fin heights were used to reflect variations in heat flux. The analysis has shown that use of a single fin height is feasible and even desirable. The resulting increase in pressure drop is within acceptable limits and aids in assuring better flow distribution than could be obtained with the very low pressure drop encountered in the two-fin approach. Use of a single fin also is expected to simplify manufacture and assembly of the shell.

5.2 INNER BODY-OUTER SHELL SUPPORT STRUT

5.2.1 Design Ground Rules

The design of this critical interface used the loads generated during Phase I of the program. The primary objective of the conceptual design work accomplished on this assembly was to achieve a bolted assembly as opposed to a brazed assembly of the strut to the inner body and the outer shell. The advantages afforded by the possibility for assembly and disassembly were secondary to the advantages expected in accomplishing the initial assembly. While the brazed assembly represents a basically feasible concept, it entails requirements for relatively complex fixturing during brazing to ensure that the required tolerances and concentricities are maintained. The use of a bolted assembly offers an opportunity for mechanical adjustment to obtain the necessary alignments and concentricities. The bolted assembly that evolved from this study has been evaluated for structural and thermal performance and appears adequate for the predicted loads.

5.2.2 Features

Drawing L-980608 shows the conceptual design of the selected support strut assembly. This drawing necessarily shows an assembly which will eventually be encountered only on the final assembly drawing for the inner body-outer shell support strut. Although the basic features of the design shown in the layout are expected to be retained, layout of the inner shell and of the outer shell is expected to lead to modifications of the strut mounting details.

5.2.2.1 Assembly

Assembly of the inner body and outer shell by the support strut will involve first, the placement of the two shells and alignment of the cutouts in the shells. The strut will then be inserted from outside and bolted to the socket in the inner body. The bolts will be tightened to predetermined torque values. The mounting flange on the outer shell has brazed,threaded studs which pass through clearance holes in the strut flange. The nuts used on these studs are again tightened to preselected torque values. The air seal is formed by a flat gasket type seal. Material tentatively selected for the seal is annealed copper.

The exit tube for the leading edge requires its own seal (not shown in the layout) which is expected to be formed by a bellows joined to the inner shell and the exit tube after assembly. Use of this separate seal avoids the need to extend the flat gaskets into the leading edge area and eliminates the resulting ledge on the gas side of this area. Analyses have shown that cooling of such a ledge requires special provision.

5.2.2.2 Manifolding and Structural Attachment

Adequate cooling of the strut requires two separate flow routes, one for the leading edge and one for the main portion of the strut. The leading edge is cooled using $100^{\circ}R$ hydrogen at a flow rate equivalent to that required to provide cooling to the entire inner body. The main strut is cooled with outer shell coolant, taken from the aft manifold shown in the layout, flowed axially along the strut and then discharged into the fuel plenum.

Structural loads are reacted at the fuel injection manifolds near the leading edge of the strut and at the manifolds near the trailing edge of the strut. The basic structural design problem is the attachment of the strut mounting to these manifold rings. The fuel injection manifold at the center of the strut is not necessary as a structural member and has, therefore, been made lightweight and is not tied to the strut mountings.

All hydrogen plumbing connections that are required to pass through the strut will be metallurgically joined to their mating lines. Disassembly of the shells, therefore, will require cutting of the lines. This is considered preferable to the use of a multiplicity of threaded connections.

In addition to the critical structural attachments required in the strut assembly, thermal stress problems are expected to be serious. The presence of relatively large masses on the thermally responsive shells is unattractive. The extent of the thermal stress problem will be evaluated experimentally in the full-scale tests.

5.2.3 Fabrication Requirements

The strut itself is not expected to involve serious fabrication problems. The machining operations on the strut, although numerous, can be accomplished with conventional machine tools or by electrical discharge machining. The critical areas for manufacturing are the interface of the strut mountings with the manifold rings at the two ends. Extremely precise fitup is required here to facilitate the necessary brazing operations.

Assemby will involve tacking of the rings and strut mountings to the already brazed shell and joining of these components to the shell in a single braze cycle. The tie-in of the strut mountings to the rings by gussets is expected to require an additional braze cycle. Since this part of the structure will be operating at maximum temperatures of $1600^{0}R$, considerable flexibility exists in the selection of braze filler alloys and no problems with remelt of the alloys or dissolution in previously brazed assemblies is anticipated.

5.3 OUTER BODY LEADING EDGE

5.3.1 Design Ground Rules

The objectives sought in the conceptual design layout studies of the leading edge were:

> Increase of the gap for coolant flow at the leading edge stagnation line. It is considered that reliable manufacture requires a gap of approximately 0.020 in. Gaps less than this are subject to plugging by braze alloy and require extremely careful control of braze alloy quantity and braze cycles.
>
> A manifolding arrangement into and out of the leading edge which permits flexibility in the selection of manifold cross-sectional area and number of inlet and outlet lines. This flexibility, in turn, assures opportunity for control of leading edge flow distribution.
>
> Temperature matching at the inlet and outlet stations of the leading edge section. Temperature differences up to about $300^{0}R$ at these sections are expected to be tolerable. Much larger temperature differences are likely to lead to serious thermal stress problems.

5.3.2 Concepts

Drawing L-980600 shows a number of leading edge concepts. All concepts shown in this drawing follow the arrangement evolved during Phase I of the program. Emphasis in these concepts is, therefore, on use of small gaps in the stagnation line area and control of the plugging by various mechanical means. In general, none of the concepts shown in this drawing are considered particularly attractive. Flow around the leading edge was, therefore, re-studied in terms of leading edge and outer shell cooling requirements.
Use of all of the coolant required in the forward portion of the outer shell through the leading edge was found to yield an attractive solution and meets the basic design ground rules. Drawings SK-51305, SK-51306, SK-51307, and SK-51308 show concepts incorporating this flow routing. Drawing SK-51306

is the simplest and most direct of the concepts. The two principle areas of uncertainity involved in this concept are the nature of the coolant flow around the leading edge and the feasibility of a welded joint along the stagnation line. This concept has been selected for experimental verification to establish the adequacy of cooling.

Drawing SK-51305, shows a more complete arrangement of the leading edge and a leading edge configuration which involves flow parallel to the stagnation line. The principle problems with this concept involve the flow routing out of the leading-edge channel into the main stream. Fabrication of the skin joint at the leading edge is, similarly, a considerable manufacturing problem. A braze joint in this area appears required since welding in the presence of braze alloy would constitute a questionable procedure. The detail shown for the manifolding of the leading edge represents the current concept. The ablatively cooled cowl is brought forward to near the midpoint of the leading edge section. Removal of the cowl makes available the manifold joints in the leading edge which is expected to facilitate manufacturing assembly. This configuration of the leading edge will be experimentally evaluated as a leading-edge straight section.

Drawings SK-51307 and SK-51308 show two concepts for the use of copper tips in the stagnation area. The difficulty of reliably joining the copper tip to the remainder of the leading edge has caused rejection of the concept.

5.3.3 Test Section

Figure 5.1-1 schematically shows the cowl leading-edge straight section to be used in the evaluation of the concept shown in Drawing SK-51306.

5.3.3.1 Design Objectives

The purpose of this test section is to evaluate thermal fatigue and coolant-side heat transfer in the area of the immediate leading edge. In addition, the manifolds have been so scaled as to permit a qualitative assessment of flow distribution that is expected to be applicable to the full-scale outer body leading edge.

5.3.3.2 Features

The leading section of Drawing SK-51306 is duplicated in the leading, edge straight section. The internal portion of the test section will be sealed against gas pressure to simplify instrumentation and plumbing connections. The webs shown in Figure 5.1-1 provide buckling strength to the surface panels. Cast zirconia pieces are used on the manifold and at top and bottom to protect these uncooled or inadequately cooled areas.

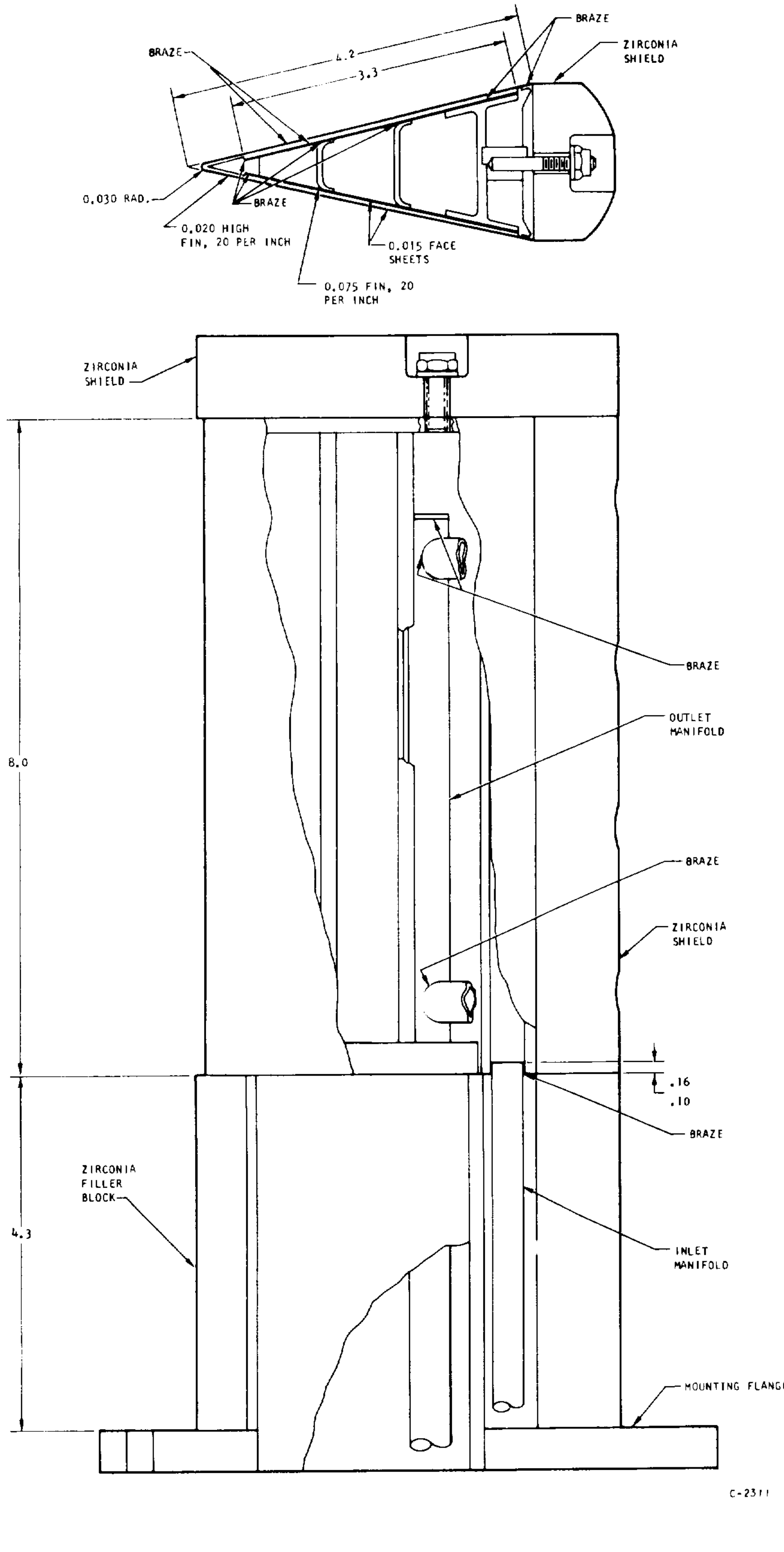

Figure 5.1-1. Outer Body Leading Edge
Straight Section

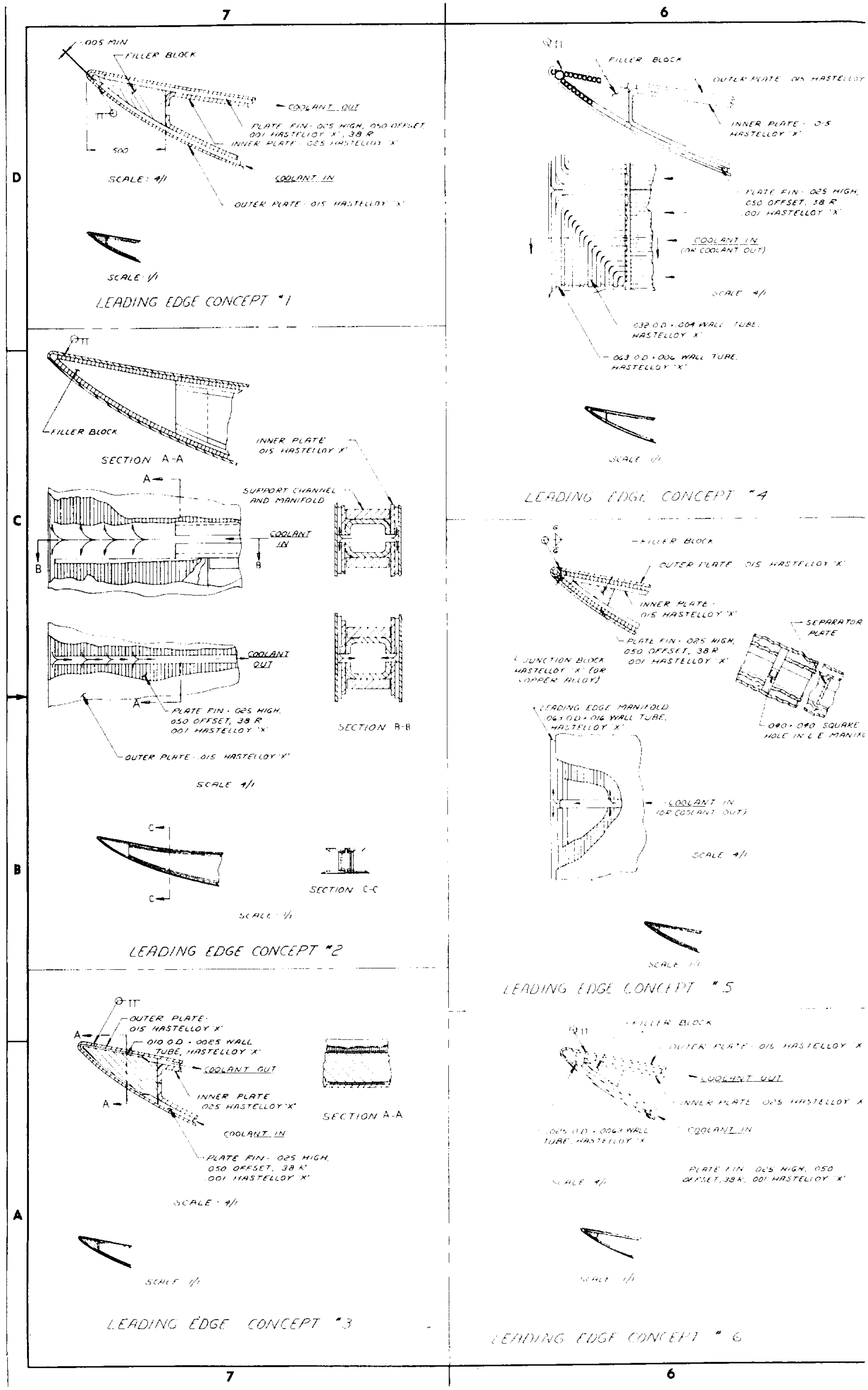

FOLDOUT FRAME /

5

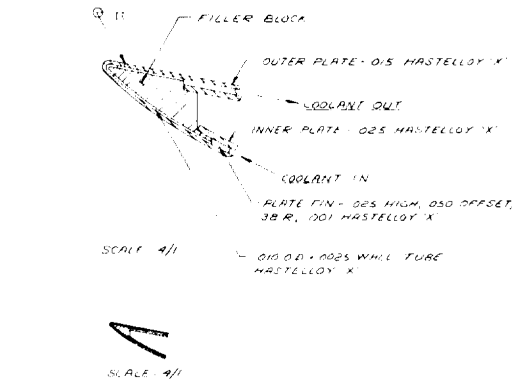

LEADING EDGE CONCEPT # 7

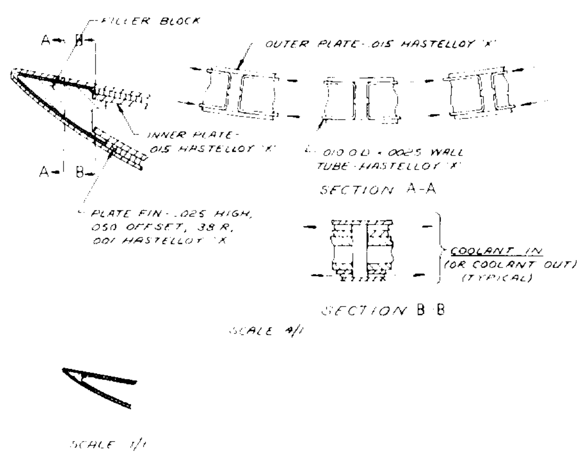

LEADING EDGE CONCEPT # 8

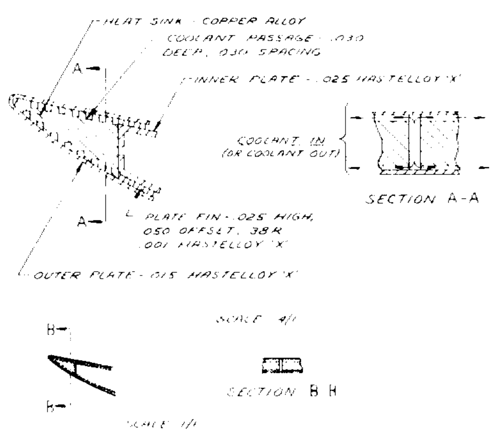

LEADING EDGE CONCEPT #9

VARIATIO
WITH

BEND RAD
× DIA
½ D
1 D
1½ D
2 D

BEND RADI
(.040Ø S

5

FOLDOUT FRAME 2

4 3

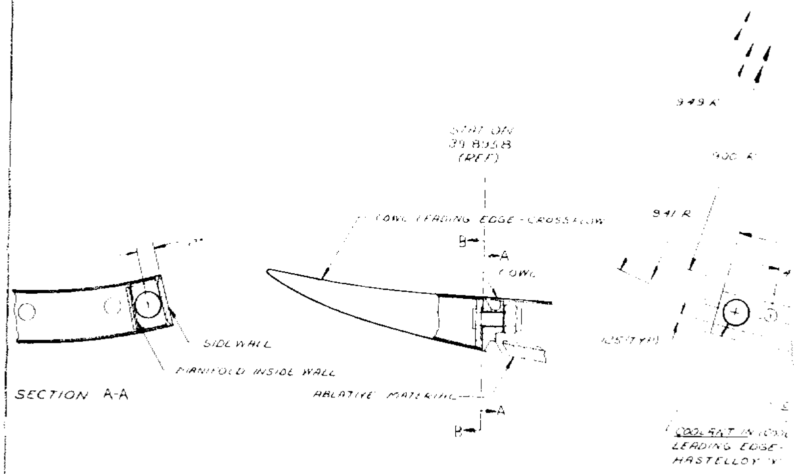

LEADING EDGE ATTACH CONCEPT #1 - CROSSFLOW

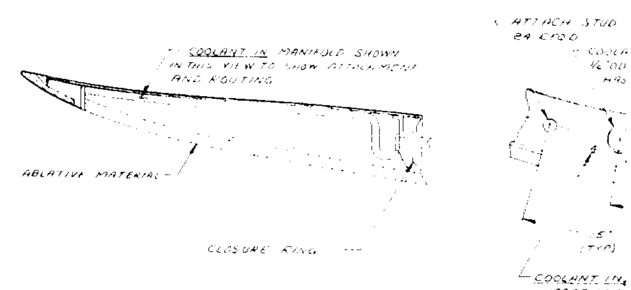

LEADING EDGE ATTACH CONCEPT #2 LATERAL FLOW

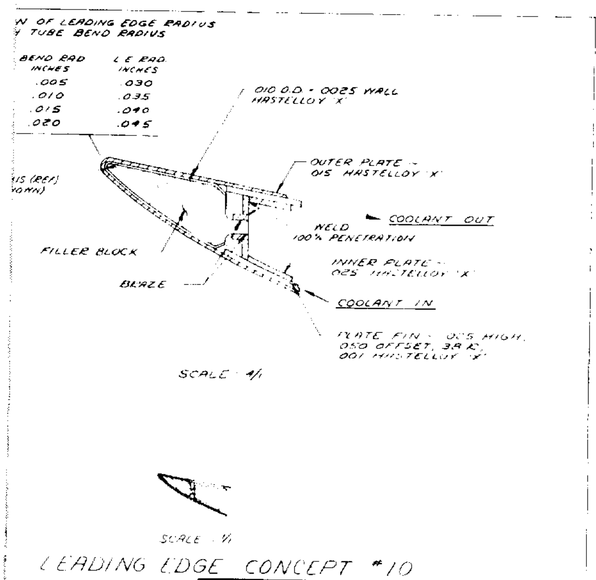

LEADING EDGE CONCEPT #10

4 3

FOLDOUT FRAME 3

2

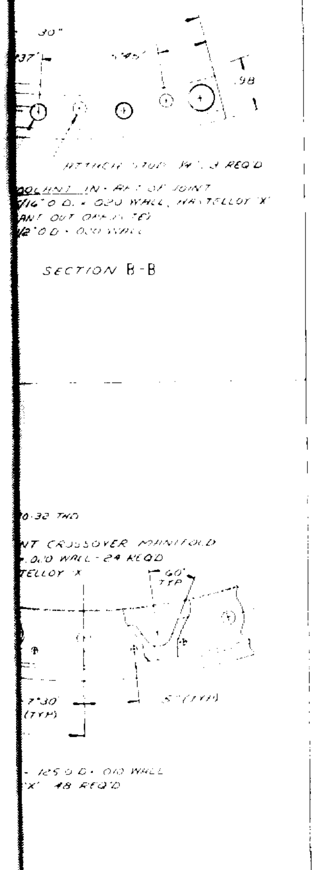

NOTES: UNLESS OTHERWISE SPECIFIED

REQD	NEXT ASSY
	APPLICA

2

FOLDOUT FRAME 4

1

REVISIONS				
ZONE	LTR	DESCRIPTION	DATE	APPROVED

D

C

B

Z980600

A

QTY REQD	ITEM NO	PART NO.	SYM	DESCRIPTION	CODE IDENT	MATERIAL AND SPECIFICATION	ZONE
	←ASSY						

LIST OF MATERIAL

UNLESS OTHERWISE SPECIFIED:
DIMENSIONS ARE IN INCHES
MACHINE FILLET RADII .013 — .030
SURFACE ROUGHNESS PER MIL-STD-10
BURR CONTROL PER SC002
DIMENSION LIMITS HELD AFTER PLATING
IDENT MARKING PER MCM
DIMENSIONING AND TOL PER MIL-STD-8

HEAT TREATMENT	PROCESS
HARDNESS AND SPEC	NAME AND SPEC

SIGNATURES	DATES
DFT W.L. GALLAGHER	11-23-66
CHK	
VALUE ENGR	
MATL	
STRESS	
APPD	
APPD	

AIRESEARCH APPD

OTHER ACTIVITY APPD

USED ON

AIRESEARCH MANUFACTURING COMPANY
A DIVISION OF THE GARRETT CORPORATION
LOS ANGELES, CALIFORNIA

COWL & LEADING EDGE
DESIGN CONCEPTS
H.R.E.

SIZE	CODE IDENT NO.	DWG NO.
J	70210	L 980600

SCALE ½ & NOTED

SHEET 1 OF 1

1

FOLDOUT FRAME 5

11 10

D

C

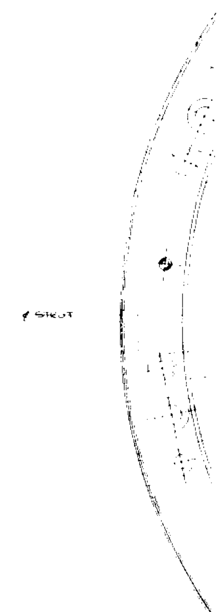

B

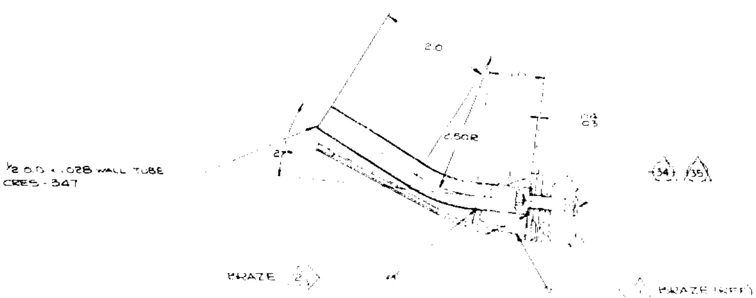

SECTION **C-C**
(TYP 20 PLACES)

A

11 10

FOLDOUT FRAME 1

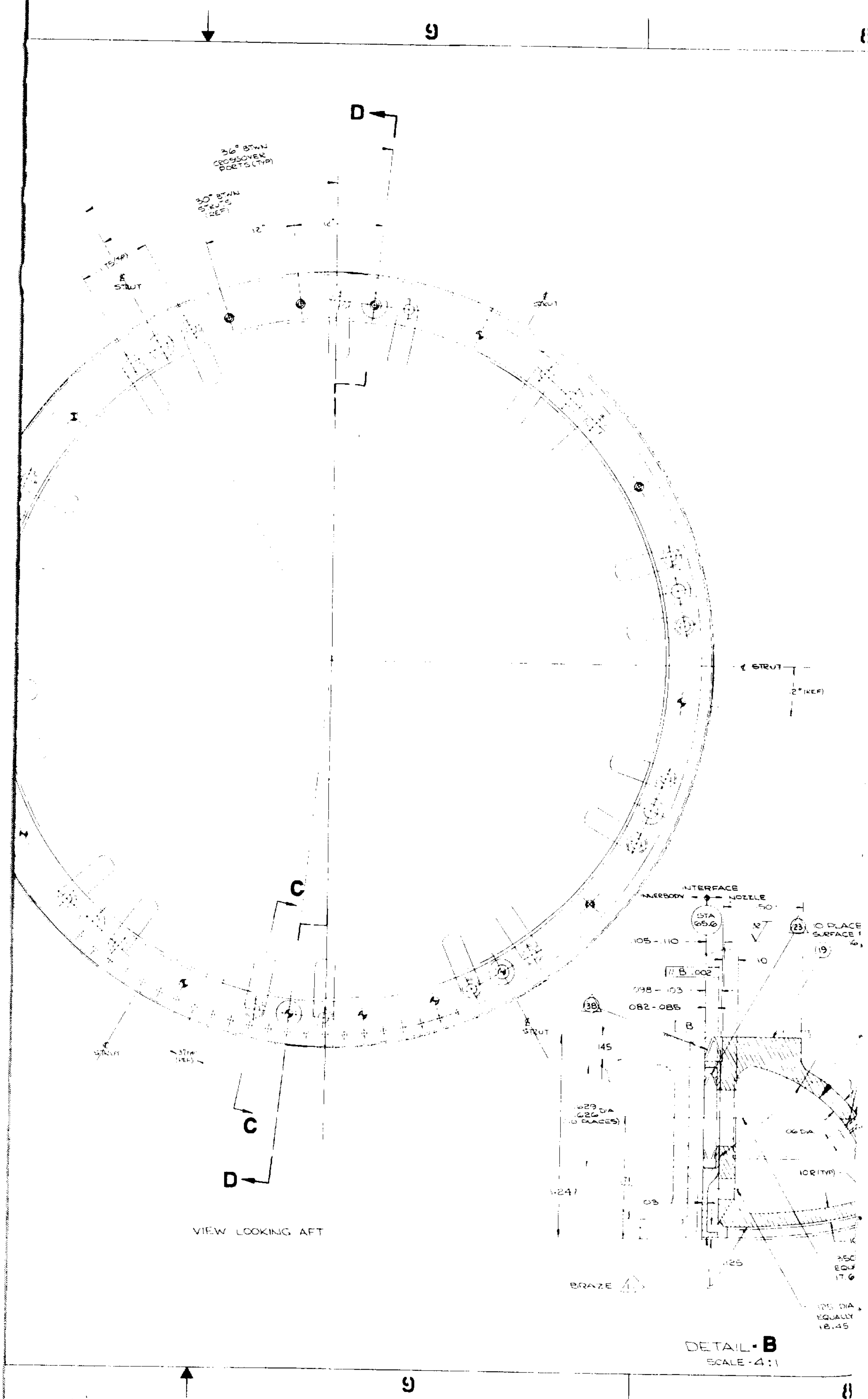

FOLDOUT FRAME 2

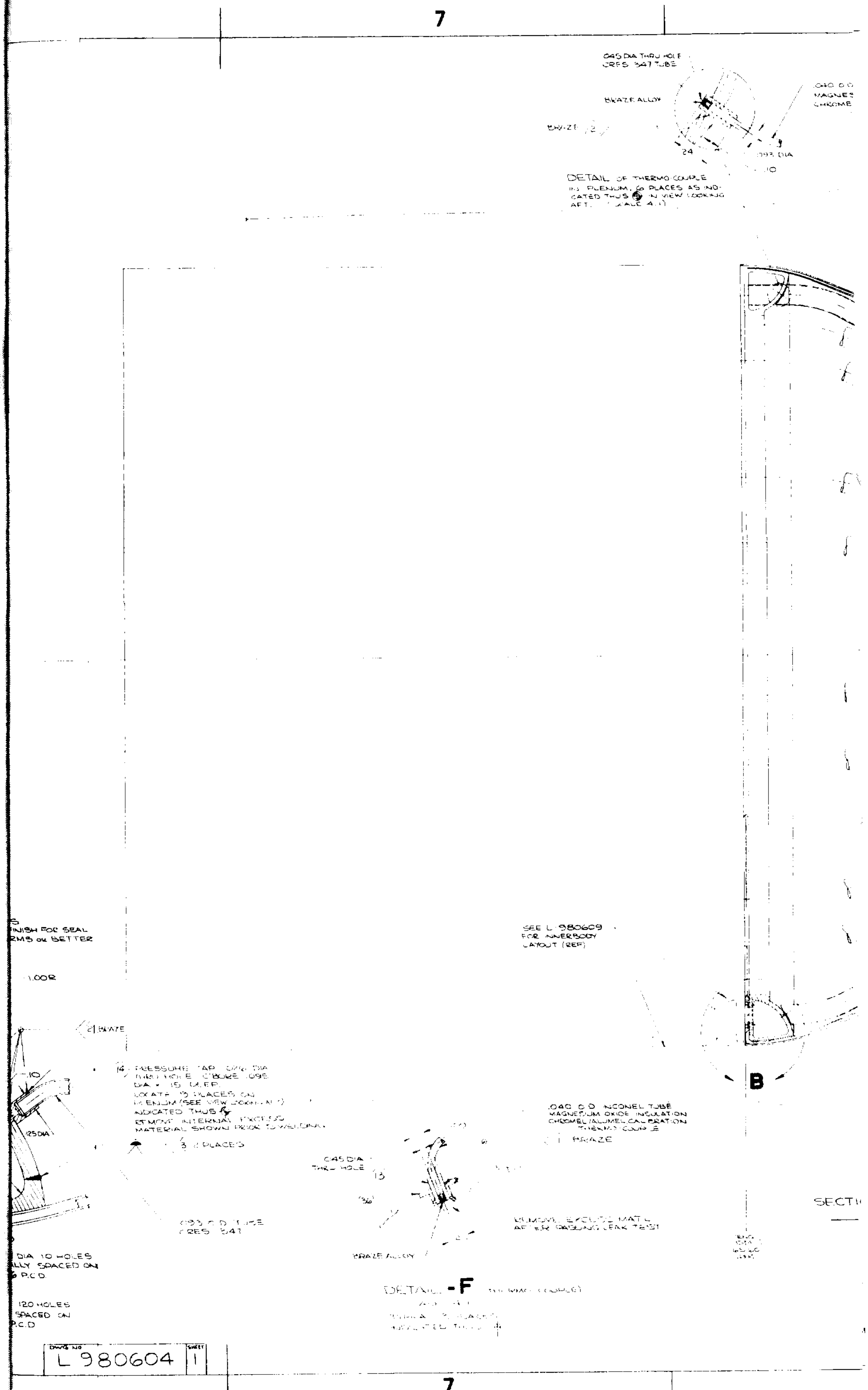

FOLDOUT FRAME 3

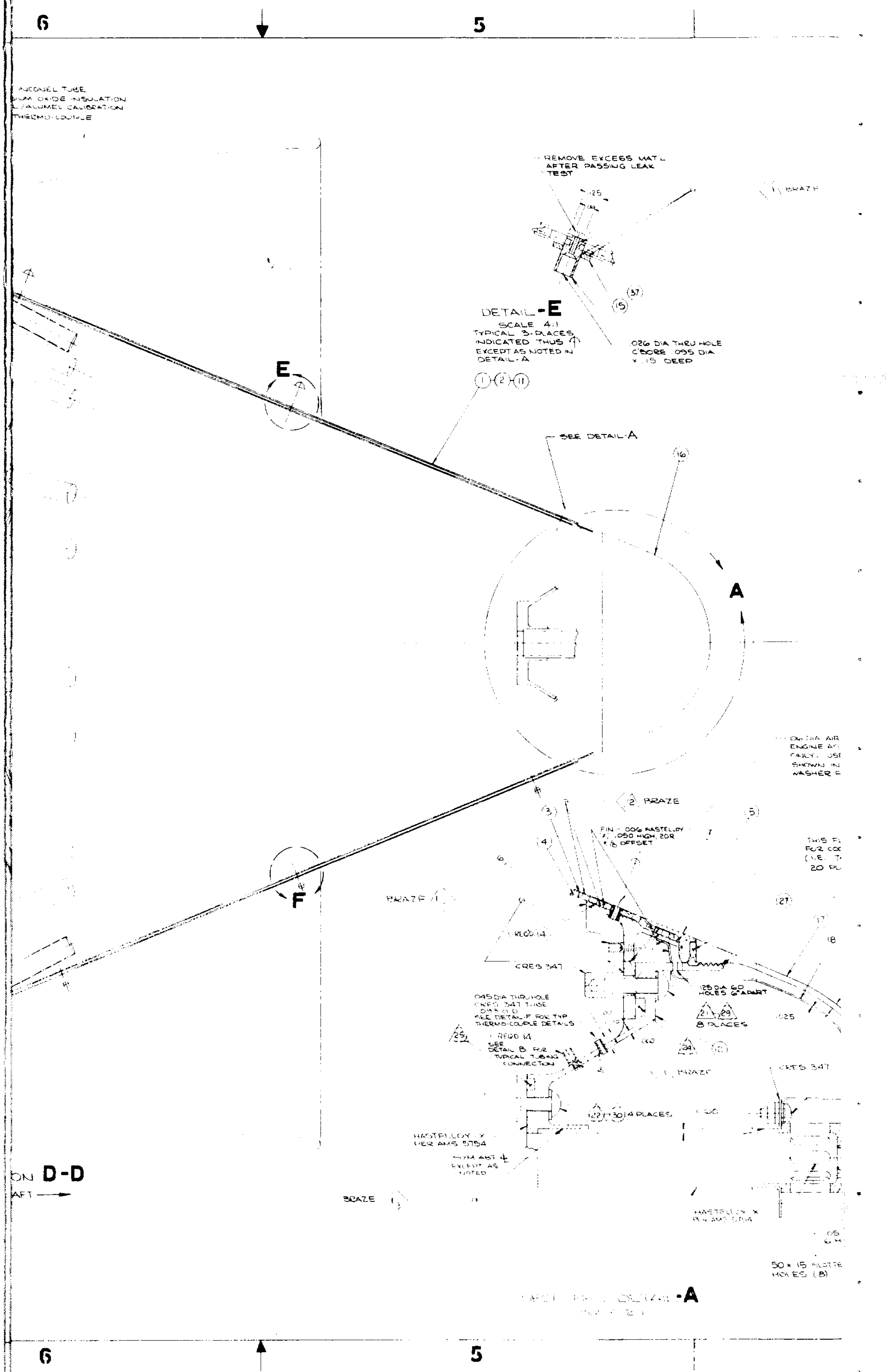

FOLDOUT FRAME 4

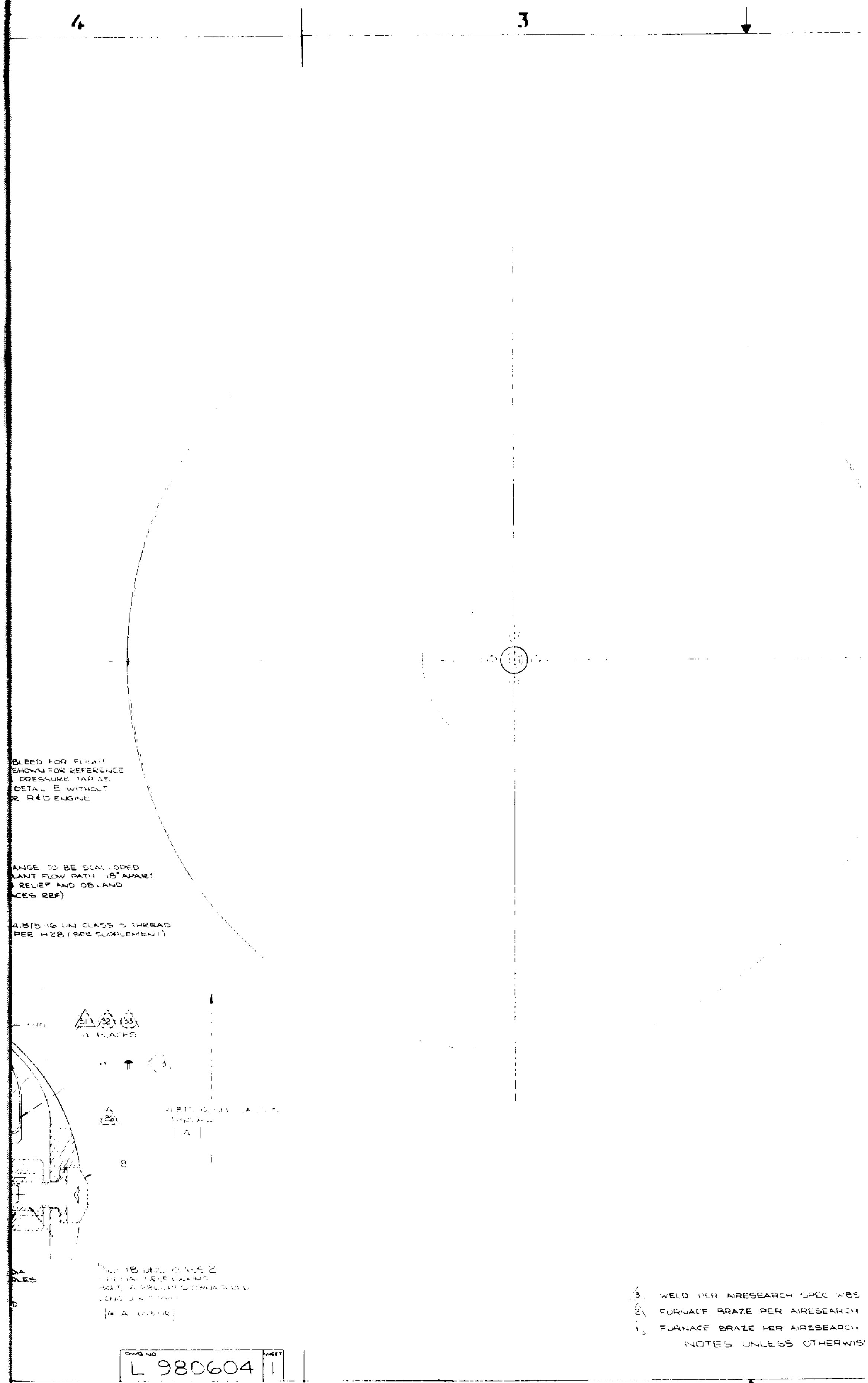

FOLDOUT FRAME 5

E

C

B

NEW	OLD	PART NUMBER	NO REQ	DESCRIPTION	N/A ITEM	MATERIAL	REF	REMARKS (HEAT TREATING, PLATING PROCESS OF MANUFACTURE, ETC.)	SPEC	DRAFT	CHECK	APPROVAL REMARKS OF CHECKER
	38	TVMV 540-8-5	1	SEAL - AIR				TETRAFLOUR INC INGLEWOOD CALIF				
37		980042-1	2	WASHER	11	HASTE-LLOY-X		AMS 5536				
36		980041-1	3	WASHER	11	HASTE-LLOY-X		AMS 5536				
	35	5815TN222-032	20	WASHER	1	CRES						
	34	DT43U048J11	20	BOLT - SELF LOCK'G	1	CRES		18-8 CRES ¼-28 THD LONG-LOK CORP'N				
	33	MS21048L04W	4	NUT PLATE	1							
	32	NAS1635-04-6	4	SCREW	1							
	31	NAS 620C4	4	WASHER	1							
	30	AN 960 C8	4	WASHER	1							
	29	NAS 620C10L	8	WASHER	1							
28												
27		980034-1	1	SEAL - PORT (SPCL)	1			HARRISON MFG.				
	26	12190AA-5	1	SEAL - PORT	1			HARRISON MFG.				
	25	22022NA2000	1	SEAL - FACE	1			HARRISON MFG				
	24	22023NA4000	1	SEAL - FACE	1			HARRISON MFG				
	23	22021NA625	10	SEAL - FACE	1			HARRISON MFG				
	22	DT43AB2Q11	4	SCREW - SELF LOCK'G	1	CRES		18-8 CRES 8-32 THD LONG LOK CORP'N				
	21	DT43A02Q11	8	SCREW - SELF LOCK'G	1	CRES		18-8 CRES 10-32 THD LONG LOK CORP'N				
20												
19		980037-1	1	PLENUM ASSY	11	HASTE-LLOY-X		AMS-5754				
18		980040-1	1	BAFFLE ASSY	1	CRES		CRES 347				
17		980036-1	1	CAP	1	HASTE-LLOY-X		AMS-5754				
16												
15		980039-1	3	PRESSURE TAP	11	HASTE-LLOY-X		AMS 5754				
14		980038-1	11	PRESSURE TAP	19	CRES		CRES 347				
13		980029-1	3	THERMO-COUPLE	11	HASTE-LLOY-X		AMS 5754				
12		980035-1	1	DOOR ASSY	1							
11		980028-1	1	NOZZLE ASSY	1							
10												
9												
8		980033-1		SCREW - CAP SELF LOCKING	1	CRES		CRES A286 DYNA-THRED LONG LOK CORP'N				
7		980032-1		RING FLOW GUIDE	11	CRES		.025 CRES 347				
6		980031-1	1	RING - COLD NOZZLE	11	HASTE-LLOY-X		AMS 5754				
5		980030-1	1	RING - HOT NOZZLE	11			AMS 5754				
4		980023-1	1	SHELL - COLD NOZZLE	2			AMS 5536				
3		980022-1	1	SHELL HOT NOZZLE	2	HASTE-LLOY-X		AMS-5536				
2		980021-1	1	SHELL ASSY - BRAZED	11							
1		980020-1		NOZZLE - ASSY								

18

SPEC WBS-27 USING PALNIRO 4

SPEC WBS-27 USING PALNIRO 1

E SPECIFIED

SIGNATURES	DATES	DATE STARTED	WITNESSED BY
DES B OGDEN	4-2-67		
MATL JOHNNE	5-1-67	4-7-67	
STRESS	5-1-67	DATE COMPLETED	WITNESSED BY
WEIGHT			
APPD	4-28-67	5-2-67	
APPD	5-8-67	WORK ORDER NO	
APPD	5/9/67	3402-250052-27-0500	
FEATURES			

AIRESEARCH MANUFACTURING COMPANY
A DIVISION OF THE GARRETT CORPORATION
LOS ANGELES, CALIFORNIA

LAYOUT

NOZZLE
H.R.E

SIZE	CODE IDENT NO.	DWG NO
	70210	L 980604

SCALE 1:1 & NOTED | WT | SHEET 1 OF 1

DWG NO L980604

2 1

FOLDOUT FRAME 6

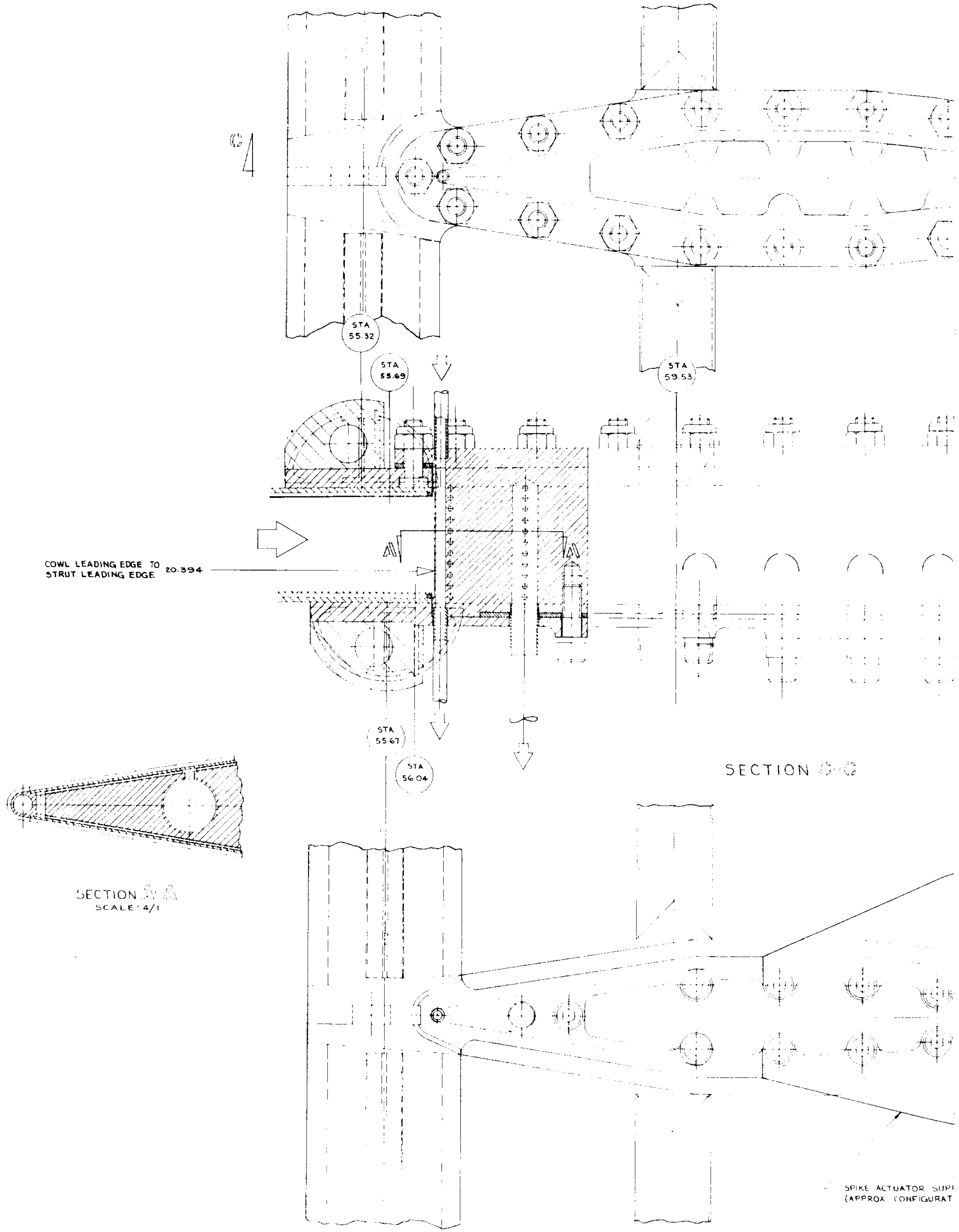

FOLDOUT FRAME 1

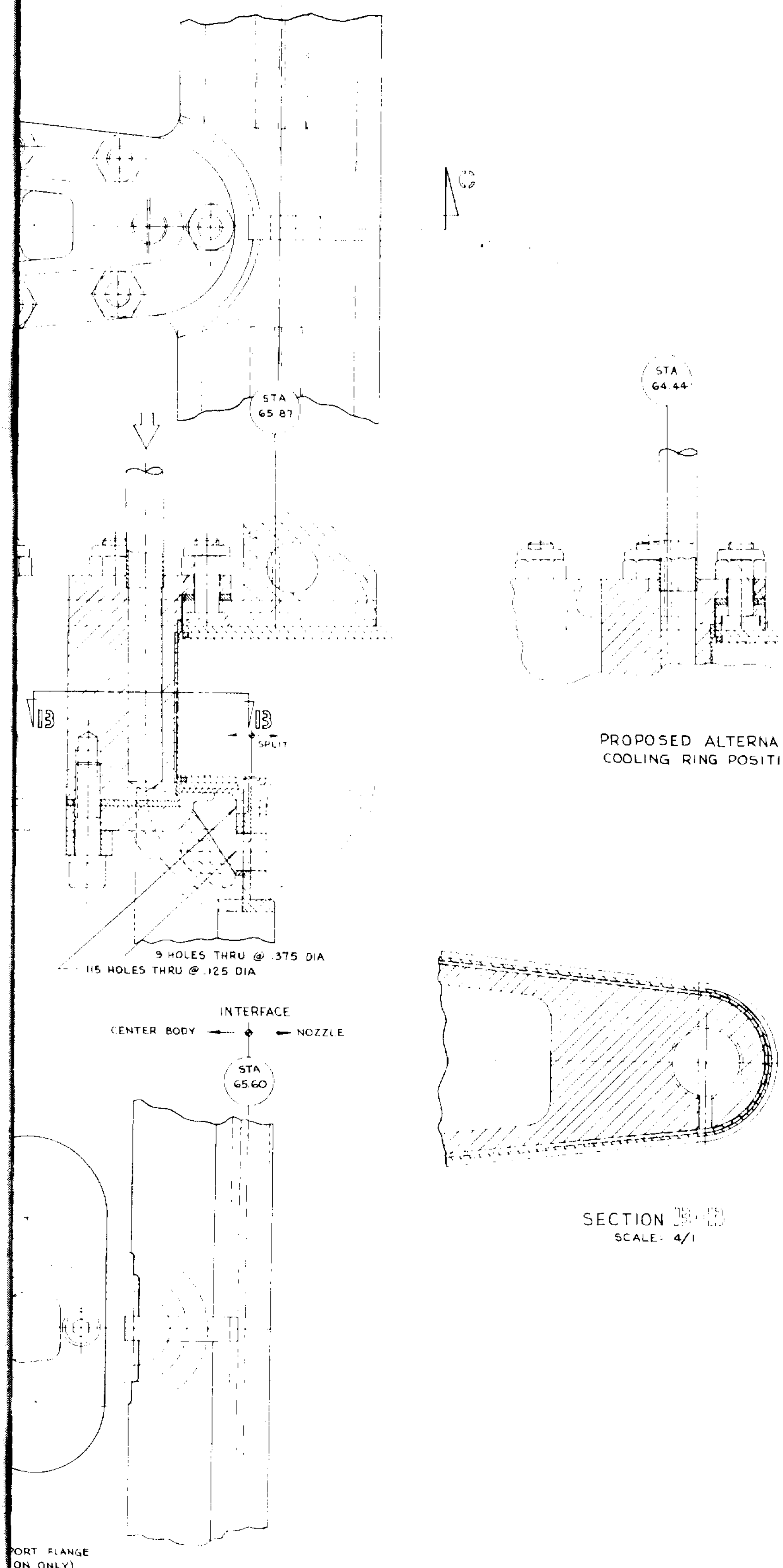

FOLDOUT FRAME 2

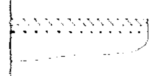

TE
ON

FOLDOUT FRAME 3

PROPRIETARY NOTICE

THIS LAYOUT DRAWING EMBODIES A PROPRIETARY DESIGN OWNED BY THE GARRETT CORPORATION, AND IS SUBMITTED UNDER A CONFIDENTIAL RELATIONSHIP. EXCEPT FOR USES EXPRESSLY GRANTED IN WRITING, ALL RIGHTS ARE RESERVED BY THE GARRETT CORPORATION. THIS DRAWING SHALL BE RETURNED WHEN THE NEED FOR IT HAS BEEN CONCLUDED.

SIGNATURES		DATES		
DES	M. E. COOKE	4-20-67	DATE STARTED	WITNESSED BY
MATL			4-14-67	
STRESS			DATE COMPLETED	WITNESSED BY
WEIGHT				
APPD			4-20-67	
APPD			WORK ORDER NO	
APPD			3402-250052-21-2500	

FEATURES
REVISED AERODYNAMIC STRUT SHAPE

AIRESEARCH MANUFACTURING COMPANY
A DIVISION OF THE GARRETT CORPORATION
LOS ANGELES, CALIFORNIA

LAYOUT

SUPPORT ASSY, STRUT,
H.R.E.

SIZE	CODE IDENT NO	DWG NO
J	70210	L-980608

SCALE 2/1	WT	SHEET 1 OF 1

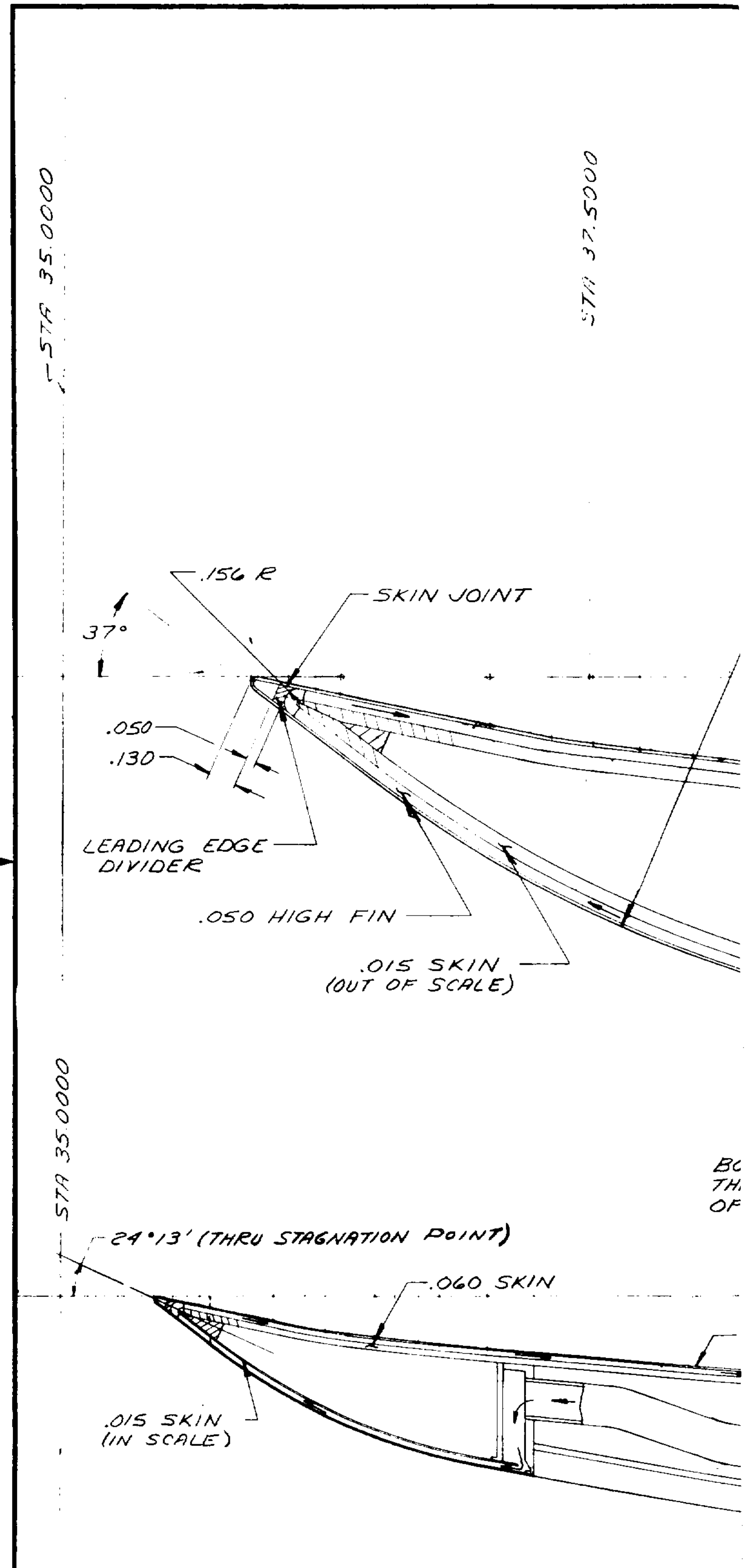

EXHAUST LEADING ED
COOLANT OUTLET FLOW

FOLDOUT FRAME /

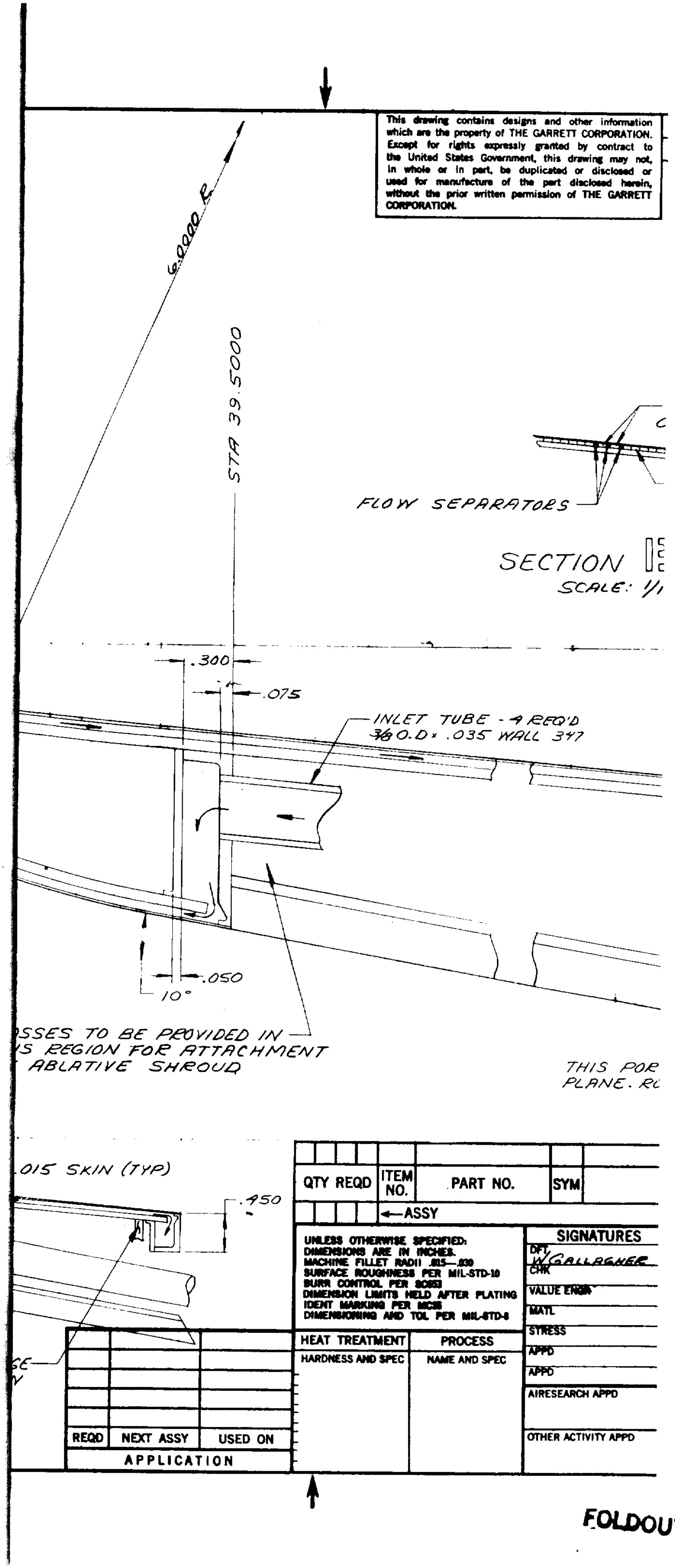

FOLDOUT FRAME 2

REVISIONS			
LTR	DESCRIPTION	DATE	APPROVED

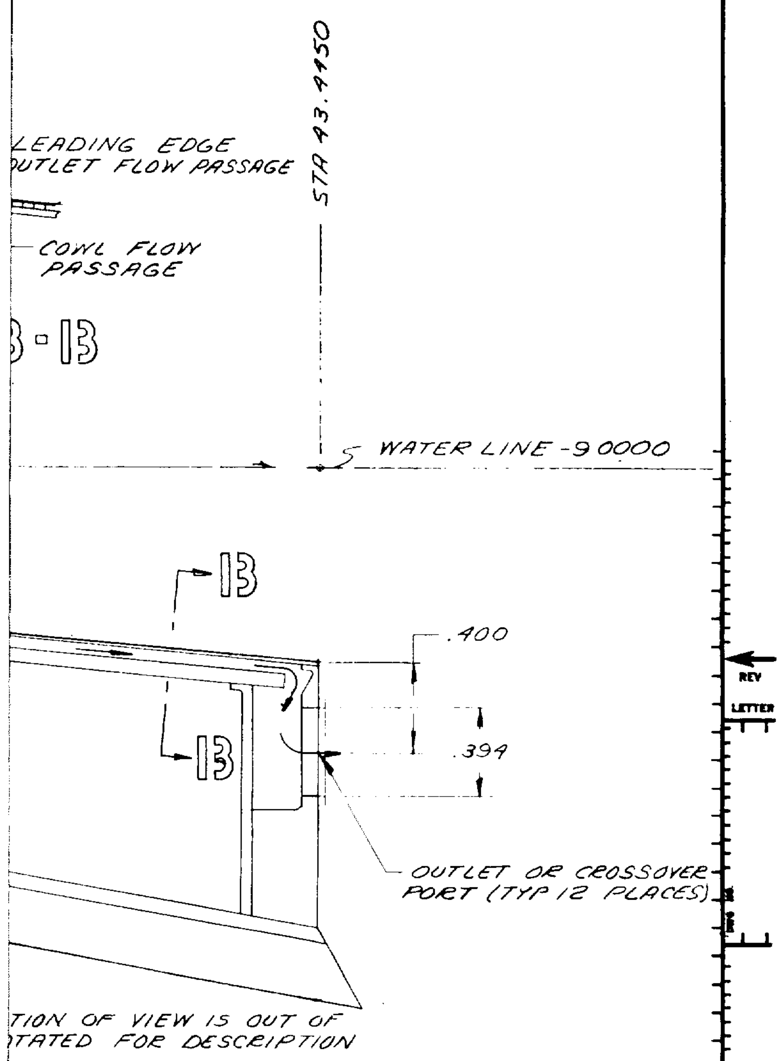

DESCRIPTION	CODE IDENT	MATERIAL AND SPECIFICATION
LIST OF MATERIAL		

DATES
5-1-67

AIRESEARCH MANUFACTURING COMPANY
A DIVISION OF THE GARRETT CORPORATION
LOS ANGELES, CALIFORNIA

LAYOUT - COWL LEADING EDGE
CONCEPT NO. 1
(PARALLEL)

SIZE	CODE IDENT NO.	DWG NO.
C	70210	SK 51305

SCALE 3/1 & 1/1 | SHEET OF

FOLDOUT FRAME 3

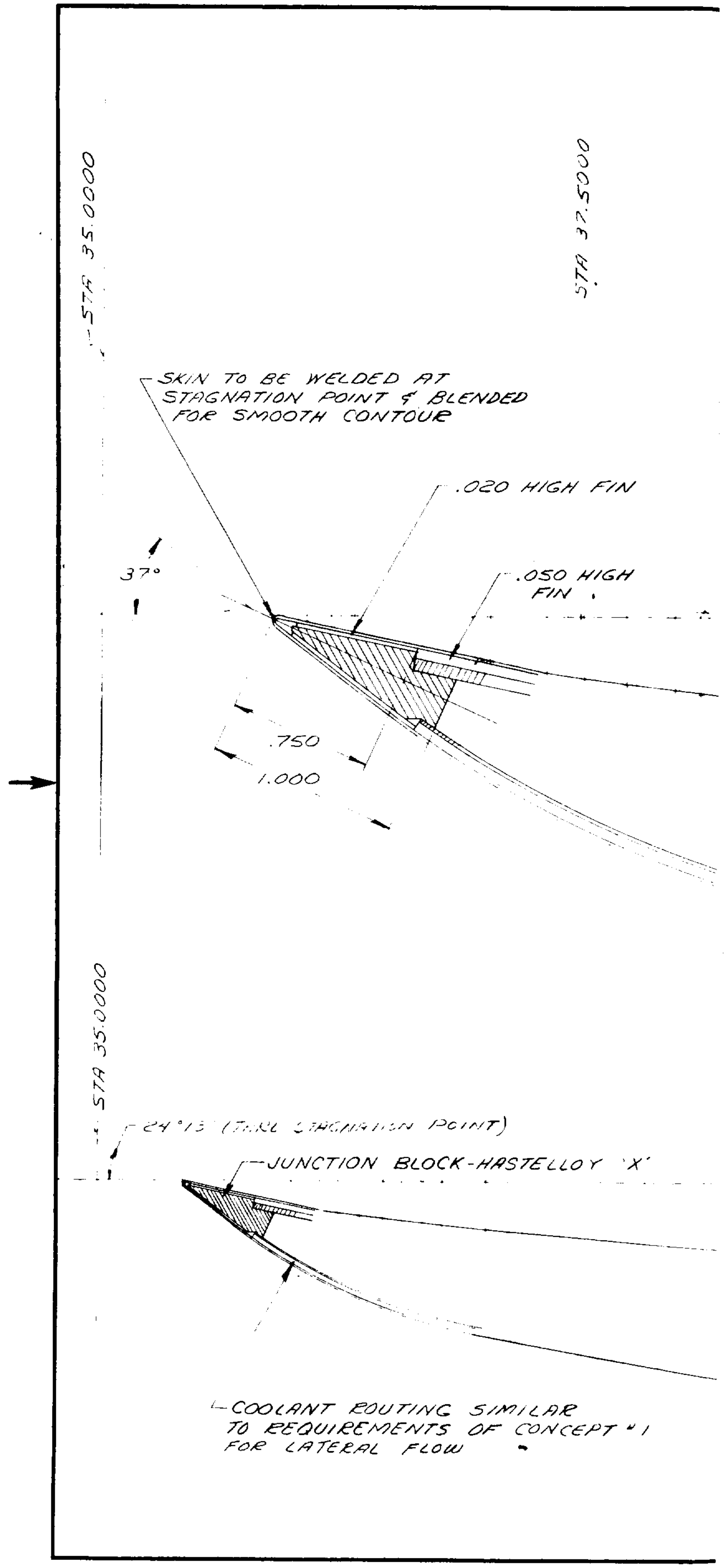

FOLDOUT FRAME 1

This drawing contains designs and other information which are the property of THE GARRETT CORPORATION. Except for rights expressly granted by contract to the United States Government, this drawing may not, in whole or in part, be duplicated or disclosed or used for manufacture of the part disclosed herein, without the prior written permission of THE GARRETT CORPORATION.

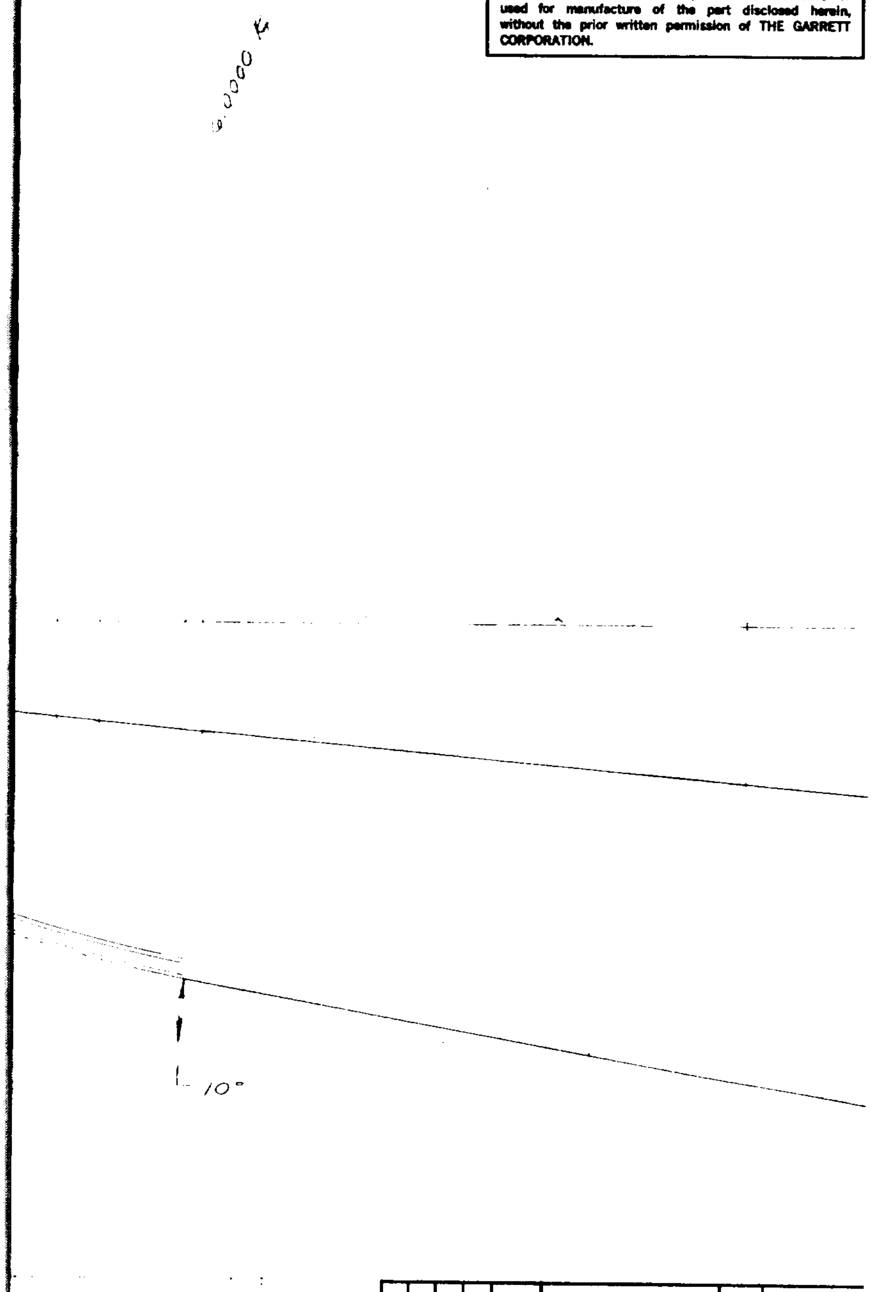

QTY REQD	ITEM NO.	PART NO.	SYM
←ASSY			

UNLESS OTHERWISE SPECIFIED:
DIMENSIONS ARE IN INCHES.
MACHINE FILLET RADII .015—.030
SURFACE ROUGHNESS PER MIL-STD-10
BURR CONTROL PER SC653
DIMENSION LIMITS HELD AFTER PLATING
IDENT MARKING PER MC35
DIMENSIONING AND TOL PER MIL-STD-8

SIGNATURES
DFT W. GALLAGHER
CHK
VALUE ENGR
MATL
STRESS
APPD
APPD
AIRESEARCH APPD
OTHER ACTIVITY APPD

HEAT TREATMENT	PROCESS
HARDNESS AND SPEC	NAME AND SPEC

REQD	NEXT ASSY	USED ON

APPLICATION

FOLDOUT FRAME 2

REVISIONS			
LTR	DESCRIPTION	DATE	APPROVED

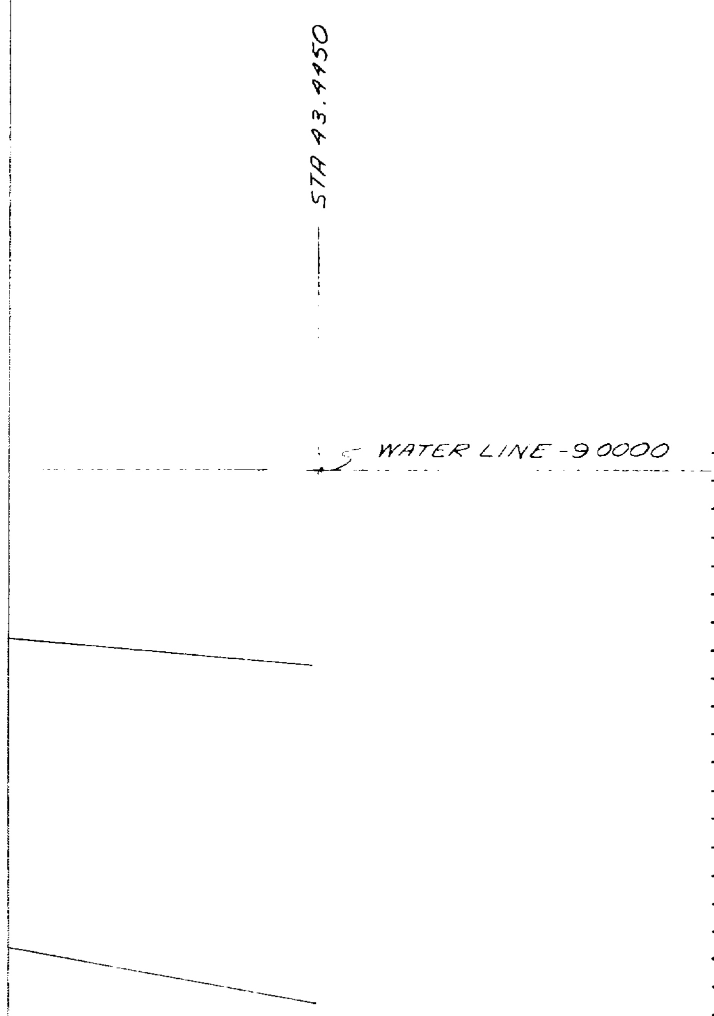

DESCRIPTION	CODE IDENT	MATERIAL AND SPECIFICATION

LIST OF MATERIAL

DATES	
5-1-67	AIRESEARCH MANUFACTURING COMPANY A DIVISION OF THE GARRETT CORPORATION LOS ANGELES, CALIFORNIA

LAYOUT - COWL LEADING EDGE
CONCEPT NO. 2
(PERPENDICULAR)

SIZE	CODE IDENT NO.	DWG NO.
C	70210	SK 51306

SCALE 4/1		SHEET	OF

FOLDOUT FRAME 3

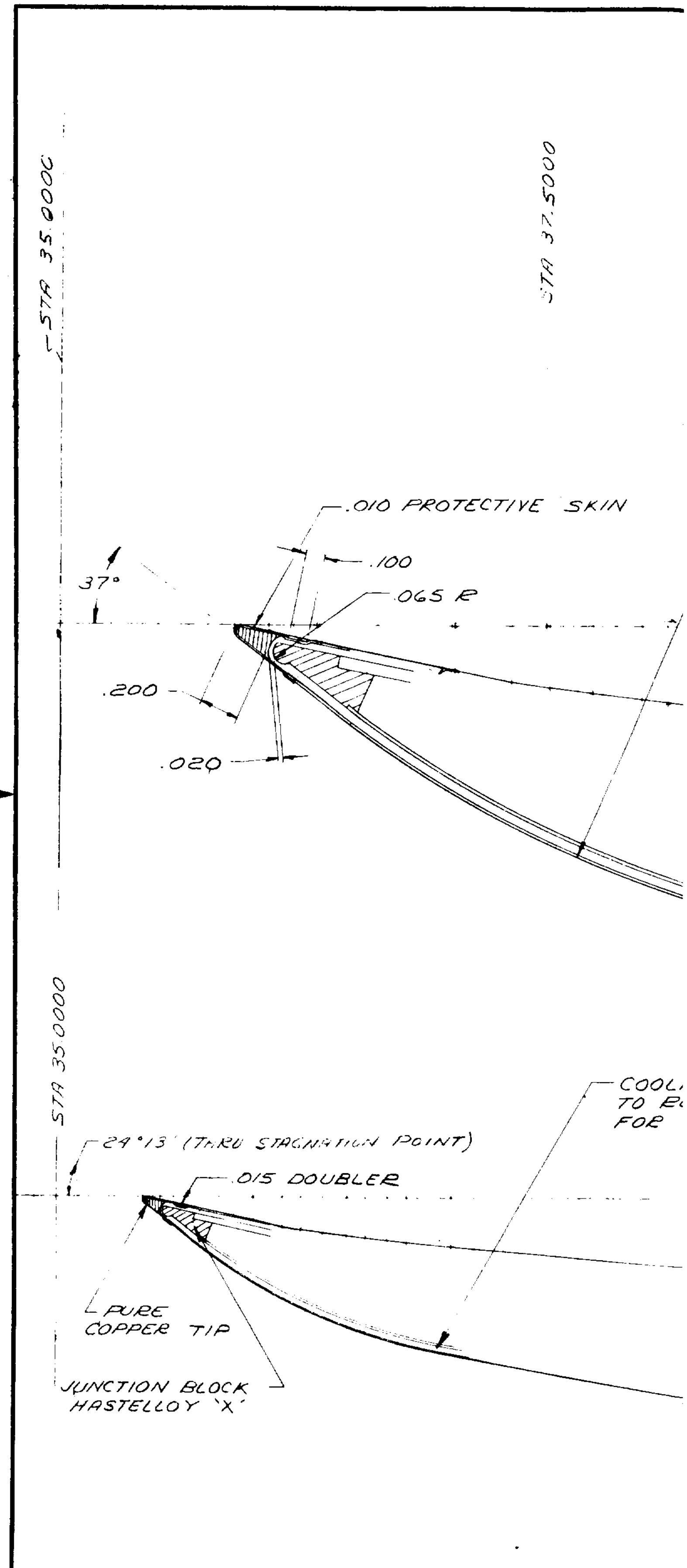

FOLDOUT FRAME 1

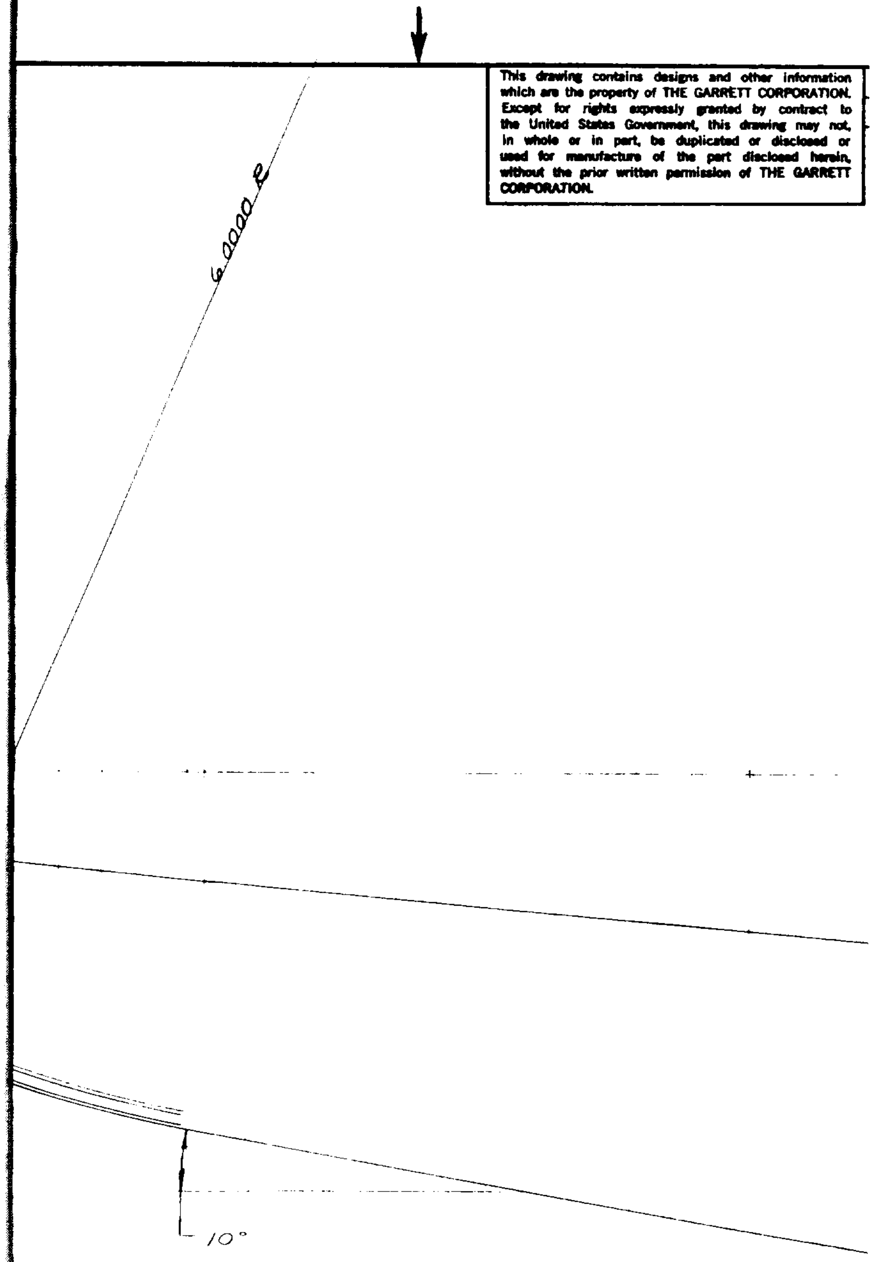

ANT ROUTING TO BE SIMILAR
EQUIREMENTS OF CONCEPT #1
LATERAL FLOW

QTY REQD	ITEM NO.	PART NO.	SYM
	←ASSY		

UNLESS OTHERWISE SPECIFIED:
DIMENSIONS ARE IN INCHES.
MACHINE FILLET RADII .015—.030
SURFACE ROUGHNESS PER MIL-STD-10
BURR CONTROL PER SC553
DIMENSION LIMITS HELD AFTER PLATING
IDENT MARKING PER MC36
DIMENSIONING AND TOL PER MIL-STD-8

HEAT TREATMENT	PROCESS
HARDNESS AND SPEC	NAME AND SPEC

SIGNATURES
DFT W GALLAGHER
CHK
VALUE ENGR
MATL
STRESS
APPD
APPD
AIRESEARCH APPD
OTHER ACTIVITY APPD

REQD	NEXT ASSY	USED ON
APPLICATION		

FOLDOUT FRAME 2

REVISIONS			
LTR	DESCRIPTION	DATE	APPROVED

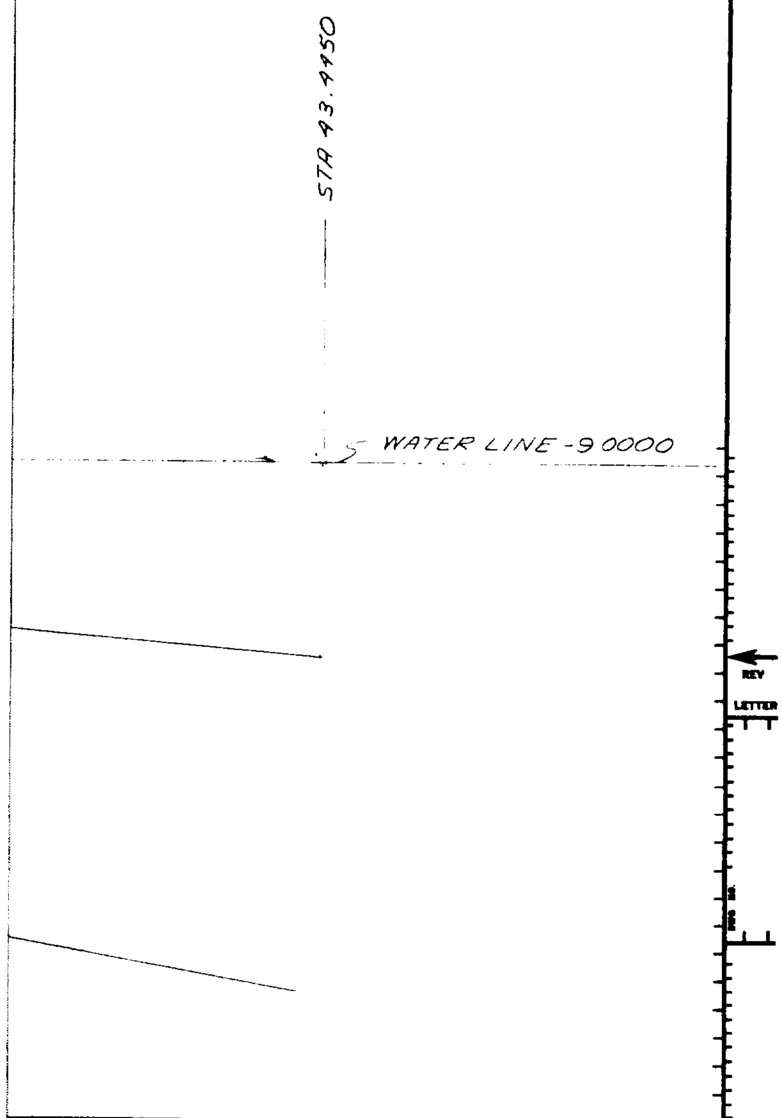

DESCRIPTION	CODE IDENT	MATERIAL AND SPECIFICATION
LIST OF MATERIAL		

DATES		
5-1-67	AIRESEARCH MANUFACTURING COMPANY A DIVISION OF THE GARRETT CORPORATION LOS ANGELES, CALIFORNIA	
	LAYOUT-COWL LEADING EDGE CONCEPT NO. 3 (COPPER TIP #1)	

SIZE	CODE IDENT NO.	DWG NO.
C	70210	SK51307
SCALE 3/1 [illegible]		SHEET OF

FOLDOUT FRAME 3

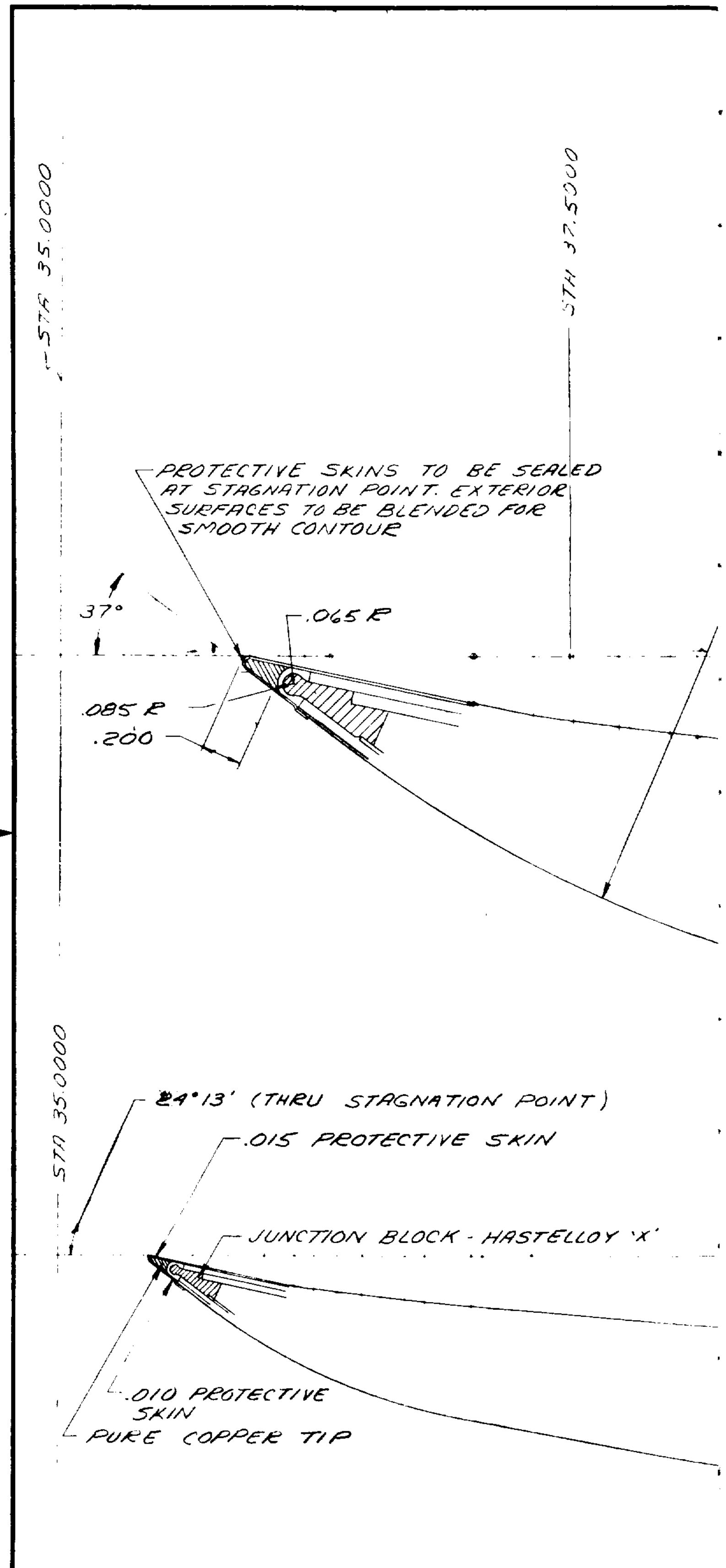

FOLDOUT FRAME /

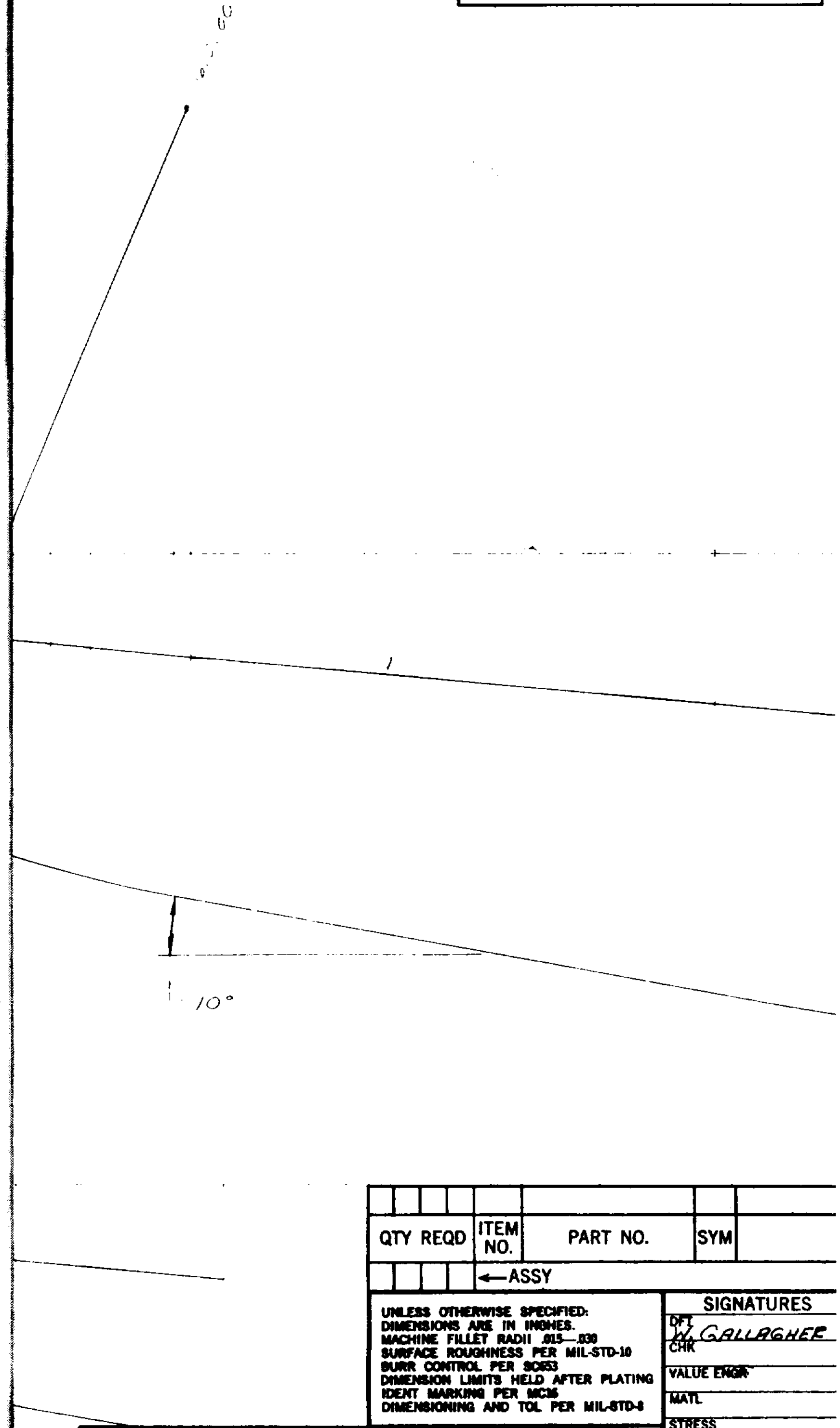

QTY REQD | ITEM NO. | PART NO. | SYM

←ASSY

UNLESS OTHERWISE SPECIFIED:
DIMENSIONS ARE IN INCHES.
MACHINE FILLET RADII .015—.030
SURFACE ROUGHNESS PER MIL-STD-10
BURR CONTROL PER SC653
DIMENSION LIMITS HELD AFTER PLATING
IDENT MARKING PER MC36
DIMENSIONING AND TOL PER MIL-STD-8

HEAT TREATMENT | PROCESS
HARDNESS AND SPEC | NAME AND SPEC

SIGNATURES
DFT W. GALLAGHER
CHK
VALUE ENGR
MATL
STRESS
APPD
APPD
AIRESEARCH APPD
OTHER ACTIVITY APPD

REQD | NEXT ASSY | USED ON
APPLICATION

FOLDOUT FRAME 2

REVISIONS			
LTR	DESCRIPTION	DATE	APPROVED

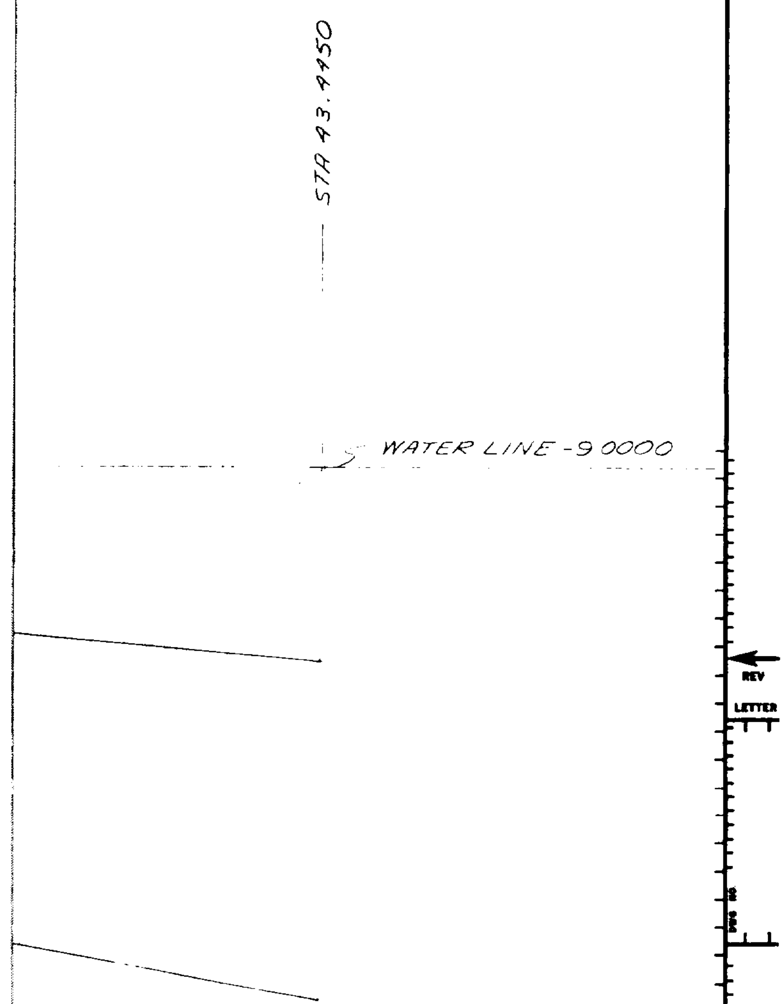

DESCRIPTION	CODE IDENT	MATERIAL AND SPECIFICATION

LIST OF MATERIAL

DATES	AIRESEARCH MANUFACTURING COMPANY A DIVISION OF THE GARRETT CORPORATION LOS ANGELES, CALIFORNIA		
5-1-67	LAYOUT- COWL LEADING EDGE CONCEPT NO. 4 (COPPER TIP NO.2)		
	SIZE C	CODE IDENT NO. 70210	DWG NO. SK51308
	SCALE 2/1		SHEET OF

FOLDOUT FRAME 3

6.0 MANUFACTURING

6.1 COMPOUND-CURVED MODEL

The compound-curved model, shown in Figure 6.1-1, is a half-scale section of a portion of the inlet spike incorporating inner and outer skins, fins, end closures, and manifold rings.

6.1.1 Purpose

The purpose of the compound-curved model is to evaluate manufacturing methods, assembly, and brazing procedures for guidance in fabrication of the full-scale cooled structures components.

6.1.2 Approach

Manufacturing processes and tooling for the model details are similar to those set up for the full-scale structure. Modifications found necessary to produce acceptable components can then be incorporated in the initial processing and tooling for the full-scale components.

Methods of brazing, using a self-fixturing arrangement and/or graphite fixtures, will be investigated.

6.1.2.1 Manufacturing Sequence and Tooling

6.1.2.1.1 Inner and Outer Skins

The inner and outer skins of the compound-curved model are fabricated from Hastelloy X sheet stock in the following sequence of operations:

a. Cut and trim sheet stock from blank to form cone

b. Roll-form cone and weld joint

c. Spin flange on large end of cone

d. Stretch-form to die contour

e. Anneal

f. Chemically mill to specified thickness

g. Trim to specified length and end diameters

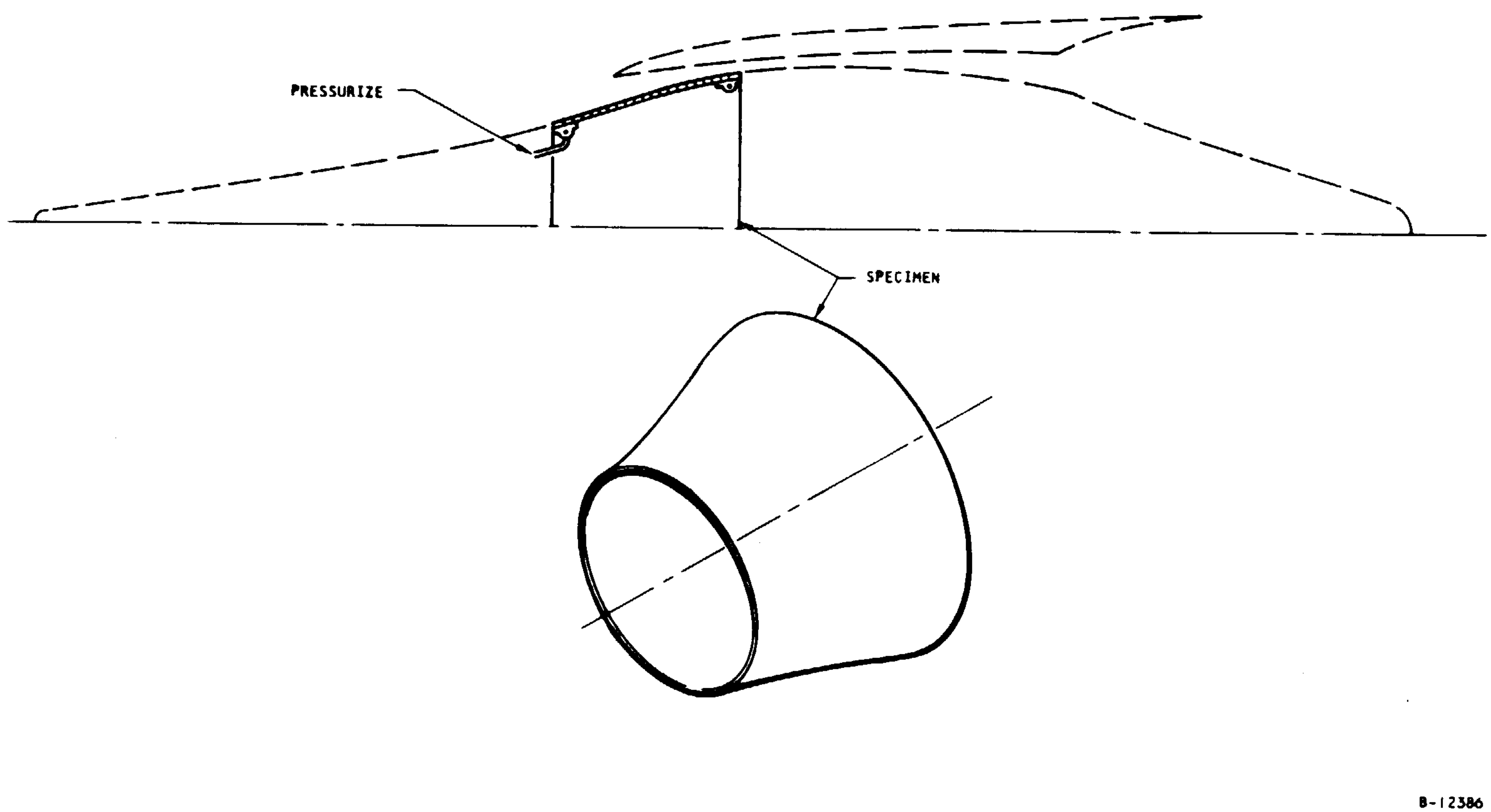

Figure 6.1-1. Compound-Curved Model with Reference to HRE Contours

h. Grind weld flush

i. Polish surface

j. Electrohydraulically form to final contour

k. Trim to final length

Inspection and/or cleaning operations which are made after each of the above operations have not been listed.

Special tooling consists of templates for checking contours, forming dies for the stretch and electrohydraulic forming, spin chuck for spinning flange, and trimming fixtures for sizing length of skins.

An inner skin after stretch forming, is shown in Figure 6.1-2.

6.1.2.1.2 Other Detail Components

All other details of the compound-curved model assembly (fins, headers, and manifolds) are fabricated by conventional machine shop and sheet metal shop practices and require no special tooling except for the manufacture of the fins, which are made with available fin dies.

6.1.2.2 Brazing

A two-cycle brazing operation will be used to accomplish the assembly of the compound-curved model; the first cycle, using a high temperature braze alloy (Palniro 4), to braze the basic assembly of skins, fins, and headers; and the second cycle, using a lower temperature braze alloy (Palniro 1 or Palniro 7), to braze the manifolds to the basic assembly.

6.1.2.2.1 Assembly of Components

Components are assembled by tack welding brazing foil, large end header ring, fins, and small end header ring to the inner skin in the order listed. Brazing foil is tack welded to the inner surface of the outer skin, then the outer skin is heated, slipped down over the inner skin, and on cooling provides a tight fit between components. To ensure retaining assembly alignment, the outer skin is tack welded to the header rings.

Brazing foil is tack welded to the joint surface of the manifold rings, then the ring and foil assembly is installed and tack welded to the inner surface of the inner skin for the second braze cycle.

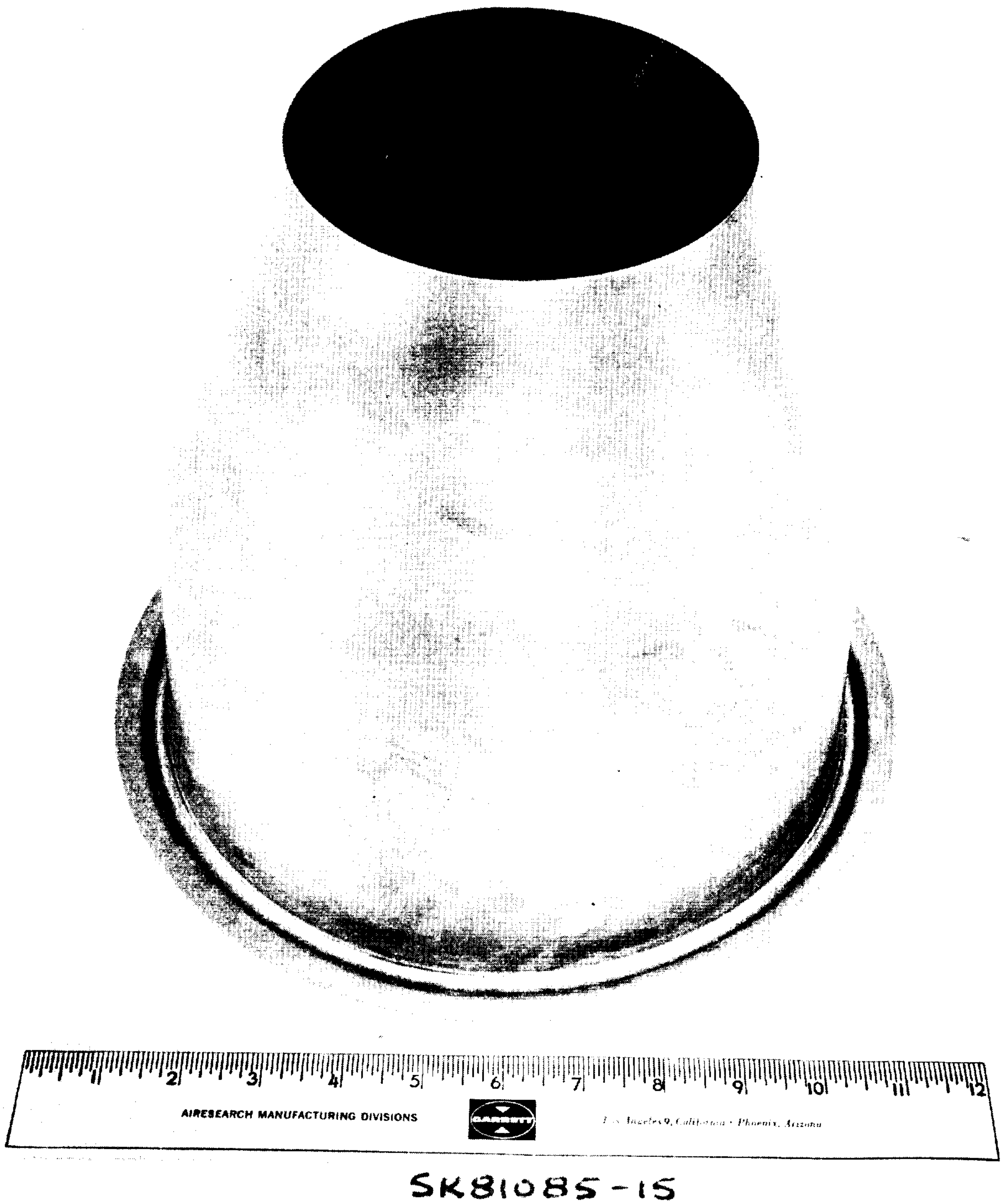

58831-12

Figure 6.1-2. Stretch-Formed Inner Skin of Compound-Curved Model

6.1.2.2.2 Brazing Fixtures

Fixturing methods being considered for the brazing operation are:

Self-fixturing - Shrink-fitting of outer skin with and without use of seal-welded header to skin joint and internal vacuum.

Graphite fixtures - To hold and load the assembly during the brazing cycle.

6.1.3 Tooling and Fixtures

Tooling and fixtures are shown in the figures listed below.

Figure No.	Tool No.	Title
6.1-3	T-607302	Tracer Template
	T-607306	Tracer Template
	T-607311	Tracer Template
	T-607312	Tracer Template
6.1-4	T-607317	Stretch-Form Tooling
6.1-5	T-607305	Trim Fixture
6.1-6	T-607318	Spin Chuck
6.1-7	T-607310	Graphite Braze Fixture
6.1-8	T-607309	Assy Tack Weld Fixture
6.1-9	T-607307	Final Sizing Die

6.2 FLAT PANELS

6.2.1 Purpose

Flat panels are being used to evaluate the effects of braze alloy foil thickness, brazing cycle time, and fin material thickness on the structural strength of the cooled structures.

6.2.2 Approach

Flat panels are used to permit close control of all variables in order to accurately evaluate specific variables affecting the structural strength of the cooled structure.

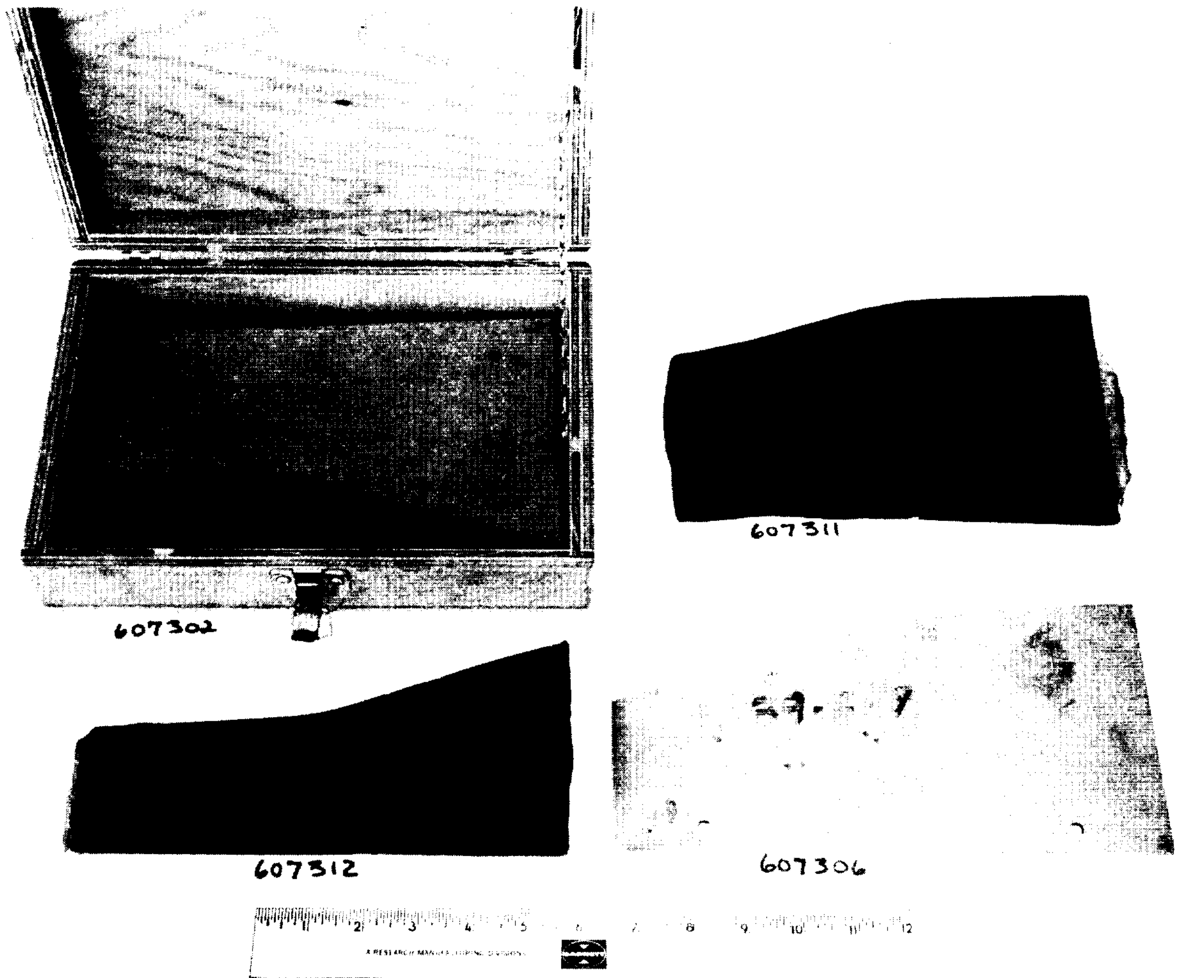

58831-9

Figure 6.1-3. Tracer Templates (Tool No. T-607302, T-607306, T-607311, and T-607312)

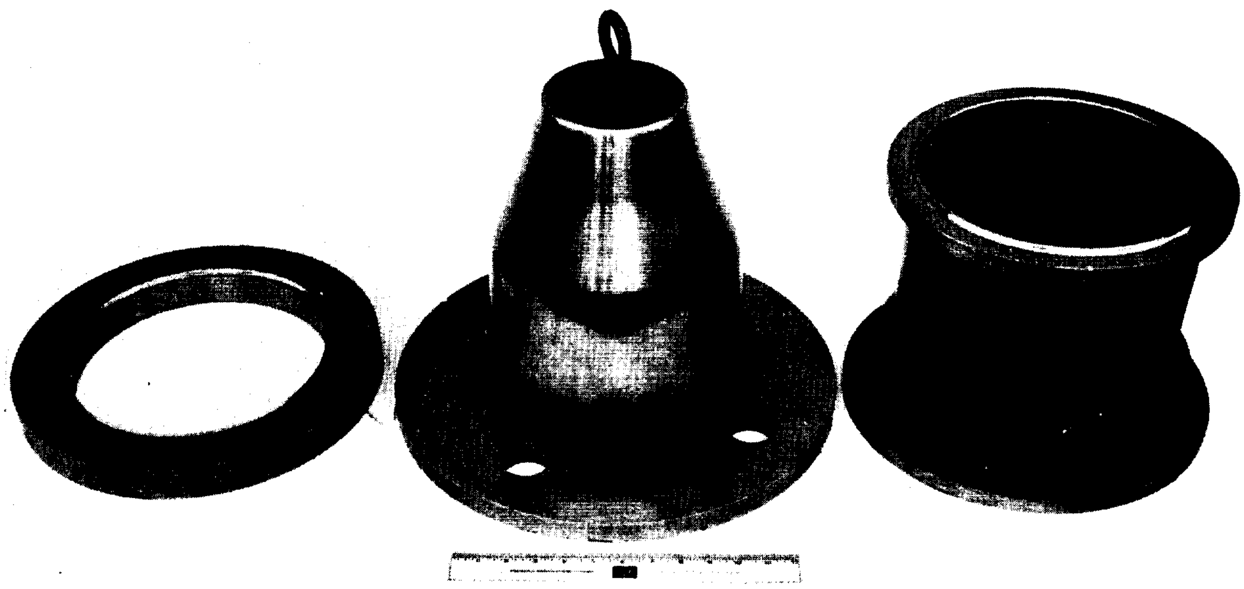

58831-13

Figure 6.1-4. Stretch Form Tooling (Tool No. T-607317)

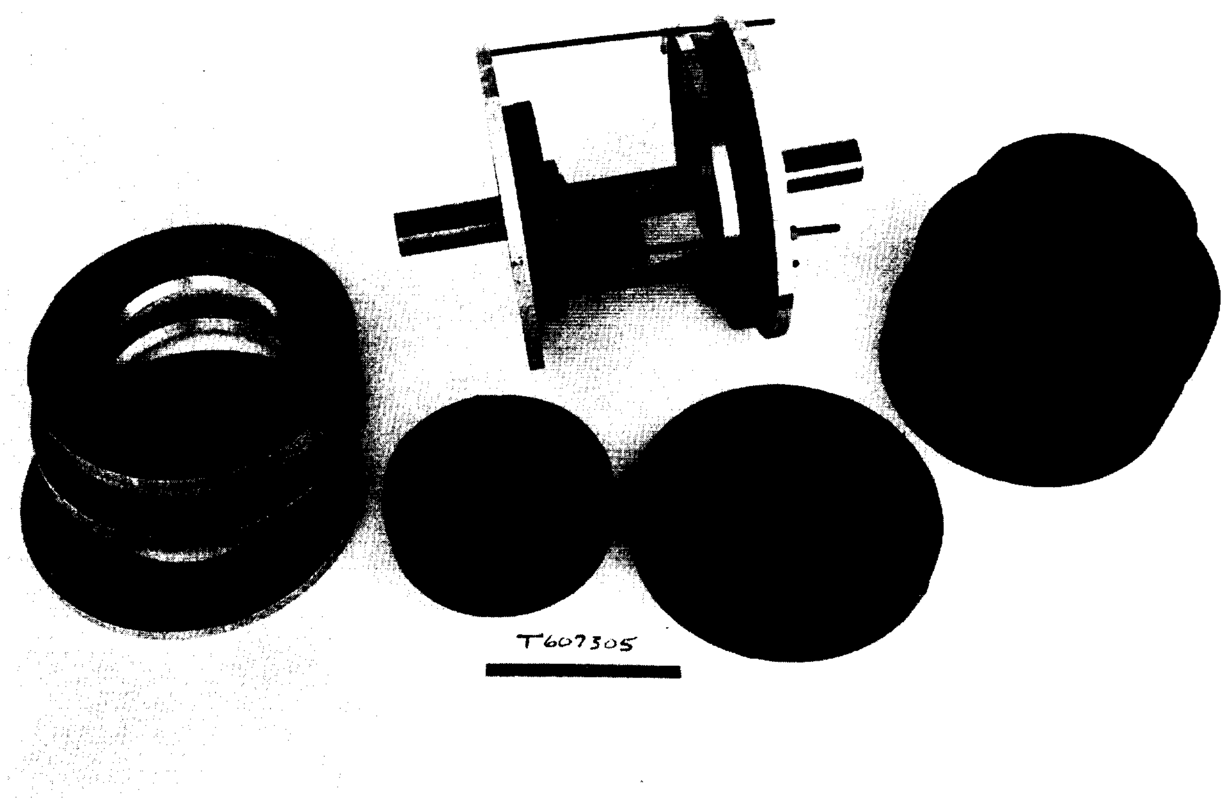

58831-2

Figure 6.1-5. Trim Fixture (Tool No. T-607305)

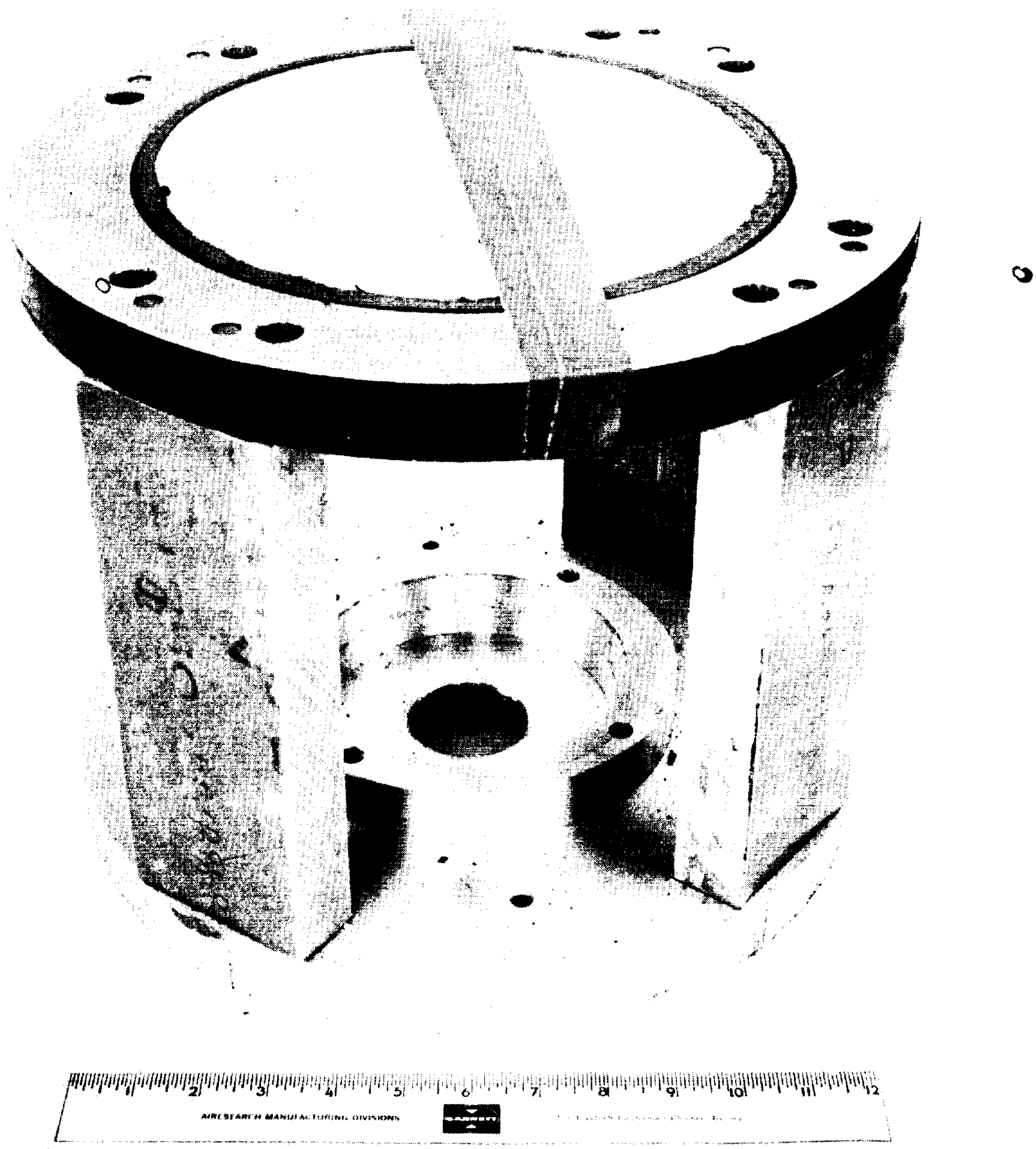

T-607318

58831-11

Figure 6.1-6. Spin Chuck (Tool No. T-607318)

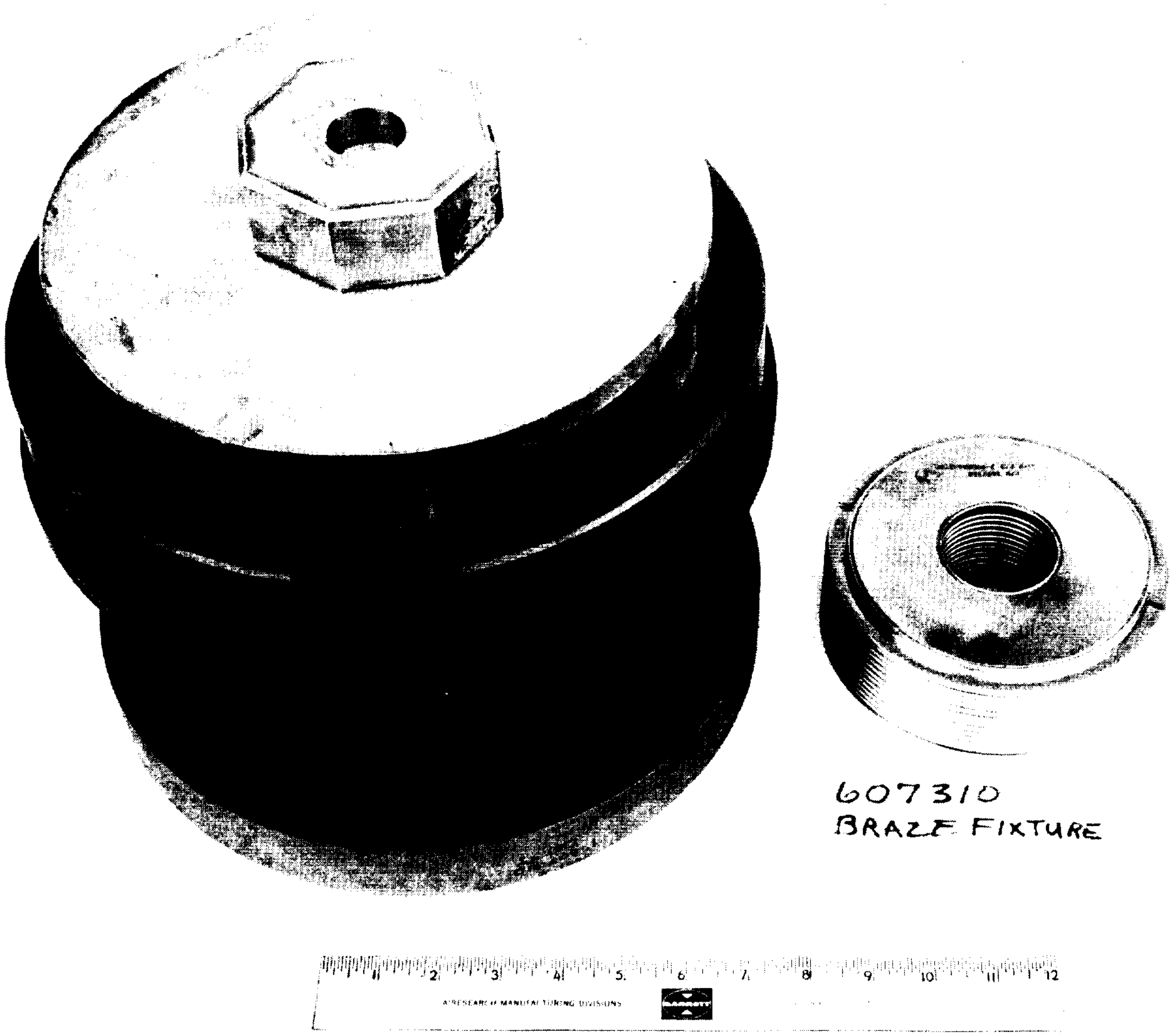

58831-5

Figure 6.1-7. Assembled View of Graphite Brazing Fixture (Tool No. T-607310)

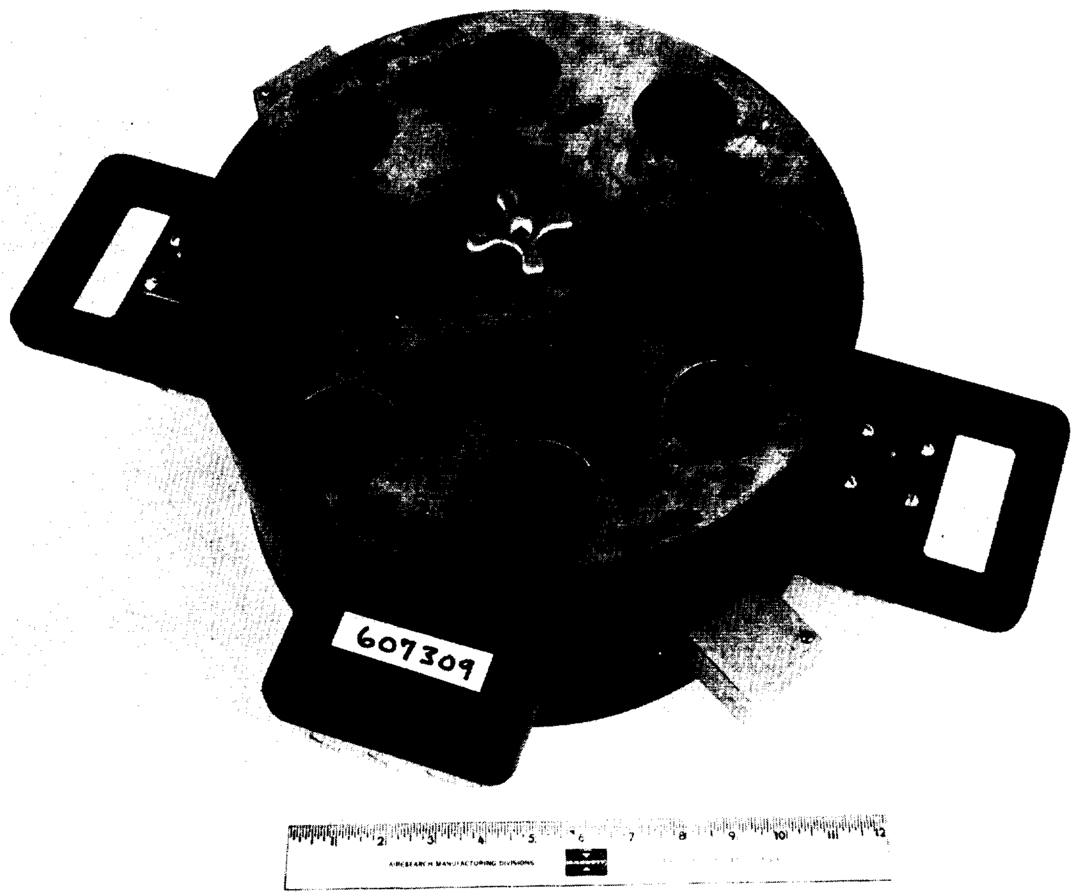

58831-8

Figure 6.1-8. Assembly Task Weld Fixture (Tool No. T-607309)

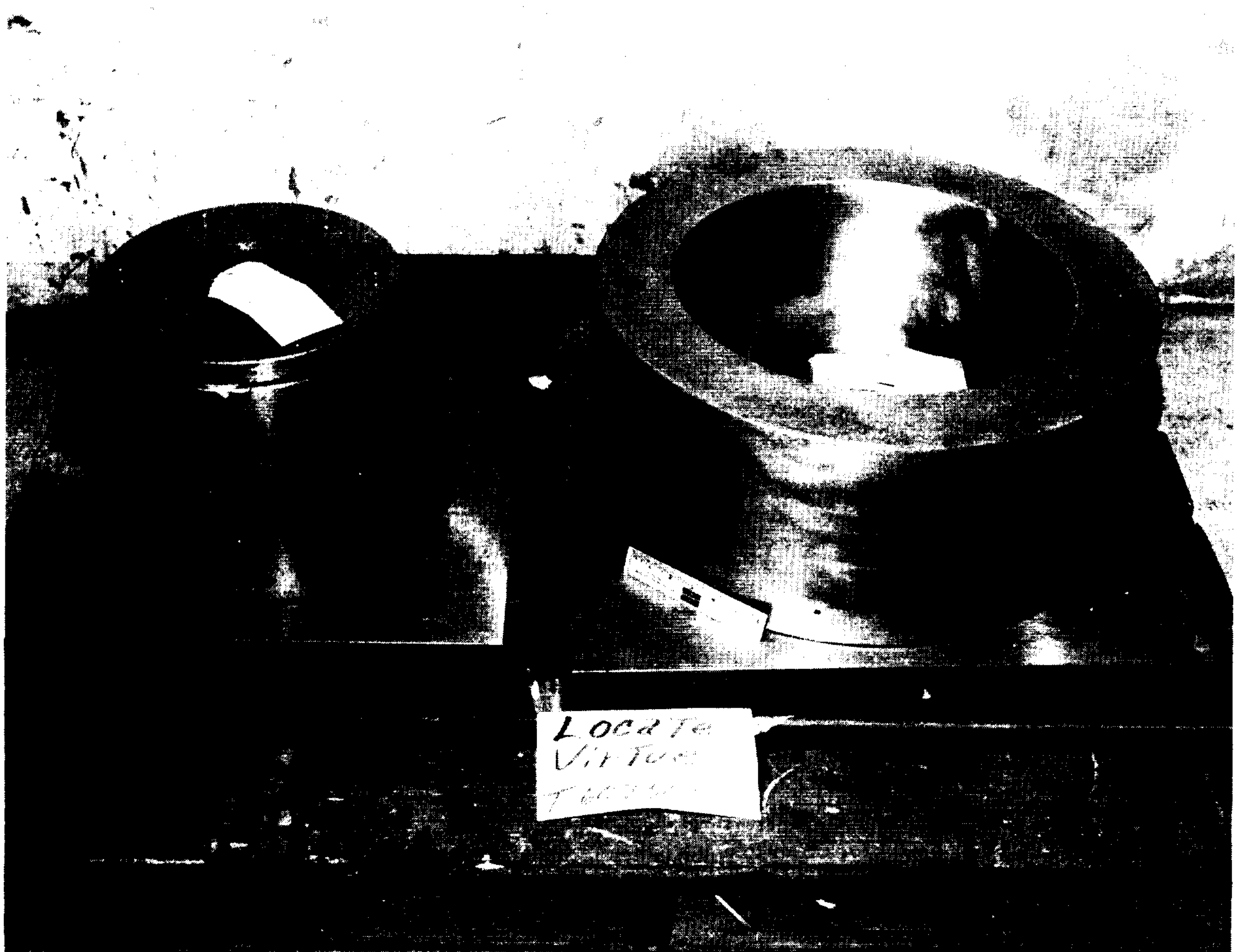

58831-1

Figure 6.1-9. Final Sizing Die (Tool No. T-607307)

6.2.2.1 Manufacturing Sequence and Tooling

The detail parts for the flat panels are fabricated by conventional machine shop and sheet metal shop practices. Available dies are used for fabricating fins and one-piece headers. No special tooling or manufacturing processes are required.

6.2.2.2 Brazing

A single brazing cycle is used for the panels shown in Figure 6.2-1. Panels shown in Figure 6.2-2 are brazed in two cycles, the first cycle brazing the flat panels, and the second cycle, with a different braze alloy at a lower temperature, used to attach the tubes and washers to the panels.

Panels are brazed by stacking and loading the stack with weights to apply a uniform pressure during the brazing operation. A vacuum furnace with temperature control is used for the brazing operations.

6.3 NOZZLE BOLTING TEST SECTION

Limited space and access is available to install the bolts attaching the nozzle assembly to the inner shell assembly. The test section duplicates the available space and will be used to develop special wrenching tools for installing and removing the nozzle-to-inner shell attaching bolts.

Figure 6.3-1 is a photo of the test section, the sheet metal section simulating the available space in nozzle and the block simulating the inner shell flange.

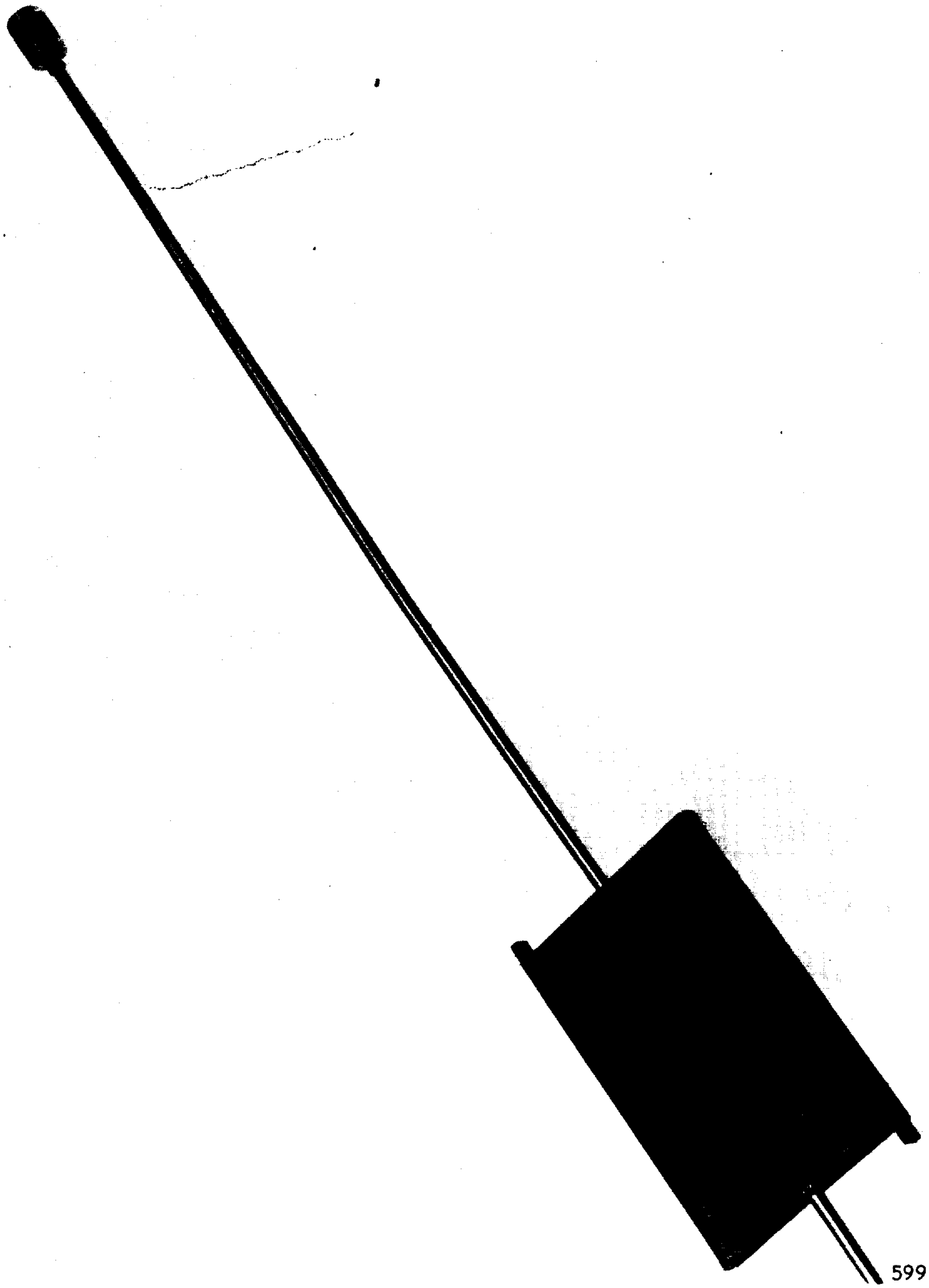

Figure 6.2-1. Type 1 Flat Panel Configuration

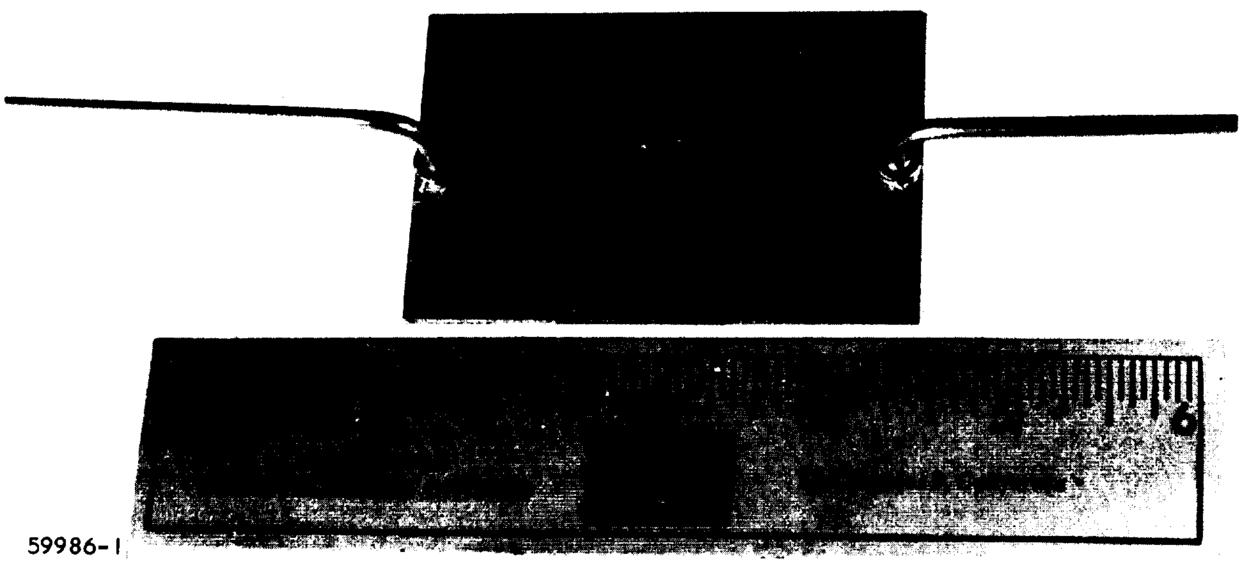
59986-1

Figure 6.2-2. Type 2 Flat Panel Configuration

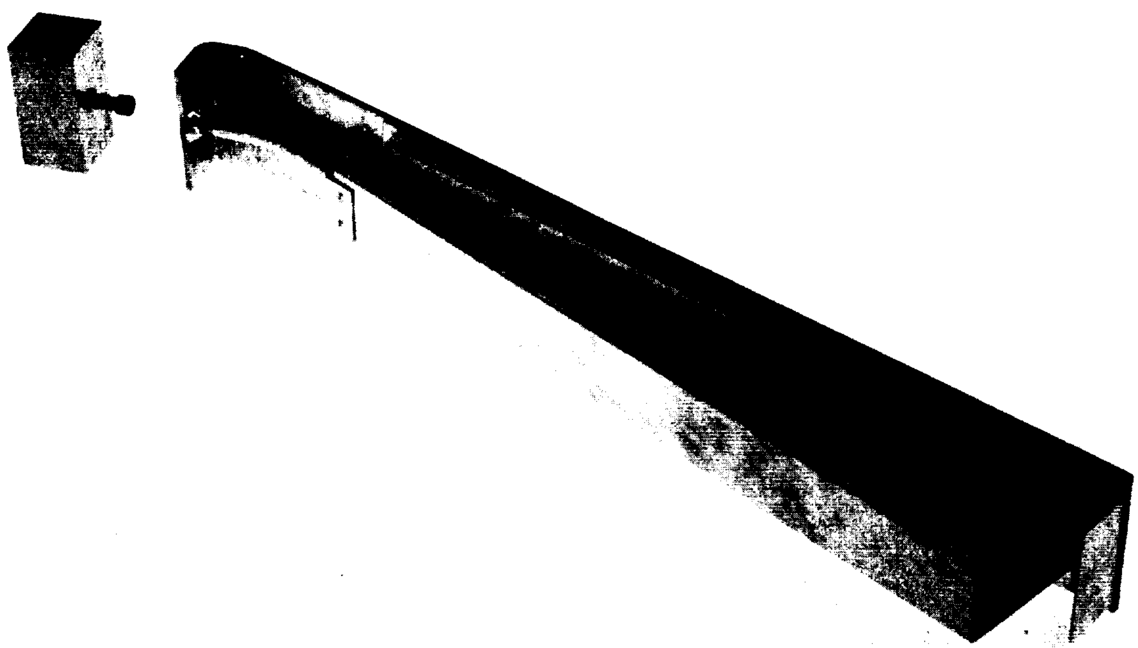

F-7657

Figure 6.3-1. Nozzle Bolting Test Section

7.0 TESTING

7.1 FLAT PANEL TEST OBJECTIVES

Tests were conducted on flat panels to evaluate the brazing procedures and short term burst and creep rupture strengths for three types of brazed test panels, using brazing foil thicknesses and brazing cycle times as tabulated in Table 7.1-1.

7.2 DESCRIPTION OF TEST PANELS

The test panels shown in Figure 6.2-1, Type 1 panel, and Figure 6.2-2, Type 2 panel, are also typical for the Type 3 panels. They are 2 by 3 in. sections consisting of a single layer of fin, brazed between two sheets separated by header bars, as shown in the exploded view, of Figure 7.2-1. Basic construction is the same for all three types, although details of the header construction and tube connection on Type 1 differs from that on Types 2 and 3 for reasons of manufacturing convenience.

7.3 FLAT PANEL TEST PROCEDURE

7.3.1 Leakage and Proof Pressure Test

Panels were connected to a nitrogen gas supply, pressurized to 1050 psig, and checked for leaks and any indications of permanent deformation to test the structural integrity of the brazed assembly. All test panels were subjected to this test before being instrumented with thermocouples for short term burst or creep rupture tests.

7.3.2 Short Term Burst Test

Test panels were instrumented to measure panel temperature and pressure and installed in one of the Marshall muffle furnaces shown in Figure 7.3-1 for elevated temperature tests, or in a water tank for ambient temperature tests. Pressure was applied and slowly and continuously increased until failure by rupture or deformation occurred.

7.3.3 Creep Rupture Test

Panel instrumentation and test setup for this test were the same as used for the short term burst elevated temperature tests. Test panels were installed in the furnace. Furnace temperature was then raised to bring the test specimen to specified temperature in approximately one-half hour. Specified pressure was then applied and both temperature and pressure held at specified values until failure occurred.

7.4 TEST RESULTS

7.4.1 Leakage and Proof Pressure Test

All test panels, fabricated to date, completed this test satisfactorily.

TABLE 7.1-1

FLAT PANEL DATA

Configuration	Serial No.	Finish	Braze Filler Alloy Foil Thickness, in.	Time at Braze Temperature, min	Braze Filler Alloy Type	Braze Temperature, ^{o}F
Type 1		16R-.153-.100-.006			Palniro 4	2160
	1-6		0.001	5		
Type 2		34R-.025-.050-.002			Palniro 4	2160
	1-4		0.001	5		
	5		0.001	20		
	6		0.0005	20		
	7-10		0.0005	5		
Type 3		20R-.075-.100-.004			Palniro 4	2160
	1-5		0.001	5		

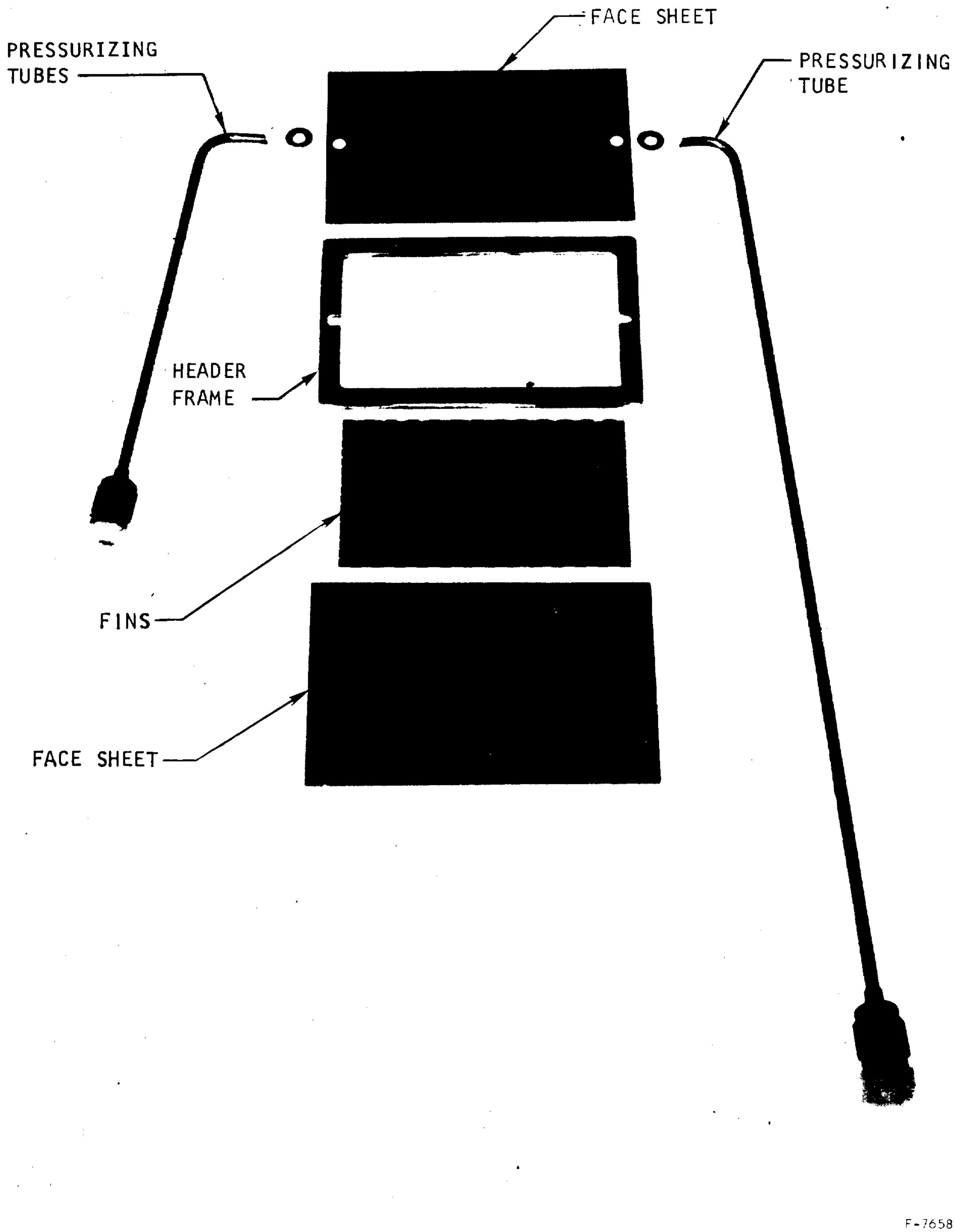

Figure 7.2-1. Exploded View of Flat Panel

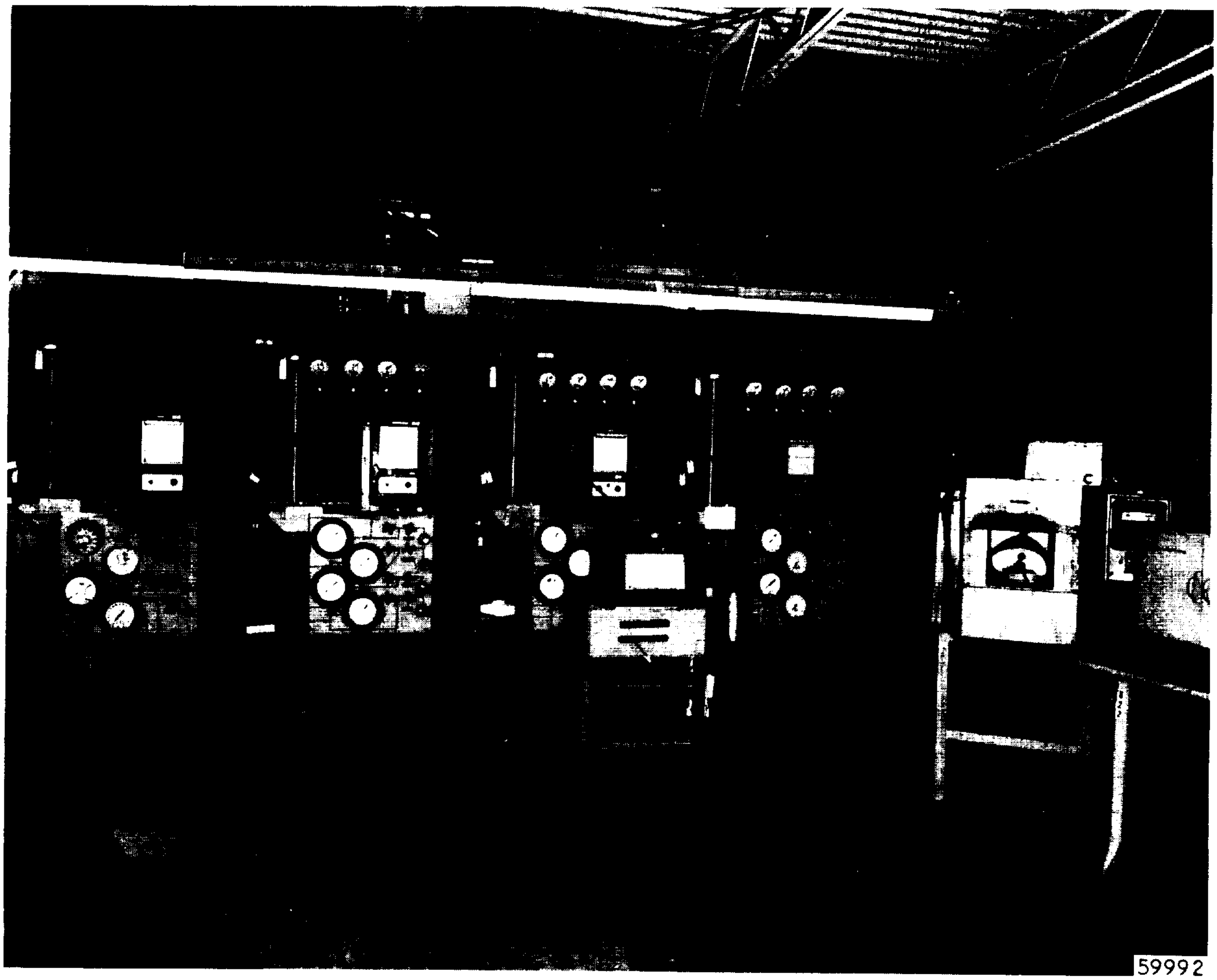

Figure 7.3-1. Regenerative Cooled Panels High Temperature Test Facility

7.4.2 Short-Term Burst Tests

Results are tabulated in Table 7.4-1, but have not been fully analyzed. Visual inspection of fail test panels indicates that all braze joints were satisfactory and that ruptures occurred as tensile ruptures of the fin material. Typical failures for each type of panel are shown in Figures 7.4-1, 7.4-2, and 7.4-3. Metallurgical inspection of typical failed panels is in progress for further evaluation.

Results for the Type 2 test panels indicate that the ultimate strength decreased with increase in the brazing cycle time. Further evaluation of the effect of brazing cycle time will be made on additional Type 1 and Type 3 test panels which have been brazed using a 20-min cycle time.

7.4.3 Creep-Rupture Tests

Results which have not been fully analyzed are tabulated in Table 7.4-1 and typical creep rupture test failures are shown in Figures 7.4-4 and 7.4-5 for Type 2 and Type 3 panels.

Visual inspection and preliminary analysis of the test results indicate the same conditions for rupture as obtained on short-term burst tests. Additional test panels of Type 1 and Type 3 configurations will be used for further evaluation of the effect of braze cycle time on creep-rupture strength.

TABLE 7.4-1

FLAT PANEL TEST DATA

Configuration	Serial No.	Short-Term Burse Test		Creep Rupture Test		
		Temperature, °F	Burst Pressure, psig	Temperature, °F	Pressure, psig	Time to Rupture, Hr:min
Type 1	1	1600	2125	NA	NA	NA
	2	RT	7400	NA	NA	NA
	3	1200	3600	NA	NA	NA
	4	1200	3400	NA	NA	NA
	5	1200	3750	NA	NA	NA
	6	RT	7300	NA	NA	NA
Type 2	1	NA	NA	1500	850	6:24
	2	NA	NA	1500	750	4:41
	3	1500	3650	NA	NA	NA
	4	1500	3250	NA	NA	NA
	5	1500	2125	NA	NA	NA
	6	1500	1400	NA	NA	NA
	7	NA	NA	1500	750	6:46
	8	NA	NA	1500	700	10:36
	9	1500	2575	NA	NA	NA
	10	1500	2575	NA	NA	NA
	1	NA	NA	1600	780	3:21
	2	NA	NA	1600	650	5:14
	3	NA	NA	1600	700	3:30
	4	1600	2680	NA	NA	NA
	5	1600	2375	NA	NA	NA

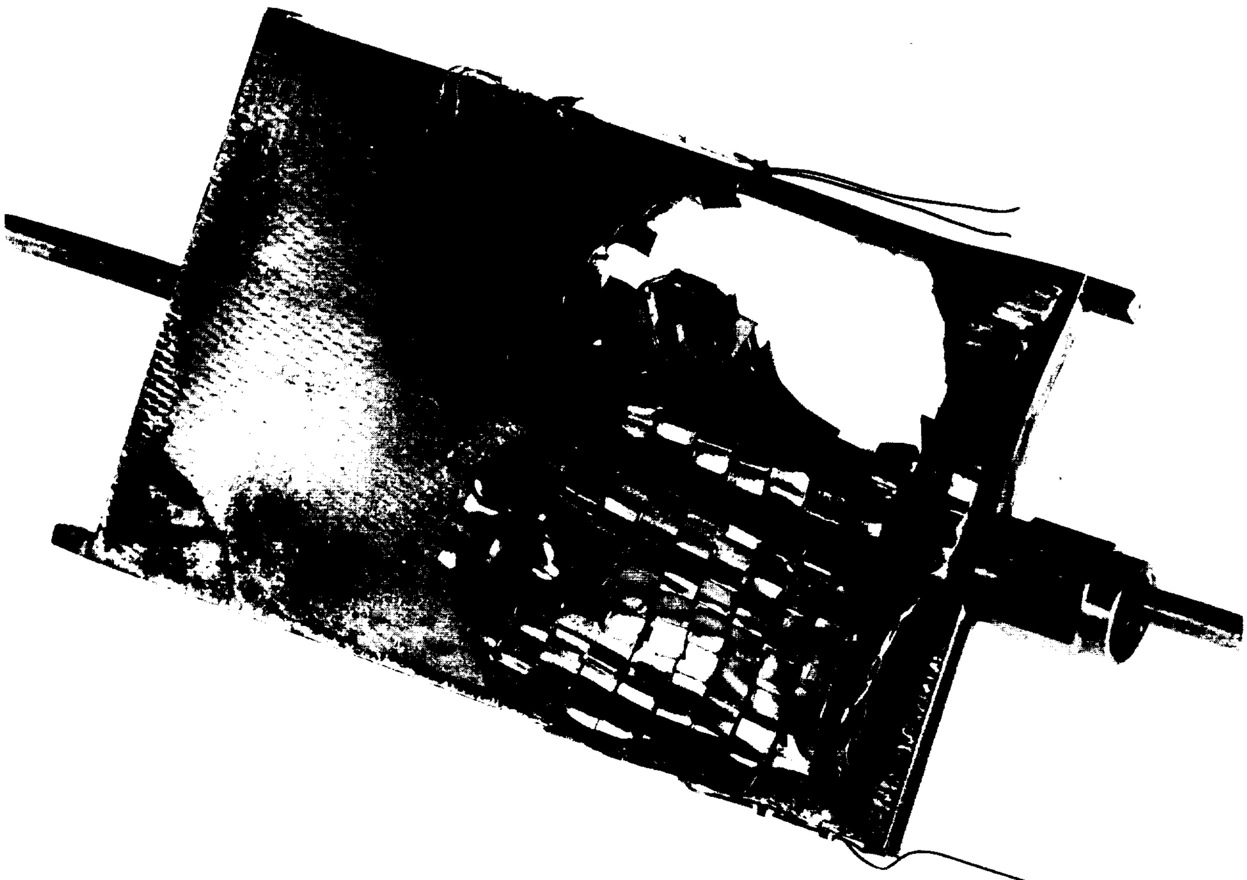

59946-2

Figure 7.4-1. Short-Term Burst Rupture,
Type 1 Flat Panel Configuration

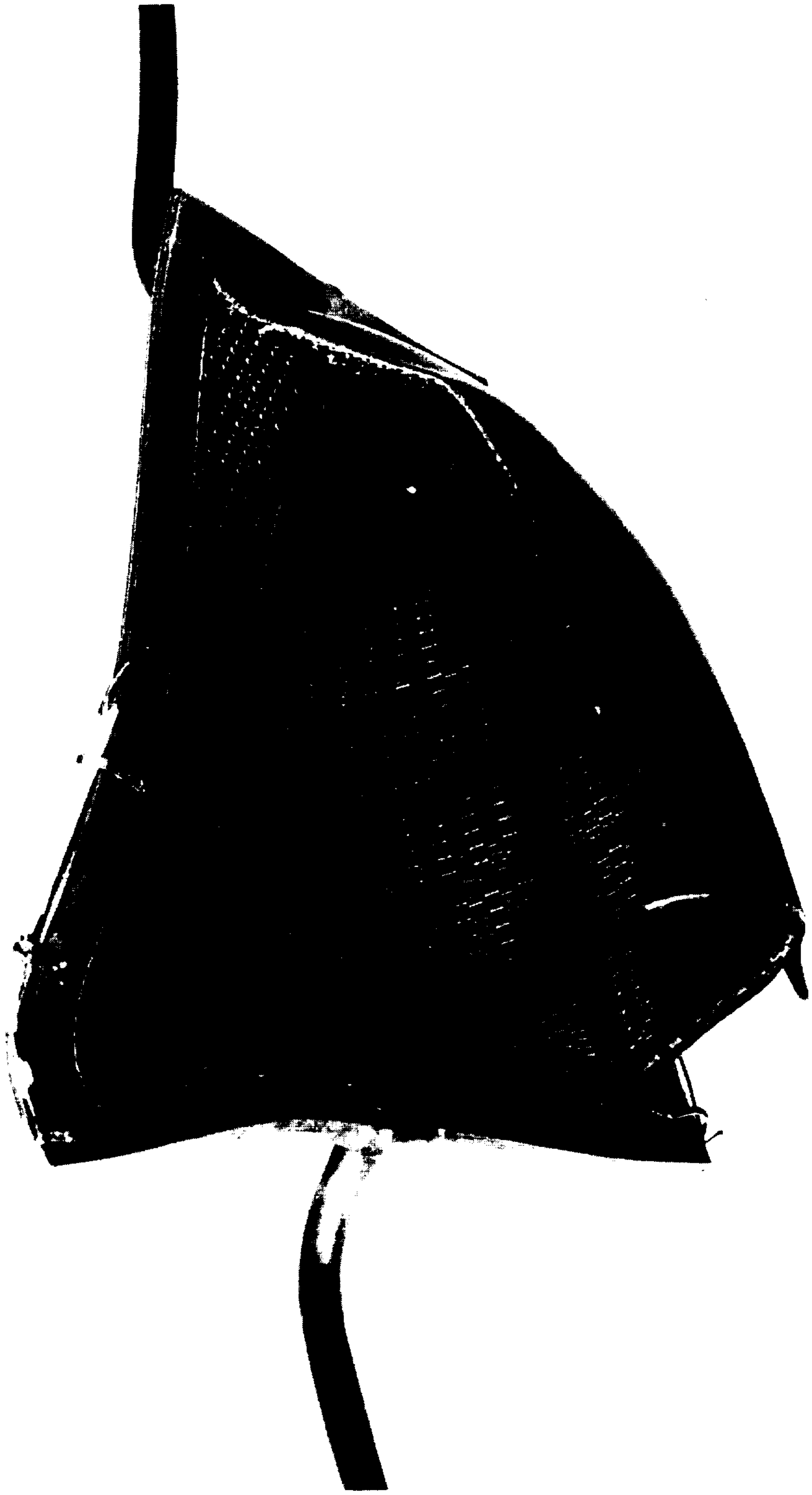

60046-2

Figure 7.4-2. Short-Term Burst Rupture, Type 2 Flat Panel Configuration

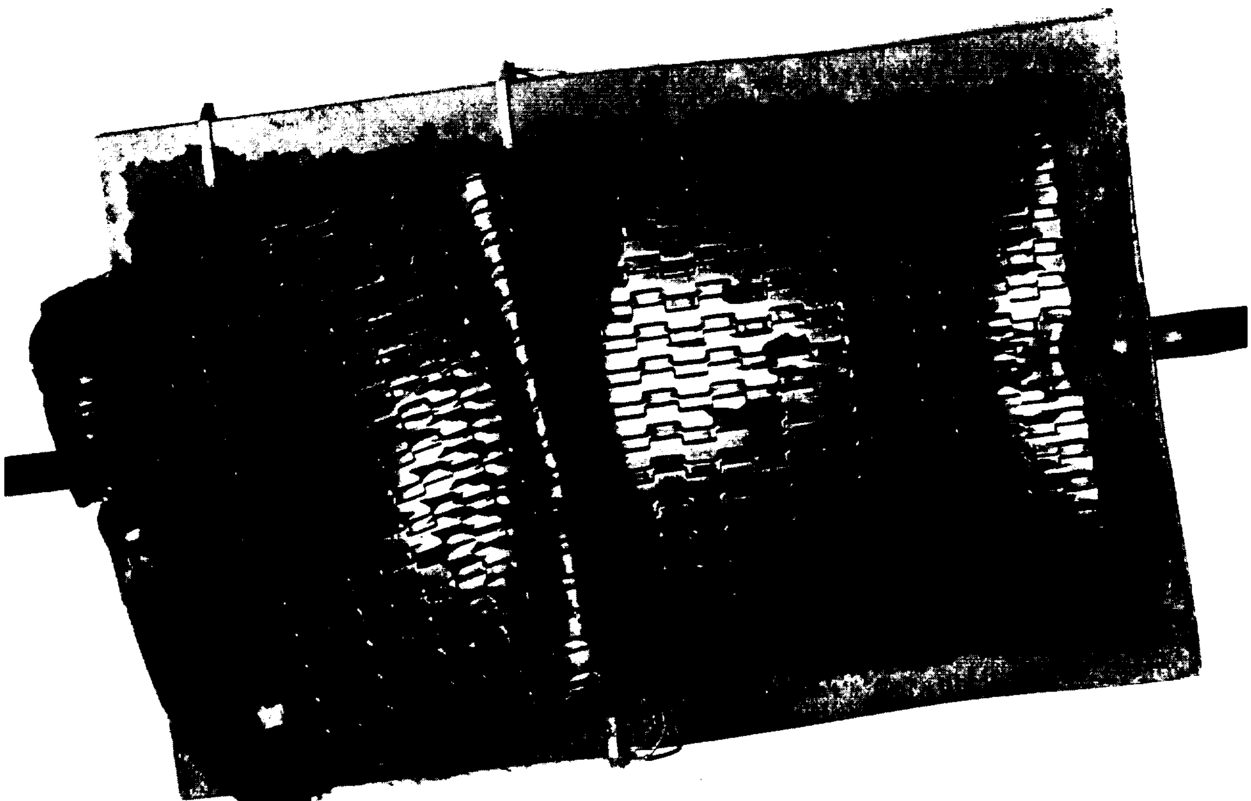

60122-4

Figure 7.4-3. Short-Term Burst Rupture, Type 3
Flat Panel Configuration

60046-3

Figure 7.4-4. Creep Rupture, Type 2
Flat Panel Configuration

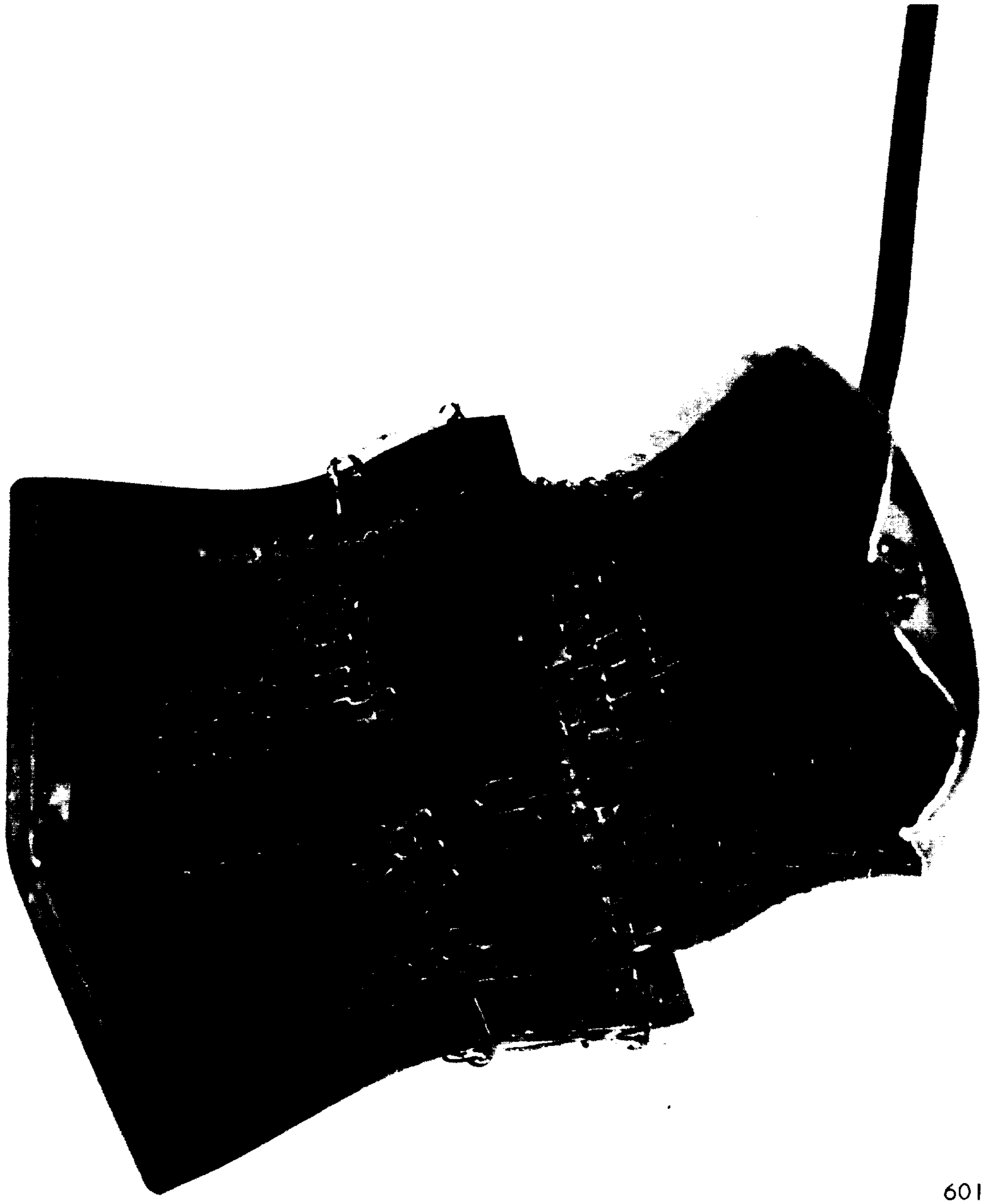

60122-6

Figure 7.4-5. Creep Rupture, Type 3
Flat Panel Configuration

8.0 SUMMARY OF STATUS

8.1 OVERALL ENGINE DESIGN

The design conditions and loads, as established during Phase I of the program, were used to review the thermal and structural design of the engine. The purpose of the review was to verify the adequacy of the general design as opposed to detail designs. Analyses of the regeneratively cooled shells has shown satisfactory margins of safety for the gauges and stiffening selected during Phase I. Heat transfer analysis has shown opportunities for simplification of the coolant side configuration (reduction of the number of different fins and fin heights required), but substantiated the adequacy of the solutions established during Phase I. The results of the design review are being used as a basis for definition of the sizing dies required for forming of the shell face sheets. Early definition and fabrication of these tools is being scheduled.

8.2 INNER BODY NOZZLE

The principle problems encountered in design of the nozzle are the method of attachment of the nozzle to the burner assembly and design of a nozzle cap compatible with the assembly procedure. A bolted flange, using metallic face seals, was the solution selected for nozzle assembly to the engine. A threaded cap will be used to form the remainder of the nozzle.

8.3 INNER BODY-OUTER SHELL SUPPORT STRUT

The design for the inner body-outer shell support strut has been revised and involves a bolted assembly as opposed to the brazed assembly used in the Phase I design. The bolted assembly was selected because it is expected to reduce risk during final engine assembly. The critical problems in achieving a satisfactory bolted assembly are the provisions necessary to react the strut loads into the shells by means of the stiffening rings (manifolds). To minimize section thickness and ensure efficient design, relatively detailed and complex analyses are required. The design that was involved is considered satisfactory for the structural and thermal loads used in the analyses.

Revision of the strut stagnation line heat flux relative to the value used during Phase I resulted in a critical cooling problem at the leading edge. Satisfactory solution of the problem required the use of a separate flow route along the leading edge. The large heat flux predicted and local heat flux steps due to boundary layer interactions at the leading edge led to adoption of an 0.080-in. strut leading edge radius.

Since the bolted design tends to reduce the open cross section of the strut that is required for plumbing and wiring pass-through, the aerodynamic shape of the strut was reviewed and modified. A minimum drag body having the required cross sectional area was designed and will be used in subsequent work.

8.4 COMPOUND-CURVED MODEL FABRICATION

Fabrication of compound-curve models was initiated with shells fabricated as part of an in-house R&D program. A total of 13 shells were available. Of these, 12 were rejected following chemical milling because of excess material removal. The procedure had been verified by use of one of the satisfactory shells. Splitting of 4 replacement thin shells during bulge forming has resulted in modification of the welding procedure and addition of trim material to the end of the shell.

8.5 FLAT PANEL EVALUATION

The results of burst and creep rupture tests on the specimens indicate that the design factors used in establishing fin thicknesses for pressure containment are satisfactory. The test indicate that fin thickness does not have to be increased in any area relative to what was used during Phase I and that reductions in fin thickness are possible in some areas.

The effect of the amount of braze filler alloy and time at brazing temperature were also investigated as part of this work. Significant effects were demonstrated for both of these variables. Evaluation of additional test specimens for extended times at brazing temperature (20 minutes) has, therefore, been scheduled. The significant reduction in strength obtained with 0.0005-in. braze foil thickness compared to 0.001-in. braze foil thickness indicates that the heavier foil should be used for best strength.

8.6 INLET SPIKE ACTUATOR DESIGN

As a first step in the inlet spike actuator design, the operating conditions for the actuator have been established in light of a more detailed knowledge of engine operating conditions and design. The magnitude of the loads and the load profile impose design problems for the actuator as to size and weight, quantity of pressurant for operation, and response. The solution being investigated involves a pneumatic piston combined with a hydraulic damper.

9.0 FUTURE ACTION

Critical problem areas or activities that will extend into the next quarterly reporting period include the following:

a. Definition of inlet spike to inner body shell interface.- In addition to constituting a problem in its own right, the design of this interface will directly affect the design of the inlet spike actuator. The best solution appears to involve the use of a welded bellows. Such a bellows can provide a zero-leakage seal. On the other hand, the high pressure loads that must be sustained by this bellows during inlet unstart make the design of the bellows itself problematical.

b. Preliminary design of inlet spike actuator.- For the loads and load profiles currently predicted for the actuator, a pneumatic device appears marginal. The actuator loading, however, is very strongly influenced by the design of the inlet spike/inner body interface and makes resolution of this interface important. Preliminary design of the actuator will be based on currently known loads, which are considered realistic.

   In addition to its actuation function, the actuator serves as the support for the inlet spike. The structural design problem is one of limiting deflection of the moveable spike. Evaluation of this problem, in turn, requires definition of actuator size and configuration. The contribution of the actuator to the total engine weight is significant. Incentives, therefore, are strong for finding ways to minimize actuator loads to the point where the structural deflection limits design.

c. Computer programming of a structural model of the engine.- Engine static loads can be and have been reasonably well defined. Dynamic loads are being approximated by use of assumed dynamic input amplification factors. Verification of the assumption requires the results of the model analyses. Computer programming was started during this reporting period and will extend into the next reporting period.

d. Full-scale component sizing die fabrication.- These dies constitute the pacing item in fabrication of the components. The design drawing for the sizing dies have been completed and submitted to forging vendors for bid.

e. Thermal transient analysis of the engine based on predicted mission profiles.- Detailed estimates of the thermal response of the engine structure is required to establish adequacy of the design. Preliminary transient analyses performed during Phase I have shown acceptable thermal transients. The detailed analysis to be initiated during the next reporting period will be studying the designs evolved during the current phase of the program, since significant differences have occurred.

f. Coolant flow distribution as a function of engine operating conditions.- A preliminary analysis of this problem was performed during Phase I. This data has been reviewed during the reporting period. Further analyses to establish the requirement for orificing and for valves to ensure flow balancing in the various routes for different mission profiles is planned. The possibility of adjusting pressure drops in the various flow routes for individual missions prior to each mission is being considered.

REFERENCES

1. Phase I Aerodynamic, Heat Transfer, and Cooling Data for Hypersonic Ramjet Off-Design Flight Conditions, AiResearch Report AP-1001-10

2. NASA Statement of Work, Hypersonic Research Engine Project, L-4947-B, January 15, 1967

3. E. Reshotko and C. B. Cohen, "Heat Transfer at the Forward Stagnation Point of Blunt Bodies", NACA Technical Note 3513

4. J. A. Fay and F. W. Riddell, "Theory of Stagnation Point Heat Transfer in Dissociated Air", Journal of the Aeronautical Sciences, Vol. 25, No. 2, February 1958

5. L. Lees, "Laminar Heat Transfer Over Blunt-Nosed Bodies at Hypersonic Flight Speeds", Jet Propulsion, April 1956

6. F. Krieth, "Principles of Heat Transfer", Internation Textbook Co., 2nd Ed. P 408, 1966

7. Conceptual Design Study Report, AiResearch Report AP-67-0167-1, Vol. I (CONFIDENTIAL)

8. Conceptual Design Study Report, AiResearch Report AP-67-0167-2, Vol. II, Appendix A (CONFIDENTIAL)

9. Conceptual Design Study Report, AiResearch Report AP-67-0167-3, Vol. III, Appendix B (UNCLASSIFIED)

10. Preliminary Design Report, AiResearch Report AP-67-0168-1, Vol. I (CONFIDENTIAL)

11. Preliminary Design Report, AiResearch Report AP-67-0168-2, Vol. II, Appendix A (CONFIDENTIAL)

12. Preliminary Design Report, AiResearch Report AP-67-0168-3, Vol. III, Appendix B (CONFIDENTIAL)

13. Preliminary Design Report, AiResearch Report AP-67-0168-4, Vol. IV, Appendix C (CONFIDENTIAL)

14. Engine Development Plan, Technical Proposal for Phase II, AiResearch Report AP-67-0169 (CONFIDENTIAL)

15. Computer Program H1940, AiResearch Report AP-1001-3

16. Computer Program H1930